Covid Impact Statement

Frequent disruptions from the Covid-19 pandemic throughout 2021 and 2022 included a lack of access to testing facilities, an inability to collect experimental data under strictly controlled, laboratory conditions, and fewer available participants. Visual psychophysics involves testing participants for extended periods of time, typically with testing sessions broken up across multiple days, and often requires intensive piloting processes. To mitigate risk, exploratory research was disregarded in favour of experimental approaches which required less-intensive periods of experimental setup, piloting, and data collection. An initial research question (which could not be explored) was how long-term adaptation would impact orientation perception, whereby participants would be devoid of normal vision, by exposure to prism lenses that would optically rotate their perceived world around the line of sight.

To mitigate the impacts of the pandemic, I designed a psychophysical experiment for a cohort of undergraduate students to perform as part of their 'Practical Methods' module, which was completed on participants' web-browsers at home. This enabled a substantial body of data to be collected that otherwise would have been impossible during Covid restrictions. Due to the lack of previous research using web-based, psychophysical experiments, the level of agreement between web-based and lab-based methods was evaluated to establish the validity of the web-based testing protocol (see Section 6.3). To utilise these data, the reliability of web-based methods and individual differences were investigated for the orientation-identification task (see Chapter 7).

Investigations of orientation anisotropies in the human visual system: psychophysics and modelling

Richard Leadbeater

Thesis submitted to the University of Nottingham

for the degree Doctor of Philosophy

December 2023

Abstract

Visual performance is worse for the detection and discrimination of stimuli at oblique orientations, than for cardinal (horizontal and vertical) orientations, i.e., the 'oblique effect'. The classical view is that the oblique effect is generated by an overrepresentation of orientation-selective mechanisms which prefer cardinal orientations, however there are aspects of the behavioural oblique effect which are inconsistent with this account. In the empirical Chapters of this thesis, a variety of psychophysical techniques were employed to measure the behavioural oblique effect in humans.

Computational models of orientation coding are inspired by decades of psychophysical and neurophysiological research, and can serve as tools for testing explicit hypotheses about visual function. Through a combination of psychophysical testing and computational modelling, this thesis systematically investigated various accounts of the oblique effect, and aimed to provide a thorough account of the neuronal mechanisms underlying anisotropic perception. To capture the psychophysical data for contrast detection, orientation discrimination, and orientation identification tasks, model performance was assessed on a series of analogous, computational tasks.

A novel account is proposed for why the oblique effect for contrast detection emerged at high spatial frequencies (16c/°), yet was abolished at low spatial frequencies (2c/°). An overrepresentation of cardinal-tuned neurons effectively increases the signal-to-noise ratio (SNR) for cardinal orientations relative to oblique orientations, however this difference in the signal-to-noise ratio is diminished by the broad, overlapping orientation-tuning curves of neurons selective for low spatial frequencies. Conversely, the narrowed orientation bandwidths of neurons selective for high spatial frequencies increases this difference in the

signal-to-noise ratio, such that cardinal orientations can be detected at lower contrasts than oblique orientations.

A unified model could not account for the empirical, behavioural data on both the contrast-detection and orientation-discrimination tasks, challenging the classical view of the oblique effect. Specifically, model simulations revealed that anisotropic orientation bandwidths were required to capture the oblique effect for orientation discrimination, yet this anisotropy abolished the oblique effect for contrast detection. Therefore, the oblique effect may not be a unitary phenomenon, such that the oblique effects measured for various behavioural tasks may be generated by independent mechanisms, each with their own distinctive orientation anisotropies.

A visual masking paradigm generated psychophysical estimates of orientation bandwidths, on contrast-detection and orientation-discrimination tasks, and confirmed two key predictions from the preceding modelling work. First, the bandwidths of detection mechanisms were equal for cardinal and oblique orientations, and second, the bandwidths of discrimination mechanisms were substantially narrower for cardinals than for obliques. In a further challenge to the classical view of the oblique effect, the number of orientation-selective mechanisms underlying visual perception was estimated to be equal about the cardinal and oblique axes.

Notably large oblique effects were found for an orientation-identification task, which required participants to judge which of two stimuli was presented at the standard orientation. A novel computational framework was proposed to account for these data, where the decision stage of the model compared each encoded orientation with the memory of the standard orientation, in order to quantify its degree of similarity to the standard orientation. To capture the larger oblique effect for identification, relative to discrimination, the standard orientation

had to be decoded from an anisotropic population of orientation-selective mechanisms which was independent of the population which encoded the stimulus orientation. The reliance of orientation identification on higher-level, cognitive mechanisms was supported by findings of an increased oblique effect when spatial attention was divided between two stimuli, presented simultaneously, in separate spatial locations. Attentional mechanisms may serve to lessen the anisotropic representations of orientation (i.e., 'whitening' perception).

Overall, the ubiquity of the oblique effect in the human visual system indicates that it should be a feature for models of orientation perception. The novel findings of this thesis demonstrate the utility of this approach for understanding the initial stages of visual perception, including the computations of detection and orientation perception, the modularity of visual function, and the integration of cognitive information. So long as visual performance varies systematically along a particular stimulus dimension, these methods can be adopted by future research in other domains of visual function, beyond orientation perception.

Acknowledgements

I would like to thank my friends and family for their support during my PhD. I want to thank my PhD supervisors, Tim and Paul for their invaluable guidance and supportive nature throughout the last few years. I would like to give a special thanks to Tim for his encouragement over the past year, and for his excellent supervision in my BSc, MSc and PhD studies. I want to show an enormous amount of love and gratitude for Luka, whose support, kindness, and patience seemingly knows no bounds.

Finally, I want to acknowledge myself for writing such a ridiculously long document, and my examiners for having to read it.

Table of Contents

1. Introduction 13
1.1 The visual pathways 13
1.1.1 Optics 13
1.1.2 Retina 14
1.1.3 Lateral geniculate nucleus 20
1.1.4 Primary visual cortex 21
1.1.5 Extrastriate visual areas 31
1.2 Orientation encoding 33
1.2.1 Orientation selectivity 33
1.2.2 Feedforward 33
1.2.3 Challenges to the feedforward model 35
1.2.4 Cortical inhibition 39
1.2.5 Models of orientation encoding 41
1.3 Psychophysical evidence of the oblique effect 49
1.3.1 Overview 49
1.3.2 Visual sensitivity 50
1.3.3 Orientation discrimination 53
1.3.4 Orientation channels 55
1.3.5 Higher visual areas 58
1.4 Neurophysiological evidence for the oblique effect in animals 63
1.4.1 Overview 63
1.4.2 Single-cell recordings 64
1.4.3 Optical imaging 68
1.5 Brain imaging evidence for the oblique effect in humans 71
1.5.1 Electrophysiology 71
1.5.2 Functional magnetic resonance imaging 76
1.6 Individual differences in visual function 80

141 1.6.1 Variations in the visual pathways 80
142 1.6.2 Assessing individual differences 82
143 1.6.3 Stability of individual differences 85
144 1.7 Unresolved issues 87
145 2. General methods 90
146 2.1 Participants 90
147 2.2 Apparatus 90
148 2.3 Monitor calibration 91
149 2.3.1 Gamma correction 91
150 2.3.2 Noisy-bit method 93
151 2.4 Stimuli 94
152 2.5 Adaptive staircase 97
153 2.6 Method of constant stimuli 99
154 2.7 Bandwidth estimation 100
155 2.8 Oblique effect index 101
156 2.9 Reliability analyses 102
157 2.10 Web-based testing 105
158 3. Modelling 106
159 3.1 Population Response 106
160 3.1.1 Tuned responses 106
161 3.1.2 Internal noise 108
162 3.2 Decoding orientation 109
163 3.3 Detection 111
164 3.4 Model performance 113
165 3.4.1 Orientation discrimination 113
166 3.4.2 Contrast detection 116
167 3.5 Model parameters 117
168 3.5.1 Stimulus orientation 117
169 3.5.2 Number of neurons 119

3.5.3 Orientation bandwidth 122
3.5.4 Response variability 122
3.5.5 Peak firing rate 123
3.5.6 Spontaneous firing rate 124
3.5.7 Contrast-response function 124
3.6 Modelling the oblique effect 127
3.6.1 Orientation anisotropies 127
3.6.2 Comparisons with behavioural performance 129
4. Understanding the mechanisms of the oblique effect through the manipulation contrast and spatial frequency 130
4.1 General introduction 130
4.2 Contrast detection and spatial frequency 134
4.2.1 Introduction 134
4.2.2 Methods 136
4.2.3 Results 137
4.2.4 Modelling 141
4.2.5 Discussion 146
4.3 Orientation discrimination and spatial frequency 150
4.3.1 Introduction 150
4.3.2 Methods 152
4.3.3 Results 154
4.3.4 Modelling 157
4.3.5 Discussion 162
4.4 Orientation discrimination and stimulus contrast 165
4.4.1 Introduction 165
4.4.2 Methods 167
4.4.3 Results 168
4.4.4 Modelling 170
4.4.5 Discussion 176
4.5 Summary of findings 179

5. Psychophysical investigations of the orientation-selective mechanisms underlying perception 182
5.1 General introduction 182
5.2 Estimating the number of cardinal and oblique mechanisms underlying perception 184
5.2.1 Introduction 184
5.2.2 Methods 186
5.2.3 Results 190
5.2.4 Discussion 194
5.3 Estimating the orientation bandwidths of the mechanisms for detection and discrimination 197
5.3.1 Introduction 197
5.3.2 Methods 199
5.3.3 Results 205
5.3.4 Discussion 210
5.4 Summary of findings 214
6. Investigating the contributions of cognitive factors to the oblique effect 217
6.1 General introduction 217
6.2 Remote measurements of the oblique effect for orientation-identification 221
6.2.1 Overview 221
6.2.2 Methods 222
6.2.3 Results 225
6.2.4 Summary 226
6.3 Lab-based measurements of the oblique effect for orientation identification 228
6.3.1 Overview 228
6.3.2 Methods 228
6.3.3 Results 232
6.3.4 Summary 236
6.4 Examining the cognitive factors underlying the oblique effect for orientation

identification 237
6.4.1 Overview 237
6.4.2 Methods 237
6.4.3 Results 240
6.4.4 Summary 242
6.5 Comparing the oblique effects for orientation identification and discrimination 244
6.5.1 Overview 244
6.5.2 Methods 245
6.5.3 Results 247
6.5.4 Summary 252
6.6 Modelling the oblique effect for orientation identification 254
6.7 Summary of findings 264
7. Individual differences in the oblique effect 269
7.1 Introduction 269
7.2 Methods 271
7.3 Results 273
7.3.1 Within-groups 273
7.3.2 Between-groups comparisons 277
7.4 Discussion 280
8. General Discussion 283
8.1 Summary of main findings 283
8.1.1 The oblique effect for contrast-detection 283
8.1.2 The oblique effect for orientation-discrimination 284
8.1.3 The oblique effect for orientation-identification 285
8.1.4 Distinct mechanisms for detection and discrimination 286
8.1.5 The number of perceptual mechanisms 287
8.1.6 The computation of detection 288
8.1.7 The computation of orientation perception 288
8.1.8 The reliability of web-based testing 289

8.2 Unanswered questions 290
8.2.1 The independence of mechanisms for encoding and perception 290
8.2.2 Predicting visual performance 291
8.2.3 Investigating the mechanisms of contrast discrimination 293
8.2.4 Quantifying the number of perceptual mechanisms 293
8.2.5 How is cognitive information integrated with sensory visual information? 294
8.2.6 The role of attention in the oblique effect 295
8.2.7 Insight from individual differences 296
8.2.8 The reliability of web-based methods in clinical populations 296
8.3 Concluding remarks 298
9. References 299

1. Introduction

1.1 The visual pathways

1.1.1 Optics

Light entering the eye is focussed onto the retinal surface by the optics of the eye (Figure 1.1). The cornea and lens refract light projecting from locations in three-dimensional (3D) space onto photoreceptors at corresponding locations of the spherical retina. This encodes changes in light intensity across space. The cornea has a fixed, curved shape that is partially flattened in the central section, which refracts a greater proportion of light to central vision. The lens is elastic and can stretch and shrink, through relaxation and tension of surrounding ciliary muscles, which provides variable optical power to central vision (De Valois & De Valois, 1990; Kandel et al., 2021).

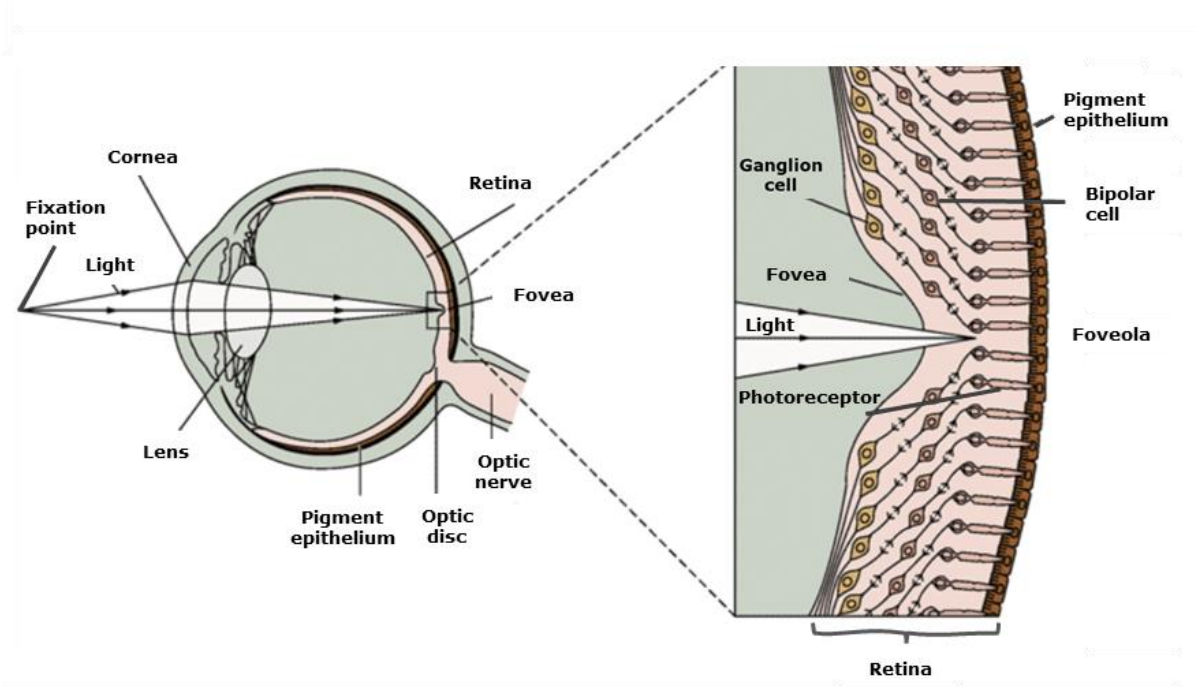

Figure 1.1. The main structures of the eye involved in the detection and of transduction of light information. Adapted from Kandel et al. (2021).

Imperfections in the optics of the eye introduce errors into the retinal image (for review, see Lombardo & Lombardo, 2010). Refractive errors occur due to spherical aberrations of the cornea and lens, impaired ciliary muscle function, pupil diffraction, and structural abnormalities in the shape of the retina. The eye is also unstable during periods of fixation, with microsaccades which typically range from 0.05 to 1° in amplitude (Deubel & Elsner, 1986; Poletti & Rucci, 2016) with a median amplitude of 0.5° (Otero-Millan et al., 2008; Rolfs, 2009), and are predominantly horizontal in direction (Engbert, 2006). Blurring of the retinal image impairs the positional accuracy of light information on the retina, placing a physiological limit on the highest spatial frequency that can be encoded by the visual system (De Valois & De Valois, 1990). Additional error is introduced by intraocular light scatter (or 'retinal straylight'), caused by reflections off retinal structures, such as blood vessels, the optic disc, and the myelin sheath of nerve fibres (Franssen et al., 2006).

1.1.2 Retina

Overview

Light information passes through three major functional layers of the retina (Figure 1.2), namely photoreceptors (rods and cones), interneurons (bipolar, horizontal, and amacrine cells), and ganglion cells (Hedges, 2022; Masland, 2012). Light traverses through each layer before being absorbed by photopigments in the outer segments of photoreceptors which penetrate the pigment epithelium of the outermost layer of the retina. The pigment epithelium absorbs light that is not absorbed by the photoreceptors. The absorption of light in photoreceptors induces biochemical changes that converts light into neural activity (for review, see Luo et al., 2008). Variations in light intensity (i.e., the rate of photons) modulates the hyperpolarisation of the membrane potential of photoreceptors, which in turn determines

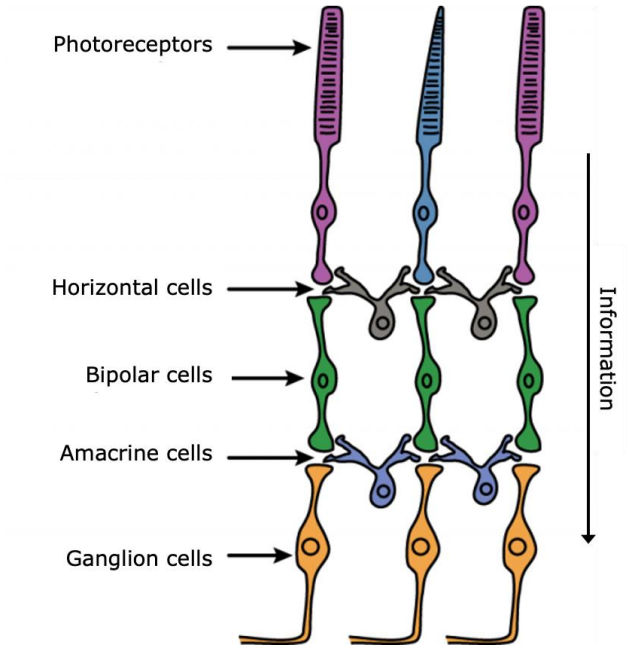

Figure 1.2. The flow of information through the retinal layers through direct and lateral connections. Adapted from Hedges (2022).

the magnitude of synaptic release at connections with bipolar and horizontal cells (for review, see Masland, 2012). Owing to similarities in the basic structure and function of the retina across vertebrate species, various animal models (e.g., non-human primates, cats, rabbits, rodents, zebrafish, etc.) have been used to understand the mechanisms of phototransduction in the retina (Luo et al., 2008; Masland, 2012). Electrophysiological techniques, typically intracellular and extracellular recordings of neuronal activity, have provided insight into the response properties of retinal cells (Mahroo, 2023).

Photoreceptors

Photoreceptors display three key response characteristics that specialise them for light detection. First, there is a substantial amplification of the detected signal, caused by a cascade of molecular and biochemical changes in the photoreceptor, which generates large changes in membrane polarisation despite relatively small variations in light intensity (Lagnado, 2002).

For example, human observers can reliably detect the absorption of five to seven photons in a retinal region containing 500 rods (Hecht et al., 1942; Van Der Velden, 1946), indicating that individual rods can themselves detect a single photon (for review, see Rieke & Baylor, 1998).

Second, visual perception in scotopic conditions (i.e., low-light) is facilitated by photon capture which occurs over time, such that the membrane potential of a photoreceptor at a given point in time reflects signal changes integrated over a period of milliseconds. The response to light (both for bright flashes and for single photons) in vertebrate photoreceptors follow a delayed Gaussian as a function of time (Lamb & Pugh, 1992).

Third, adaptation is demonstrated in photoreceptor sensitivities that vary with the mean light level, such that the whole response range of a photoreceptor is utilised across an enormous range of light levels (Choi et al., 2005; Fain et al., 2001). Shifting of the operational range is often termed 'variable gain control'. This mechanism was first discovered in extracellular recordings (measuring the firing rates) of macaque LGN neurons (De Valois et al., 1962), before being captured by intracellular recordings (measuring changes in membrane potential) of photoreceptors in the Necturus, or 'mudpuppy' (Normann & Werblin, 1974).

Rods and cones

Photoreceptors in the outer retinal layer consist of rods and cones. Rods have a higher sensitivity and a longer integration time than cones, meaning they are specialised for low-light conditions, but become unresponsive under photopic conditions (Ingram et al., 2016). In contrast, cones become unresponsive in low-light conditions but have an operating range which extends beyond the photopic levels of everyday visual experience (Barbur & Stockman, 2010). Early investigations quantified the density of rods and cones across the vertebrate retina by staining sections of post-mortem retinal tissue, and then counting the

density of photoreceptors within these regions (Curcio et al., 1990; Gresh et al., 2003). Modern techniques, such as 'adaptive optics scanning laser ophthalmoscopy' (AO-SLO), compensate for aberrations in the optics of the eye to enable such measurements in healthy human eyes (Wells-Gray et al., 2016). There are approximately 90 million rods and 5 million cones in the average human retina (Curcio et al., 1990), although these are non-uniformly distributed along the retinal meridians. The majority of cones are located in the fovea (a small depression in the centre of the retina), whereas rods are largely absent here, and reach their highest density at about 20 to 25° from the fovea (Curcio et al., 1990; Wells-Gray et al., 2016; Zhang et al., 2015). Neurophysiological investigations using macaques have revealed that the neural pathways of rods and cones are largely separated in the retina and through to early visual cortex (Grünert & Martin, 2020; Lee et al., 2010).

By measuring the proportion of light that is absorbed at different wavelengths, microspectrophotometry has been used to characterise the spectral absorption curves of photopigments in rods and cones, in the retina of various vertebrate species (Bowmaker, 1984), including humans (Merbs & Nathans, 1992). As the rod system contains only one type of photopigment, rhodopsin, the change in photoreceptor response is a combined function of both the intensity and wavelength of light. Therefore, the rod system cannot distinguish between a change in wavelength, and a corresponding change in intensity (i.e., the 'principle of univariance') (Rushton, 1972). Colour perception is mediated by the combined responses of three cone subtypes with distinct peak absorption wavelengths, S-cones (~ 420 nm), M-cones (~ 535 nm) and L-cones (~ 560 nm) (Bowmaker, 1984), in that their combined responses can distinguish between a change in light intensity and a change in wavelength.

Retinal ganglion cells

Information passes from photoreceptors to bipolar cells to ganglion cells (Grünert & Martin, 2020; Masland, 2012). Bipolar cells receive convergent inputs from photoreceptors, through direct, synaptic connections and lateral connections mediated by horizontal cells. A similar pattern of convergent connections is observed from bipolar to ganglion cells, with lateral connections from amacrine cells (Cook & McReynolds, 1998). Horizontal cells modulate the synaptic gain between photoreceptors and bipolar cells, forming the classical centre-surround, antagonistic receptive field organisation of bipolar cells (Normann & Werblin, 1974), which is subsequently inherited by ganglion cells (Mangel, 1991). Inhibitory interactions mediated by amacrine cells also contribute to the surround antagonism of ganglion cell receptive fields (Cook & McReynolds, 1998).

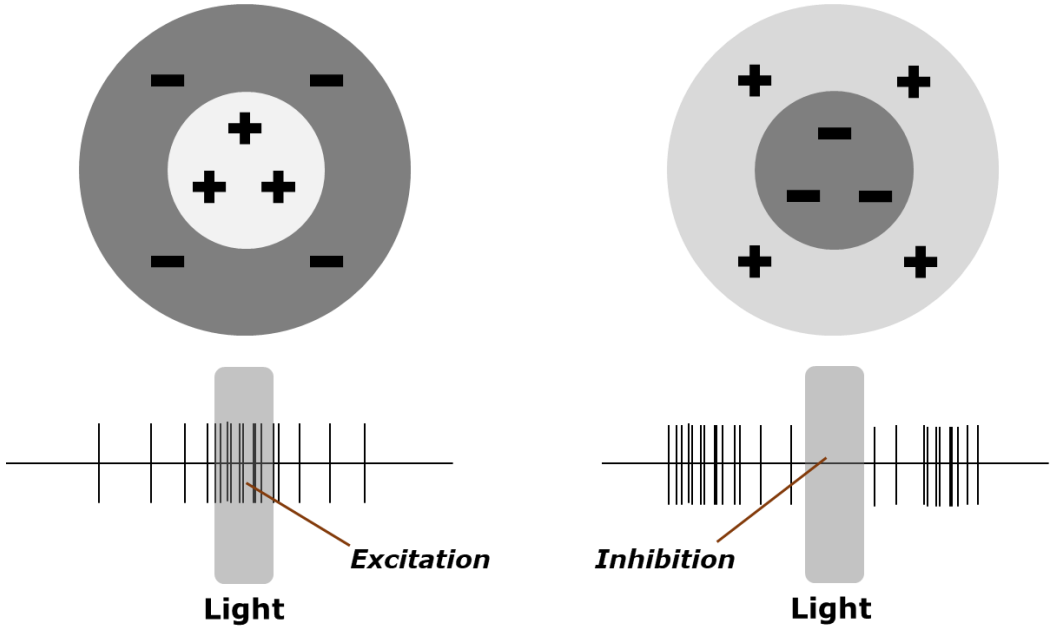

Figure 1.3. Bipolar and ganglion cells have circularly symmetric receptive fields in an antagonistic centre-surround arrangement. Light stimulation localised to the central region of the ganglion cell receptive field either increases or decreases the firing rate of ganglion cells for 'centre-on surround-off' (left) and 'centre-off surround-on' (right) cells, respectively.

This centre-surround arrangement takes two main forms (Figure 1.3). 'On-centre off-surround' receptive fields are formed through depolarising direct connections that dominate the centre of the receptive field, and hyperpolarising lateral connections that dominate the outer portion. Conversely, 'off-centre on-surround' receptive fields are formed from hyperpolarising direct connections and depolarising lateral connections. Put simply, 'on-centre off-surround' cells respond maximally to light in the centre of their receptive field, with a sharp drop in response to luminance in the surround. Whereas 'off-centre on-surround' ganglion cells respond maximally to light in the surround, with a sharp drop in response to stimulation of the centre.

There is substantially more neural convergence through the retinal layers for rod pathways than cone pathways. One study quantified convergence by measuring the spatial extent of ganglion cells across the human retina, and calculating the average number of photoreceptors within the corresponding spatial regions (Goodchild et al., 1996). At eccentricities over 20° from the fovea, measures of convergence approached 10,000 rods per ganglion cell, and under 500 cones per ganglion cell. In the fovea, relative to more peripheral locations, cone neural pathways are far less convergent and the receptors themselves are more tightly spaced (Borwein, 1981), with approximately 80 to 100 cones per ganglion cell (Goodchild et al., 1996). These patterns of convergence are consistent with findings that the receptive field sizes of cat and monkey ganglion cells increase with eccentricity from the fovea (Wassle & Boycott, 1991). A perceptual consequence of neural convergence is the spatial smoothing of the retinal image, which reduces sensitivity to high spatial frequency information to a greater extent with increasing eccentricity, as evidenced by eccentricity-dependent losses in visual acuity (Anderson et al., 1991).

1.1.3 Lateral geniculate nucleus

Ganglion cell axons traverse the inner retinal surface, bypassing the fovea, to exit the eye at the optic disc, located about 15° temporally from the fovea. Photoreceptors are entirely absent from this portion of the retina, which results in a functional blind spot that is elliptical in shape and approximately 7.5 x 5.5° in size at its widest and narrowest points, respectively (Jonas et al., 1991). The axons of ganglion cells form the optic neural tract that projects from the retina to thalamic regions of the brain. At the optic chiasma, the nasal fibres from each eye cross to the other side, such that information from the right visual field passes to the left hemisphere of the brain, and information from the left visual field passes to the right hemisphere (for review, see Katz & Shatz, 1996).

The two main destinations of ganglion cell axons are the lateral geniculate nucleus (LGN) and the superior colliculus. The superior colliculus receives approximately 20% of ganglion axons, and its primary role has been identified as the control of eye movements (Wurtz & Goldberg, 1971). LGN relay cells are organised retinotopically with interneurons mediating lateral connections (Pasik et al., 1973), in a manner resembling that of bipolar and horizontal cells in the retina. Extracellular recordings in cat LGN revealed that relay cells exhibit circular, antagonistic, centre-surround receptive fields (P. Hammond, 1973), although there is evidence of weak orientation selectivity in some of these neurons (Ghodrati et al., 2017; Vidyasagar & Siguenza, 1985). The LGN is generally considered as a simple, linear relay stage between retina and visual cortex, however there are indications that the LGN may play a more active role in visual perception (Ghodrati et al., 2017), either through generating feature selectivity (Vidyasagar & Eysel, 2015) or through the modulation of neuronal responses through inhibitory connections, via selective attention (Briggs et al., 2013). One example of efferent control in LGN, is the transient disinhibition of the LGN in cats that

coincides with rapid eye movements, thought to act as a gating mechanism to reset neurons to a neutral state whenever fixation is changed (Singer, 1977).

1.1.4 Primary visual cortex

Structure

The majority of retinogeniculate connections project to primary visual cortex (V1), located in the occipital lobe. V1 is subdivided into 6 layers, from layer 1 at the cortical surface through to layer 6, which is adjacent to the white matter (axonal projections). Projections between different brain regions are often recorded using tracer injections, which label the axons of connecting neurons (Amir et al., 1993). LGN cells primarily make synaptic contacts with layer 4 of V1 (McLaughlin et al., 2000; Wilson et al., 1969), although there are also projections to layers 1, 3, and 6. There are even projections from LGN cells to other visual areas, as found in macaques (Fries, 1981; Ghodrati et al., 2017), such as V2 (Markov et al., 2011), V3 (Yoshida & Benevento, 1981), and V4 (Gattass et al., 2014; Lyon & Rabideau, 2012; Yoshida & Benevento, 1981). V1 interneurons form connections vertically between the cortical layers, primarily through the extended dendritic trees of large pyramidal cells (Callaway, 1998). Compared to subcortical structures, V1 circuitry is less well-understood (Callaway, 1998; S.-H. Lee et al., 2012), due to the vast amount of intracortical connections and feedback connections from higher visual areas (Budd, 1998; Douglas & Martin, 2007; Felleman & Van Essen, 1991).

Studies of macaque visual cortex have revealed separate neuronal pathways, born from axonal projections out of V1 (J. S. Lund et al., 1975). The majority of macaque V1 projections are to V2 (El-Shamayleh et al., 2013; J. S. Lund, 1973), although there are also projections to various extrastriate visual areas, such as V4 (Pettine et al., 2019) and middle

temporal (MT) visual area (Vanni et al., 2020), which largely bypass the classical visual hierarchy. Additionally, neurons in layer 6 of V1 in macaques have direct feedback connections to LGN neurons in corresponding receptive field locations (Mohan et al., 2019; Vidyasagar & Urbas, 1982). Similarly, it has been shown that there are many more feedback connections from extrastriate visual areas to V1, than there are feedforward projections out from V1 (Budd, 1998; Felleman & Van Essen, 1991).

Retinotopy

The retinotopic organisation of V1 was clearly demonstrated in macaques (Tootell et al., 1982) using the 'C-labelled 2-deoxy-D-glucose' (2DG) method, which labels cortical regions according to their long-term metabolic activity (Hand, 1981; Sokoloff et al., 1977). This revealed a retinotopic mapping of the contralateral visual field onto each hemisphere of V1, such that retinal regions of each eye project to corresponding regions of V1 in a systematic fashion (for review, see Katz & Shatz, 1996). Projections from foveal ganglion cells terminate in the most lateral regions of V1, whereas ganglion cells from the periphery project to the more medial regions. Cortical regions with receptive fields close to the vertical meridian of the visual field also form interhemispheric lateral connections, via the corpus callosum, as demonstrated in cat visual cortex (Altavini et al., 2017; Hubel & Wiesel, 1967).

Retinal ganglion cell density is highest in the fovea, with a logarithmic drop-off in density with increasing eccentricity, as demonstrated in both cats (Hubel & Wiesel, 1974) and macaques (Strasburger, 2022; Tootell et al., 1982). This dedication to the central visual field was demonstrated to be further magnified in the LGN, and through its projections to V1 (Van Essen et al., 1984), such that approximately 25% of the cortical representation in V1 is dedicated to the central 2.5° of the visual field (Strasburger, 2022). The degree of cortical magnification as a function of eccentricity can be quantified by the 'cortical magnification

468 factor' (mm/°), which decreases with eccentricity (Rovamo & Virsu, 1979; Strasburger, 2022;
469 Tootell et al., 1982). This is consistent with receptive field sizes that increase as a function of
470 eccentricity, as demonstrated by single-cell recordings in monkeys (Hubel, 1982) and by
471 population-receptive field mapping in humans (Dumoulin & Wandell, 2008).

472 Monocular inputs from corresponding retinal regions (i.e., with overlapping receptive
473 fields) in each eye are carried by separate neural pathways that converge in V1 (Hubel &
474 Wiesel, 1970), outside of layers 4 and 6, which are largely monocular (Hubel & Wiesel,
475 1968). The convergence of monocular inputs provides the neural circuitry needed to generate
476 a unified representation of visual space, i.e., binocular vision, and the ability to utilise
477 stereoscopic depth information (Parker, 2007, 2016). Around 80% of visual cortical neurons
478 are binocular (Hubel & Wiesel, 1962, 1968). The response characteristics of binocular V1
479 neurons are modulated by the summation of signals from the left and right eyes (H. B.
480 Barlow et al., 1967; G. Poggio et al., 1988). The relative contribution of each eye can be
481 quantified by indices of ocular dominance (LeVay & Voigt, 1988; Prince et al., 2002; Read &
482 Cumming, 2004). Early investigations in cats and monkeys revealed an ordered structure of
483 eye dominance throughout V1, in ocular dominance columns (Hubel & Wiesel, 1962, 1968).

Receptive fields

The classical V1 receptive field is symmetrical, and is composed of elongated excitatory and inhibitory subregions, arranged in an antagonistic arrangement (Figure 1.4). Classical receptive fields have often been characterised as Gabor functions, in that their response profiles resemble a sinusoidal waveform that is spatially windowed by a Gaussian (Hubel & Wiesel, 1959, 1962). Receptive fields in cosine and sine phase are sometimes referred to as 'even' and 'odd' receptive fields, respectively, although any phase is possible. Pairs of simple cells in quadrature phase (i.e., with responses 90° out of phase with each other) have been proposed to extract the cosine and sine components of stimulus features in order to extract edges or textural details (Liu et al., 1992; Pollen & Ronner, 1981, 1983).

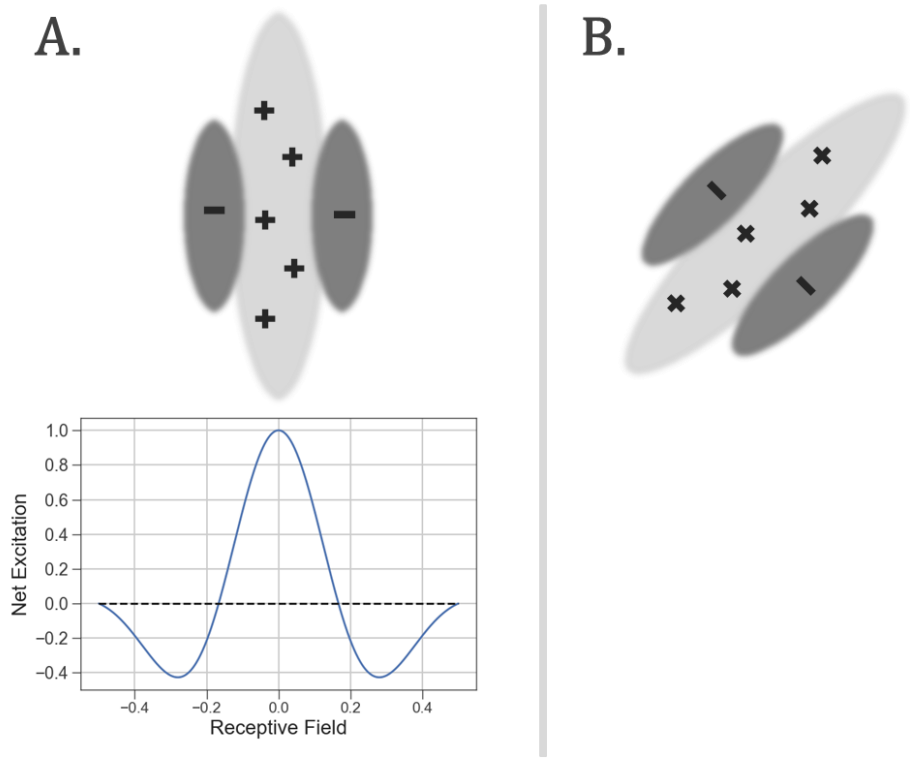

Figure 1.4. Antagonistic receptive field arrangement of orientation-selective neurons in early visual cortex. Receptive fields of neurons which responds preferentially to 90° (A) and 135° (B).

Orientation selectivity

The majority of V1 neurons in cats and macaques are selective for simple stimulus features, such as orientation (Hubel & Wiesel, 1959, 1962) and spatial frequency (De Valois, Albrecht, et al., 1982; H.-H. Yu & Rosa, 2014). Selectivity refers to the differential response of a neuron to variations along a specific feature dimension, that is maximal for a 'preferred' value in feature space. For example, a given orientation-selective neuron will respond maximally to its preferred orientation, with decreasing responsivity towards the orthogonal orientation. For a given cortical locus in V1, orientation preferences are shared through the cortical layers, forming orientation columns (Hubel & Wiesel, 1974). Orientation columns themselves are arranged in a 'pinwheel' arrangement, such that orientation preferences are distributed radially around a pinwheel centre, changing in a continuous fashion that covers the 180° range of orientation space (Ohki et al., 2006; Ts'o et al., 1990). This cortical architecture is found in a variety of mammals, including ferrets, cats, and non-human primates (Freeman et al., 2011; Ohki et al., 2006; Ts'o et al., 1990).

There are various methods to quantify the level of orientation selectivity from the responses of a singular neuron or a population of neurons. The 'orientation-selectivity index' (OSI) is commonly defined as the difference in response to the preferred and orthogonal orientations, divided by the sum of these responses. Requiring recordings for just two stimulus orientations means that the OSI is a relatively quick method to implement, but that it is particularly unreliable for neurons with low orientation selectivity or high levels of response variability (Mazurek et al., 2014).

Circular Variance (CV) is an alternative measure of orientation selectivity that treats responses to different orientations as vectors in a polar coordinate system. The CV value is given by one minus the amplitude of the average vector (normalised between 0 and 1), and

thus indexes the uniformity of responses across all tested orientations. The CV method is able to capture more subtle variations in orientation tuning than the OSI, although CV values can be greatly inflated by high levels of response variability (Mazurek et al., 2014).

Crucially, neither OSI nor CV methods can identify neuronal response parameters to describe such variations in orientation selectivity. To achieve this, orientation-tuning curves can be approximated by measuring the firing rates of a given neuron as a function of stimulus orientation (for review, see Swindale, 1998). These data can often be well-fit by a Gaussian function, where the mean (peak) corresponds to the preferred orientation of the neuron, and the standard deviation reflects its tuning bandwidth. Orientation bandwidth can be quantified as the orientation difference, either side of the peak, producing half of the maximum firing rate, i.e., 'full-width half-max' (FWHM). Strict control over other stimulus properties that modulate neural responses (e.g., contrast, spatial frequency, size) is required to accurately quantify orientation tuning (Swindale, 1998).

There are instances where neuronal responses are not well-described by a Gaussian function, such as neurons with asymmetric orientation-tuning curves (Heggelund & Albus, 1978; Swindale, 1998), or neurons with multiple peaks in their response profile (Mazurek et al., 2014; Ringach et al., 1997). Such complexities in neural responses can be captured by statistical methods such as hierarchical Bayesian modelling (Cronin et al., 2010), however the vast majority of orientation-selective neurons have a singular peak and symmetric tuning curves (Hubel, 1982; Ringach, 2002). Therefore, Gaussian approximations of orientation-tuning curves are still useful for the estimation of typical neuronal response parameters (e.g., Albrecht & Hamilton, 1982; Geisler & Albrecht, 1997), and consequently for computational simulations of visual function (e.g., May & Solomon, 2015a; Rokem & Silver, 2009).

Estimates of the average orientation bandwidth (full-width half max) in macaque V1

neurons typically range from 40 to 60° (Y. Chen et al., 2020; De Valois, William Yund, et al., 1982; J. B. Levitt et al., 1994; Nauhaus et al., 2008; G. F. Poggio et al., 1977; Ringach et al., 2002; Schiller et al., 1976b; Xing et al., 2004), although in individual neurons these measurements can vary from extremes of non-selectivity, to narrow orientation bandwidths under 20° (De Valois, Albrecht, et al., 1982; Schiller et al., 1976b). The average orientation bandwidth in macaque V1 is invariant with eccentricity from the fovea, at least up to 50° eccentricity (Battaglini et al., 1993; H.-H. Yu & Rosa, 2014). Typically, neurons in superficial layers are more selective (i.e., narrower tuning) for orientation than those in deeper layers (Ringach et al., 2002; Schummers, 2007). Additionally, neurons closer to pinwheel centres are typically less selective than those further out (Koch et al., 2016; Mariño et al., 2005; Nauhaus et al., 2008; Schummers et al., 2002, 2005). For a discussion of the origins of orientation selectivity, see Section 1.2.

Spatial frequency selectivity

Early neurophysiological studies did not uncover spatial frequency selectivity in the response profiles of V1 neurons, as they used bar stimuli which have broad spatial frequency spectra (Hubel & Wiesel, 1959, 1962). Periodic stimuli such as gratings, with defined spatial frequencies, revealed that the majority of V1 neurons are selective for spatial frequency, in cats (De Valois, Albrecht, et al., 1982; Issa et al., 2000) and macaques (Y. Chen et al., 2020).

Neurons with similar spatial frequency preferences are clustered together in domains which run tangentially to the cortical surface. Although the average preferred spatial frequency varies across domains, the periodicity of spatial frequency preferences is markedly less consistent than found in the pinwheel maps of orientation columns (Issa et al., 2000). Furthermore, spatial frequency preferences within a given domain can range up to two octaves from the average preferred spatial frequency. Thus, nearly all combinations of

orientation and spatial frequency preferences can be represented in V1 (Hübener et al., 1997; Issa et al., 2000).

Whereas neural convergence in the retina and LGN results in the sharp attenuation of high spatial frequencies (akin to low-pass filtering), most cortical cells demonstrate attenuation at both low and high spatial frequencies (i.e., are spatially band-pass) (De Valois, Albrecht, et al., 1982). It is customary to specify spatial frequency bandwidths on a logarithmic scale, in terms of octaves, where it refers to a 2:1 ratio. The human visual system is sensitive to a range of more than 8 octaves (Y. Chen et al., 2020; De Valois, Albrecht, et al., 1982), with an upper visual acuity limit of roughly 50c/° (R. S. Anderson et al., 1996). The average spatial frequency bandwidth of macaque V1 neurons is approximately 2 octaves for neurons with preferred spatial frequencies of 2c/°, and this decreases with increasing spatial frequency (De Valois, Albrecht, et al., 1982). There are also far fewer neurons which are selective for high spatial frequencies than for low spatial frequencies in cat V1 (De Valois, Albrecht, et al., 1982; Issa et al., 2000) and V2 (J. B. Levitt et al., 1994), although the precision of these estimates is often limited by restricted sample sizes in single-cell studies. One study reported that roughly 20% of simple cells had preferred spatial frequencies near 2c/°, under 5% had preferred spatial frequencies near 8c/°, and substantially fewer were selective for even higher spatial frequencies (De Valois, Albrecht, et al., 1982).

Orientation bandwidths are narrower for V1 neurons which prefer higher spatial frequencies, relative to those selective for low spatial frequencies (Y. Chen et al., 2020; B. Li et al., 2003; G. Shen et al., 2014; Webster & De Valois, 1985). For example, neurons in macaque V1 with a preferred spatial frequency of approximately 2c/° were reported to have orientation bandwidths of 50°, whereas neurons preferring higher spatial frequencies, at or above 8c/°, had orientation bandwidths under 30,° (Y. Chen et al., 2020; De Valois, Albrecht,

et al., 1982; P. Hammond & Pomfrett, 1990; J. P. Jones et al., 1987; Lampl et al., 2001; Webster & De Valois, 1985; Xing et al., 2004).

Eccentricity

With increasing eccentricity, fewer V1 neurons in cats and macaques prefer high spatial frequencies (De Valois, Albrecht, et al., 1982; H.-H. Yu & Rosa, 2014), consistent with neural convergence in the retinocortical pathways (see Section 1.1.2) and the associated increase in V1 receptive field size (Hubel, 1982). The distribution of orientation preferences across the visual field is suggested to vary with eccentricity, such that there may be an overrepresentation of neurons which prefer orientations aligned with the meridional axes, i.e.,

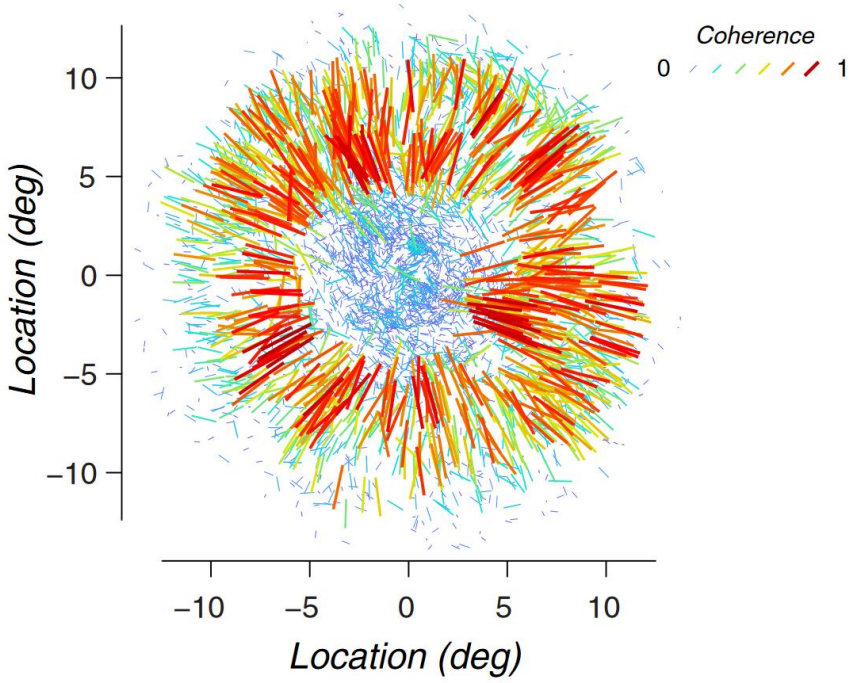

Figure 1.5. Line-vector plot showing radial bias in the orientation preferences of voxels across the visual field, in human V1. Each line corresponds to a voxel. The centre of each line is the voxel's retinotopic position (angular position and eccentricity). The angle of each line indicates the voxel's orientation preference. Line colour and size indicate 'coherence' (i.e., the strength of bias) from an orientation-mapping experiment.
Reproduced from Freeman et al. (2013).

a 'radial bias'. This is evidenced by a coarse-scale radial bias in the global responses of V1 subregions (see Figure 1.5), uncovered in humans and macaques with fMRI (Roth et al., 2018; Sasaki et al., 2006; Sun et al., 2013), and in macaques using optical imaging techniques (Fang et al., 2022; J. Freeman et al., 2011). One study using single-cell recordings reported the absence of a radial bias in macaque V1, however these measurements were taken from neurons at eccentricities under 5° (G. Shen et al., 2014). The radial bias is reflected in improved psychophysical performance for radial orientations relative to tangential orientations (Davey & Zanker, 1998), at eccentricities of approximately 15°, on contrast-detection (Sasaki et al., 2006) and orientation-discrimination tasks (Westheimer, 2003b).

Simple cells and complex cells

Early neurophysiological investigations proposed two distinct categories of V1 neurons, namely simple cells and complex cells (Hubel & Wiesel, 1959, 1962). Simple cells are considered to have receptive fields with distinct excitatory and inhibitory regions that summate and are antagonistic. Thus, the responses of simple cells are modulated by the spatial phase (or position) of a pattern within its receptive field. For example, a simple cell that is stimulated by its optimal pattern (e.g., preferred orientation, spatial frequency) will receive maximal excitation when that pattern is in its preferred spatial phase, and will receive maximal inhibition for the opposite phase**.** Complex cells have non-discrete, excitatory and inhibitory subregions, such that they respond to an optimal pattern regardless of its position within the receptive field. Thus, complex cells are phase-insensitive (for review, see De Valois & De Valois, 1990).

In primates, cells in input layer 4 tend to be simple cells and those in more superficial layers tend to be complex cells (Hubel et al., 1977; Hubel & Wiesel, 1962; Martinez & Alonso, 2003). Classical feedforward models hence propose a simple hierarchy, where LGN

afferents converge to form phase-sensitive, orientation-selective simple cells in V1, whose intracortical projections converge to form phase-insensitive complex cells, which in turn project out of V1 (Pollen & Ronner, 1983). There is debate as to whether simple and complex cells are truly distinct cell types (De Valois, Albrecht, et al., 1982; Skottun et al., 1991). For instance, measurements of membrane potentials rather than firing rates, which rely on a threshold non-linearity, reveal a continuous distribution of phase-sensitivity across cells in V1 (Priebe et al., 2004). Other challenges to the feedforward model, in the context of orientation selectivity, will be discussed in Section 1.2.

1.1.5 Extrastriate visual areas

Regions of visual cortex beyond V1 (i.e., extrastriate visual areas) have been demarcated based on their laminar structure, patterns of connectivity, and functional specialisations (Angelucci & Bressloff, 2006; Kritzer et al., 1992; Vanni et al., 2020). Originally, visual information was considered to progress serially, from V1, through a hierarchy of increasingly specific feature detectors (Neisser, 1967). Simple local features which are encoded in V1, such as orientation, were proposed to progress serially through V2, V3, and V4 to generate selectivities for more complex visual features, such as curvature (Hu et al., 2020; Y. Lu et al., 2018) or shape (Nandy et al., 2013). This is consistent with increasing receptive field sizes across sequential stages of the visual pathways (Dumoulin & Wandell, 2008; A. T. Smith, 2001). Additionally, although the ordered pinwheel arrangement of orientation columns is maintained in V2 (Vanni et al., 2020), this is mostly absent in area V4, where there is an abundance of cells with complex selectivities across multiple feature dimensions (Nandy et al., 2013).

It has been suggested that different regions of visual cortex are specialised for

different visual functions, exemplified by demonstrations of functional dissociations between the dorsal stream and ventral stream across visual cortex, i.e., the 'perception-action model' (Goodale & Milner, 1992; Milner & Goodale, 2008). In this view, visual information is thought to flow from early visual areas (V1, V2, V3) along independent visual pathways, either to ventral regions (e.g., V4) associated with form and image understanding, or to dorsal regions (e.g., MT) associated with motion and visually guided action. However, the two streams are not entirely independent of each other (Schenk & McIntosh, 2010), with cortical connections between V4 and MT being reported in macaques (Ungerleider et al., 2008; Ungerleider & Desimone, 1986).

The distributed nature of feedforward and feedback connections in extrastriate visual areas (e.g., Amir et al., 1993; Budd, 1998; Ungerleider et al., 2008) demonstrates the combinations of serial and parallel arrangements in visual cortex. For example, macaque MT receives direct input independently from V1, V2 (El-Shamayleh et al., 2013; Vanni et al., 2020), and V4 (Ungerleider et al., 2008). A combination of feedforward, lateral, and feedback connections is thought to contribute to various receptive field properties in extrastriate visual areas (Angelucci et al., 2017; Angelucci & Bressloff, 2006), including extra-receptive field contextual modulations (Zipser et al., 1996) that may also subserve putative attentional (Carrasco, 2014) and predictive coding mechanisms (Petro et al., 2014). However, the function of the extensive connections between visual areas remains largely unknown (Hubel & Wiesel, 1962; Ringach et al., 2002).

1.2 Orientation encoding

1.2.1 Orientation selectivity

The receptive field of an orientation-selective neuron in V1 is characterised by the arrangement of flanking, excitatory and inhibitory subregions, which are elongated along an axis of orientation that corresponds to the preferred orientation of that neuron. Such a neuron will respond maximally to a stimulus presented at its preferred orientation, and will respond less as the stimulus progressively deviates from the preferred orientation (see Section 1.1.4). More complex selectivities develop in extrastriate visual areas, such as selectivity for curvature and shape in V4 (Hu et al., 2020; Nandy et al., 2013), or global motion in MT (Rokem & Silver, 2009; Vanni et al., 2020). However, to understand such complex transformations in receptive field properties, the mechanisms underlying the emergence of simpler selectivities in V1 should first be understood. For instance, the vast majority of V1 neurons exhibit strong orientation selectivity (Hubel, 1982), despite a general invariance of retinal ganglion cell and LGN-relay cell responses to orientation, as observed in primates (Xu et al., 2002). Accounts of the emergence of orientation selectivity in V1 have been informed by the relatively simple and tractable circuitries of retinal-cortical pathways and intracortical V1 connections (Callaway, 1998; Grünert & Martin, 2020; Katz & Shatz, 1996). However, there is long-standing debate surrounding the contributions of intracortical connections and feedback from extrastriate visual areas in generating orientation selectivity in V1, which warrants further consideration (for review, see Priebe, 2016).

1.2.2 Feedforward

The classical 'feedforward model' for the emergence of orientation selectivity in V1 (Hubel & Wiesel, 1962) proposes that the specific linear combination of excitatory inputs,

690 from LGN relay cells with spatially offset receptive fields, determines the properties of
691 orientation-selectivity. In this model, the circularly symmetric, centre-surround receptive
692 fields of LGN afferents are aligned along an axis of orientation that determines the preferred
693 orientation of a given neuron. Orientation selectivity is then considered to result from the
694 relative extent of excitation and inhibition across space.

695 The feedforward model makes testable predictions about the response properties of
696 V1 orientation-selective neurons (for review, see Priebe et al., 2016). One prediction is the
697 correspondence of spatial polarity in the receptive fields (i.e., the size of excitatory and
698 inhibitory regions) of V1 neurons and the LGN cells from which they receive input. Indeed,
699 simultaneous recordings of connected pairs of LGN relay cells and V1 neurons, in the cat,
700 revealed correspondence between ON and OFF subregions in the receptive fields of LGN-V1
701 cell pairs (Reid & Alonso, 1995; Tanaka, 1983, 1985). Additionally, the degree of overlap for
702 each LGN-V1 cell pair was correlated with the strength of synaptic connection (Reid &
703 Alonso, 1995).

704 A second prediction is that the axis of alignment of LGN receptive fields (i.e., the
705 angle at which they are spatially offset from each other) determines the preferred orientation
706 of the connected V1 neuron. In support of this, Chapman et al. (1991) analysed the spatial
707 offset of LGN neurons that were connected to a single orientation column, in cats, before and
708 after the application of a GABA agonist to inactivate the visual cortex. They reported that the
709 aggregate receptive field of LGN afferents was orientated along the same axis as the
710 preferred orientation of the connected V1 orientation column (R. W. Chapman et al., 1991).

711 Cortical inactivation abolishes neural spiking in visual cortex, along with silencing
712 any additional cortical circuitry that could modulate orientation selectivity. Therefore, during
713 cortical inactivation, orientation-tuning curves which are estimated from subthreshold

changes in membrane potential should be driven solely by LGN afferents. Using intracellular recordings to measure the membrane potential of V1 neurons in the cat, orientation selectivity was demonstrated to be generally unaffected by cortical inactivation (Chung & Ferster, 1998; Ferster et al., 1996), indicating that the feedforward model is sufficient to explain the emergence of orientation selectivity in visual cortex. However, there are certain response properties of orientation-selective neurons in V1 that suggest a role for intracortical mechanisms in shaping orientation selectivity.

1.2.3 Challenges to the feedforward model

Narrowed orientation tuning

If orientation selectivity is derived solely from the spatial combination of LGN relay cell afferents, then the orientation bandwidth of a given V1 neuron should be accurately estimated from a detailed map of its receptive field by a simple linear model. For example, neurons with wider and shorter subregions should produce broadened orientation tuning, because a bar stimulus could be rotated far from the preferred orientation and still overlap with a large portion of the excitatory subregion. However, linear predictions of V1 orientation bandwidths from receptive field maps (i.e., LGN inputs), in cats, are up to three times larger than the orientation bandwidth of an individual cell measured using firing rates (Gardner et al., 1999; J. P. Jones & Palmer, 1987). Mechanisms of cortical inhibition may thus be required to account for the size of this effect (Ben-Yishai et al., 1995; Hirsch et al., 2003; Somers et al., 1995; Sompolinsky et al., 1990; Sompolinsky & Shapley, 1997; Troyer et al., 2002), however the feedforward model can partially account for this effect.

The membrane potential of a V1 neuron rests far below its spiking threshold, with very little spontaneous activity (DeWeese et al., 2005; Tan et al., 2014). Orientations further

737 from the preferred orientation will induce smaller changes in membrane potential, which are
738 less likely to reach threshold. Therefore, orientation bandwidths estimated from firing rates
739 (i.e., above threshold) are narrowed relative to those estimated from changes in membrane
740 potential (Carandini & Ferster, 2000). In support, orientation bandwidths measured from
741 membrane-potential responses in cat V1 neurons match those predicted from receptive field
742 maps (Lampl et al., 2001). However, an unfeasibly high spiking threshold would be required
743 to account for the narrow orientation bandwidths of V1 neurons, supporting the need for an
744 alternative explanation.

745 ## Contrast-invariant orientation tuning

746 The activity of LGN-relay cells (which are typically not selective for orientation)
747 increases with stimulus contrast, thereby increasing the excitation of target V1 cells
748 regardless of their preferred orientation. Classical feedforward models thus predict that
749 increasing stimulus contrast should broaden the orientation bandwidths of visual cortical
750 neurons (Figure 1.6). However, the orientation bandwidth of V1 neurons as measured with
751 firing rates is invariant to changes in stimulus contrast (Alitto & Usrey 2004; Sclar &
752 Freeman 1982, Skottun et al. 1987). Thus, classical feedforward models fail to capture the
753 principal of contrast invariance.

754 An alternative feedforward account for contrast-invariant orientation selectivity relies
755 on evidence from intracellular recordings in cat V1 neurons. Trial-to-trial variability in
756 membrane potentials may be contrast dependent, such that an increase in stimulus contrast
757 corresponds with a decrease in membrane-potential variability (Finn et al., 2007; Sadagopan
758 & Ferster, 2012). At high contrasts, a reduction in membrane-potential variability would

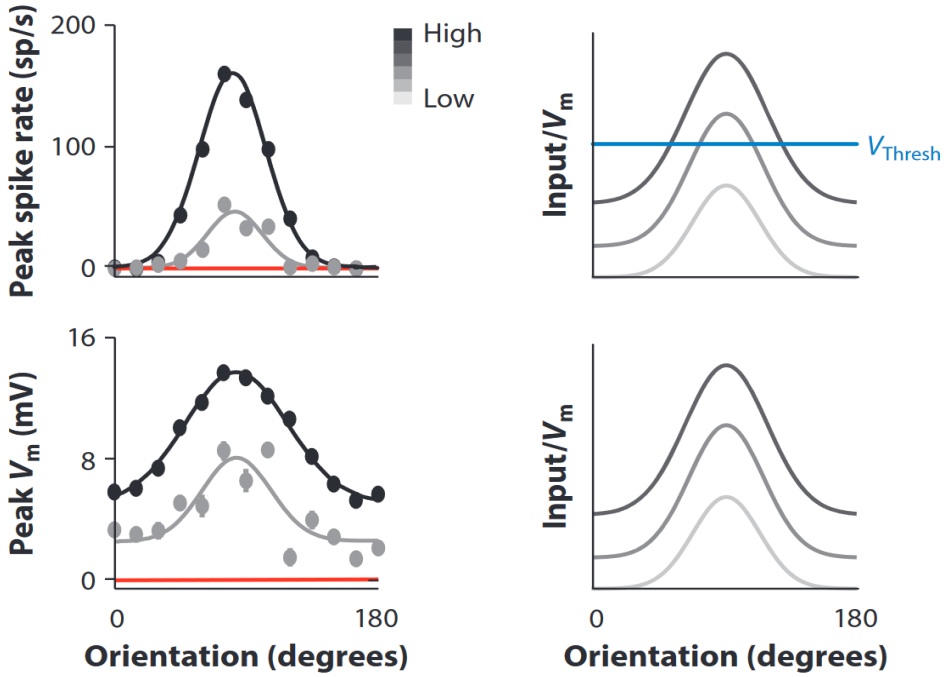

Figure 1.6. Contrast-invariant orientation tuning is observed in the firing rates (top-left) but not the membrane potential (bottom-left) of visual-cortical neurons, which may be partially mediated by the spiking threshold (top-right). Adapted from Priebe et al. (2016).

759 decrease the likelihood of non-preferred orientations reaching the spiking threshold, thus
760 generating contrast invariance. However, contrast-dependent response variability is not an
761 exclusive feature of feedforward models, and could also arise from subcortical (Sadagopan &
762 Ferster, 2012) or cortical sources (Monier et al., 2003), hence this issue has yet to be
763 resolved. Furthermore, inhibitory connections between orientation-selective neurons have
764 also been proposed to contribute to contrast-invariant orientation selectivity, by raising the
765 spiking threshold of visual cortical neurons (for review, see Priebe, 2016).

Cross-orientation suppression

Compelling evidence against the classical feedforward model comes from interactions between stimuli of different orientations. Cross-orientation suppression can be demonstrated behaviourally in humans, where the detectability of an orientated grating is lowered by superimposing a masking grating of orthogonal orientation (Meese & Holmes, 2010). Consistent with this, firing rates of cat V1 neurons in response to non-preferred orientations are suppressed by the presence of a superimposed, orthogonal grating stimulus (Bishop et al., 1973; Freeman et al., 2002).

One explanation is that the superimposition of gratings causes reductions in the average local contrast, which will inevitably suppress V1 responses for the preferred orientation. Indeed, cat V1 responses to a grating stimulus are also suppressed by the simultaneous presentation of dynamic white noise with the target stimulus (Carandini et al., 2002), suggesting that this phenomenon is not necessarily related to the orientation of the masking stimulus. However, cross-orientation suppression has also been demonstrated in the firing rates of cat V1 neurons when there is a temporal gap between bar stimuli at the preferred and orthogonal orientations, with the strength of suppression increasing as the duration of the temporal gap increased from 50 to 200ms (Nelson, 1991a).

Unlike in V1 neurons, cross-orientation suppression in LGN neurons does not remain over such long temporal gaps (Nelson, 1991b), indicating a cortical basis for this phenomenon. In support of a cortical mechanism, cross-orientation suppression in visually evoked potentials (VEPs) is reduced by cortical disinhibition, induced by the application of GABA antagonists in cat visual cortex (Morrone et al., 1982). Consistent with this notion, cross-orientation suppression in cat visual cortex is increased by the induction of cortical inhibition through the application of GABA agonists (Morrone et al., 1987).

However, there are characteristics of cross-orientation suppression which do not reflect a cortical locus. First, although V1 neurons are largely binocular, extracellular recordings in the cat revealed that cross-orientation suppression is predominantly driven by monocular inputs (Ferster, 1981; Walker et al., 1998). Second, strong suppression of cat V1 neurons is reported for masks at high temporal frequencies (> 8 Hz) (Freeman et al., 2002), above the typical sensitivity range of V1 neurons in cats (Saul & Humphrey, 1992). Lastly, the activation of inhibitory circuits should be observable in the time course of neural responses (i.e., the onset of suppression should be delayed), yet cross-orientation suppression coincides with the temporal onset of cortical responses (M. A. Smith et al., 2006). All of these properties of cross-orientation suppression are more typical of LGN relay cells, than of cortical neurons (Carandini et al., 2002; B. Li et al., 2006; Priebe & Ferster, 2008).

1.2.4 Cortical inhibition

Cortical inhibition models propose an important role for intracortical connections and V1 inhibitory circuits in generating orientation selectivity (Adorján et al., 1999; Ben-Yishai et al., 1995, 1997; Hansel & Sompolinsky, 1996; Somers et al., 1995). For example, the application of GABA antagonists to cat V1 induces the disinhibition of visual cortical circuits, resulting in a broadening of orientation tuning bandwidths (Sillito, 1975). This is proposed to be caused by the inactivation of inhibitory interneurons with preferred orientations different to that of their target cell (Eysel et al., 1990).

There are various models of how cortical inhibition modulates orientation selectivity, each of which operates based on the relative strength and selectivities of inhibitory inputs. For example, some models suggest that inhibitory input may be more broadly tuned for orientation than excitatory input (Ben-Yishai et al., 1995; Somers et al., 1995). This predicts

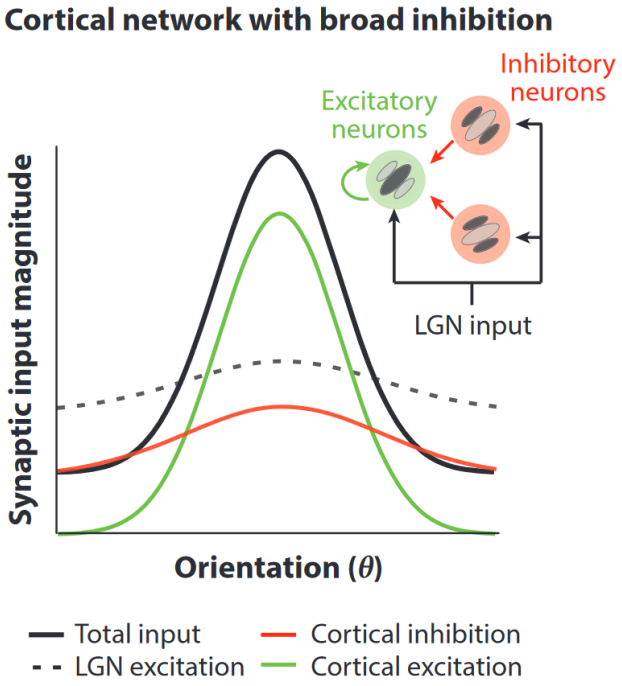

Figure 1.7. Orientation selectivity could arise from a combination of excitatory feedforward connections, and a mixture of excitatory and inhibitory, orientation-selective intracortical connections. Adapted from Priebe et al. (2016).

that V1 neurons receiving strong inhibitory inputs should have sharpened orientation tuning (Somers et al., 1995; Sompolinsky & Shapley, 1997), due to an effective increase in the spiking threshold (Figure 1.7). Alternatively, normalisation models implement inhibition that is proportional to the stimulus contrast at all orientations (Carandini et al., 1997; DeAngelis et al., 1992; Heeger, 1992).

A role for cortical inhibition in generating orientation selectivity is consistent with associations between the functional architecture and orientation selectivity of V1 neurons. For instance, V1 neurons in iso-orientation domains (i.e., surrounded by neurons with similar preferred orientations) have narrowed orientation relative to neurons in pinwheel centres, which are surrounded by neurons with heterogeneous orientation preferences (Koch et al., 2016; Mariño et al., 2005; Schummers, 2007; Schummers et al., 2002). Additionally, greater

cross-orientation suppression is reported for neurons in iso-orientation domains than for those in heterogeneous orientation domains (Koch et al., 2016). Along with the absence of 'pinwheel' orientation maps in preceding, subcortical visual areas (Mazade & Alonso, 2017), which are not selective for orientation, these findings indicate that there are aspects of orientation selectivity that emerge due to intracortical influences.

In general, orientation selectivity can emerge in more diverse ways than considered by many individual models. For example, excitation and inhibition share the same orientation preference for some neurons but have distinct orientation selectivities for others (Frégnac & Bathellier, 2015; Monier et al., 2003; Volgushev et al., 1993). Diversity in cortical mechanisms could result from variability in the distribution of preferred orientations across the cortical surface (Stimberg et al., 2009) or from variations in circuit elements across the cortical layers (Martinez et al., 2005). For example, neurons in superficial regions of V1 are more narrowly tuned than those in deeper layers (Ringach et al., 2002; Schummers, 2007). Although orientation selectivity is a fundamental property of most V1 cells, its neural origins are complex and are unlikely to be captured by a singular mechanism.

1.2.5 Models of orientation encoding

Orientation mechanisms

Although orientation-selectivity in V1 neurons provides a basis for orientation encoding in the visual system (Hubel & Wiesel, 1962), it is important to understand the mechanisms and computations underlying how this information is utilised in visual perception. Early psychophysical research inspired the first models of orientation encoding with investigations into the tuning properties of orientation mechanisms (i.e., 'orientation channels') in human vision (Braddick et al., 1978; Campbell & Kulikowski, 1966; Thomas &

847 Gille, 1979). In visual masking experiments, subjects detect a target orientation in the
848 presence of a superimposed mask stimulus, and the orientation difference between the two
849 stimuli is varied systematically (Figure 1.8). Masking effectively reduces the signal-to-noise
850 ratio (SNR) for the target orientation (Meese & Holmes, 2010). Therefore, mask orientations
851 closer to the target orientation cause the strongest impairment in detection performance, and
852 this masking effect gradually lessens as the orientation difference between the two stimuli
853 increases. Psychophysical estimates of orientation bandwidth (full-width half-max) in
854 humans can vary greatly between studies (for review, see Graham, 1979), ranging from
855 approximately 60° (Blake & Holopigian, 1985; Phillips & Wilson, 1984) to 40° (Meese &

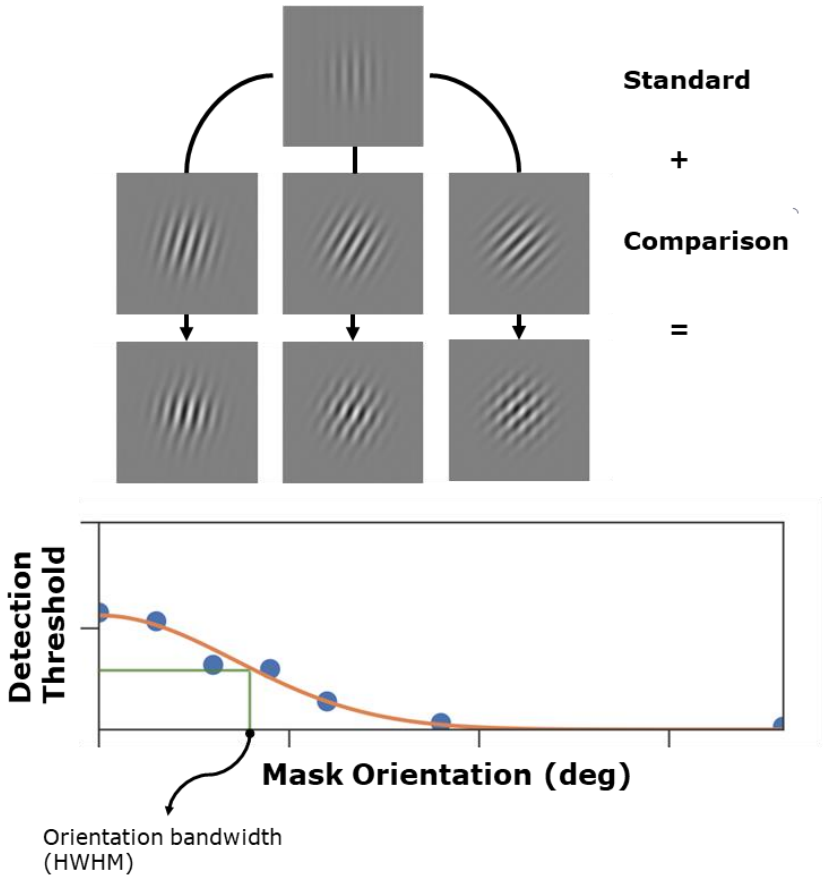

Figure 1.8. The orientation bandwidth (half-width half-max, HWHM) of a given orientation channel (at the standard orientation) can be estimated from detection thresholds in the presence of differently orientated masks.

Holmes, 2010) to 30° (Campbell & Kulikowski, 1966; Thomas & Gille, 1979). Although psychophysical estimates are broadly consistent with single-cell estimates of orientation bandwidths in V1 neurons of macaques (see Section 1.1.4), the level of variation between studies indicates the need for further investigation with rigorous experimental controls.

The vast majority of these studies used only one orientated mask, meaning that the detection of the target orientation may have been determined by the responses of neighbouring orientation mechanisms, i.e., 'off-channel looking'. This phenomenon was first identified in auditory masking where it is termed 'off-channel listening' (R. D. Patterson & Nimmo-Smith, 1980). In terms of contrast detection, this occurs when the observer does not use the orientation channel centred on the target stimulus for detection, because its signal-to-noise ratio is reduced by the mask, but instead uses a channel less sensitive to the target that is unaffected by the mask. This can distort estimates of channel bandwidth suggesting it is more narrowly tuned than it really is. One solution to this problem, from psychophysical measures of spatial frequency bandwidths (Hutchinson & Ledgeway, 2004), is to present two masks simultaneously, such that they bracket (are equidistant from) the target orientation. Model simulations of empirical visual masking data validate the use of such dual masks to prevent 'off-channel looking' when estimating channel bandwidths (Serrano-Pedraza et al., 2013).

Similar measures of orientation channels can be obtained using adaptation (Blakemore & Nachmias, 1971; Movshon & Blakemore, 1973) or subthreshold summation paradigms (Kulikowski et al., 1973). However, psychophysical estimates of orientation bandwidth are roughly 15° in adaptation experiments and just 6° in subthreshold summation paradigms (Graham, 1989). The reason for the difference between bandwidth estimates derived from masking and adaptation is unclear, but it is worth noting that the mechanisms

underlying visual adaptation are still not well-understood. Narrowed tuning bandwidths for subthreshold summation paradigms could be generated by cross-orientation suppression (Bishop et al., 1973; Meese & Holmes, 2010), such that the responses to orientated subthreshold stimuli would be suppressed to a greater extent than the stimulus at the target orientation.

The outputs of orientation channels are a combined function of stimulus contrast and orientation. Although early models of contrast detection could explain the detection of a stimulus from the activity of orientation channels, these could not explain how the visual system distinguishes between orientations (Watson & Robson, 1981). For the responses of orientation channels to be meaningful, the visual system must have some knowledge of their tuning characteristics. Reports of a lower contrast threshold for detection than for the identification of stimulus orientation (Watson & Robson, 1981) led to suggestions that each orientation channel is known to the visual system by its preferred orientation. 'Labelled line' models propose that an orientation can only be identified once the associated orientation channel has reached some perceptual threshold, and that the perceived orientation is determined by the strongest responding orientation channel. These models were proposed to account for the tilt-aftereffect (i.e., the temporary misperception of the orientation of a target stimulus following prolonged viewing of a differently orientated adaptation stimulus), because the strongest responding channels would be those that are selective for orientations rotated away from the adapted orientation. Labelled line models were also proposed to explain the shift in perceived spatial frequency arising from adaptation in the spatial frequency domain (Blakemore et al., 1970).

However, the maximally responding orientation channel does not necessarily correspond to the perceived orientation. One study reported that after visual adaptation,

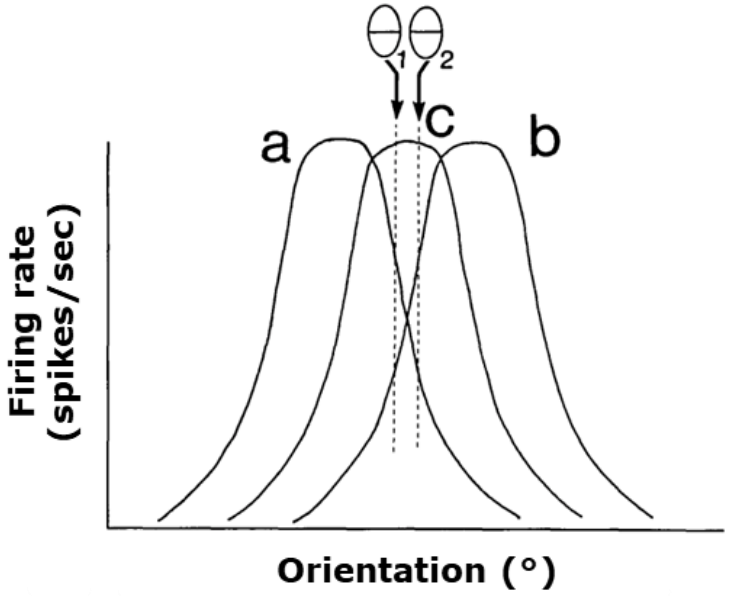

Figure 1.9. Changes in stimulus orientation (from θ_1 to θ_2) results in larger signal changes for neurons with tuning curve slopes that are steepest about the stimulus orientation (*a* and *b*), than for neurons with orientation preferences centred on the stimulus orientation (*c*). Adapted from Regan & Beverley (1985).

orientation-discrimination thresholds were higher when the adapting orientation was rotated about 15° from the test stimulus, than when presented at the same orientation as the test stimulus (Regan & Beverley, 1985). These findings suggest that the precision of orientation encoding may be determined by the slopes of orientation-tuning curves, which are higher for more narrowly tuned channels. In other words, for a given change in stimulus orientation, the change in the responses of orientation channels will be maximal around the steepest part of the curve (Figure 1.9).

Inspired by Hering's theory of colour vision, in which difference signals between the three colour channels provide the basis of colour perception, Westheimer et al. (1976) proposed that interactions between ensembles of orientation channels may be required to explain how such broadly tuned orientation channels could produce such precise judgements of stimulus orientation (Westheimer et al., 1976).

Population codes

The clustering of orientation columns into pinwheel arrangements in early visual cortex (Freeman et al., 2011; Ohki et al., 2006; Ts'o et al., 1990) provides a structural basis for the encoding of visual orientation in populations of orientation-selective neurons. Combined knowledge from psychophysics, neurophysiology, and computational investigations has guided the understanding of 'population coding models' in the visual pathways. Population codes have been highlighted across the brain, including superior colliculus neurons encoding saccade direction (C. Lee et al., 1988), middle temporal (MT) cells serving local velocity computations (J. H. Maunsell & van Essen, 1983), and inferotemporal (IT) neurons responding to compositions of human faces (Perrett et al., 1985).

The mechanisms by which multiple neurons can represent a single variable, and how this information is decoded (i.e., read-out) by the visual system, have traditionally been investigated through combined neurophysiological and computational modelling approaches (Abbott & Dayan, 1999; Salinas & Abbott, 1994). The classical model of population coding comes from the cercal system of the cricket which encodes the direction of air currents, sensed by hair cells on antenna-like protrusions called cerci (Miller et al., 1991; Theunissen & Miller, 1991). The cercal system consists of four interneurons, each sensitive to air speed

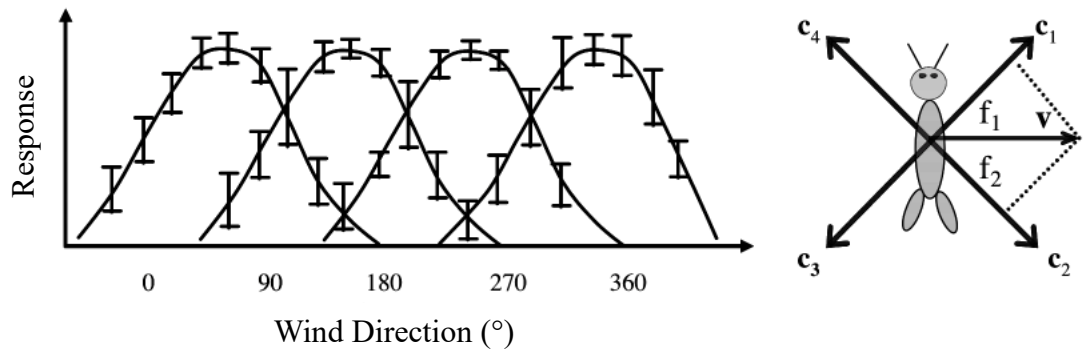

Figure 1.10. Cartesian coordinate system where the responses of four differently tuned neurons are combined to produce an estimate of wind direction. Adapted from Dayan & Abbott (2001).

but selective for different air directions (Figure 1.10). Air direction tuning curves can be approximated by rectified cosines, with the preferred air directions of each of the four neurons being equally spaced, thus forming a Cartesian coordinate system for wind velocity (Salinas & Abbott, 1994).

To estimate the stimulus value (in this case air direction) from the population response, various decoders can be implemented. The winner-take-all (WTA) estimate (sometimes called the 'max rule') is taken as the preferred air direction of the neuron with the highest firing rate, similar to labelled line models of orientation encoding (Watson & Robson, 1981). The population vector (PV) estimate is calculated from the firing rate (amplitude) and preferred air direction (direction) of each neuron in the population code (Georgopoulos et al., 1986). The maximum likelihood (ML) estimate is taken as the air-direction that was most likely to produce the observed neural response. Even for a Cartesian system, the precision of air direction estimates is remarkable for PV and ML decoders (Salinas & Abbott, 1994). The implementation of these decoders in a population code for visual orientation has been described previously (Webb et al., 2010).

Despite its relative simplicity, the cricket cercal system has revealed computational principles that could apply to the human visual system. Visual features, such as orientation, are commonly assumed to be encoded within dense populations of neurons with uniformly distributed orientation preferences and homogeneous response characteristics (Abbott & Dayan, 1999; Goris et al., 2015; Pouget et al., 2000; Rokem & Silver, 2009; Webb et al., 2010). In a noiseless system, the higher the number of elements in a population code, the greater the precision of the encoded estimate, since more neurons can provide more information about the stimulus feature. However, the responses of neurons in sensory systems are invariably noisy (for review, see Faisal et al., 2008), such that the firing rates of individual

957 neurons within a short time window will likely deviate from that predicted by a tuning
958 function, thus placing an internal limit on the precision of a population code. Variability in
959 neural responses tend to follow a Poisson-like distribution (Tolhurst et al., 1983), such that
960 the variance is proportional to the square root of the mean firing rate, as revealed by single-
961 cell recordings in cats (Villeneuve & Casanova, 2003) and macaques (Ecker et al., 2014; Gur
962 et al., 1997; Gur & Snodderly, 2006).

963 Population coding models based on time-averaged firing rates (i.e., 'rate coding') may
964 ignore important information in the temporal characteristics of spike trains (Thorpe et al.,
965 2001). For example, rate coding omits potentially meaningful information in spike-timing
966 correlations, synchronised spike discharges, and burst firing (de la Rocha et al., 2007; T. Lu et
967 al., 2001). Alternative coding schemes, such as spiking neural networks, can capture these
968 temporally varying response properties (Ponulak & Kasinski, 2011) and account for certain
969 neural functions that may be too fast to achieve a reliable rate-based code (Thorpe et al.,
970 2001). However, rate coding is suitable for modelling neural responses to static stimuli which
971 are presented for longer durations.

972 Decoding is a useful computational tool for assessing the precision of stimulus
973 encoding within a neuronal population, and provides an estimate (or at least a lower bound)
974 of the fidelity of the information contained in the population response (Borst & Theunissen,
975 1999; Rieke et al., 1999). Explicit decoding of the stimulus from each population code in
976 visual cortex may not be necessary, as evidenced by orientation pinwheels in V1 of macaques
977 which project directly to pinwheels in V2 (Vanni et al., 2020). Rather, the information
978 represented in population codes may support the encoding of simple and complex stimulus
979 features at subsequent stages of the visual pathways, which may form the mechanisms
980 underlying perception.

1.3 Psychophysical evidence of the oblique effect

1.3.1 Overview

Visual performance is impaired for oblique orientations relative to cardinal orientations (i.e., horizontal and vertical) for a variety of behavioural tasks, including visual acuity (Campbell et al., 1966; Mitchell et al., 1967), contrast detection (Campbell et al., 1966; Heeley & Timney, 1988; Westheimer & Beard, 1998), orientation discrimination (Heeley & Timney, 1988; Westheimer & Beard, 1998), and motion-direction discrimination (Dakin et al., 2005; Pilz & Papadaki, 2019). For stimuli at suprathreshold contrasts, the oblique effect is only found for tasks that require the explicit encoding of stimulus orientation. For example, no oblique effect is observed for contrast discrimination (or 'intensity discrimination') of single lines (Westheimer & Beard, 1998), spatial-frequency discrimination (Caelli et al., 1983; Heeley & Timney, 1989), line-length estimation (Lyakhovetskii et al., 2023), shape discrimination (Westheimer, 2003a), nor motion-speed discrimination (Matthews & Qian, 1999). The oblique effect has been characterised behaviourally not only in humans but also in a variety of other animal species, such as non-human primates, cats, ferrets, and even goldfish (Appelle, 1972).

The 'carpentered environment' hypothesis for the oblique effect posits that biases in orientation perception reflect a functional adaptation to the orientation statistics of natural images, in which there is a higher proportion of cardinal orientations than oblique orientations (Coppola, Purves, et al., 1998; Girshick et al., 2011; Keil & Cristóbal, 2000). This aligns with principles of efficient coding, such that coding resources may be preferentially allocated to stimulus features that are highly probable during natural vision (H. Barlow, 1961; Girshick et al., 2011). Alternatively, biases in orientation perception could also

arise through statistical inference, in which noisy representations of encoded orientations are fused with a probabilistic model of the environment. In either case, visual experience is assumed to refine the observer's 'internal model' to match that of the environment (Girshick et al., 2011), however the neurophysiological principles underlying such accounts are unclear. Psychophysical investigations of low-level visual function and associated cognitive factors have generated theoretical models of orientation perception and the oblique effect, forming predictions about the nature of the oblique effect that can be evaluated with neurophysiological evidence (see Sections 1.4 and 1.5). Computational models are a tool with which to explicitly test these predictions, and in turn, psychophysical data can be used to assess the validity of models of orientation perception. However, this requires a systematic approach which has rarely been utilised in previous work.

1.3.2 Visual sensitivity

The oblique effect in humans was first demonstrated for measures of visual acuity (Higgins & Stultz, 1950; Jastrow, 1892; Nachmias, 1960), where the highest detectable spatial frequency for cardinal orientations is approximately 30% higher than for obliques (Mitchell et al., 1967). Due to methodological limitations, early accounts could not rule out orientation anisotropies in the physical properties of the eye, such as asymmetric optics, sparse photoreceptor spacings along oblique meridians, and microsaccade eye movements along the cardinal axes. However, later work demonstrated that the oblique effect is still found when gratings are projected directly onto the retina using laser interference fringes which bypass any optical aberrations (Campbell et al., 1966; Mitchell et al., 1967), and that the magnitude of eye movements during viewing does not contribute substantially to the oblique effect (Higgins & Stultz, 1950; Nachmias, 1960). Additionally, anisotropies in

photoreceptor spacings along the oblique and cardinal meridians of the retina are not substantial enough to support the oblique effect, although photoreceptors are more tightly packed along the horizontal meridian than the vertical meridian (Chui et al., 2008).

For measures of contrast sensitivity, the oblique effect is absent at low spatial frequencies but increases with spatial frequency (Berkley et al., 1975; Campbell et al., 1966; Heeley & Timney, 1988; Pointer, 1996). At 10 c/°, contrast-detection thresholds are approximately 1.5 to 2 times higher for obliques relative to cardinals (Heeley & Timney, 1988). A dependency on spatial frequency is consistent with findings that the oblique effect for visual acuity diminishes with increasing retinal eccentricity (Berkley et al., 1975; Rovamo et al., 1982), commensurate with the associated loss of high spatial frequency information in the periphery (see Section 1.1.1). However, when scaling stimuli to account for cortical magnification (i.e., increased receptive field sizes in the periphery), the oblique effect for contrast sensitivity is still observed at eccentricities of 40° (Figure 1.11) with sensitivity profiles shifted to lower spatial frequencies (Pointer, 1996).

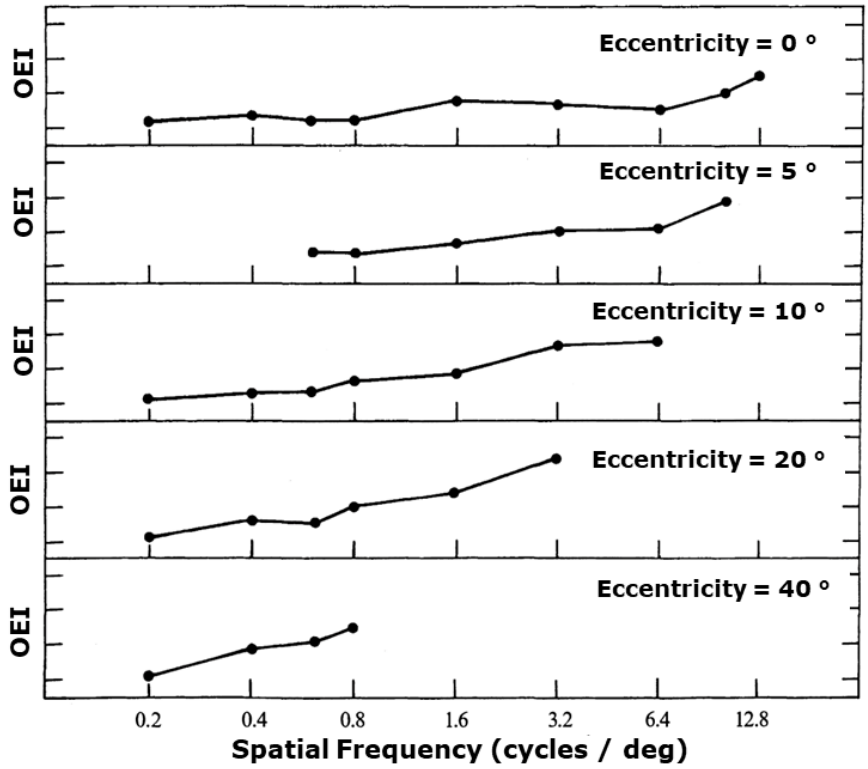

Figure 1.11. The oblique effect for contrast sensitivity increases with increasing spatial frequency, although this is shifted to a lower spatial frequency range at greater eccentricities. Adapted from Pointer (1996).

The spatial frequency-dependency of the oblique effect for contrast sensitivity suggests an anisotropy that may be restricted to populations of orientation-selective neurons that prefer higher spatial frequencies. This is supported by neurophysiological single-cell recordings in cats (B. Li et al., 2003) and macaques (G. Shen et al., 2014). However, optical imaging in macaques (Fang et al., 2022) and fMRI in humans (Sun et al., 2013) indicates that the overrepresentation of cardinal-tuned neurons also occurs at low spatial frequencies. To resolve this conflict, computational models of contrast detection (e.g., Goris et al., 2013) could be a useful tool for understanding how the oblique effect could be generated from anisotropies in populations of orientation-selective neurons.

An 'inverse oblique effect' (i.e., worse performance for cardinals) has been observed

for the detection of orientated gratings superimposed on images of natural visual scenes (Hansen & Essock, 2004; Nasr & Tootell, 2012), or on 1/f noise (Haun & Essock, 2010) which is thought to approximate the Fourier power spectra of natural scenes. One explanation is that the overrepresentation of cardinal-tuned neurons forms a larger, inhibitory normalisation pool for cardinal orientations than for the obliques, consequently dampening the responses of cardinal-tuned neurons in response to broadband stimuli (Hansen & Essock, 2006). However, these studies also report much higher detection thresholds for horizontal than vertical orientations, which indicates (according to this theory) a larger proportion of neurons that are selective for horizontal than vertical orientations. Although there is some single-cell evidence for this in V1 of cats (B. Li et al., 2003) and macaques (G. Shen et al., 2014), this is restricted to high spatial frequencies and is inconsistent across studies (see Section 1.4.2). Alternatively, the 'inverse oblique effect' may emerge if the cardinal-tuned mechanisms serving detection in noise had narrower orientation bandwidths than oblique mechanisms, such that the extent of neural recruitment would be smaller for cardinals than for obliques. However, no alternative models have been explored to explain this finding.

1.3.3 Orientation discrimination

Orientation-discrimination thresholds (i.e., the just-noticeable difference values for stimulus orientation) are typically two to four times larger for oblique orientations relative to cardinals (Heeley & Timney, 1988; G. A. Orban et al., 1984a; Vogels et al., 1984; Westheimer, 2003a; Westheimer & Beard, 1998). This oblique effect is reported to be invariant with stimulus spatial frequency (Heeley & Timney, 1988), indicating that the source of the oblique effect for orientation discrimination may be distinct from that underlying the oblique effect for contrast sensitivity. If an overrepresentation of cardinal-tuned neurons

generated the oblique effect for orientation discrimination, then one might expect an oblique effect for spatial frequency discrimination (which may rely on similar mechanisms), however this is not found (Caelli et al., 1983; Heeley & Timney, 1989).

For line stimuli of shortened lengths, < 1°, the oblique effect for orientation discrimination is reduced in magnitude relative to larger stimuli (G. Orban et al., 1984; Vandenbussche et al., 1986). This can be attributed to the broadened orientation content in the Fourier power spectra of shorter stimuli (Figure 1.12), which would generate noisier

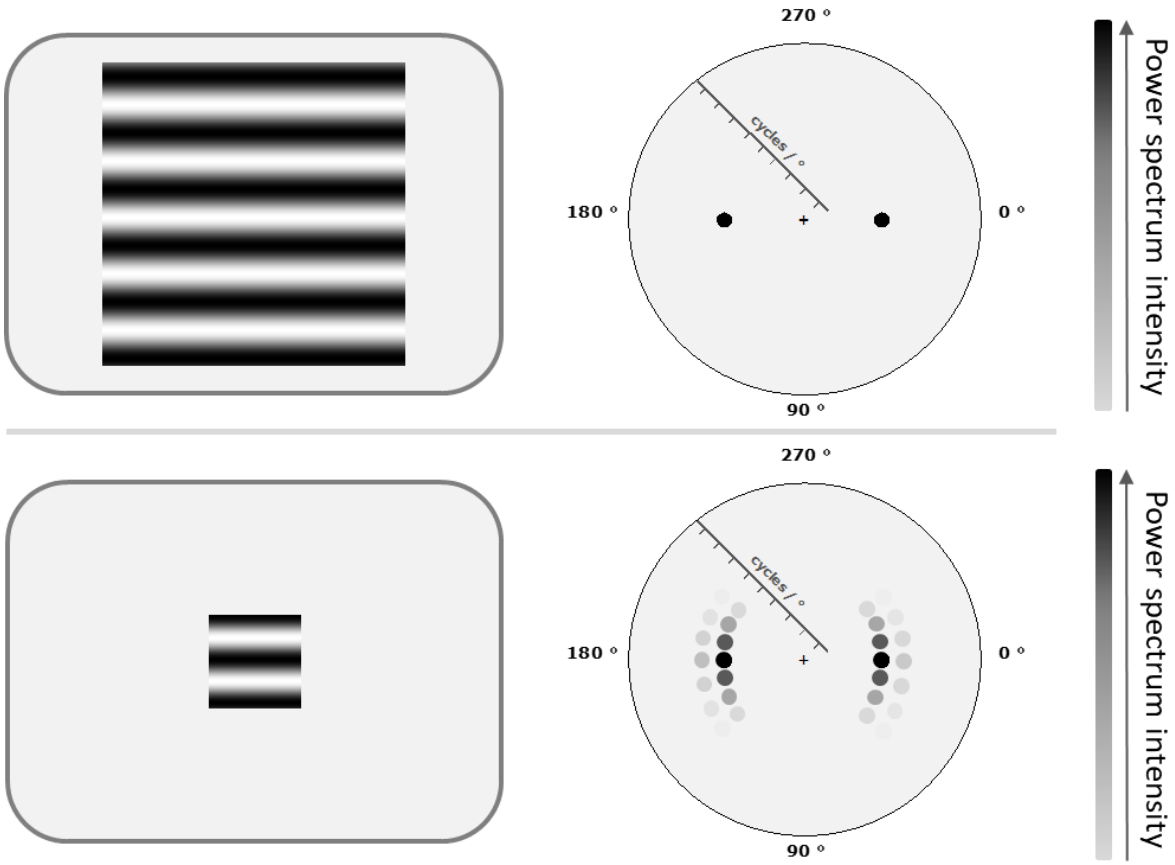

Figure 1.12. For large (*top*) and small (*bottom*) stimuli of equal spatial frequency (*left*), the spatial frequency content is represented on polar plots (*right column*). For the polar plots, the spectral intensity values represent the amplitude at each frequency (scaled to cover the available brightness range, such that darker values indicate greater amplitude). Smaller stimuli have broadened orientation and spatial frequency spectra.

responses from orientation-selective receptive fields. Additionally, sharp changes in luminance along the edges of stimuli cause 'stimulus vignetting' (Roth et al., 2018), which introduce spurious orientation and spatial frequency information into the stimulus. Therefore, when measuring the oblique effect, it is prudent to use oriented stimuli that are both relatively large and presented within a smooth-edged (e.g. Gaussian) spatial window to reduce the presence of potential image artefacts.

The size of the oblique effect for orientation discrimination is also reduced with increasing eccentricity (Davey & Zanker, 1998; Vandenbussche et al., 1986; Westheimer, 2003b), but is not abolished. However, this is not the case if larger stimuli are used (Vandenbussche et al., 1986), commensurate with the receptive field sizes of V1 neurons which increase with eccentricity (Hubel, 1982). For example, orientation-discrimination thresholds for a line stimulus, 1° in length, is relatively unchanged up to 8° eccentricity (G. Orban et al., 1984; Vandenbussche et al., 1986). Eccentricity-dependent modulations of the oblique effect may be partially mediated by a radial bias, whereby performance is improved for orientations aligned with the axis of the retinal meridian (see Section 1.1.4).

1.3.4 Orientation channels

Orientation-discrimination performance may be determined by the slopes of orientation channels (see Section 1.2.4), indicating that the oblique effect for orientation-discrimination may be generated by an orientation anisotropy in the tuning bandwidths of orientation channels. However, there is little neurophysiological support for such a claim (see Section 1.4). Psychophysical estimates of orientation bandwidths, thought to reflect the orientation tuning of channels underlying perception, have been measured for cardinal and oblique stimuli using an orientation-masking paradigm with contrast detection. An overview

of this method is described in Section 1.2.4. Despite initial reports that cardinal bandwidths were 20% smaller than oblique bandwidth (Campbell & Kulikowski, 1966), the majority of studies report no consistent difference between the two orientations (Blake & Holopigian, 1985; Phillips & Wilson, 1984; Saarinen & Levi, 1994; Thomas & Gille, 1979). The lack of supporting psychophysical evidence suggests that either orientation bandwidths are isotropic (i.e., not anisotropic), or that the orientation-masking paradigm with contrast detection is unsuitable for measuring the orientation bandwidths of channels serving visual perception. For instance, if the mechanisms serving detection were independent of those underlying visual perception, then orientation bandwidth estimates from a detection task may not be informative about the visual system as a whole.

With thousands of trials of practice on an orientation discrimination task with only oblique orientations, the oblique effect for orientation discrimination is partially diminished (Vogels & Orban, 1985; Westheimer & Lavian, 2013), whereas the oblique effect for contrast detection can be abolished or even reversed with practice (Mayer, 1983). Feature-based attentional mechanisms, which boost the effective contrast of a practiced orientation (Bloem & Ling, 2017a; Carrasco, 2014), may account for the reduction in the oblique effect. Alternatively, there are suggestions from animal neurophysiology that perceptual learning may sharpen the selectivity of oblique-tuned neurons in V1 and V4 of monkeys (Schoups et al., 2001; Yang & Maunsell, 2004).

Another mechanism by which perceptual learning mechanism may improve visual performance for obliques is the reduction of internal noise (i.e., response variability) for oblique-tuned orientation channels (Dosher & Lu, 2017; Wang et al., 2013). The 'equivalent-noise method' is often employed to characterise the internal noise within the human visual system (e.g., Dakin et al., 2005; Heeley et al., 1997; Yu et al., 2002). This involves measuring

psychophysical performance for various levels of external noise, in order to estimate the level of internal, equivalent noise (i.e., the internal limit on performance).

One study implemented the equivalent-noise method by measuring orientation-discrimination thresholds at various levels of stimulus-orientation bandwidth (Heeley et al., 1997). With the variance of the external noise being known (i.e., the stimulus bandwidth) they fit a variance-summation model to their data which provided estimates of two free parameters, the number of sampled local orientations (assumed to reflect the number of orientation channels) and the variance within each orientation sample (i.e., internal noise). They reported higher levels of internal noise for oblique orientations than for cardinals, and a substantial oversampling of cardinal orientations, which could reflect an overrepresentation of cardinal mechanisms. These findings are consistent with an investigation of the oblique effect for motion-direction discrimination, which implemented a similar methodology (Dakin et al., 2005).

Psychophysical estimates of internal noise are relatively broad, in that they could reflect the contributions of various response parameters, such as sampling density, orientation bandwidth, response variability, and response gain (Regan & Beverley, 1985). Furthermore, estimates of internal noise may also reflect inhibitory interactions between orientation channels (i.e., cross-orientation inhibition) (D. H. Baker & Meese, 2012; Baldwin et al., 2016). To avoid this, future research could utilise the 'double-pass method' to estimate internal noise, which measures the changes in behavioural responses across multiple presentations of the same stimulus, i.e., response variability (Green, 1964; Z.-L. Lu & Dosher, 2008).

1.3.5 Higher visual areas

The oblique effect for orientation discrimination is not entirely consistent with low-level accounts, which attribute anisotropic perception to anisotropies in the response characteristics orientation-selective neurons. A prominent oblique effect for orientation discrimination is found for stimuli comprised of widely separated elements, positioned to evoke a percept of an orientated contour, which would elicit little response in orientation-selective neurons in early visual cortex (Figure 1.13). For example, an oblique effect for orientation discrimination is found for illusory lines, formed from two circles that are spatially separated by 5°, that is larger than that for normal (luminance-defined) lines (Westheimer, 2003a). The typical receptive field sizes for central vision are far below 5° in V1 and V2, however the larger receptive fields of some neurons in V4 could feasibly encode the orientation of such illusory lines (J. Freeman & Simoncelli, 2011).

In a typical temporal, two-alternative forced choice (2AFC), orientation-discrimination task, the orientation in the first interval must be encoded and stored for

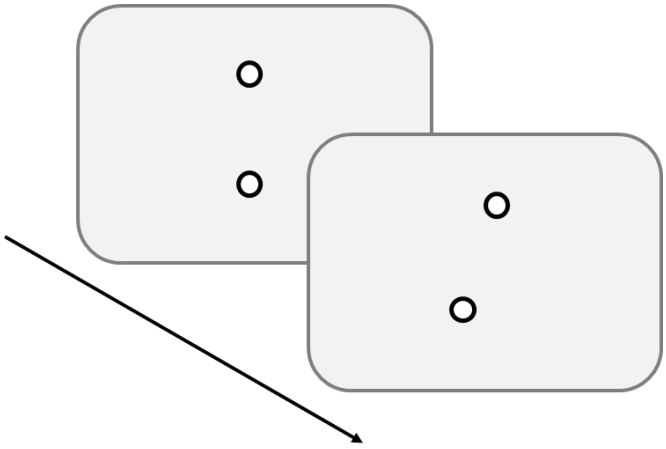

Figure 1.13. Schematic of an orientation-discrimination task with illusory contours, perceived as the inferred connection between two spatially separated circles, as in Westheimer (2003). Participants judged which of the two stimuli was perceived as being rotated more clockwise.

comparison in the second interval. For cardinal orientations, the precision of this representation is unaffected by a ten-fold increase in the interstimulus interval (Regan & Beverley, 1985). However, larger oblique effects for orientation discrimination have been reported for temporal 2AFC tasks compared to spatial 2AFC tasks, where stimuli are presented simultaneously (Heeley & Buchanan-Smith, 1992; Westheimer, 2003a). This could reflect anisotropic storage mechanisms of visual working memory (Westheimer, 2003a), such that the representation of oblique orientations may decay at a faster rate that of cardinal orientations.

However, the spatial 2AFC task in Heeley & Buchanan-Smith (1992) involved presenting the target and comparison in a centre-surround arrangement (Figure 1.14A). This stimulus configuration would be confounded by tilt effects (e.g., the simultaneous presence of nearby lines or gratings is known to alter the perceived orientation of target contours), which are also reported to be anisotropic (McMahon & MacLeod, 2003; Westheimer, 2017). The

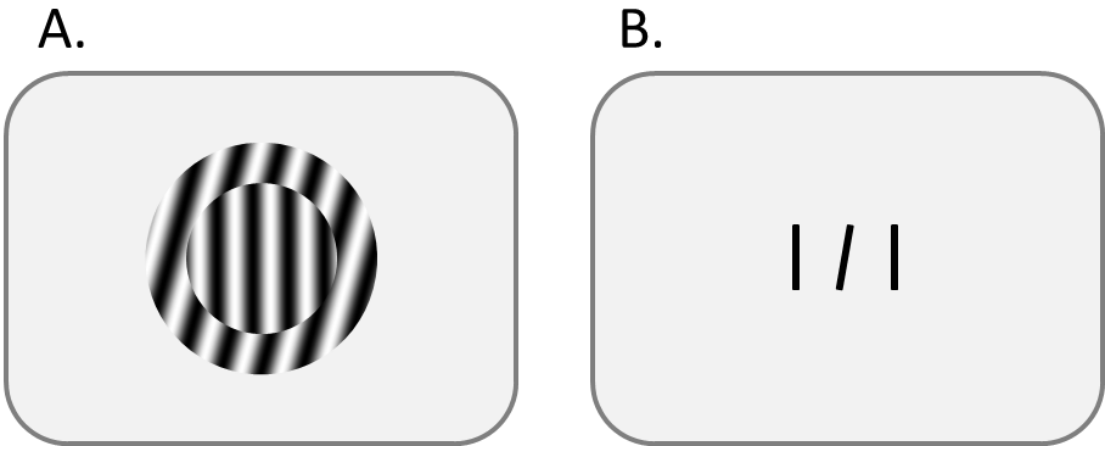

Figure 1.14. Spatial orientation-discrimination tasks for a centre-surround arrangement (*A*) (Heeley & Buchanan-Smith, 1992) and for closely spaced small lines (*B)* (Westheimer, 2003a). Such stimuli are not well-suited to measure orientation perception, in that the simultaneous presence of adjacent stimuli can affect the perceived orientation of the central target (Schwartz et al., 2007).

spatial 2AFC condition used by Westheimer (2003) involved the close arrangement of short lines (Figure 1.14B), 0.25° in length, separated by just 0.2°, which was proposed to adequately minimise orientation interactions (Westheimer et al., 1976). However, such closely spaced lines are smaller than the typical receptive field sizes of V1 neurons in macaques (J. Freeman & Simoncelli, 2011), such that this information may have been pooled together. Performance on this task has been proposed to reflect a mechanism that is sensitive to the changes in the 'synchronicity' of orientated components (Westheimer & Lavian, 2013).

In the presence of distractor stimuli, an oblique effect for judgements of simultaneity has been reported for pairs of Gabors, of the same orientation, spaced roughly 30° apart (Kelly & Matthews, 2011). Conversely, in the absence of distractor stimuli, this effect was abolished, suggesting that attentional mechanisms may serve to reduce the perceptual oblique effect. Indeed, it was reported that having less attentional resources available (participants attended a rapid stream of letters at fixation) impairs orientation-discrimination performance for oblique orientations more so than for cardinal orientations (Bloem & Ling, 2017a), although this finding was highly variable across participants.

If the oblique effect is determined by orientation anisotropies in the retinotopic maps of early visual cortex, then the oblique effect should follow retinal coordinates. In other words, with the head tilted by 45°, the oblique effect should be reflected in impaired performance for the physical orientations of 0° and 90°, respectively. To note, for these measurements, it is crucial to correct for ocular-counter roll (Bockisch & Haslwanter, 2001) and variations in the subjective visual vertical that occur with head tilt (S. Chen & Levi, 1996; Howard & Templeton, 1966). The oblique effect for contrast sensitivity indeed follows retinal coordinates (Corbett & Carrasco, 2011; Frost & Kaminer, 1975), supporting an early cortical locus in the visual pathways. However, the oblique effect for orientation

discrimination is reported to follow gravitational coordinates (Buchanan-Smith & Heeley, 1993; Mikellidou et al., 2015). When the head is tilted by 45°, orientation-discrimination performance is still superior at the physical-cardinal orientations (0 and 90°), despite these corresponding to oblique orientations in retinal coordinates. Furthermore, when participants are supine (i.e., lying down on their back) and facing a screen directly above them, such that gravitational cues (e.g., vestibular information) are discounted, the oblique effect for orientation discrimination follows retinal coordinates (Mikellidou et al., 2015). These findings implicate a higher-level contribution to the oblique effect, potentially independent of low-level mechanisms, such as those serving detection.

Orientation reproduction

In orientation-reproduction tasks, participants manually rotate a stimulus to match the orientation of a previously presented stimulus. There are two key components of the oblique effect for orientation reproduction. First, there is more variable error when reproducing oblique orientations than the cardinals, which may reflect the lesser precision of the encoded oblique orientation (Balikou et al., 2015; Gentaz et al., 2008). Second, for angles in between the cardinals and obliques (e.g., 22.5°), there is a tendency for errors to be biased towards the oblique axes (Balikou et al., 2015; Tschopp-Junker et al., 2010), which is proposed to reflect higher-level cognitive mechanisms, reflecting biased, internal representations of orientation. However, there have been few attempts to model the nature of these hypothesised biases. A bias in the error towards oblique axes is also found for an orientation-estimation task, where participants had to estimate the visual orientation of a visual line stimulus (Ye & Liu, 2020). The extent of this bias is markedly reduced when a known reference line, at 45°, is presented simultaneously with the test stimulus (Figure 1.15), suggesting that this bias may reflect the imprecision of participants' internal representations of oblique orientations.

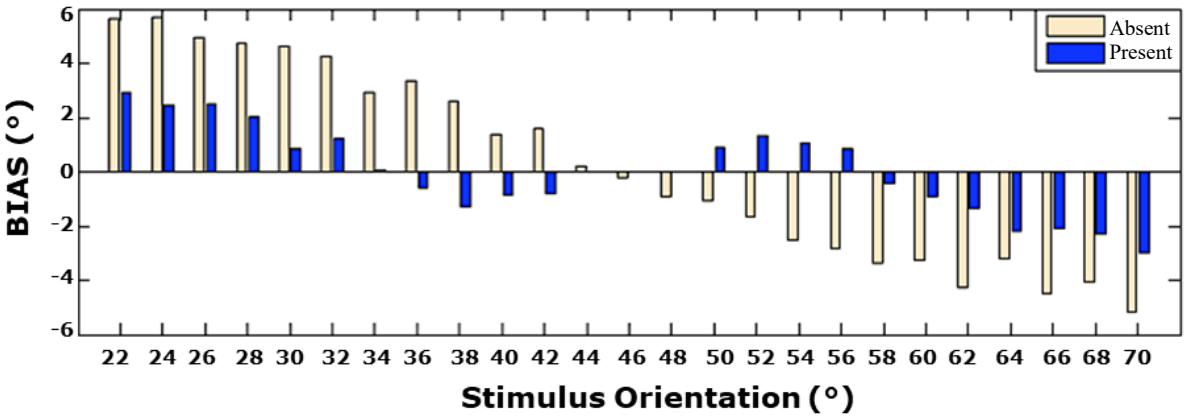

Figure 1.15. Errors in an orientation-estimation task are biased towards the oblique axes, however this is bias is abolished in the presence of a 45° reference-line. BIAS is the average error of the estimated orientation from the stimulus orientation. Participants' may have an imprecise internal reference-frame for the obliques. Adapted from Ye & Liu (2020).

One study manipulated the working memory load (and attentional load) before each orientation-reproduction judgement, such that a variable number of distinct orientations had to be perceived and then remembered over a brief temporal interval, before one of these orientations was signalled to be reproduced (Balikou et al., 2015). They found that the bias in error towards the oblique axes increased with the number of distractor orientations, whereas the extent of variable error was unchanged. These findings suggest that there may be two independent sources of the oblique effect, an anisotropic low-level component that encodes the visual orientation, and an anisotropic higher-level component that is sensitive to increasing cognitive demands. Beyond orientation perception, a systematic bias towards the oblique axes has also been demonstrated in smooth pursuit eye movements (Krukowski & Stone, 2005), haptic orientation perception (Gentaz et al., 2008), and manual pointing movements in 3D space (Kaspiris-Rousellis et al., 2017; Smyrnis et al., 2014).

1.4 Neurophysiological evidence for the oblique effect in animals

1.4.1 Overview

Theoretical accounts of the oblique effect can be tested through neurophysiological measurements of activity in visual cortex. Despite advances in non-invasive brain imaging techniques for human participants, invasive neurophysiological techniques in animals provide a level of spatial and temporal precision that can greatly inform our understanding of the cortical circuitry that may underlie the oblique effect. The oblique effect has been demonstrated behaviourally in animals (for review, see Appelle, 1972), such as the cat (G. A. Orban et al., 1984b; Parriss, 1964; Vandenbussche & Orban, 1983), monkey (J. A. Bauer et al., 1979; Boltz et al., 1979), and other non-mammalian species, including goldfish (Mackintosh & Sutherland, 1963) and octopus (Sutherland, 1957). Some studies have failed to reveal a behavioural oblique effect in animals (Bisti & Maffei, 1974; Blake & Holopigian, 1985; De Weerd et al., 1990), however such inconsistencies may result from differences in training schedules prior to formal testing.

In certain species of mammals, common developmental mechanisms have led to similar cortical architectures across species (Krubitzer, 2007). For example, humans, non-human primates, cats, and ferrets each have a retinogeniculate pathway which projects to an initial cortical input stage, primary visual cortex (V1), that is formed of six anatomically defined layers with orientation columns arranged into pinwheels (Ibbotson & Jung, 2020). Therefore, neurophysiological investigations into the oblique effect have typically been focused on non-human primates (G. Shen et al., 2014), cats (B. Li et al., 2003), and ferrets (Grabska-Barwińska et al., 2009). Other mammals such as mice and rats have 'salt-and-pepper' orientation-selectivity maps, with a seemingly random distribution of orientation

preferences, both across the retinotopic map and along the six cortical layers (Murgas et al., 2020; Ohki et al., 2005; Van Hooser et al., 2005).

Macaque monkeys are considered to provide the closest model for human vision (Vanni et al., 2020), with similar foveal cone densities (Curcio et al., 1990), photoreceptor distributions in the peripheral retina (Wilder et al., 1996), topographic organisation of the LGN (Kastner et al., 2006), and laminar patterns in V1 (Balaram et al., 2014; Kastner et al., 2006). Additionally, macaques are sensitive to a similar spatial frequency range as humans (De Valois et al., 1974). However, although V1, V2, and MT of humans and macaques are highly similar, other visual areas such as V4 lack clear homologues (Vanni et al., 2020). Additionally, much of the macaque visual cortex beyond V1 and V2 is buried within sulci and is therefore less accessible for neurophysiological recording techniques. Investigations into extrastriate visual areas sometimes focus on marmoset visual cortex, which has a smooth cortical structure that allows simultaneous access to multiple visual cortical areas (Solomon & Rosa, 2014).

1.4.2 Single-cell recordings

Sampling

Single-cell recordings involves the insertion of microelectrodes into the visual cortex of animals in order to record the activity of individual neurons. These animals are typically anaesthetised, although recordings can be made in awake behaving animals (e.g., Celebrini et al., 1993). Single-cell recordings first characterised orientation selectivity from the firing rates of V1 neurons (Hubel & Wiesel, 1962). Many early single-cell studies reported a larger proportion of orientation-selective neurons that prefer cardinal than oblique orientations, in V1 of cats (R. Bauer & Jordan, 1993; Kalia & Whitteridge, 1973; Kennedy & Orban, 1979;

Pettigrew et al., 1968) and non-human primates (De Valois, William Yund, et al., 1982; Mansfield, 1974). However, numerous other investigations failed to find such a difference in V1 (Campbell et al., 1968; Finlay et al., 1976; Henry et al., 1974; Noda et al., 1971; G. F. Poggio et al., 1977; Rose & Blakemore, 1974). However, these early single-cell studies used restricted sample sizes (typically under 100 individual cells) and were thus prone to sampling biases due to the ordered nature of visual-cortical architecture, which likely confounded attempts to quantify the distributions of response characteristics across visual cortex (for review, see Li et al., 2003). For example, orientation-selective neurons in superficial layers of V1 display narrower orientation tuning than those in deeper layers (Ringach et al., 2002; Schiller et al., 1976b), neurons in pinwheel centres are more broadly tuned than those in iso-orientation domains (Koch et al., 2016), and there may be a higher proportion of neurons tuned to meridional axes (Roth et al., 2022).

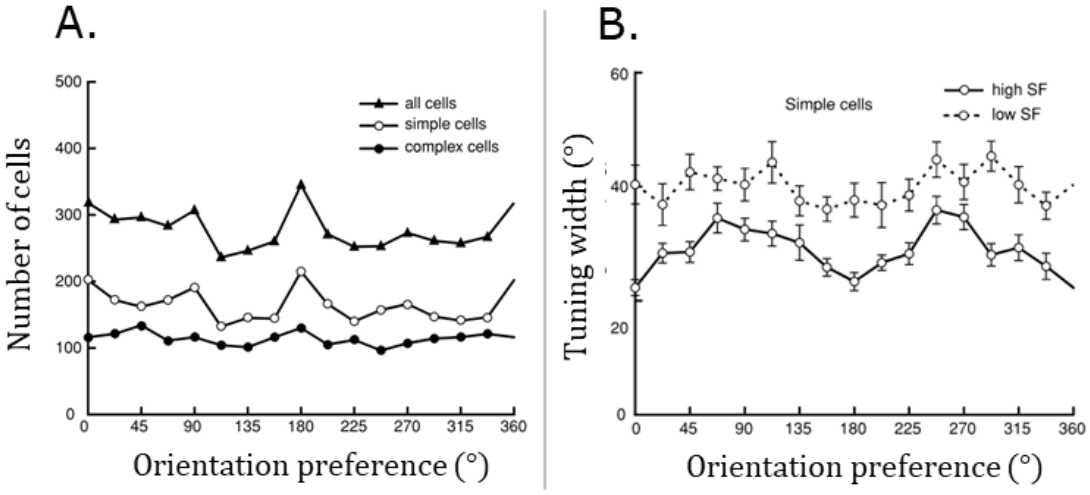

Figure 1.16. In cat V1, more neurons prefer cardinal orientations than oblique orientations (A) and cardinal-tuned simple cells are more narrowly tuned than oblique-tuned neurons (B). Adapted from Li et al. (2003).

The most comprehensive single-cell account in the cat comes from an analysis of 4,418 cells in V1 (B. Li et al., 2003). They reported that approximately 56% of neurons were tuned to cardinal orientations (Figure 1.16A) and that this effect was predominantly driven by anisotropies in simple cells (G. A. Orban et al., 1984b; G. A. Orban & Kennedy, 1981). In contrast, from recordings of 1,369 individual cells in macaque V1, there was no reported difference in the numbers of cardinal-tuned and oblique-tuned neurons (G. Shen et al., 2014). This could simply reflect genuine species differences, however the sampling of cells in either study could have been biased by the overrepresentation of neurons that prefer orientations about the meridional axes (J. Freeman et al., 2011), which should be accounted for when quantifying orientation anisotropies in neuronal populations (e.g., Fang et al., 2022).

Various mammals, such as cats and ferrets, have high density regions of retinal ganglion cells and V1 neurons that are elongated along the horizontal meridian, termed the 'visual streak' (Hübener & Bonhoeffer, 2002; Hughes, 1975; Law et al., 1988; McIlwain, 1977; Stone, 1978), whereas macaques and humans have a circular foveal region. Both cats and macaques have an overrepresentation of preferred orientations in V1 which are aligned with the retinal meridians (Leventhal, 1983), i.e., a 'radial bias' (see Section 1.1.4). Therefore, horizontal-biases in cat visual cortex (B. Li et al., 2003) may be attributable to a radial bias that is accentuated along the horizontal meridian.

However, in macaques, an overrepresentation of horizontal-tuned neurons was found in area V2 (G. Shen et al., 2014), such that 40% of all sampled neurons preferred horizontal orientations, versus roughly 20% preferring orientations that were about the vertical or oblique axes. Notably, this difference was larger for neurons tuned to high spatial frequencies, consistent with suggestions that orientation anisotropies were greater for neurons with small receptive field sizes (Kennedy & Orban, 1979; Leventhal & Hirsch, 1977;

Mansfield, 1974; G. A. Orban & Kennedy, 1981). However, an equal number of neurons tuned to vertical and oblique orientations is difficult to reconcile with behavioural findings of an oblique effect for measures of visual sensitivity (where oblique performance is worse than for vertical), such as visual acuity and contrast-sensitivity (see Section 1.3.2). Future research should measure the distributions of cardinal-tuned and oblique-tuned neurons in distinct visual areas, to investigate the progression of orientation anisotropies along the visual pathways (e.g., V1, V2, and V4).

Orientation selectivity

Early investigations reported that neurons preferring cardinal orientations have narrower orientation-tuning bandwidths than those preferring obliques (Kennedy & Orban, 1979; B. Li et al., 2003; J. I. Nelson et al., 1977; G. A. Orban & Kennedy, 1981; Rose & Blakemore, 1974). However, in other work, no such anisotropy was observed (Finlay et al., 1976; Mansfield, 1974; G. Shen et al., 2014; J. R. Wilson & Sherman, 1976). Single-cell recordings from the V1 of the cat demonstrated that narrowed orientation tuning may only be found for horizontal-tuned neurons which are selective for higher spatial frequencies (Figure 1.16B), with no differences in tuning bandwidth for vertical and oblique orientations (B. Li et al., 2003).

Comparisons with predicted bandwidths, estimated from linear 2D receptive fields in the cat, indicated that the narrowed bandwidths of horizontal-tuned neurons may be mediated by intracortical, inhibitory mechanisms (B. Li et al., 2003) (see Section 1.2.3). Although there is partial support for these findings in macaque V2, narrowed cardinal-orientation bandwidths were absent in V1 (G. Shen et al., 2014). Interspecies differences may again be related to interactions between the radial bias in V1 (Leventhal, 1983) and the 'visual streak' in cats (Hübener & Bonhoeffer, 2002) that is not present in macaque visual cortex.

Other response characteristics

There are relatively few single-cell studies that explore orientation anisotropies for characteristics other than sampling and orientation bandwidth. It has been reported that there is no orientation-specific variation in the maximum firing rate or spontaneous firing rate of simple cells in cat V1 (B. Li et al., 2003) or in macaque V1 and V2 (G. Shen et al., 2014). Contrast thresholds for individual neurons, taken as the contrast at which a cell fired reliably above its spontaneous firing rate, may be lower for cardinal-tuned neurons relative to oblique-tuned neurons (Anzai et al., 1995; B. Li et al., 2003). However, despite extensive study, there are no reports of orientation anisotropies in the contrast-response functions of V1 neurons (Albrecht & Hamilton, 1982; Geisler & Albrecht, 1997).

1.4.3 Optical imaging

Overview

Intrinsic signal optical imaging (ISOI) is a functional imaging technique that indirectly measures neuronal activity by the changes in light reflectance that are associated with activity-dependent levels of oxygenated haemoglobin. Small changes in intrinsic signals (< 1% of the total signal) are captured by highly sensitive imaging cameras positioned over the cortical surface. For image analysis, the signal-to-noise ratio is improved through spatial and temporal filtering to produce functional maps with a high spatial resolution (< 100μm) and relatively broad temporal resolution (< 100ms) (Frostig & Chen-Bee, 2009; Grinvald et al., 1999; H. D. Lu et al., 2017).

The spatial resolution of ISOI has been instrumental in revealing the functional organisation of visual cortex (H. D. Lu et al., 2010; Roe et al., 2005; Ts'o et al., 1990). For example, the radial arrangement of orientation columns in pinwheels was revealed using ISOI

(Bonhoeffer & Grinvald, 1991; Ohki et al., 2006). To generate orientation-preference maps, typically recordings are made for four orientations, then maps of signal change are generated for each orientation. These data are combined by vector summation to generate an estimate of 'orientation bias' (mean response vector) for each pixel represented along the cortical surface.

One limitation of ISOI is that the signal recorded in each pixel reflects the combined activity of many neurons through the cortical layers, and across the cortical surface due to spatial smoothing of the images. Variability in signal amplitude across visual cortex therefore reflects not only the total number of responding neurons, but also the pooled response characteristics of sampled neurons. Additionally, ISOI records signals predominantly from superficial cortical layers, where V1 neurons have narrower orientation tuning relative to neurons in middle and deeper layers (Ringach, 2002; Schiller et al., 1976a). Therefore, bandwidths may be systematically underestimated by this technique.

Cardinal bias

Compared with single-cell recordings, optical imaging of population responses has consistently revealed an orientation anisotropy in early visual cortex of macaques (Fang et al., 2022), cats (Huang et al., 2006; Liang et al., 2007; Ribot et al., 2008; Sengpiel et al., 1999; W. Shen et al., 2008; G. Wang et al., 2003), and ferrets (B. Chapman & Bonhoeffer, 1998; Coppola, White, et al., 1998; Coppola & White, 2004; Grabska-Barwińska et al., 2009). Despite substantial individual variation, roughly 55 to 60% of the cortical surface in V1 is biased toward cardinal orientations in ferrets (Grabska-Barwińska et al., 2009) and cats (W. Shen et al., 2008). Consistent with contrast-invariant tuning (Section 1.2), orientation biases within localised regions of ferret visual cortex were reported to be invariant with stimulus contrast, even when close to response threshold (Grabska-Barwińska et al., 2009).

Visual experience may have a role in the development of the oblique effect, due to the

overrepresentation of cardinal orientations in the visual environment (Girshick et al., 2011). In support of this, kittens reared in a single-orientation environment developed an overrepresentation of neurons tuned to the experienced orientation in V1, such that the surface area devoted to the experienced orientation was up to twice that of the orthogonal orientation (Sengpiel et al., 1999). However, dark-reared ferrets (i.e., no visual input during development) still have a cortical surface that is dominated by cardinal-tuned responses (Coppola & White, 2004), despite severe losses in orientation selectivity. In fact, the extent of this cardinal bias has been suggested to decrease during development (Coppola & White, 2004; Hoy & Niell, 2015), although the extent of this effect becomes unclear due to the collapsing of data across orientation conditions (i.e., pooling data for horizontal and vertical orientations into a singular, cardinal condition).

The extent of cardinal bias in V1 responses may be modulated by feedback from extrastriate visual areas. Disinhibition of visual responses in the cat, via the administration of GABA in area 21a, abolished the cardinal bias in V1 and was associated with a general loss in orientation selectivity (Liang et al., 2007; W. Shen et al., 2008), whereas administration of glutamate in area 21a (an excitatory neurotransmitter) increased the strength of the cardinal bias (Liang et al., 2007). These findings indicate that inhibitory feedback connections from higher visual areas to V1 may modulate anisotropies in tuning bandwidths. Importantly, these findings indicate that the cardinal bias (as measured using various imaging techniques, such as ISOI and fMRI) may reflect the response characteristics of visual cortical neurons, and does not necessarily provide information about the relative numbers of cardinal-tuned and oblique-tuned neurons. For a given cortical region or pixel, a cardinal bias could reflect a combination of orientation anisotropies in sampling, tuning bandwidths, firing rates, or response variability. Furthermore, a recent ISOI study revealed that contributions from the

radial bias (see Section 1.1.4) can obscure measurements of cardinal biases in V1 of macaques (Fang et al., 2022).

An optical imaging study in macaques reported a cardinal bias in visual cortex, which progressively increased from V1 to V2 and V4 (Fang et al., 2022). This is consistent with single-cell findings of a more prominent overrepresentation of cardinal-tuned neurons in macaque V2, relative to V1 (G. Shen et al., 2014). This is also consistent with a stronger cardinal bias in area V2 of the marmoset (G. B. Liu & Pettigrew, 2003), area MT of the owl monkey (Xu et al., 2006), and in area 21a of the cat (Huang et al., 2006). Cardinal biases which are larger in extrastriate visual areas than in V1 are consistent with psychophysical findings that the size of the oblique effect for orientation-discrimination is larger for illusory contours than physical, luminance-defined lines (Westheimer, 2003a). The source of the oblique effect may therefore exist beyond V1 (see Section 1.3.5).

1.5 Brain imaging evidence for the oblique effect in humans

1.5.1 Electrophysiology

Evoked activity

Neuronal activity in response to a visual stimulus can be captured through electrophysiological methods measuring visual evoked potentials (VEPs), which reflect the synchronised activity of large populations of neurons within a recorded cortical region. VEPs are typically recorded using electroencephalography (EEG) where electrode arrays are

applied to the scalp. EEG has an extremely high temporal resolution on the order of milliseconds but, despite advancements in data quality and source-localisation algorithms, it has a relatively poor spatial resolution that is restricted to the cortical surface (Michel & Brunet, 2019). Indeed, there may be a spatial 'smearing' of signals that originate in distinct visual areas (Koelewijn et al., 2011).

Upon the presentation of a visual stimulus, individual VEP components can be identified by their polarity and their latency (Figure 1.17). For example, P100 has a positive polarity and typically appears 100ms after stimulus-onset. Simultaneous EEG and fMRI recordings have identified P100 as the electrical correlate of feedforward activity in V1 (Di Russo et al., 2005; Whittingstall et al., 2007). Alternatively, the N140 is a negative potential with a latency of 140ms, with generators in V1 and extrastriate visual areas (Di Russo et al., 2005). The relative amplitude of VEP components over time provides insight into the temporal characteristics of neural activity within a particular region of interest. In general, larger VEPs (positive or negative) suggest stronger activation of visual cortex, however the mechanisms underlying such activity (e.g., feedforward or feedback) are undefined and poorly localised.

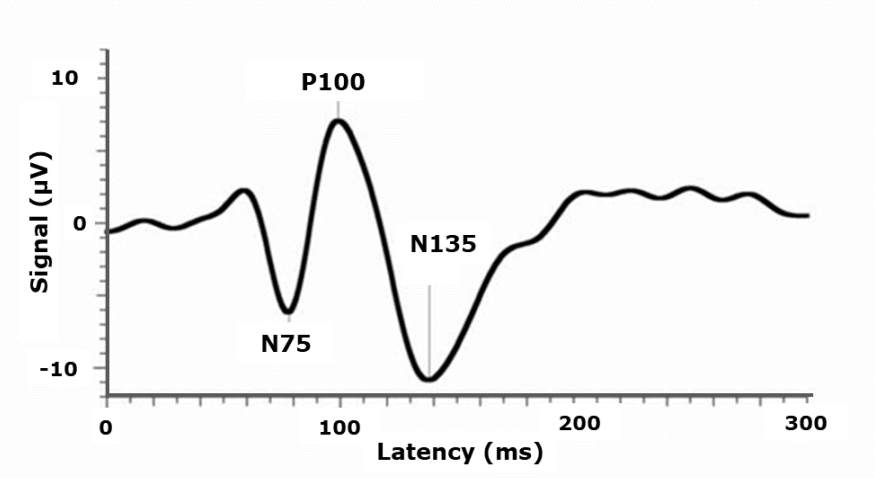

Figure 1.17. Examples of early VEPs associated with V1 activity. See text for further details. Adapted from Odom et al., 2016.

The post-retinal locus of the oblique effect in human vision was first demonstrated using electrophysiological techniques. Using an electroretinogram, the amplitude of evoked potentials in the optic nerve were found to be similar for cardinal and oblique orientations. Whereas, EEG recordings found larger VEPs in visual cortex upon viewing grating stimuli at cardinal orientations than at oblique orientations (Maffei & Campbell, 1970). There is overwhelming support for such a cardinal bias in the amplitude of VEPs from recordings across extended regions of visual cortex, with latencies at or beyond 100ms (Arakawa et al., 2000; Maffei & Campbell, 1970; Moskowitz & Sokol, 1985; Proverbio et al., 2002).

The extent of the cardinal bias in VEP amplitude has been reported to increase with increasing spatial frequency (R. D. Freeman & Thibos, 1975; Moskowitz & Sokol, 1985), although this effect may be minimal (Arakawa et al., 2000). These findings are partially consistent with an oblique effect that is modulated by spatial frequency, as evidenced psychophysically (see Section 1.3) and neurophysiologically in animals (see Section 1.4). Additionally, the cardinal bias in VEP amplitude may increase with stimulus contrast (Zemon et al., 1983). However, this is in stark opposition to an oblique bias that has been reported to emerge at high contrasts in fMRI recordings (see Section 1.5.2).

One study measured VEPs upon the onset of a Gestalt stimulus (an emergent shape formed from moving and rotating lines) and reported an oblique bias in the P300 component, far stronger than expected from small variations in the amplitudes of early VEP components (Heinrich et al., 2008). In classical P300 paradigms, less frequent visual stimuli tend to elicit larger responses (Friston, 2005), and this extends to stimuli that deviate from long-term experience (Daffner et al., 2000). This is consistent with the lower prevalence of oblique orientations in natural visual scenes (Coppola, Purves, et al., 1998; Girshick et al., 2011). However, although P300 is often proposed as a marker of high-level cognitive processes

(Friston, 2005; Linden, 2005), whether this reflects an interaction with feedforward networks is unclear. P300 may simply be a cognitive response to unexpected stimuli, such as unexpected auditory tones (Gaeta et al., 2003), with no functional significance for visual processing. Consistent with a pre-attentive cortical mechanism for the oblique effect, the visual mismatch negativity (vMMN) component, presumed to reflect the automatic comparison of stimuli to visual memory representations, is larger for cardinal gratings than oblique gratings (Takács et al., 2013).

Magnetoencephalography (MEG) detects the magnetic fields of tangentially orientated, synchronised neural activity within the cortex. MEG has a similar temporal resolution to EEG but a much improved spatial resolution, allowing the clear dissociation of VEPs from V1 and extrastriate visual areas (Koelewijn et al., 2011). In contrast with EEG

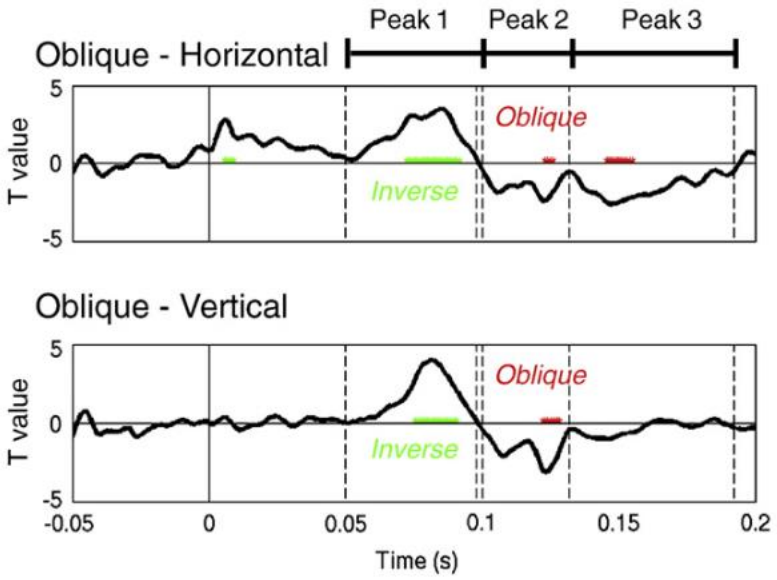

Figure 1.18. Larger early-VEPs and smaller late-VEPs were recorded for oblique orientations contrasted with either horizontal (*top*) or vertical (*bottom*). Adapted from Koelewijn et al. (2011).

findings, one MEG study found an oblique bias in the early VEP components associated with V1 activity, and a classical cardinal bias in the later VEP components (Figure 1.18) which were dominated by extrastriate visual areas (Koelewijn et al., 2011). An oblique bias in V1 responses has been confirmed in a high-density EEG study (Mikhailova et al., 2015).

Induced activity

Whereas VEPs reflect the brain activity that is locked to the onset of a visual stimulus, induced activity refers to the ongoing rhythmic activity of certain brain functions (Koelewijn et al., 2011). Induced activity is analysed in the frequency domain. First, spectral analysis identifies the power (equal to the amplitude squared) of brain oscillations within specific frequency bands, such as alpha (8-12 Hz) and gamma (30-70 Hz). Secondly, time-frequency analysis examines how the power of different frequency bands fluctuates over time. Gamma waves are robustly induced in V1 (Muthukumaraswamy, 2013) and may reflect feedforward activity that propagates from the input layer of V1 to extrastriate visual areas, whereas alpha waves may reflect feedback synaptic activity within the circuity of V1 (Bastos et al., 2015; Buffalo et al., 2011; Mejias et al., 2016; Michalareas et al., 2016; van Kerkoerle et al., 2014).

Orientation-discrimination performance may require the cooperative activity of dense neuronal populations (see Section 1.2). Orientation-sensitive gamma waves (Frien et al., 2000) are thought to reflect such population activity (Samonds & Bonds, 2005). In V1, an oblique bias in gamma power is evident roughly 200ms after stimulus onset (Koelewijn et al., 2011; Pantazis et al., 2018) which increases with stimulus contrast (Butler et al., 2020). Whereas, alpha power exhibits a cardinal bias which dominates the overall signal at low stimulus contrasts (Butler et al., 2020). A cardinal bias at low contrasts and an oblique bias at high contrasts is consistent with findings from fMRI studies (see Section 1.5.2).

1.5.2 Functional magnetic resonance imaging

Overview

Functional magnetic resonance imaging (fMRI) is a non-invasive neuroimaging technique that measures localised brain activity corresponding to localised changes in blood flow. The blood oxygen level-dependent (BOLD) signal serves as an indirect measure of neural activity by capturing the haemodynamic response. Typical 3T scanners have a resolution of approximately 3 mm^3, whereas high-resolution scanners (7T and beyond) can provide a spatial resolution in the sub-millimetre range. The lag between neural activity and the coupled vascular response constrains the temporal resolution of fMRI, with the BOLD signal reaching its peak roughly 5 seconds after stimulus-onset.

As with optical imaging (see Section 1.4.3), the BOLD signal in each voxel reflects the pooled activity of thousands of individual neurons. Early studies measured the relative amplitude of signals across regions of interest (Furmanski et al., 2004; Furmanski & Engel, 2000), whereas more recent studies determined the preferred orientation of individual voxels (Roth et al., 2022; Sun et al., 2013). Using a continuously rotating, high-contrast grating, the orientation tuning of visually responsive voxels can be revealed (Gardner et al., 2005; Sun et al., 2013; Yacoub et al., 2008). Voxels with statistically significant indices of selectivity are assumed to be orientation columns, and are used in further analyses (Sun et al., 2013; Yacoub et al., 2008). However, to reiterate, it is unclear to what extent the BOLD signal reflects the distribution of orientation preferences, or the response characteristics of individual neurons (see Section 1.4.3). Additionally, the BOLD response cannot distinguish between feedforward or feedback synaptic activity (Logothetis et al., 2001; Yen et al., 2011).

Cardinal bias

Early fMRI investigations reported a cardinal bias in the overall BOLD signal in V1 (Furmanski et al., 2004; Furmanski & Engel, 2000). However, subsequent studies reported either no such effect (Kamitani & Tong, 2005; Sun et al., 2013), or a stronger BOLD response to oblique orientations (Mannion et al., 2010; McDonald et al., 2012; Serences et al., 2009; Swisher et al., 2010). These later studies involved the passive viewing of grating stimuli, whereas the initially reported cardinal bias was recorded during an orientation-discrimination task (Furmanski et al., 2004; Furmanski & Engel, 2000) which may recruit attentional mechanisms that modulate V1 activity (Samonds & Bonds, 2005).

An oblique bias in the overall BOLD signal has been proposed to reflect a normalisation mechanism, whereby cardinal responses are reduced relative to obliques due to a larger inhibitory pool (Hansen & Essock, 2006; Mannion et al., 2010). In support of this, the magnitude of the oblique bias in V1 and V2 increases with stimulus contrast (Butler et al., 2020; Maloney & Clifford, 2015). However, this appears to be mostly driven by changes in the BOLD signal to vertical and oblique stimuli (Figure 1.19). Contrast-dependency of the

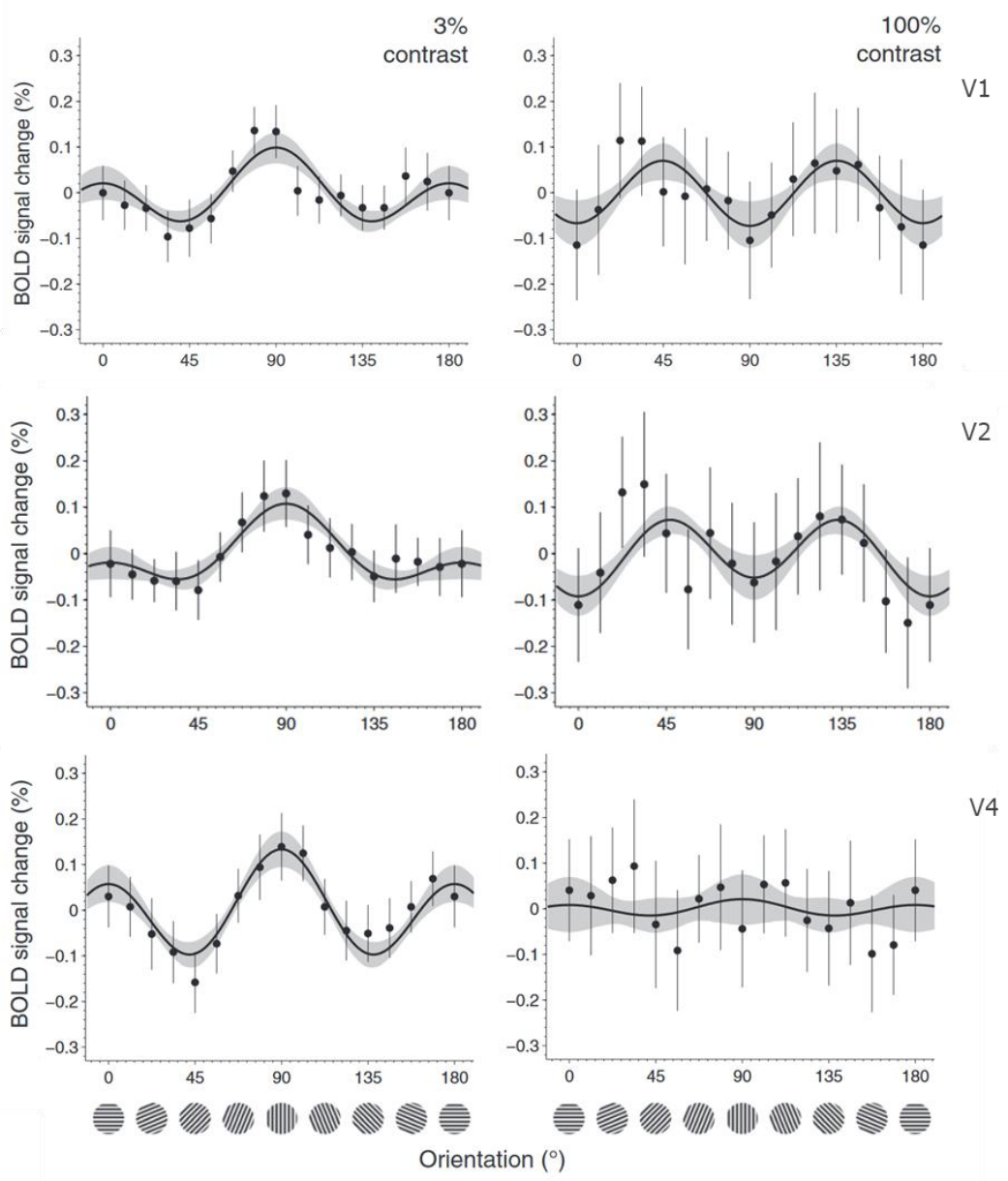

Figure 1.19. At low contrasts (left column) a cardinal bias is observed for V1, V2 and V4. At high contrasts (right column) an oblique bias is observed for V1 and V2, but not for V4. Adapted from Maloney & Clifford (2015).

BOLD signal may cast uncertainty onto previous investigations using fMRI and optical imaging, which measure a similar signal (see Section 1.3.2). Electrophysiological studies (see Section 1.4.1) reported an oblique bias in early visually evoked potentials (VEPs) followed by a cardinal bias in the sustained response (Koelewijn et al., 2011). Therefore, due to the

poor temporal resolution of the BOLD signal, it is unclear to what extent these findings reflect the early and late components of neuronal responses in early visual cortex.

Sampling

Sun et al. (2013) isolated the orientation preferences of individual voxels in human V1, using high-resolution fMRI, and reported a larger proportion of voxels in V1 selective for cardinals than for obliques, consistent with initial suggestions (Yacoub et al., 2008). However, they also reported no difference in the overall BOLD signal in V1 for cardinal and oblique orientations, independent of the orientation-selectivity criteria used. This demonstrates that biases in the overall BOLD signal (i.e., the global response) may not be informative for inferences about the response characteristics of neuronal populations. The orientation selectivity of voxels in higher visual areas, such as V4, have not been investigated, although this is likely due to the lack of clearly defined orientation columns in visual areas beyond V1 and V2 (Nandy et al., 2013).

This Chapter has highlighted various limitations of neurophysiological and electrophysiological techniques in understanding the neural mechanisms underlying the oblique effect. There is a need for a complementary computational approach, which can serve as a tool to test hypotheses generated from neurophysiological investigations. Crucially, such an approach can make causal inferences about how the distributions and response characteristics of orientation-selective neurons may impact visual performance.

1.6 Individual differences in visual function

1.6.1 Variations in the visual pathways

Overview

Substantial individual differences in visual performance can arise due to structural and functional variations across all stages of the visual pathways, including the optics of the eye (B. R. Hammond et al., 2010), the retina (B. R. Hammond et al., 2013; Stringham & Hammond, 2008), primary visual cortex (Bergmann et al., 2016; Himmelberg et al., 2022), and extrastriate visual areas (Huang et al., 2014; Kirchhoff & Buckner, 2006; Schwarzkopf et al., 2014). These contribute to individual differences observed psychophysically, from low-level measures of visual sensitivity (Hawkins et al., 2003; Himmelberg et al., 2022) to recognition mechanisms (Huang et al., 2014) and visual-cognitive biases (Grzeczkowski et al., 2017; Samaey et al., 2020).

Pre-cortical variation

In the optics of the eye, variations in the density of lens pigment (B. R. Hammond et al., 2010), which biases the wavelength spectrum reaching the photoreceptors, was reported to be the primary source of individual differences in a colour-matching task (Webster & MacLeod, 1988). Conversely, in a sample of 2,000 participants, large variations in the levels of intraocular light scatter did not predict individual differences in visual acuity (Van Den Berg et al., 2007). This may be because neural convergence within the retinal-cortical pathways provides a cut-off to determine the highest resolvable spatial frequencies (Section 1.1.2). However, it is important to note that compensatory mechanisms could also normalise sensitivity limits across observers (Webster, 2015).

For participants with normal ocular health, neither optical nor retinal factors can

reliably predict individual differences in psychophysical performance for visual function associated with early visual cortex, such as contrast detection or orientation discrimination (D. H. Baker, 2013; B. R. Hammond & Buch, 2020; Himmelberg et al., 2022). Although, in patients with macular disease, individual differences on a global orientation-identification task are associated with variations in the severity of structural changes due to accumulated retinal fluid (Fu et al., 2017).

Cortical variation

Typical orientation-discrimination thresholds range from 0.5 to 2.5° for cardinal orientations, and range from 2 to 8° for obliques (Vogels et al., 1984; Westheimer & Beard, 1998). Individual differences in orientation-discrimination performance likely arise from variations in orientation-selective neural populations in early visual cortex. In support, the extent of learning on an orientation-discrimination task was correlated with training-specific increases in the orientation-selective responses of voxels in human V1, V2 and V4 (Jehee et al., 2012). Orientation-discrimination performance for oblique orientations is also correlated with resting concentration levels of GABA in visual cortex (Edden et al., 2009), suggesting that the strength of inhibitory circuits is important for the precision of orientation encoding. This is consistent with the broadening of orientation tuning upon the application of $GABA_A$ antagonists in cat V1 (Eysel et al., 1990; Sillito, 1975), and the associated reduction of cross-orientation suppression (Morrone et al., 1982).

Development

Despite large individual differences in visual capacity, the oblique effect seems to be a ubiquitous property of the visual system. For example, from the investigations of orientation discrimination described in Section 1.3.3, every single participant displayed an oblique effect.

The oblique effect is hypothesised to reflect the higher proportion of cardinal orientations, than obliques, in natural images (Coppola, Purves, et al., 1998; Girshick et al., 2011; Keil & Cristóbal, 2000), suggesting that differences in visual experience could guide inter-individual variation in the visual pathways. This is supported by evidence of stripe-reared kittens that developed an overrepresentation of the experienced orientation in striate cortex (Sengpiel et al., 1999). However, many individual stripe-reared kittens revealed no such anisotropy, suggesting that visual experience is not the sole factor in the generation of the oblique effect. The absence of an overrepresentation of cardinal-tuned neurons is often reported in individual animals, despite the average data indicating the presence of substantial anisotropies (Coppola, White, et al., 1998; Ju et al., 2021; G. Shen et al., 2014).

Although the development of the visual system may be shaped by the orientation statistics of visual experience, which is generally common across observers, it is likely that genetic and physiological factors mediate individual differences in anisotropic visual function. For example, individual differences in resting levels of GABA are correlated with the size of the oblique effect for orientation discrimination (Edden et al., 2009), suggesting a role for cortical inhibition in generating the oblique effect. However, individual differences in the oblique effect have received little attention, however these may provide insight into the mechanisms of the underlying neuronal anisotropy.

1.6.2 Assessing individual differences

Group-level differences are the most commonly assessed individual differences. Typically, differences between groups of individuals are assessed through comparisons of the 'standard observer' (i.e., the average dataset) for each group. However, a focus on overall differences treats potentially meaningful deviations from the norm as expected variations. For

example, the size of the oblique effect for orientation discrimination is larger on average for older adults, relative to younger adults, suggesting that visual experience drives the development of anisotropic perception (Pilz et al., 2020). However, this was not the case for all individuals, and the reason for this deviation from the norm was explored. Identifying common factors for performance differences between individuals may serve as a powerful tool to identify common or dissociable mechanisms of visual function (Emery et al., 2017; Grzeczkowski et al., 2017; McGovern et al., 2017; Shavit et al., 2013; Witzel et al., 2017), validate methodologies with similar aims (Meinhardt et al., 2019; Thurman et al., 2016), guide experimental hypotheses (Bosten et al., 2017), and potentially to inform flexible parameters for computational models.

There is an important distinction to be made between the measured inter-observer variation in data, and 'true' individual differences that reflect variations in the structural and functional properties of the visual pathways (Mollon et al., 2017). Measured inter-individual variation arises from a combination of 'true' individual differences and various sources of measurement error, including differences in overall performance, internal noise state (i.e., random variability), attentional state, and response criteria. Additionally, although the typical equipment used in vision science is precisely calibrated, there are inevitable fluctuations across time and testing sessions. For example, the gamma function of traditional cathode-ray-tube (CRT) displays used in vision experiments, which characterises the relationship between its input voltage and its output luminance, varies systematically with the total operating hours (Mollon & Baker, 1995). This introduces another potential extrinsic source of variability into measurements on visual tasks.

Time-varying sources of variance can influence task performance from one testing session to another, such as 'state' factors (e.g., physical health, fatigue, and mood). Specific

time-dependent factors have been formally studied, such as the impact of 'very-long-term' chromatic adaptation on colour perception (Belmore & Shevell, 2008), fluctuations in contrast sensitivity associated with the circadian rhythm (Andrade et al., 2018), or changes in motion discrimination-thresholds throughout the 'migraine cycle' (Shepherd, 2020). A clear demonstration is the positive correlation between the strength of an audiovisual illusion, 'the McCollough effect', and the amount of sleep participants had the previous night (N. J. Lund & MacKay, 1983). This indicates, ideally speaking, that experimental data collection and subsequent measures of reliability should be taken across testing sessions broken up into chunks across multiple days.

There are design choices that can minimise sources of measurement error. For example, systematic variations in task performance due to order effects can be reduced by randomising the order of testing and by implementing counterbalancing. To control for individual differences in visual capacity (e.g., level of visual performance), a visual stimulus can be standardised across participants in order to isolate desired neural mechanisms. For instance, stimulus visibility can be equated by setting stimulus contrast in multiples of individual observers' detection thresholds (Delahunt et al., 2008). This is crucial for investigations of mechanisms which are dependent on stimulus contrast, especially considering the vast individual differences exhibited for measures of contrast sensitivity (Hawkins et al., 2003; Himmelberg et al., 2022; Thurman et al., 2016) and suprathreshold contrast discrimination (Vilidaite & Baker, 2017). Similarly, the scale of cortical magnification across the visual field can be controlled for by scaling stimulus size as a function of eccentricity (Pointer, 1996; Rovamo & Virsu, 1979).

Alternatively, relative measures of visual function control for individual differences in visual capacity by normalising the scale of measurement. For example, the 'oblique effect

index' (OEI) is a ratio measure that quantifies the size of the oblique effect for each participant, by dividing performance measures for the obliques by those for the cardinals (Westheimer, 2003a). This enables the comparison of oblique effect magnitude between individuals or groups, and across various psychophysical tasks (Westheimer, 2003, 2017).

1.6.3 Stability of individual differences

Between-groups

Between-groups assessments of reliability in large samples can be used to evaluate the consistency of group-level estimates (i.e., the average performance) across different participant populations. For instance, performance on a series of visual, cognitive tasks was similar for independent cohorts of university students who were measured at either the start, middle, or end of an academic term (Chan et al., 2017). This form of reliability is important for clinical assessments of visual function, such as measures of visual acuity (Lupión Durán et al., 2021; Rubin, 1993; Tsou & Bressler, 2017), to ensure that the measured differences between clinical and control populations reflect 'true' differences between the two groups.

Within-groups

Measurement noise is inevitable for psychophysical measurements of visual function. If variations in performance reflect 'true' individual differences, then the same participants should reproduce the same (or similar) data across multiple testing sessions. Assessments of agreement can be implemented to quantify the measurement error that may occur in a given testing session. Additionally, assessments of agreement can be used to quantify the extent to which two separate measures capture the same underlying property of visual function. For instance, one study reported good agreement between two measures of visual acuity (the 'Kay picture test' and the 'logMAR crowded test') in paediatric subjects (D. Jones et al., 2003).

Reliability analyses

The overall relationship between individual differences on two separate tasks can be quantified by the correlation coefficient. However, this statistic can only assess the degree of a linear relationship between measurements, meaning that this statistic is unsuitable for assessments of agreement. It is also highly dependent on the variability between subjects, whereby larger correlation coefficients are obtained from samples with greater individual differences (McAlinden et al., 2011). In other words, highly precise measurements that are consistent across participants, will generate a lower correlation coefficient than 'noisier' measures of the same property. Correlational analyses also provide no information about the stability of individual differences at the one-to-one level, the precision of estimates, and are insensitive to systematic biases between measures. For example, parameter estimates for one method of measurement could be twice as large and twice as variable as the other, yet the correlation coefficients would be relatively unaffected (McAlinden et al., 2011).

The limits of agreement method was developed as an alternative to correlational approaches (Bland & Altman, 1986, 1999), and has been used extensively in the assessment of agreement for clinical measures (for review, see McAlinden et al., 2011). This method is also appropriate for evaluating the stability of individual differences across testing sessions. Bland-Altman analysis estimates the systematic bias between two measures, and generates 95% confidence intervals (i.e., limits of agreement) for the one-to-one differences between measurements. This approach appears to be well-suited to the of study individual differences in psychophysical tasks (Eisen-Enosh et al., 2017; Klein & Birch, 2009; Vancleef et al., 2017), such as investigations of orientation perception, and should be utilised in future research in this area.

1.7 Unresolved issues

Orientation anisotropies in the visual pathways cause oblique orientations to be encoded less precisely than cardinal orientations, i.e., the oblique effect. However, the neuronal mechanisms underlying the oblique effect remain unclear, with little scrutiny of classical accounts. Computational models of orientation coding are inspired by decades of psychophysical and neurophysiological research, and can serve as tools for testing explicit hypotheses about visual function. Overall, this thesis aims to use a combination of psychophysical techniques and computational modelling to test predictions about anisotropic visual function, informed by previous psychophysical (see Section 1.3) and neurophysiological (see Section 1.4) work. The aims of each experimental Chapter within this thesis are outlined below.

Chapter 4 — The oblique effect for contrast sensitivity occurs only at high spatial frequencies (Campbell et al., 1966), however the mechanisms underlying this effect are unclear. Additionally, there are suggestions that stimulus contrast may modulate anisotropic orientation perception (Bloem & Ling, 2017b). The classical view of the oblique effect is that an overrepresentation of cardinal-tuned neurons in early visual cortex generates anisotropic performance in various visual tasks, however this claim remains to be formally tested. Chapter 4 aims to measure the behavioural oblique effect for contrast detection and orientation discrimination, whilst varying spatial frequency and contrast, and to subsequently capture these data with a biologically-inspired population-coding model.

Chapter 5 — There are no psychophysical investigations which directly measure the relative number of cardinal-tuned and oblique-tuned mechanisms serving visual perception.

Furthermore, previous psychophysical estimates of orientation bandwidths used methodologies that were prone to confounds, such as 'off-channel looking' (Hutchinson & Ledgeway, 2004), and used contrast-detection tasks which may recruit distinct mechanisms to visual perception (Regan & Beverley, 1985). Using established psychophysical techniques (Richards, 1979; Serrano-Pedraza et al., 2013), Chapter 5 investigates the response characteristics of the mechanisms underlying visual function, with a view to testing model predictions from the previous Chapter.

Chapter 6 — The development of a cardinal bias in orientation perception is proposed to be driven by the anisotropic orientation statistics of natural visual scenes (Girshick et al., 2011). Consistent with this, the oblique effect has been reported for visual tasks which are seemingly independent of the initial encoding of visual orientation (Gentaz et al., 2008). Orientation anisotropies in visual short-term memory have been proposed (Heeley & Buchanan-Smith, 1992; Westheimer, 2003a), however methodological limitations of previous work prompts further investigation (see Section 1.3.5). Although higher-order visual biases are well documented, they have typically not been tested using objective, psychophysical procedures. Chapter 6 aims to elucidate interactions between the oblique effect and cognitive factors, such as visual short-term memory, attentional load, and internal representations of visual orientation.

Chapter 7 (see Covid Impact Statement) — The oblique effect is assumed to be a ubiquitous phenomenon of the human visual system, but this remains to be demonstrated empirically in large samples of participants. Additionally, individual differences in the extent of anisotropic perception have been overlooked in investigations of the oblique effect.

Chapter 7 investigates the size and stability of individual differences for the oblique effect, in two versions of an orientation-identification task. Additionally, the suitability of the web-based testing protocol will be assessed.

2. General methods

In this Chapter, the methodological approaches used throughout this thesis are described. Unless stated otherwise, the information below presented applies to all subsequent experimental chapters. Variations across experiments are given in the corresponding sections.

2.1 Participants

All participants had self-reported normal or corrected-to-normal vision. Informed consent was given by all participants. All experimental procedures complied with the Declaration of Helsinki, and were approved by the local ethics committee (School of Psychology, University of Nottingham, UK).

2.2 Apparatus

Laboratory experiments were run on an *Apple Macintosh* computer and presented on a 20-inch CRT monitor (*iiyama Vision Master Pro 514*) with a refresh rate of 60 Hz, display resolution of 1152 x 870 pixels, and a maximum luminance of 52.24 cd/m^2. Monitor luminance output was carefully linearised through photometric gamma correction (*Minolta LS110 Luminance Meter*). Precise control over luminance resolution was achieved by a widely used dithering algorithm, the 'noisy-bit method' (Allard & Faubert, 2008). Testing was conducted in a darkened, quiet room. The viewing distance was fixed by means of a chinrest. Stimulus generation, presentation, and response collection were achieved using *PsychoPy* (Peirce et al., 2019) and custom written Python code.

2.3 Monitor calibration

2.3.1 Gamma correction

Luminance intensities for each colour channel (red, green, blue) are determined by their input voltage, which is converted from integer digital-to-analogue (DAC) values ranging from 0 to 255. However, the measured luminance output of CRT monitors does not change in a linear fashion with corresponding changes in the DAC values (Figure 2.1). To rectify this, the luminance output of the monitor was linearised using gamma correction. To achieve this, the output luminance values were measured using a photometer for eight uniformly sampled DAC values, from 0 to 255. Measured luminance values for each colour channel were fit by a gamma function, given by

$$L(V) = a + kV^{\gamma}$$

Equation 2.1

Where V is the input voltage (nominally scaled from 0 to 1), a is the minimum measured

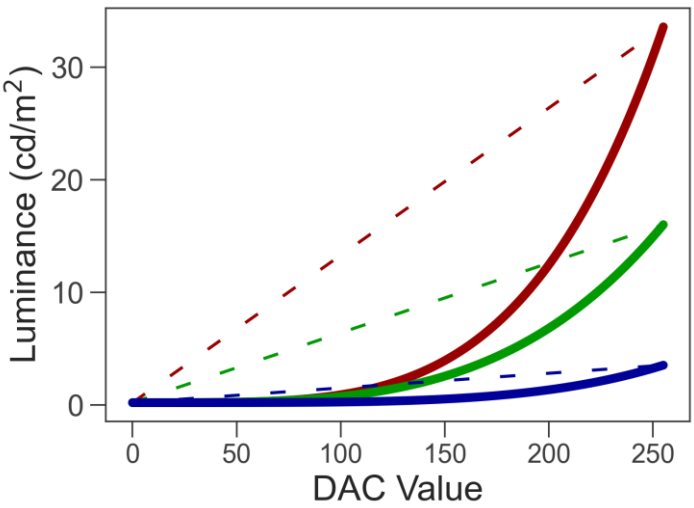

Figure 2.1. Luminance values for the red, green, and blue guns of the CRT monitor (*solid lines*) are plotted alongside the measured luminance values after gamma correction (*dashed lines*).

luminance value, k is the gain, and γ is the gamma value. This commonly used form of gamma correction assumes that the monitor itself does not contribute significantly to a (Peirce et al., 2019). The inverse gamma function was used to build a look-up table (LUT) for all values of V (desired luminance values) that correspond to linearised output luminance values,

$$LUT(V) = V^{1/\gamma}$$

Equation 2.2

Where V is the entry in the LUT between 0 ('black') and 1 ('white'). The quality of gamma correction was confirmed by repeating the initial measurements with the gamma-corrected values. Additionally, γ varied as a function of the total operating time of the monitor (Figure 2.2). All data collection was completed with a minimum total operating time of three hours, after which variation in γ was minimal (Metha et al., 1993).

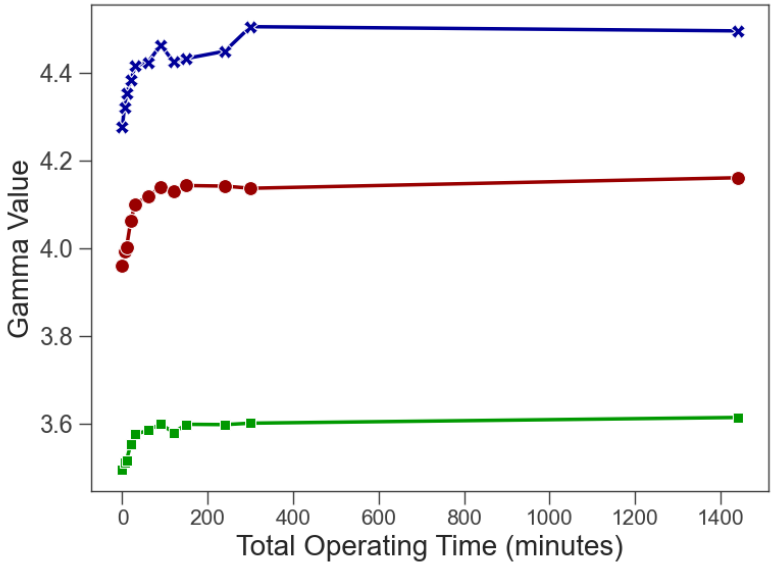

Figure 2.2. Measured gamma values for the red, green, and blue guns of the CRT monitor as a function of the total operating time of the monitor.

2.3.2 Noisy-bit method

As mentioned above, desired luminance intensities (input voltages) are converted from DAC values prior to stimulus presentation. Typically, this is achieved by rounding the desired luminance values to an integer scale, typically from 0 to 255. This is an issue for experimental procedures that require precise control of stimulus contrast, especially for measures of contrast sensitivity where detection thresholds are often around 1% Michelson contrast (for review, see Pelli & Bex, 2013).

The 'noisy-bit method' is a random dithering method that involves choosing between the two DAC values nearest to the desired luminance value, on each frame, according to a probability distribution (Allard & Faubert, 2008). The probability of choosing either the upper or lower DAC value is given by

$$P\left(V = r_{upper}\right) = r \,\%\, 1$$

$$P(V = r_{lower}) = 1 - (r \,\%\, 1)$$

Equation 2.3

Where r is the continuous DAC value,% is the modulo operator, $r\%\ 1$ is the remainder (fractional part or mantissa) of r, and the two nearest DAC values to r are given by r_{upper} and r_{lower}. For example, if the desired luminance value for a pixel was 130.75, the probability of choosing 131 on each frame would be 0.75, and the probability of choosing 130 would be 0.25, thus resulting in an expected value of 130.75. Although the noisy-bit method introduces error between the desired and displayed luminance values, this is imperceptible at the relatively high image update rates and spatial resolutions used for displays in psychophysical experiments. The noisy-bit method is perceptually equivalent to displaying continuous luminance intensities, and has no significant impact on measures of contrast sensitivity (Allard & Faubert, 2008).

2.4 Stimuli

The measurement of Michelson contrast captures local luminance changes in simple stimuli used throughout this thesis, such as gratings (Kukkonen et al., 1993). Therefore, visual stimuli are described in terms of their Michelson contrast (%):

$$C = 100 \cdot \frac{I_{max} - I_{min}}{I_{max} + I_{min}}$$

Equation 2.4

Where I_{max} and I_{min} represent the maximum and minimum luminance values of the stimulus, respectively. The luminance range of the monitor was 0.26 to 52.24 cd/m^2, giving a maximum Michelson contrast of 98%, however reported contrast values will refer to the coded Michelson contrast nominally ranging from 0 to 100%.

All stimuli were constructed by multiplying a given pattern with a specified Gaussian envelope (Figure 2.3). The amplitude of the Gaussian envelope defines the Michelson contrast, and the space-constants (standard deviation, σ^2) in the x and y directions determine the spatial dimensions of the stimulus. Stimulus size is described in degrees of visual angle,°. Gabors and one-dimensional (1D) noise stimuli were presented within a Gaussian window with symmetric x and y space-constants of 1.33°. Gaussian smoothing of contrast at stimulus edges is done to minimise the abrupt luminance transients associated with the effects of 'stimulus vignetting' (see Sections 1.3.3 and 1.5.2). Stimulus orientation was manipulated

using rotation and interpolation algorithms available in *PsychoPy* (Peirce et al., 2019).

Gabors are the product of a sine wave and a Gaussian envelope (Figure 2.3A), where the spatial frequency is defined by the number of cycles per degree of visual angle (c/°). Luminance values were uniformly sampled from the sinusoidal waveform at a minimum of 4 pixels/cycle, ensuring that the minimum and maximum luminance value were always sampled. Upon each stimulus presentation, the phase was randomised between 0 and 0.5 λ (shifting the sinusoid by half of a cycle) to minimise the influence of luminance artifacts and prevent local adaptation across trials. The narrowband spatial profile of Gabors closely

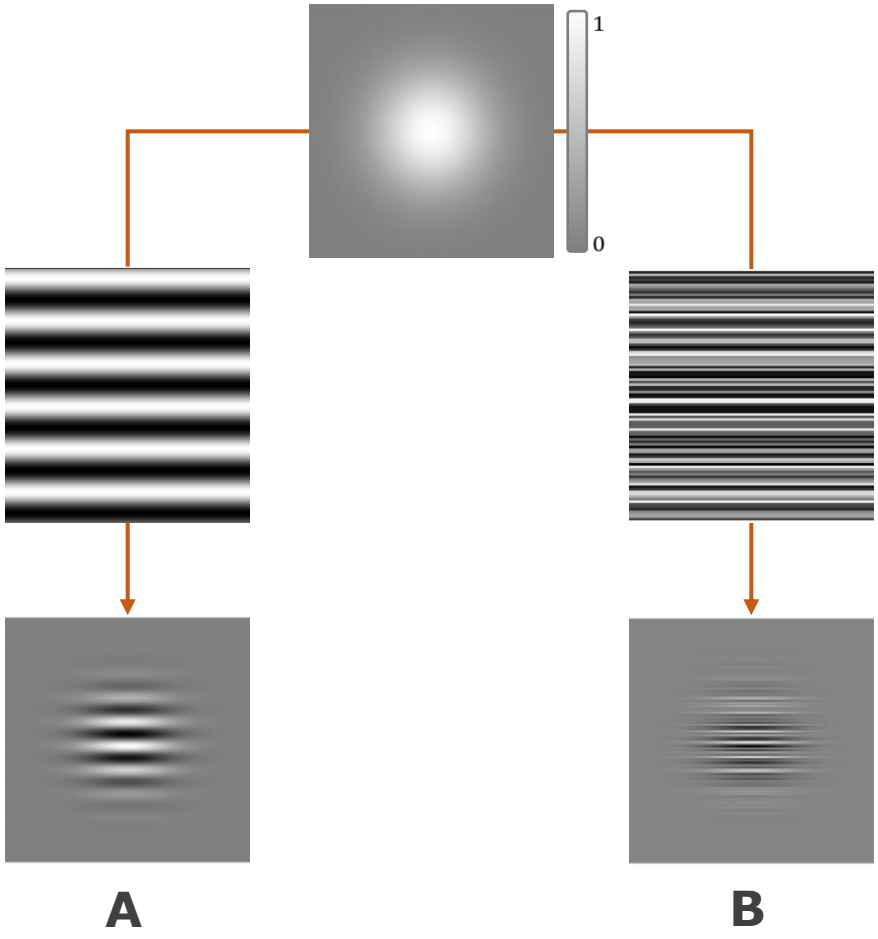

Figure 2.3. Sinusoidal gratings (*A*) and one-dimensional noise patterns (*B*) were multiplied with a two-dimensional Gaussian function (from 0 to 1), causing a smooth drop-off in contrast towards the stimulus edges.

resembles that of simple cell receptive fields (Daugman, 1984), therefore the orientation and spatial frequency (c/°) of Gabor stimuli were manipulated to probe feature-selective channels of the visual system (see Section 1.2).

1D-noise stimuli are the product of a 1D-noise pattern and a Gaussian window (Figure 2.3B). 1D-noise is constructed by uniformly sampling luminance values from a single cycle of a sinusoid (from -1 to 1), and then randomising the order of luminance values. The number of sampled luminance values is defined by the stimulus size in pixels. 1D-noise gratings have a narrowband orientation spectrum and a broadband spatial frequency spectrum, which was desired to minimise 'off-channel looking' in the spatial frequency domain during visual masking (Hutchinson & Ledgeway, 2004).

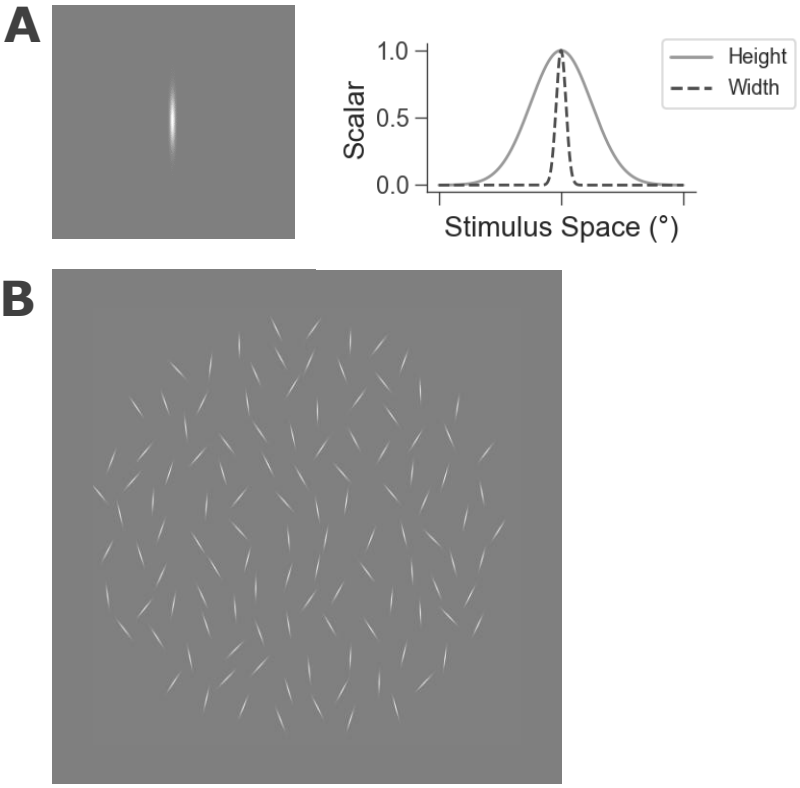

Figure 2.4. Each line stimulus was constructed as a two-dimensional Gaussian function with asymmetric space-constants (*A*). Arrays of lines are composed of numerous non-overlapping lines (*B*).

Individual line stimuli were constructed from two orthogonally orientated Gaussians, with respective space-constants that determined the height and width of lines (Figure 2.4A). Luminance values ranged from 0.5 to 1 (from 'mid-grey' to 'white'). Arrays of lines consisted of individual lines of equal length presented within a defined circular region (Figure 2.4B). Individual lines could not overlap, such that the spatial separation between the mid-points of lines was equal (at least) to the line length. Across trials, the absolute positions of lines varied in a random fashion. Other manipulations, including adjustments to the distribution of line orientations, line length, and the number of lines, are described in Section 5.1.

2.5 Adaptive staircase

The adaptive staircase procedure involves adjusting the value of a stimulus parameter until a stimulus feature is just-detectable or just-discriminable about an arbitrary threshold. The 'staircase value' (the value of the adjusted parameter) is determined by the participant's previous responses. A '3-down 1-up' adaptive staircase procedure was used in this thesis, designed to converge on the staircase value corresponding to 79.4% correct (H. Levitt, 1971). Upon every three consecutive correct responses, the staircase value was adjusted to make the task more difficult, whereas the staircase value was adjusted to make the task easier upon each incorrect response. Increments and decrements in the staircase-value were set on a log-scale:

$$s_{up} = s \cdot 10^{n}$$

$$s_{down} = s/10^{n}$$

Equation 2.5

where s is the staircase-value and n is the coded step size. For example, a step size of 0.18 roughly equates to a 50% increase or decrease from the preceding staircase value. Step

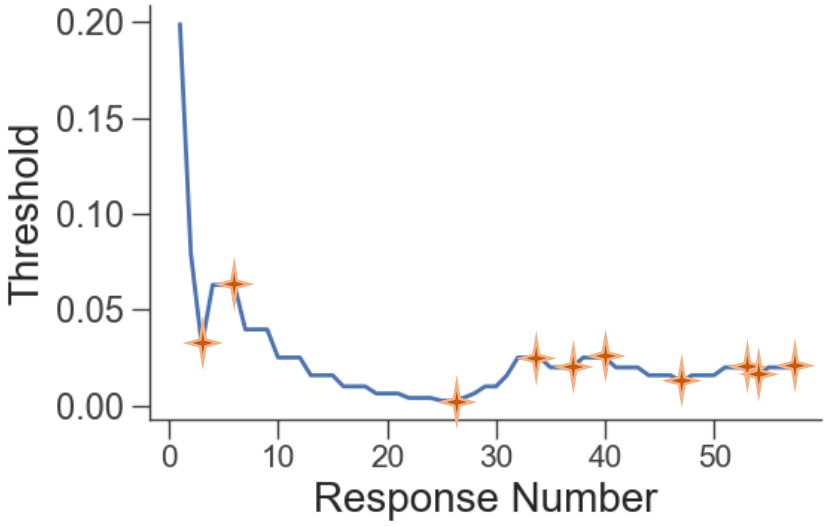

Figure 2.5. The staircase value converges around the threshold value with an increasing number of responses. Thresholds are calculated as the arithmetic mean staircase value from the last five reversals (*orange crosses*).

sizes were gradually reduced upon each 'reversal' so that the staircase converged on the threshold value (Figure 2.5). A reversal occurred whenever the direction of the staircase (i.e., ascending or descending) changed. The staircase value preceding each reversal was recorded, and each run stopped after ten such reversals. The threshold was calculated as the arithmetic-mean of the last five reversals. Substantial deviations from threshold can occur due to chance, response error, lapses in attention, etc. and therefore each staircase procedure was repeated for a minimum of four runs before the arithmetic-mean threshold (across runs) was calculated.

2.6 Method of constant stimuli

The 'method of constant stimuli' involves repeated presentations of a stimulus, where the chosen stimulus parameter is defined from a predetermined set of values, or 'stimulus levels'. Whenever this method was used, pilot data were collected to ensure that the range of chosen levels adequately captured the full performance ranges of participants, from 50% (chance-level responding) to approaching 100% correct. Stimulus levels were presented in a randomised fashion during each run, so as to minimise confounding influences of testing order. There was a minimum of ten repeats for each level in a given run. The proportion correct for each level was used to construct a psychometric function, with the proportion correct on the y-axis and the stimulus level on the x-axis (Figure 2.6). A logistic curve was fit to the psychometric function:

$$f(x) = 0.5 + \frac{0.5}{1 + \exp(-(x - x_0)/k)}$$

Equation 2.6

where k determines the slope of the curve, and x_0 is the midpoint of the curve taken as the threshold, i.e., the stimulus level corresponding to 75% correct.

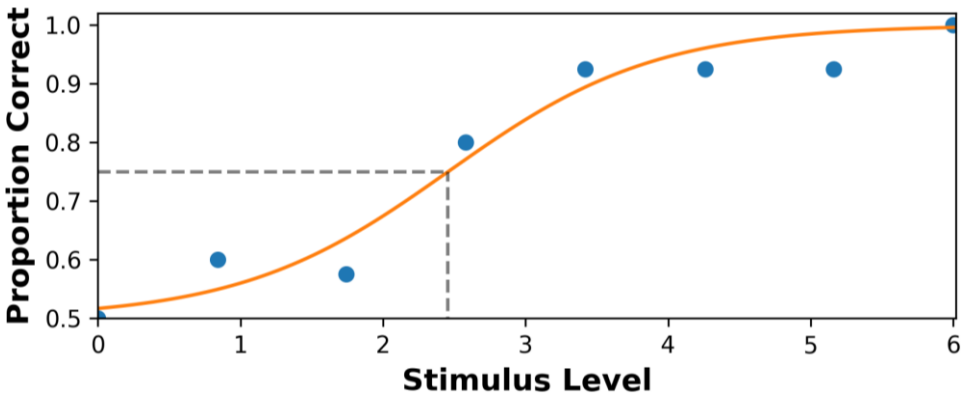

Figure 2.6. Logistic curve (*orange line*) fit to the psychometric function (*data points*) to calculate the threshold, taken as the stimulus level corresponding to 75% correct performance (grey-dotted line).

2.7 Bandwidth estimation

In Section 5.1, the bandwidths of orientation channels are estimated from thresholds for various levels of orientation difference between two masks. These bandwidths are determined from a Gaussian function that is fit to the data (Figure 2.7):

$$f(x) = a \exp\left(-\frac{(x-\mu)^2}{2\sigma^2}\right) + b$$

Equation 2.7

where μ is the mean, σ^2 is the standard deviation, a is the amplitude (maximum value - minimum value), and b defines the minimum value of the curve. The minimum value b is set to the threshold obtained in the absence of masking stimuli. The orientation bandwidth of a tuning curve is described by the distance in orientation angle between the points of the curve that correspond to half of the peak value (i.e., full-width half-max, FWHM). This can be approximated by multiplying the standard deviation σ^2 by $8 \ln 2$ (Graham, 1989).

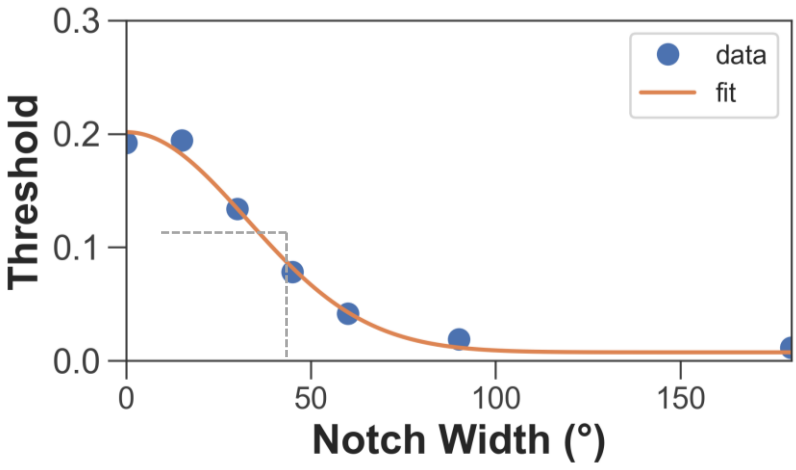

Figure 2.7. Gaussian curve (*orange line*) fit to the psychometric function (*data points*) to provide an estimate of the orientation bandwidth (full-width half-max). The half-width half-max is depicted by the grey dotted line.

To evaluate the reliability of bandwidth estimates for data fit with the Gaussian function described in Equation 2.7, the same data were also fit with a cosine function.

$$f(x) = A\cos(Bx + C) + D$$

Equation 2.8

Where A is the amplitude of the cosine wave (maximum value – minimum value), D defines the minimum value of the function, B determines the period of the cosine wave (equal to $2\pi/B$), and C is the phase shift which determines where in its cycle the cosine starts. The orientation bandwidth was given as the full-width half-max.

2.8 Oblique effect index

The 'oblique effect index' (OEI) is a ratio measure that quantifies the size of the oblique effect whilst controlling for individual differences in overall performance (Westheimer, 2003):

$$\mathrm{OEI} = \frac{-45°_T + 45°_T}{0°_T + 90°_T}$$

Equation 2.9

Where subscript T denotes a threshold value for a given orientation. Values above one indicate the presence of an oblique effect and quantify its magnitude, whereas values below one reflect an inverse oblique effect. For example, an OEI of 3.5 mean that the average threshold for oblique orientations was 3.5 times larger than that for cardinal orientations.

When calculating the average OEI score across participants, the geometric mean is used:

$$\overline{\mathrm{OEI}} = \exp\left(\frac{1}{n}\sum_{i=1}^{n} \ln \mathrm{OEI}_i\right)$$

Equation 2.10

This is preferred to the arithmetic mean as it accounts for differences on a ratio scale. For example, the arithmetic mean for OEI scores of 0.5 and 2 is 1.25 despite these scores being the reciprocal of each other. In contrast, the geometric mean would be 1. In general, the arithmetic mean tends to overestimate the mean value of scores on a ratio scale.

2.9 Reliability analyses

Assessments of reliability typically involve quantifying the consistency between two measurements of the same underlying property. Group-level reliability can be assessed by comparing the descriptive statistics of independent samples, whereas reliability at the individual-level can be described by the absolute agreement between repeated measurements of the same property (e.g., thresholds on two versions of the same task). Although correlational approaches are useful for establishing the strength of linear relationship between two independent variables, they are typically insensitive to the absolute agreement between individual measurements (McAlinden et al., 2011). For example, one measurement method could systematically overestimate thresholds relative to another, yet this would not impact the Pearson's correlation coefficient, which is independent of the intercept. Similarly, noisy measurements would lower the level of absolute agreement without necessarily impacting the Pearson's correlation coefficient (McAlinden et al., 2011).

The 'limits of agreement method' is an alternative to correlational approaches (Bland & Altman, 1986, 1999) that is widely used in the assessment of agreement between measurement methods (Giavarina, 2015). Bland-Altman plots show the differences between values from two measurement methods plotted against the average values (Figure 2.8A). The y-axis thus reflects the agreement between measurements, whereas the x-axis represents the magnitude of measurements. A difference score (y-axis) of zero indicates perfect agreement between measurement methods, whereas values extending above or below 0 indicate the

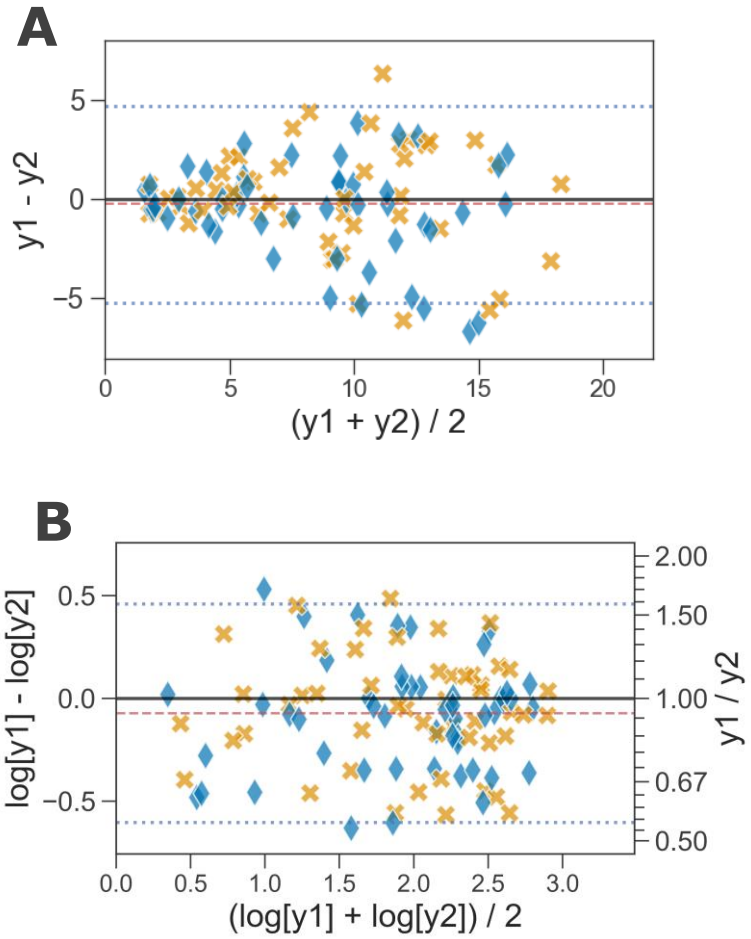

Figure 2.8. The differences between two measurements are plotted against the means for normal data (*A*) and log-transformed data (*B*). The mean difference (*red dashed line*) reflects the systematic error, and the limits of agreement (*blue dotted lines*) quantify the overall agreement between measurements.

direction and extent of deviation from perfect agreement. For example, two measures with high levels of agreement will generate data that is tightly clustered about zero on the y-axis.

The mean of the difference scores across all participants is an estimate of the systematic bias between measurement methods. For example, consider two measurement methods A and B. When assessing the difference scores $(A - B)$, a mean-difference score above 0 indicates the systematic overestimation of method A relative to B, and values below 0 indicate the underestimation of method A relative to B.

The limits of agreement ($\text{mean difference} \pm 1\text{SD} * 1.96$) provide 95% confidence intervals of the mean-difference score, with stronger reliability reflected in smaller limits of agreement. The average level of agreement (i.e., the typical variation between measurement methods) can be quantified by the median of the absolute differences between two measures, e.g., the median of $|A - B|$.

If there is a proportional relationship between the variance of difference scores (i.e., the spread along the y-axis) and the magnitude of measurements (Figure 2.8A), then Bland-Altman analyses should be performed on the log-transformed measurements (Figure 2.8B) and the limits of agreement should be calculated on a log-scale (Bland & Altman, 1999). Exponentiation of the log-transformed difference scores allows them to be examined on a ratio-scale, where a value of 1 indicates perfect agreement. In this case, the median absolute-difference score can be exponentiated to give the median 'absolute-ratio' score. For example, a median 'absolute-ratio' score of 1.2 would reflect an average change of 20% between measurement methods. All log-transformed data presented in this thesis were confirmed not to violate the assumption of normality by Shapiro-Wilk tests.

2.10 Web-based testing

An orientation-identification task was adjusted for web-based testing (see Covid Impact Statement). The web-based experiment was designed in *PsychoPy* and run through *Pavlovia*, a web-based testing platform (Peirce et al., 2019), with custom JavaScript code. Participants used their own devices and web-browsers to run the experiment. They were asked to sit in a quiet, dimly lit room with no visual distractions (e.g., flashing lights), set their screen brightness to its maximum, turn off any blue-light filters, and adjust the volume of their device to ensure that it was clearly audible. The particular devices used were not recorded. Participants were instructed to maintain a fixed viewing distance from the screen (for example, by cutting a piece of string to length and adjusting their seating position to ensure that the ends of the string, when taut, just touched both the display and the bridge of the nose). Participants also input the width, in cm, of the visible (active) portion of their visual display, and the spatial resolution of each participant's full-screen browser window was retrieved. This made it possible to standardise the size and spatial frequency of Gabor stimuli across different visual displays. The reliability of the web-based testing protocol was assessed using Bland-Altman analyses to evaluate the level of agreement between web-based and lab-based measurements.

3. Modelling

Information about the orientation of a visual stimulus is thought to be encoded by ensembles of orientation-selective neurons (J. Freeman et al., 2011). To understand how orientation anisotropies in neural encoding could result in a behavioural oblique effect, this thesis presents a biologically-inspired computational model of orientation encoding that is informed by neurophysiological research in mammals, such as macaques. In this model, orientation information is encoded in the population activity of neurons tuned for different orientations, and decoding computations are based on the mean firing rates (spikes/sec) of each neuron. In support of this approach, clear relationships between model parameters of population coding models and psychophysical performance have been established (Goris et al., 2009, 2013; May & Solomon, 2015a, 2015b; Read, 2015; Webb et al., 2007, 2011).

3.1 Population Response

3.1.1 Tuned responses

Orientation-tuning curves (Figure 3.1) were defined by a Gaussian function:

$$\overline{r}(\theta) = r_{max} \exp\left(-\frac{(\mu-\theta)^2}{2\sigma^2}\right) + r_0$$

Equation 3.1

Where $\overline{r}(\theta)$ is the tuned response for a given stimulus orientation θ (where $-90 \leq \theta < 90°$), μ is the orientation preference of a given neuron, σ is the standard deviation, r_{max} is maximum firing rate, and r_0 is the spontaneous firing rate in the absence of stimulation. To handle the circular nature of the data, Gaussian tuning functions were 'wrapped' around orientation space. The wrapped Gaussian was approximately equivalent to the von Mises distribution, such that the variance was low enough that the tails of the Gaussian distribution

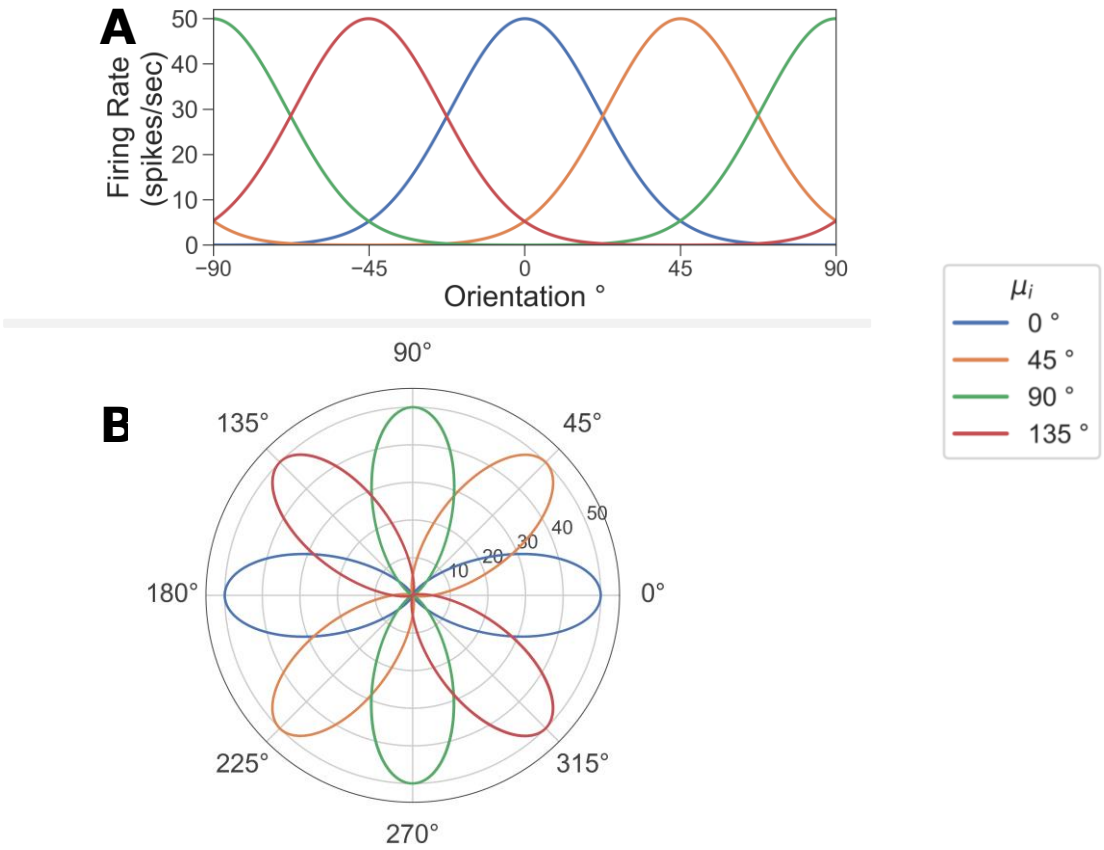

Figure 3.1. Plots of wrapped Gaussian orientation tuning curves, for four model neurons with uniformly distributed orientation preferences (*coloured lines*).

approached zero and thus had negligible impact on wrapping around the circle (Pewsey et al., 2007). The model parameter for orientation bandwidth (full width at half max, FWHM) is denoted as σ_{ori} and was equivalent to the standard deviation σ^2 multiplied by $8 \ln 2$ (Graham, 1989).

Tuned responses were also modulated by stimulus contrast in a manner that is well-described by the Naka-Rushton function (Albrecht & Hamilton, 1982; Naka & Rushton, 1966):

$$\bar{r}(c) = \frac{\overline{r} c^q}{{c_{50}}^q + c^q}$$

Equation 3.2

Where c is the Michelson contrast, the 'semi-saturation constant' c_{50} is the contrast at which

the neural response is equal to half of the tuned response $\bar{r}$, and q defines the shape of the curve.

3.1.2 Internal noise

To simulate the variable firing rates of visual cortical neurons (i.e., internal noise), noisy firing rates were generated by adding noise to the tuned response of each neuron $i = \{1, \ldots, N\}$, on a trial-to-trial basis.

$$r_i = \overline{r}_i + \eta$$

Equation 3.3

Where r_i is the noisy firing rate, calculated by summing the tuned response of each neuron $\overline{r}_i$ with an independent random variable η drawn from a Gaussian distribution centred on zero, given by:

$$f(x|\sigma) = \frac{1}{\sqrt{2\pi\sigma^2}} \cdot \exp\left(-\frac{(x-0)^2}{2\sigma^2}\right)$$

Equation 3.4

Where the standard deviation σ of the distribution in Equation 3.4 is equal to:

$$\sigma = \sqrt{\lambda_F \cdot \overline{r}}$$

Equation 3.5

Such that the scale of noise was proportional to the tuned firing rate and scaled by the Fano factor λ_F (e.g., Raiguel et al., 2006). Consequently, trial-to-trial firing rates for a single orientation had a variance which was proportional to the mean firing rate, and thus approximated a Poisson-like process (Foi et al., 2008). In the absence of a stimulus orientation, the tuned response was determined by the spontaneous firing rate r_0 (see

Equation 3.1). Firing rates were constrained to positive values only, such that $[r_i]_+ = \max(r_i = 0)$.

3.2 Decoding orientation

Estimates of the stimulus orientation θ are decoded from the firing rates of each neuron r_i that comprise the population response R. In terms of the current modelling framework, several well-known decoding ('read-out') algorithms are considered and the characteristics of each will be described in turn. Inspired by labelled line models (Watson & Robson, 1981) the winner-take-all (WTA) decoder is given by

$$\theta_{WTA} = \arg\max R(\theta)$$

Equation 3.6

where θ_{WTA} is the orientation preference of the neuron with the strongest response in the neural population. The winner-take-all decoder is a heuristic method that assumes knowledge only of the preferred orientation of each neuron.

The population vector (PV) decoder assumes that each neuron represents a vector (Georgopoulos et al., 1986; Gilbert & Wiesel, 1990; Vogels, 1990), where the orientation preference μ_i and firing rate r_i reflect the direction and the amplitude of the response vector $\overrightarrow{u_i}$, respectively. The PV estimate θ_{PV} is the vector sum of all neurons:

$$\overrightarrow{\theta_{PV}} = \sum_{i=1}^{N} r_i \overrightarrow{\mu_i}$$

Equation 3.7

This estimator is a linear function of the responses r_i and only requires prior knowledge of the orientation preference of each neuron. For uniformly distributed orientation-preference vectors $\overrightarrow{\mu_i}$, the direction of the population vector $\overrightarrow{\theta_{PV}}$ converges to the stimulus orientation θ

(Georgopoulos et al., 1986; Tanabe, 2013). Increasing the number of response vectors improves the accuracy of the population vector estimate (Tanabe, 2013). Biases in population vector estimates arise for neural populations with non-uniform distributions of orientation preferences, and in the presence of noise correlations between similarly tuned neurons (Salinas & Abbott, 1994; Shadlen et al., 1996; Zohary et al., 1994).

The maximum likelihood (ML) method is a standard statistical approach for obtaining parameter estimates from experimental data. The ML method typically performs better than linear methods for large numbers of neurons and under conditions of low noise (Salinas & Abbott, 1994; Xie, 2002). The ML estimate of orientation is optimal in the sense that it minimises the square of the difference between the orientation estimate θ_{ML} and the stimulus orientation θ. The basis of such statistical inference is Bayes' theorem, which establishes the precise relationship of the probabilities for the stimulus orientation θ and the population response R composed from $\{r_1, \ldots, r_N\}$:

$$P(R|\theta) = \frac{P(\theta|R)P(\theta)}{P(R)}$$

Equation 3.8

The value of $P(R)$ can be omitted because it is a fixed value that does not depend on the stimulus orientation θ. Similarly, $P(\theta)$ is omitted in the current model due to the absence of stimulus priors. This simplifies Bayes' theorem into a proportional relationship:

$$P(\theta|R) \propto P(R|\theta)$$

Equation 3.9

Under the assumptions of Poisson-like variability and the independence of response variability between neurons, the logarithm of the likelihood function $P(R|\theta)$ is a linear combination of the population response (Jazayeri & Movshon, 2006):

$$\log P(R|\theta) = \sum_{i=1}^{N} \log\left(\overline{r}_i(\theta)\right) \cdot r_i$$

Equation 3.10

Where the orientation tuning function of each neuron $\overline{r}_i(\theta)$ determines the weights. Given the population response R, the maximum likelihood estimator chooses the orientation θ that maximises $P(R|\theta)$:

$$\theta_{ML} = \arg\max \log P(R|\theta)$$

Equation 3.11

The neurophysiological plausibility of the ML decoder is questionable, as it requires knowledge of the full conditional probability functions for each neuron in the system. However, ML estimates approximate the quality of encoded information in a neural population, and describe the upper limit of the possible psychophysical performance level given the neuronal parameters (Dayan & Abbott, 2001; May & Solomon, 2015a).

3.3 Detection

Contrast detection tasks involve judgements about the presence or absence of a visual stimulus. Early models of contrast detection proposed a link to the underlying single-cell physiology in primary visual cortex, such that neurons with different feature-selectivities constitute 'mechanisms' (or 'channels') that act as an array of independent linear filters (Campbell & Robson, 1968; Graham, 1977; Kulikowski & Tolhurst, 1973; Watson & Robson, 1981; H. R. Wilson & Bergen, 1979). In these models, detection is determined by comparing either the output of the maximally responsive mechanism or the pooled responses of multiple mechanisms (Graham, 1977; Legge & Foley, 1980; Stromeyer & Klein, 1975). Despite challenges to the generality of these models for suprathreshold vision (Goris et al.,

2013), they have long been successful in accounting for vision at threshold (Graham, 1989; Watson & Ahumada, 2005).

In this model, the 'peak' method refers to detection based on the firing rate of the maximally responding neuron in the population:

$$R = \max R(\theta)$$

Equation 3.12

In contrast, the 'summation' method involves pooling neural responses across all neurons:

$$R = \sum_{i=1}^{N} r_i$$

Equation 3.13

The 'magnitude' method (Quick, 1974; Stromeyer & Klein, 1975) posits that neural responses are still pooled across the entire population, but that the contribution of each neuron is weighted by the magnitude of its response:

$$R = \left[\sum_{i=1}^{N} r_i^q\right]^{\frac{1}{q}}$$

Equation 3.14

Alternatively, signals for detection may be pooled across a limited range of orientation preferences, due to the limited range of lateral connections in visual cortex (Andrei et al., 2019). 'Distance-weighted' pooling in this model is defined by:

$$R = \sum_{i=1}^{N} w_i r_i$$

Equation 3.15

Where the weight w_i associated with the response of each neuron r_i is scaled according to its distance from the stimulus orientation θ:

$$w_i = \exp\left(-\frac{(\mu_i - \theta)^2}{2\sigma^2}\right)$$

Equation 3.16

Where σ^2 is the extent of pooling across neurons according to their orientation preference μ_i.

3.4 Model performance

3.4.1 Orientation discrimination

For a given stimulus orientation across multiple trials, the value of the estimated orientation varies due to stochasticity in the firing rates of model neurons (see Equation 3.3). The accuracy of orientation decoding can be measured by calculating the absolute error between the estimated orientation θ_{est} and the stimulus orientation θ:

$$\varepsilon = |\theta_{est} - \theta|$$

Equation 3.17

Although this provides insight into model performance, decoding errors alone are not directly comparable to data from human observers, where this information must be inferred through task performance. Orientation-selective mechanisms in human observers are often probed

through two-alternative forced choice (2AFC) tasks. This model used analogous 2AFC designs for orientation discrimination and contrast detection, where model decisions are based on the relative population activity across two independent stimulus intervals. This provides a basis for direct comparison with human psychophysical performance (Goris et al., 2013; May & Solomon, 2015a, 2015b; Watson & Ahumada, 2005; Webb et al., 2010).

Throughout this thesis, model performance was assessed using the 'method of constant stimuli' approach (see Section 2.6). This design was chosen as model performance can be assessed for thousands of repeats of each stimulus level at once (i.e., in a single computation). An adaptive staircase method was found to be too computationally intensive for practical use, owing to the dependency of the staircase value on the response of the preceding trial, such that computations could not be performed on multiple repeats of a given staircase level.

For orientation discrimination, the model generated independent estimates of the standard orientation θ_{std} (set to either 0 or 45 º) and the comparison orientation θ_{comp}. The comparison orientation was presented at each level of orientation difference (either clockwise or anticlockwise) from the standard:

$$\text{CLOCKWISE:} \quad \theta_{comp} = \theta_{std} + \theta_{lvl}$$

$$\text{ANTICLOCKWISE:} \quad \theta_{comp} = \theta_{std} - \theta_{lvl}$$

Equation 3.18

Where θ_{lvl} is the level of orientation difference. Clockwise and anticlockwise rotations were used to remove biases that became apparent for smaller numbers of model neurons.

The model decided which of the two decoded orientations was more clockwise or anticlockwise relative to the other:

$$\text{CLOCKWISE:} \quad D_{lvl} = \theta_{comp} > \theta_{std}$$

$$\text{ANTICLOCKWISE:} \quad D_{lvl} = \theta_{comp} < \theta_{std}$$

Equation 3.19

Where D_{lvl} is a binary array of the correct (1) and incorrect (0) responses for a given stimulus level θ_{lvl} that is combined for clockwise and anticlockwise rotations. A psychometric function was constructed from the proportion of correct responses at each level of orientation difference (Figure 3.2). A logistic curve was fit to these data and orientation discrimination threshold was defined as the orientation difference corresponding to 75% correct (see Section 2.6). When comparing model performance to behavioural data from adaptive staircase designs, thresholds were taken at 79.4% correct (Levitt, 1971).

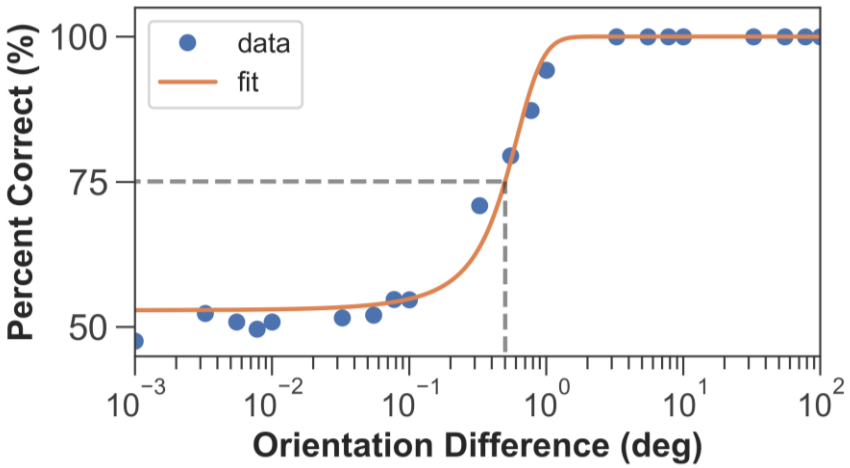

Figure 3.2. Psychometric function and logistic curve fit for the orientation discrimination 2AFC task. The threshold is taken as the orientation difference corresponding to 75% correct performance (*grey dotted line*). The logarithmic x-axis demonstrates the regular sampling of orientation-difference values across a large range.

3.4.2 Contrast detection

In the absence of a stimulus orientation, variability in the firing rates of model neurons was observed due to the constant value of the spontaneous firing rate r_0 in the tuned response of model neurons (e.g., Equation 3.1), along with Poisson-like variability in the trial-to-trial firing rates of model neurons (see Equations 3.3 to 3.5). To measure the capacity of the visual system to detect a visual stimulus at low contrasts, 2AFC contrast-detection tasks are often used (Campbell & Kulikowski, 1966; Mitchell et al., 1967; Watson & Robson, 1981). In the presented model, the pooled population response R is compared between two independent stimulus intervals. One interval presents the stimulus orientation at a given contrast level c_{lvl} and the other presents the stimulus at zero contrast c_0. The model decides which of the two population responses was largest:

$$D_{lvl} = R(c_{lvl}) > R(c_0)$$

Equation 3.20

Contrast-detection thresholds are calculated in the same manner as described above for orientation discrimination.

3.5 Model parameters

3.5.1 Stimulus orientation

For a population of neurons with homogeneous response characteristics, performance for the population vector (PV) and maximum likelihood (ML) decoders is similar, whereas winner-take-all estimates are relatively inaccurate and imprecise. Default model parameters are described in Table 3.1. In this case, the accuracy (absolute error) of orientation estimates is invariant with stimulus orientation (Figure 3.3). Even with just four neurons in the model, deviations for the PV and ML decoders are small, although orientation invariance predictably breaks down for the WTA decoder under this constraint.

Symbol	Value	Comments
$\boldsymbol{N}$	180	Total number of neurons
$\boldsymbol{\sigma_{ori}}$	50	Orientation bandwidth (full-width half-max)
$\boldsymbol{\lambda_F}$	1	Response variability as the Fano factor $\left(\frac{variance}{mean}\right)$
$\boldsymbol{r_{max}}$	50	Maximum firing rate (spikes/sec)
$\boldsymbol{r_0}$	0.03	Spontaneous firing rate as a proportion of r_{max}
$\boldsymbol{q}$	2	Exponent of the Naka-Rushton contrast response function
$\boldsymbol{c_{50}}$	24	Semi-saturation constant of the Naka-Rushton contrast response function

Table 3.1. The 'default' value for each model parameter.

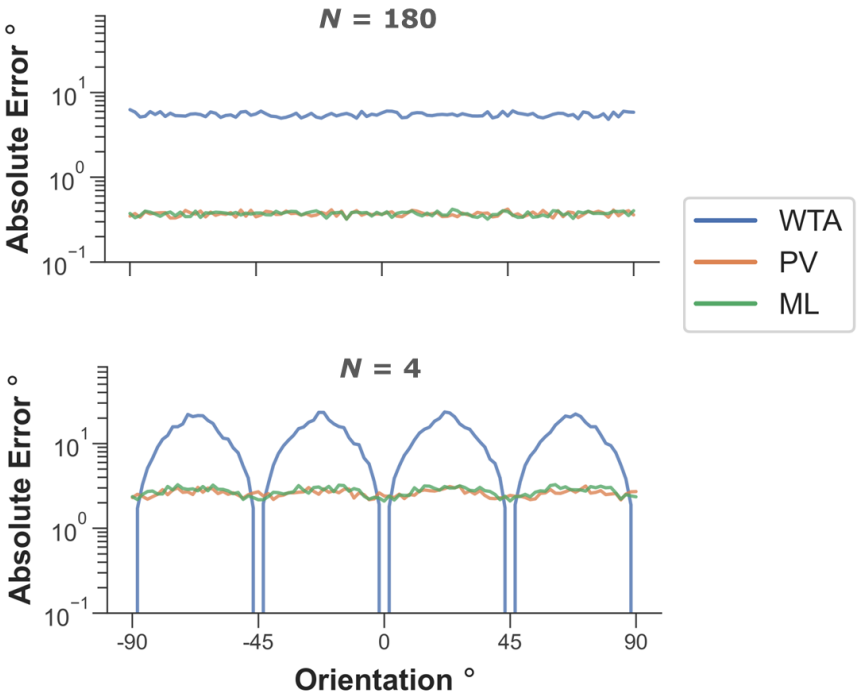

Figure 3.3. Absolute error of orientation estimates across the full range of stimulus orientations for a population composed of either 180 neurons (*top*) or four neurons (*bottom*). Values are jittered to distinguish the performance of each decoder (*coloured lines*).

An invariance to orientation is also found for thresholds measured in the 2AFC orientation-discrimination paradigm (Figure 3.4). This is consistent with previous work which suggests that discrimination thresholds reflect the accuracy and precision of model decoding, as quantified by the Fisher information (May & Solomon, 2015a). In general, there was little trial-to-trial variability in the measured thresholds owing to the high number of levels tested for each threshold measurement (see, Figure 3.2). In the following subsections, model parameters are each manipulated in isolation and model performance for orientation-discrimination and contrast-detection tasks are described for a single standard orientation θ_{std} of 0° and a contrast of 100%, unless stated otherwise. `

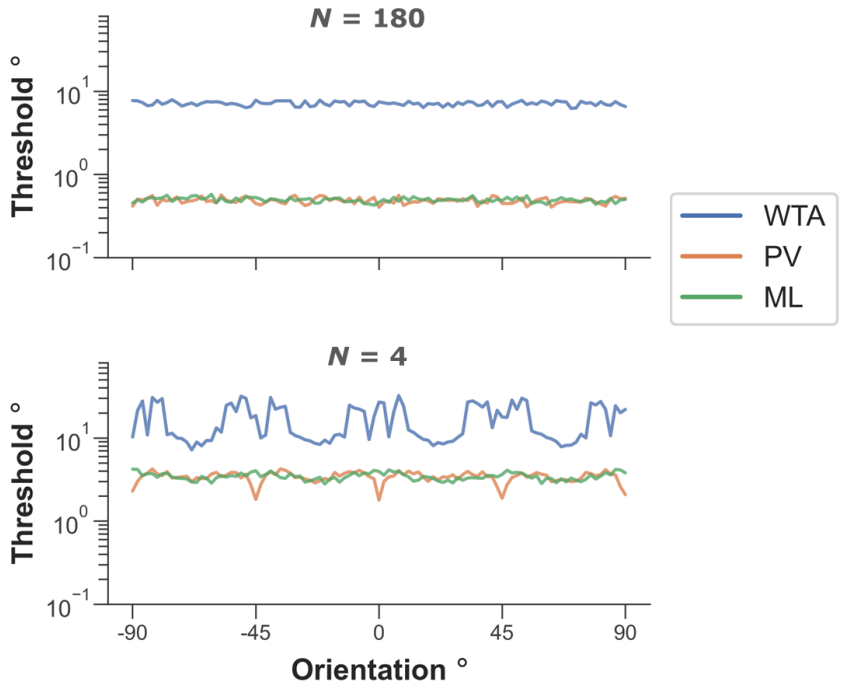

Figure 3.4. Model orientation-discrimination thresholds as a function of orientation for a population composed of either 180 (*top*) or 4 neurons (*bottom*). Values are jittered to distinguish the performance of each decoder (*coloured lines*).

3.5.2 Number of neurons

In V1 and V2, populations of orientation-selective neurons are composed of continuously distributed orientation preferences around orientation pinwheels (J. Freeman et al., 2011; Ohki et al., 2006; Ts'o et al., 1990). This was approximated in the model by uniformly sampling the orientation preference μ_i of each neuron $i = \{1, \ldots, N\}$ for the full range of orientations, 180°, such that $\mu_i = \frac{180}{N} \cdot i$.

Increasing the total number of neurons N in the model continually improved orientation-discrimination performance for the PV and ML decoders (Figure 3.5), however improvement for the WTA decoder was limited. Contrast-detection performance was remarkably unaffected by the total number of neurons N (Figure 3.6), with around a 15% reduction in detection threshold when doubling N. The default value for the total number of

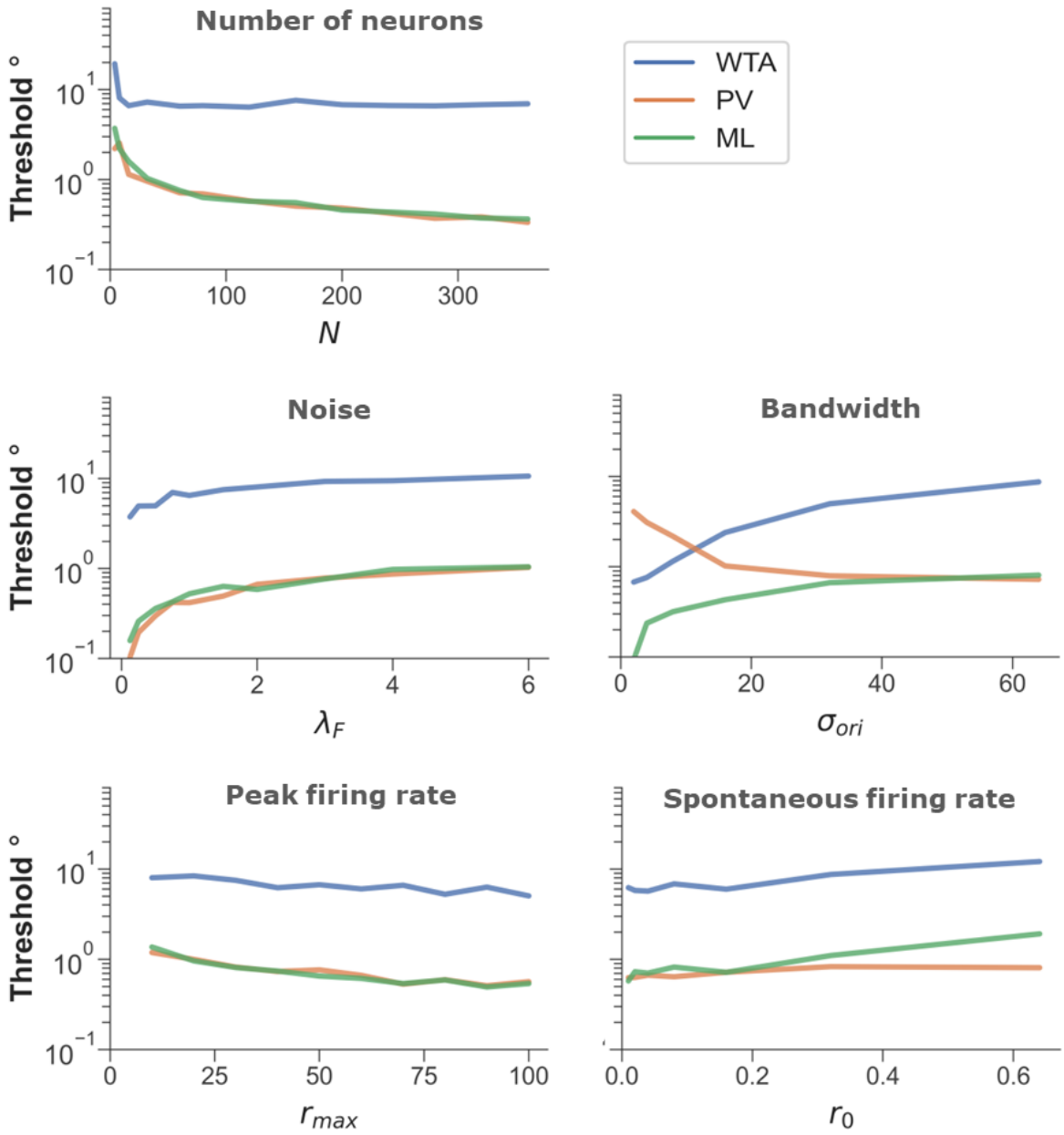

Figure 3.5. Model orientation-discrimination thresholds measured using a simulated 2AFC task as a function of each model parameter manipulated in isolation (*x-axis*). Default parameter values are set as per Table 3.1. Values are jittered to distinguish the performance of each decoder (*coloured lines*).

2267

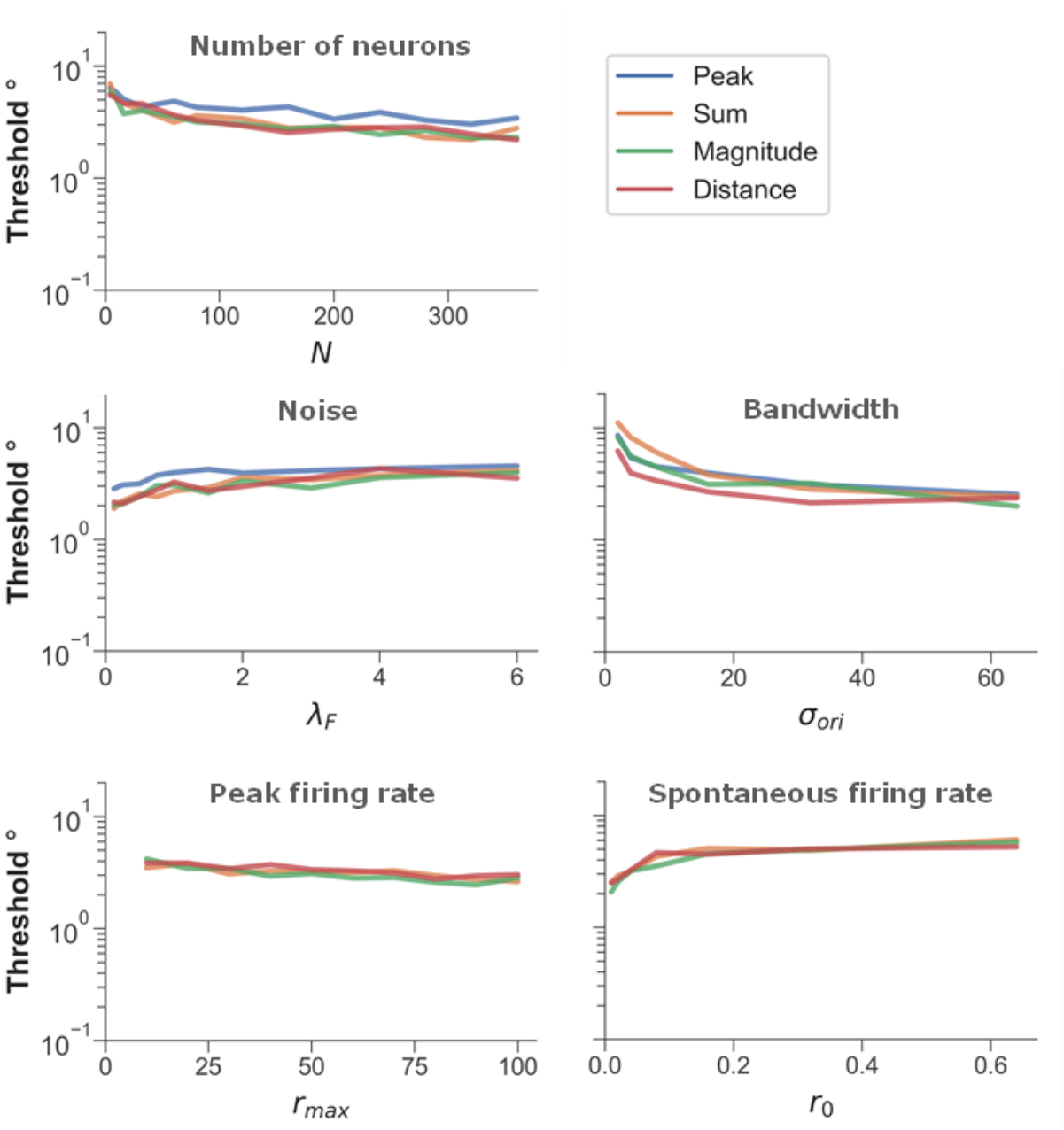

Figure 3.6. Model contrast-detection thresholds measured using a simulated 2AFC task as a function of each model parameter manipulated in isolation (*x-axis*). Default parameter values are set as per Table 3.1. Values are jittered to distinguish the performance of each decoder (*coloured lines*).

2268

neurons *N* was set to 180. Beyond this point, denser sampling vastly increased computation time with little change in the performance of the model.

3.5.3 Orientation bandwidth

The orientation bandwidth (fullwidth at half-max, FWHM) σ_{ori} of Gaussian tuning curves (Equation 3.1) are approximated by $\sigma_{ori} \approx 2.355\sigma^2$. Neurophysiological research has robustly characterised orientation selectivity for neurons in V1 of the macaque, which is considered to be a suitable analogue of V1 in humans (see Section 1.4.1). Average tuning bandwidths typically range from 40 to 60° (Y. Chen et al., 2020; De Valois, William Yund, et al., 1982; J. B. Levitt et al., 1994; Nauhaus et al., 2008; G. F. Poggio et al., 1977; Ringach et al., 2002; Schiller et al., 1976b; Xing et al., 2004). Therefore, σ_{ori} was set to 50° in the present model.

For orientation bandwidths increasing above 50°, there was relatively little change in orientation-discrimination performance for the ML and PV decoders (Figure 3.5). For narrowed bandwidths (< 20°) orientation-discrimination performance was vastly improved for the ML and WTA decoders, and was greatly impaired for the PV decoder. Contrast-detection performance generally improved with increasing orientation bandwidth (Figure 3.6), reflecting extended neural recruitment for a given stimulus orientation.

3.5.4 Response variability

The scale of response variability λ_F in this model is described by the Fano factor (see Equation 3.5), a commonly used metric of neuronal response variability (Raiguel et al., 2006). Larger values of λ_F indicate increasing levels of response variability. There are inconsistencies in the literature for estimates of response variability in V1. In anaesthetised monkeys, the typical Fano factor is around 2 (Adab & Vogels, 2011; Ecker et al., 2014;

Raiguel et al., 2006), whereas the Fano factor in V1 of awake macaques is much lower (Ecker et al., 2014). When controlling for eye movements, λ_F estimates as low as 0.35 have been reported across the cortical layers of V1 (Gur et al., 1997; Gur & Snodderly, 2006). This is supported by findings of large fluctuations in responsivity in anaesthetised animals (Tolhurst et al., 1983; Villeneuve & Casanova, 2003). A default value of $\lambda_F = 1$ was used in the present model, such that firing rates approximate a Poisson process.

In the model, orientation-discrimination performance was impaired with increasing levels of response variability (Figure 3.5). Doubling the Fano factor results in roughly a 25% difference in orientation-discrimination threshold for PV and ML decoders, and a 10% difference for the WTA decoder. The scale of response variability had little impact on contrast detection performance for all decoders (Figure 3.6).

3.5.5 Peak firing rate

The average peak firing rate r_{max} of neurons in V1 and V2 is somewhere between 25 (Levitt et al., 1994; Sclar et al., 1990; Shen et al., 2014; Zheng et al., 2007) and 60 spikes/sec (De Valois, Albrecht, et al., 1982; De Valois, William Yund, et al., 1982; Raiguel et al., 2006; Tao et al., 2012). However, estimates of firing rates are largely heterogeneous across a neural population, typically ranging from 20 to 80 spikes/sec (Ringach et al., 2002; Xing et al., 2004). Firing rates tend to be higher for neurons with less inhomogeneities in their orientation tuning profiles (Tao et al., 2012). For the idealised response characteristics of neurons in the present model, the default r_{max}value was set to 50 spikes/sec (Raiguel et al., 2006).

Increasing the peak firing rate results in improved discrimination performance (Figure 3.5). For PV and ML decoders, doubling the firing rate corresponds roughly to a 25% decrease in orientation-discrimination threshold. As expected, the peak firing rate had

minimal influence on contrast-detection performance (Figure 3.6). Minor improvements in contrast-detection performance with increasing r_{max} were due to the parameters of the contrast-response function (see Section 3.5.7).

3.5.6 Spontaneous firing rate

The majority of orientation-selective V1 neurons have little to zero spontaneous activity, with the average rate typically around 1 or 2 spikes/sec (Ringach et al., 2002; Schiller et al., 1976b; Xing et al., 2004). In the present model, the spontaneous firing rate r_0 was set to 3% of the maximum firing rate, equivalent to 1.5 spikes/sec when $r_{max} = 50$. Spontaneous firing rates are typically larger for neurons with extremely broad orientation bandwidths, above 80° (Ringach et al., 2002). However, these are associated with inhomogeneities in orientation-selectivity profiles and are far beyond the typical orientation bandwidths which are considered for this thesis.

The spontaneous firing rate r_0 is defined as a proportion of the maximum firing rate r_{max}, for example $r_0 = 0.05$ corresponds to 5% of r_{max}. For spontaneous firing rates under 0.1 (< 5 spikes/sec), there was little impact on orientation-discrimination thresholds (Figure 3.5). Both the WTA and ML decoders were greatly impacted for higher values of r_0. Contrast-detection thresholds consistently increased by ~15% when doubling the spontaneous firing rate (Figure 3.6).

3.5.7 Contrast-response function

The parameters of the Naka-Rushton contrast-response function (Equation 3.2) have been routinely investigated in macaques. The influence of the semi-saturation constant c_{50} and the exponent q on the neural response is shown in Figure 3.7. Single-cell estimates of the

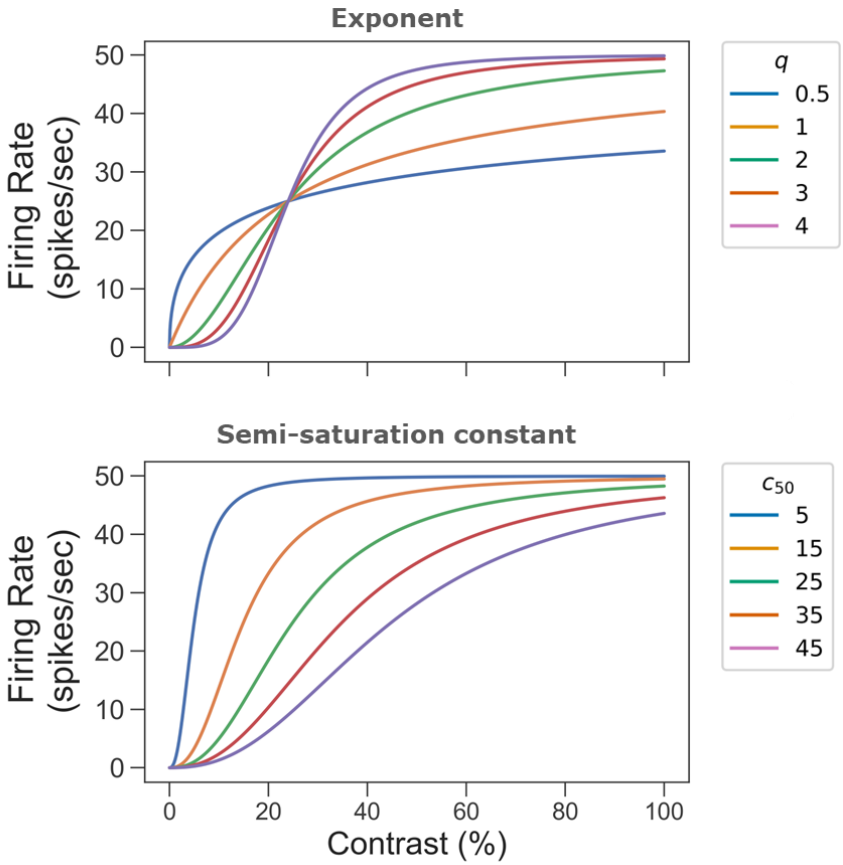

Figure 3.7. Firing rate (spikes/sec) of a model neuron as a function of stimulus contrast (%), where parameters of the Naka-Rushton contrast response function have been adjusted (*coloured lines*).

semi-saturation constant c_{50} typically range from 20 to 30%, and estimates of the exponent q lie around 1.8 to 2.4 (El-Shamayleh et al., 2013; Geisler & Albrecht, 1997; J. B. Levitt et al., 1994; Sclar et al., 1990; Zheng et al., 2007) but have been reported up to 3.4 (Albrecht & Hamilton, 1982). Psychophysical measurements of the contrast-response function in humans reveal an exponent q similar to those in neurophysiological data, however psychophysical estimates of the semi-saturation constant c_{50} are far lower, at roughly 5% contrast (DiMattina, 2016). Despite psychophysical results, the response characteristics of neurons in the present model are determined solely from the neurophysiological evidence, with values of 24% and 2.4 for the semi-saturation constant and exponent, respectively (May & Solomon,

2015b).

For orientations presented at higher contrasts (> 40%), the parameters of the contrast-response function had predictably little impact on orientation-discrimination performance (Figure 3.8A). However, at low contrasts (5%) orientation-discrimination thresholds

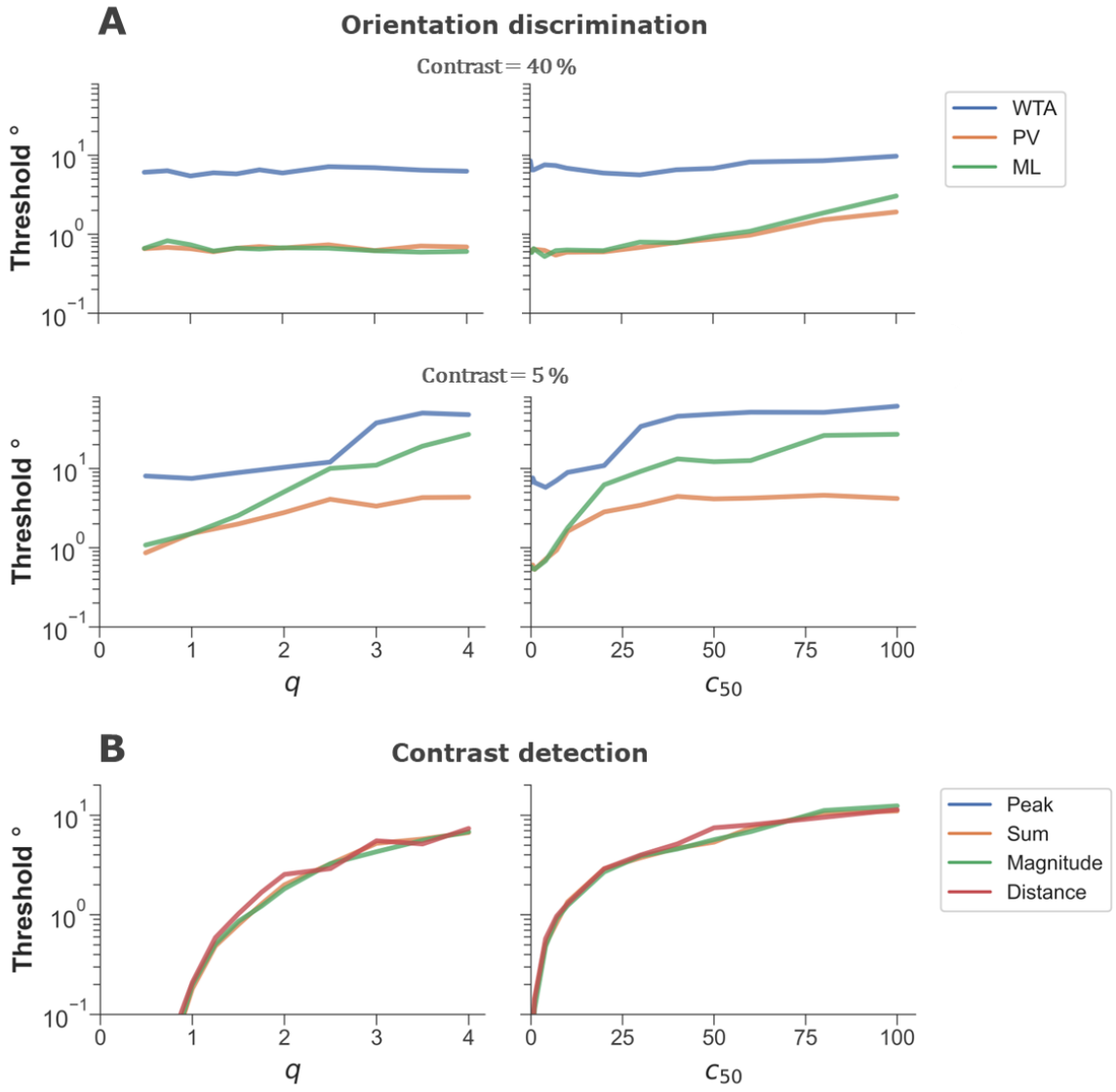

Figure 3.8. Model performance as a function of the parameters of the Naka-Rushton contrast response function, for orientation discrimination at high and low stimulus contrasts (*A*) and for contrast detection (*B*). Default parameters are set as per Table 3.1. The standard orientation is 0°. Values are jittered to distinguish the performance of each decoder (*coloured lines*).

increased with increasing values of q and c_{50}, especially for the ML decoder which performed far worse than the PV. As expected, decrements in the exponent q and the semi-saturation constant c_{50} are associated with proportional improvements in contrast-detection performance (Figure 3.8B).

3.6 Modelling the oblique effect

3.6.1 Orientation anisotropies

To explore the potential neural mechanisms of the oblique effect, parameter values were independently varied for neurons selective for cardinal orientations and those selective for oblique orientations. Orientation anisotropies that have been proposed to account for the behavioural oblique effect (see Sections 1.3, 1.4 and 1.5) were implemented in the model. Specifically, the number of neurons N, orientation bandwidth σ_{ori}, and response variability λ_F were manipulated in cardinal-tuned and oblique-tuned populations (Figure 3.9). Cardinal-tuned neurons were defined as those with orientation preferences ± 22.5° from either 0° or 90°, whereas oblique-tuned neurons were had orientation preferences ± 22.5° from either 45° or 135°. Anisotropic parameters changed gradually from oblique orientations to their peak at the cardinal orientations, according to a cosine distribution.

There were no systematic differences between the two cardinal orientations, nor between the two obliques, therefore model performance on various 2AFC tasks were measured for two stimulus orientations (0 and 45°). The oblique effect index (OEI) was calculated from the model thresholds as a measure of oblique effect magnitude (see Section 2.8), and were compared across a range of anisotropic model parameters. The neural mechanisms of the oblique effect will be explored in further detail throughout the experimental chapters of this thesis.

2373

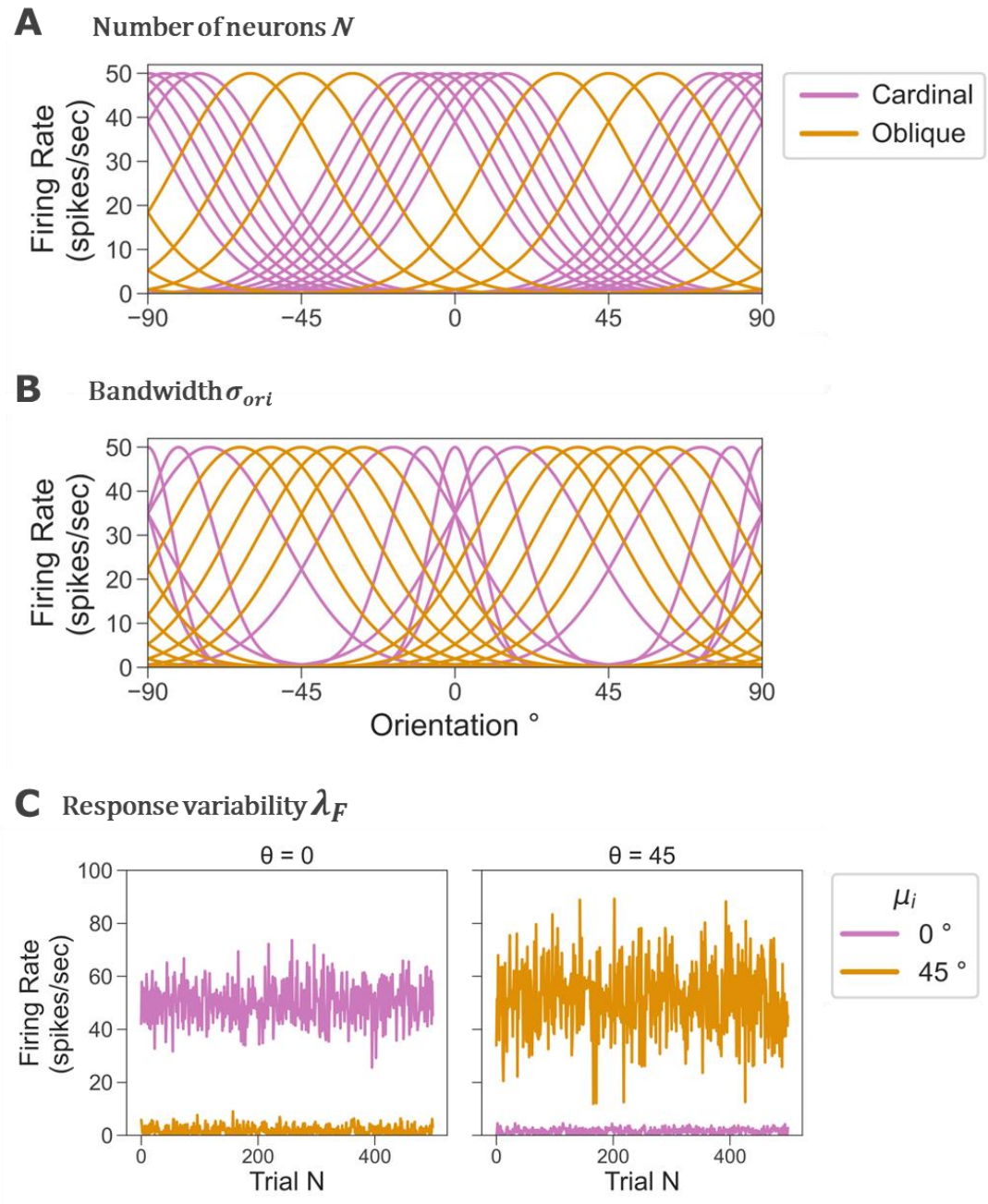

Figure 3.9. Orientation tuning curves displaying an overrepresentation of cardinal-tuned neurons (A) and narrowed orientation bandwidths (B). Anisotropic levels of noise (C) are exemplified by the trial-to-trial responses of a cardinal-tuned neuron and an oblique-tuned neuron, where λ_F is set to 1 and 3, respectively.

3.6.2 Comparisons with behavioural performance

Thresholds from model simulations on 2AFC tasks can be compared to the mean thresholds obtained psychophysically from a sample of participants. Model thresholds for PV and ML decoders on an orientation-discrimination task were remarkably close to those obtained psychophysically for cardinal orientations, ~ 1° (Figure 3.5), whereas thresholds for the WTA decoder tended to be much higher. Contrast-detection thresholds for the model were around 3%, which is around 10 times larger than detection thresholds measured behaviourally (see Section 4.2). However, when the semi-saturation constant c_{50} of the contrast-response function is informed by previous psychophysical investigations, such that $c_{50} = 5\%$ (DiMattina, 2016), model detection thresholds are much closer to those observed behaviourally.

The oblique effect index (OEI) reflects the magnitude of the oblique effect whilst controlling for overall differences in performance. This enabled direct comparisons between the oblique effect in model performance with that measured psychophysically. Crucially, this provided insight into the feasibility of the proposed mechanisms of the oblique effect. This will be explored in detail throughout the experimental chapters of this thesis.

4. Understanding the mechanisms of the oblique effect through the manipulation contrast and spatial frequency

4.1 General introduction

Overview

The oblique effect is a behavioural phenomenon where visual performance is worse for stimuli orientated about the oblique axes, relative to the cardinal axes (see Section 1.3). The oblique effect was initially discovered for psychophysical measures of visual sensitivity, such as visual acuity and contrast sensitivity (Appelle, 1972; Campbell et al., 1966; Higgins & Stultz, 1950; Mitchell et al., 1967; Nachmias, 1960) but has also been found for tasks at suprathreshold contrasts, such as orientation discrimination (Westheimer, 2003a; Westheimer & Beard, 1998). Proposed explanations of the oblique effect include on overrepresentation of cardinal-tuned mechanisms, anisotropic orientation-tuning bandwidths, and increased response variability for oblique-tuned mechanisms (see Sections 1.4 and 1.5).

Modelling

At present, the impact of such neuronal anisotropies on task performance have generally been inferred from comparisons between psychophysical and neurophysiological data. However, the need for an alternative approach is highlighted by the frequency of conflicting neurophysiological findings, and the presence of substantial methodological limitations (see Section 1.4). Computational models provide a basis for assessing the impact of neuronal anisotropies on psychophysical performance (Henderson & Serences, 2021; Rokem & Silver, 2009; Watson & Ahumada, 2005; Wong & Price, 2014), assuming that the model accurately reflects the visual mechanisms of interest.

Previous models of the oblique effect for contrast detection were descriptive and thus provided no insight into the neural basis of the oblique effect (Watson & Ahumada, 2005), whereas there are no computational investigations at present into the oblique effect for orientation discrimination. A hierarchical model of the oblique effect for motion-direction discrimination and the motion aftereffect was reported to capture psychophysical performance, in the presence of a slight overrepresentation of neurons tuned to cardinal motion directions and a large anisotropy in motion-direction tuning bandwidths (Rokem & Silver, 2009; Wong & Price, 2014). However, the authors in one study noted that similar results were found across a 'range of parameter values', but did not specify what this range was (Rokem & Silver, 2009).

Decoding

Comparisons between model performance and psychophysical data provide a basis to evaluate how stimulus features are encoded and decoded by the visual system. Previous assessments of decoding algorithms have been investigated in populations of neurons with homogeneous response characteristics which are invariant to the manipulated stimulus feature (Berens et al., 2011; Deneve et al., 1999; Jazayeri & Movshon, 2006; Tanabe, 2013; Webb et al., 2007b, 2011). Therefore, implementing orientation anisotropies within a computational framework presents an opportunity to evaluate different orientation-decoding methods in model simulations. For example, following adaptation to motion, the oblique effect for the motion aftereffect was captured by a maximum-likelihood model, whereas the population vector and winner-take-all models failed to account for the psychophysical results (Rokem & Silver, 2009). Conversely, behavioural performance could have been captured by all three decoders had a singular direction been tested, highlighting the importance of capturing anisotropic performance in order to assess the validity of a given model

Analyses of computational simulations should be comprehensive in their scope, such that the influence of each free parameter on model performance is quantified and described clearly. Drawing conclusions from limited datasets runs the risk of generating reductive or inaccurate explanations of simulation data. For example, neither study on the oblique effect for motion-direction discrimination reported the impact of adjusting various anisotropic parameter values on model performance, and only reported the relative differences between cardinal and oblique thresholds (Rokem & Silver, 2009; Wong & Price, 2014). Additionally, there are no previous attempts to account for how psychophysical performance is modulated by changes in stimulus parameters, such as spatial frequency or contrast. Therefore, the modelling work in the present Chapter attempts to address these limitations, by exploring the impact of various neuronal anisotropies and stimulus parameters on model performance.

Unified model of the oblique effect

Previous suggestions that contrast detection and orientation discrimination rely on different neural mechanisms (G. A. Orban et al., 1984b) raise the question as to whether a unified model, with a single encoding stage (i.e., model parameters are the same regardless of the task), can account for the oblique effect for both tasks. The oblique effect for contrast detection scales with spatial frequency (Campbell et al., 1966; Mitchell et al., 1967; Pointer, 1996), implicating a neural locus in early visual cortices (V1, V2), where the majority of neurons are selective for orientation and spatial frequency (De Valois, Albrecht, et al., 1982; De Valois, William Yund, et al., 1982; Issa et al., 2000). In contrast, orientation-discrimination thresholds are reported to be invariant to spatial frequency (Heeley & Timney, 1988; Matin et al., 1987), and the associated oblique effect is larger than that for contrast detection (Westheimer, 2003a; Westheimer & Beard, 1998). It has been reported that the larger oblique effect for orientation discrimination, relative to contrast detection, reflects the

same underlying anisotropy which simply scales with stimulus contrast (Bloem & Ling, 2017b). However, this fails to explain why the oblique effect for contrast detection only emerges at higher spatial frequencies, typically above 8c/° for stimuli presented in central vision (Pointer, 1996).

Aims

The present Chapter investigates the influence of spatial frequency and stimulus contrast on the oblique effects for contrast detection (Section 4.2) and orientation discrimination (Sections 4.3 and 4.4). Psychophysical results are evaluated in the context of computational model simulations of analogous two-alternative forced choice (2AFC) tasks with corresponding decision rules. Orientation anisotropies were implemented in a model population of orientation-selective neurons with the aim of capturing the oblique effect, including any modulation of task performance by stimulus parameters. Crucially, the impact of various neuronal anisotropies on model performance will be explored systematically. Finally, this work evaluates whether a unified model can account for the oblique effect for both contrast detection and orientation discrimination.

4.2 Contrast detection and spatial frequency

4.2.1 Introduction

The oblique effect for contrast sensitivity is found only for stimuli presented at high spatial frequencies, above 8c/° for stimuli presented in central vision (Pointer, 1996). This effect has been demonstrated for circular gratings using oscilloscope displays (Berkley et al., 1975; Campbell et al., 1966; Mitchell et al., 1967) and CRT monitors (Heeley & Timney, 1988; Long & Tuck, 1991; Tootle & Berkley, 1983), and for gratings presented within a spatial Gaussian window (Pointer, 1996). The cause of the oblique effect for contrast sensitivity is thought to be restricted to early visual cortex, where the majority of neurons are selective for both orientation and spatial frequency (De Valois, Albrecht, et al., 1982; Issa et al., 2000).

Previous modelling work has provided a descriptive account of the oblique effect for contrast sensitivity, formulated as a general loss of sensitivity for oblique orientations which increases with increasing spatial frequency (Watson & Ahumada, 2005), however the mechanistic basis for such a loss in sensitivity was not explored. A common explanation of the oblique effect is that there is a larger proportion of cardinal-tuned neurons relative to oblique-tuned neurons (B. Li et al., 2003; Sun et al., 2013). Neurophysiological evidence tends to support such a claim, although there are some notable inconsistencies in the literature (see Sections 1.4 and 1.5).

It remains unclear why the oblique effect for contrast sensitivity is found only at relatively high spatial frequencies. One suggestion is that the overrepresentation of cardinal-tuned neurons is accentuated for populations of neurons tuned to higher spatial frequencies, however this is only found for horizontal orientations, with similar numbers of vertical-tuned

and oblique-tuned neurons being reported in V1 of cats and macaques (B. Li et al., 2003; G. Shen et al., 2014). Furthermore, a strong cardinal bias in the voxel-wise activity of V1, in macaques and humans (see Section 1.4.3 and Section 1.5.2), has been reported even for stimuli presented at lower spatial frequencies, < 5c/° (Fang et al., 2022; Sun et al., 2013).

Alternatively, the extent of neuronal anisotropies may be invariant with respect to spatial frequency, and the oblique effect for contrast sensitivity may emerge at high spatial frequencies due to differences in the response characteristics of neuronal populations which are selective for distinct spatial frequencies. For example, neurons in macaque V1 with a preferred spatial frequency of 2c/° have typical orientation tuning bandwidths (full-width half-max) of roughly 50°, whereas neurons which prefer spatial frequencies at or above 8c/° have tuning bandwidths under 30° (Y. Chen et al., 2020; De Valois, Albrecht, et al., 1982; P. Hammond & Pomfrett, 1990; J. P. Jones et al., 1987; Lampl et al., 2001; Webster & De Valois, 1985; Xing et al., 2004). Further investigation is required to assess whether the oblique effect for contrast detection could arise due to an interaction between the proportion of cardinal-tuned neurons, and the uniformly narrowed orientation bandwidths of neurons which prefer higher spatial frequencies.

There are also far fewer neurons which are selective for high spatial frequencies than for low spatial frequencies in V1 (De Valois, Albrecht, et al., 1982; Issa et al., 2000) and V2 (J. B. Levitt et al., 1994), although the precision of these estimates is often limited by small sample sizes in single-cell studies. One study found that roughly 20% of simple cells in cat V1 had preferred spatial frequencies near 2c/°, whereas under 5% had preferred spatial frequencies near 8c/°, and substantially fewer were selective for even higher spatial frequencies (De Valois, Albrecht, et al., 1982). The total number of neurons serving detection may interact with the oblique effect, such that the responses of smaller populations may be

less robust to the impacts of neuronal anisotropies.

Using psychophysical and computational techniques, this study aimed to provide an explanatory account of the oblique effect for contrast detection, including its dependency on spatial frequency. The capacity for the model to capture the psychophysical data was explored in the presence of various neuronal anisotropies, including those which were subsequently demonstrated to contribute towards the oblique effect for orientation discrimination (see Sections 4.3 and 4.4).

4.2.2 Methods

Participants

Eight participants took part in the contrast-detection experiment, all with normal or corrected-to-normal visual acuity. Participants were not screened for ocular pathology or visual dysfunction, but were instructed to wear appropriate refractive correction, if required. All but three participants (P1, P2, P3) were naïve to the aims of the study. A subsample of three participants (P1, P5, P6) performed an additional intermediate spatial frequency condition. Ethical guidelines were followed as described in Section 2.1.

Stimuli

The testing apparatus for the present experiment is described in Section 2.2. Monitor output was carefully linearised through photometric gamma correction (Section 2.3.1) and the noisy-bit method provided precise control over the luminance resolution of the monitor (Section 2.3.2). The viewing distance was 135cm, providing a maximum-displayable spatial frequency of approximately 17c/° at 4 pixels per cycle. Visual stimuli were Gabor patterns (Section 2.4), composed of orientated sinusoidal luminance gratings presented within a spatial Gaussian window with a space-constant σ^2 of 1.33°, truncated at ±4°.

Design

For each run, the chosen spatial frequency condition (either 2, 8 or 16c/°) and orientation condition (either 0, 90, -45, or 45°) defined the corresponding parameters of the target stimulus, which were constant throughout each run of trials. Contrast-detection thresholds were determined for each condition using a temporal two-alternative forced choice task (2AFC) task, with a 3-up 1-down adaptive staircase procedure (see Section 2.5). The contrast of the target stimulus on each trial was determined by the staircase value. Each run ended after ten reversals, and thresholds were calculated as the arithmetic-mean staircase value of the last five reversals. Participants completed a minimum of four runs in each condition. All runs were completed in a randomised fashion. The 'oblique effect index' (OEI, see Section 2.8) scores quantified the magnitude of the oblique effect.

Procedure

The target stimulus was presented for 300ms in one of two temporal intervals which were separated by a 500ms homogeneous blank field. The intervals were marked by distinct audible tones. The interval containing the target stimulus was randomised on each trial. Participants judged in which interval the target stimulus appeared, using the 'F' and 'J' keys to refer to the first and second intervals, respectively. A central fixation spot was present at the end of each trial until a valid keyboard response was collected. A response signalled the initiation of the next trial after a 500ms delay. No response feedback, concerning the correctness of the participant's decision, was given.

4.2.3 Results

A two-way repeated measures ANOVA revealed a significant interaction between orientation and spatial frequency on the measured contrast-detection thresholds ($F(1,7) =$

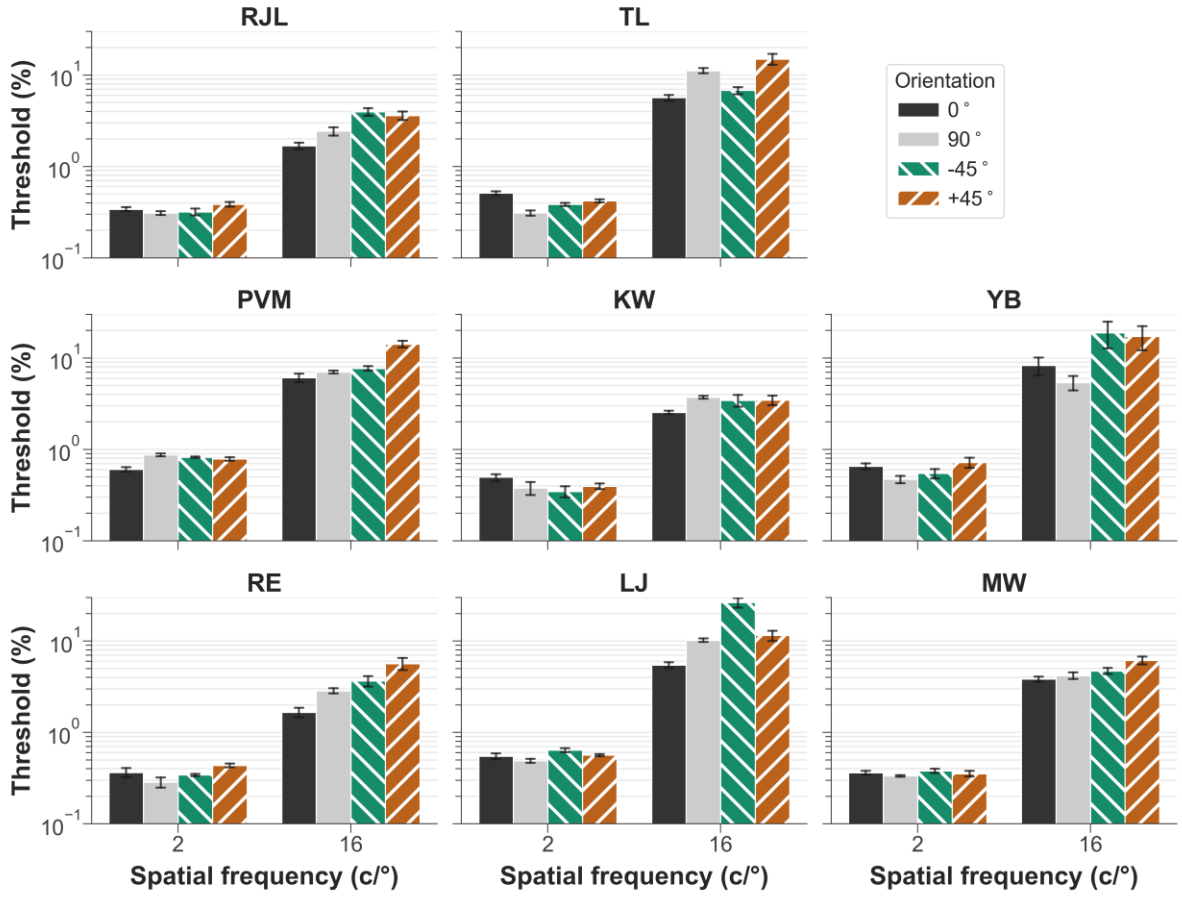

Figure 4.1. For each participant, contrast-detection thresholds are plotted against spatial frequency. Error bars reflect the standard error of the mean threshold across runs. At 16c/°, thresholds were higher for the obliques (-45 and 45°) than for the cardinals (0 and 90°).

21.6, $p = .034$, $\eta^2_p = .333$). There was little difference between cardinal (0 and 90°) and oblique (-45 and 45°) detection thresholds at 2c/°, for all eight participants (Figure 4.1). At 16c/°, pairwise comparisons revealed that thresholds for the right oblique (45°) were significantly higher than for horizontal or vertical. Although five out of eight participants showed substantially lower contrast-detection thresholds for horizontal (0°) relative to vertical (90°) at 16c/°, there was no significant difference between thresholds for horizontal and vertical, nor between the two oblique orientations. Mean thresholds are shown in Figure 4.2.

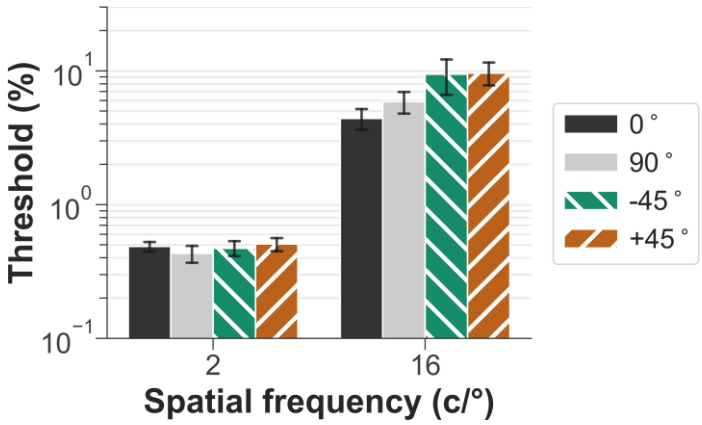

Figure 4.2. Mean contrast-detection thresholds are plotted against spatial frequency. Error bars reflect the standard error of the mean.

The absence of an oblique effect at 2c/° was demonstrated by a geometric-mean OEI (SE) score of 1.06 (0.04). At 16c/°, the geometric-mean OEI (SE) score was 1.71 (0.18), with an OEI score of 1.33 or above being measured in seven out of eight participants (Figure 4.3). A paired-samples t-test revealed that OEI scores at 16c/° were significantly larger than at 2c/° ($t(7) = 4.43$, $p = .003$), with a large effect size (Cohen's $d = 1.56$).

There was a significant main effect of spatial frequency ($F(3,21) = 3.50$, $p = .034$, $\eta^2_p = .333$), such that thresholds at 16c/° were significantly higher than at 2c/° for each tested orientation condition. Cardinal thresholds were on average 10 times higher at 16c/° than at 2c/°, whereas oblique thresholds were approximately 16 times higher. There was considerable inter-individual variation in the extent of this difference, and there was no consistent relationship between the size of the oblique effect for each individual and the change in thresholds between 2 and 16c/°.

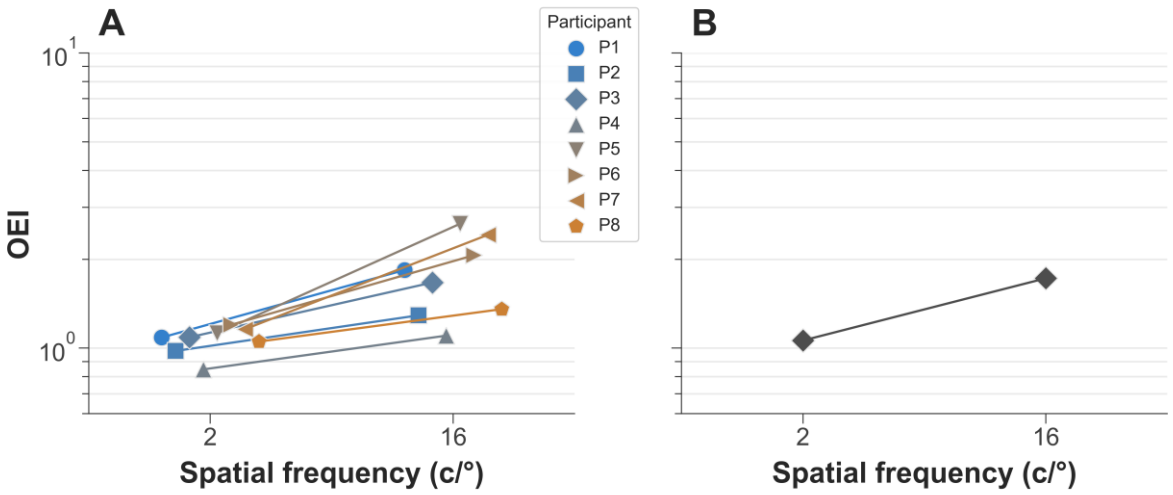

Figure 4.3. Individual oblique effect index (OEI) scores (*A*) and the geometric-mean OEI score (*B*) are plotted against spatial frequency. OEI scores at 16c/° were higher than at 2c/°.

A subsample of three participants performed the same contrast-detection task at an intermediate spatial frequency of 8c/° (Figure 4.4). For two of the three participants, OEI scores increased between 2 and 8c/°, and were relatively unchanged between 8 and 16c/°. For the remaining participant, an increase in OEI score was only observed at 16c/°.

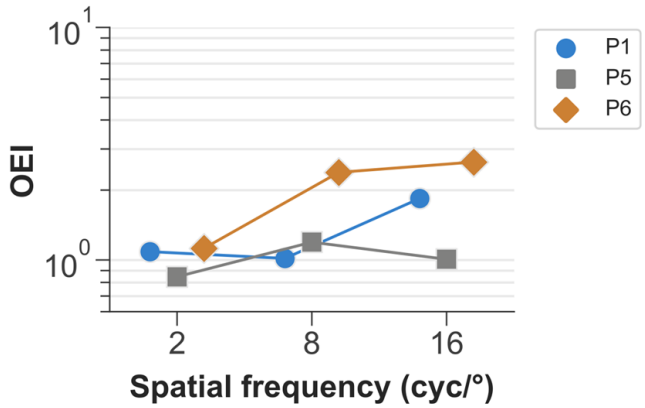

Figure 4.4. Three participants performed an additional, 8 c/° condition. The oblique effect index (OEI) scores are plotted against spatial frequency.

4.2.4 Modelling

Overview

Model performance was assessed on a simulated contrast-detection, 2AFC task, analogous to that described for the behavioural task (see Section 3.4.2). Orientation anisotropies were implemented in the model by independently varying the parameters of neurons tuned to either cardinal or oblique orientations. Unless otherwise specified, model parameters were set to the 'default' values described in Section 3.5 (Table 3.1). There were no systematic differences between the two cardinal orientations, nor between the two obliques, therefore model contrast-detection thresholds were measured for two stimulus orientations (0 and 45°). The 'oblique effect index' (OEI, see Section 2.8) quantified the size of the oblique effect. Model performance was assessed for the pooling methods described in Section 3.3.

Independent model populations were nominally selective for 'low', 'mid', and 'high' spatial frequencies, with default orientation bandwidths of 50, 30, and 20°, and a total number of neurons set to either 1620, 540, or 180, respectively. A variant of the low spatial frequency condition with an orientation tuning bandwidth of 70° was also assessed.

Overrepresentation of cardinal-tuned neurons

Model contrast-detection performance was measured across five levels of 'cardinal overrepresentation', such that the proportion of cardinal neurons was set to either 0.5, 0.6, 0.7, 0.8, or 0.9. For all pooling methods, increasing the proportion of cardinal neurons was associated with larger OEI scores (Figure 4.5), although this was dependent on the nominal spatial-frequency condition (for the 'summation', 'magnitude-weighted', and 'peak' pooling methods). Of all of the pooling methods, the oblique effect was largest for the 'summation' method, with OEI scores of roughly 1.55 at mid and high spatial frequencies when the proportion of cardinal-tuned neurons was set to 0.7. Excluding the 'distance-weighted' pooling method, the dependency of the oblique effect on spatial frequency was captured by

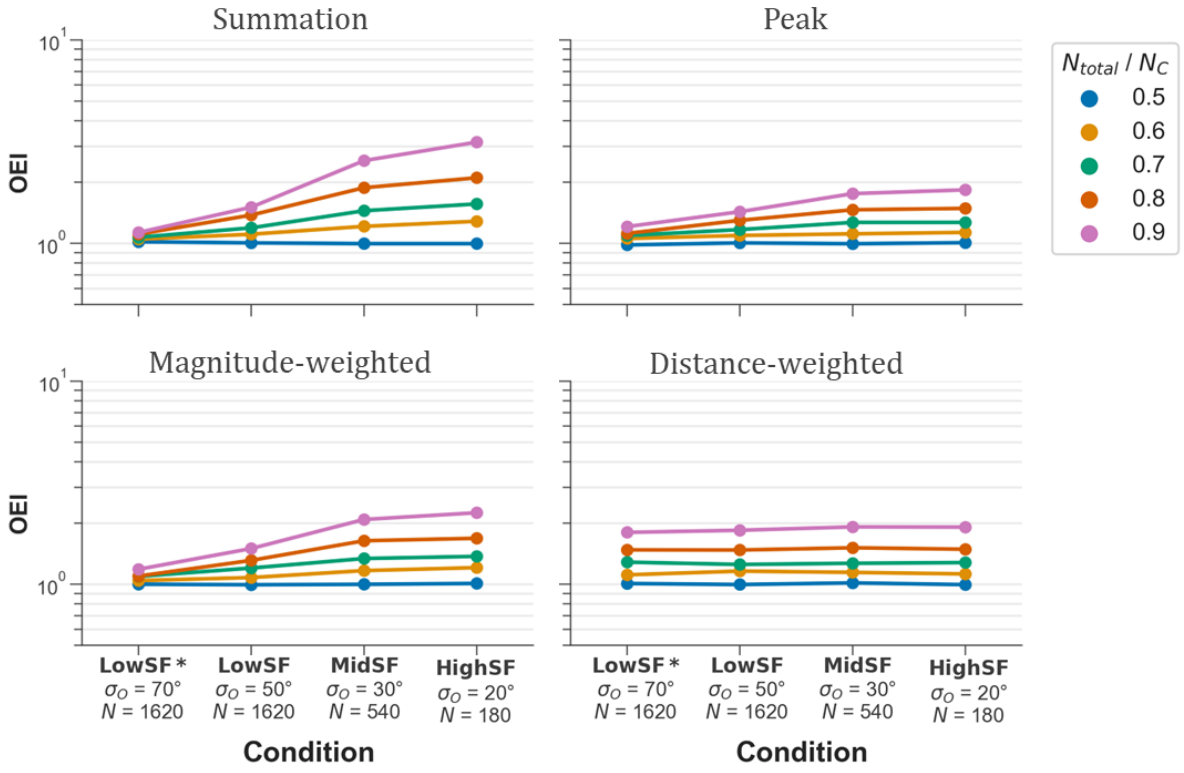

Figure 4.5. For each pooling method, OEI scores are plotted for each spatial frequency condition. The starred low spatial frequency condition had broadened orientation tuning bandwidths. Coloured lines reflect the proportion of cardinal-tuned neurons in the model.

the model, such that OEI scores increased with spatial frequency. The oblique effect was only abolished at low spatial frequencies for the variant of the model with broader orientation bandwidths (70°), and this effect was strongest for the 'summation' pooling method.

Narrowed cardinal tuning bandwidths

With the proportion of cardinal-tuned neurons set to 0.7, cardinal-orientation bandwidths were set as a fraction (either 1, 0.8, 0.6, 0.4, or 0.2) of the oblique-orientation bandwidth. In the presence of anisotropic orientation bandwidths, the spatial frequency-dependency of the oblique effect for contrast detection could not be captured, such that model OEI scores did not increase with spatial frequency (Figure 4.6). For all pooling methods, OEI

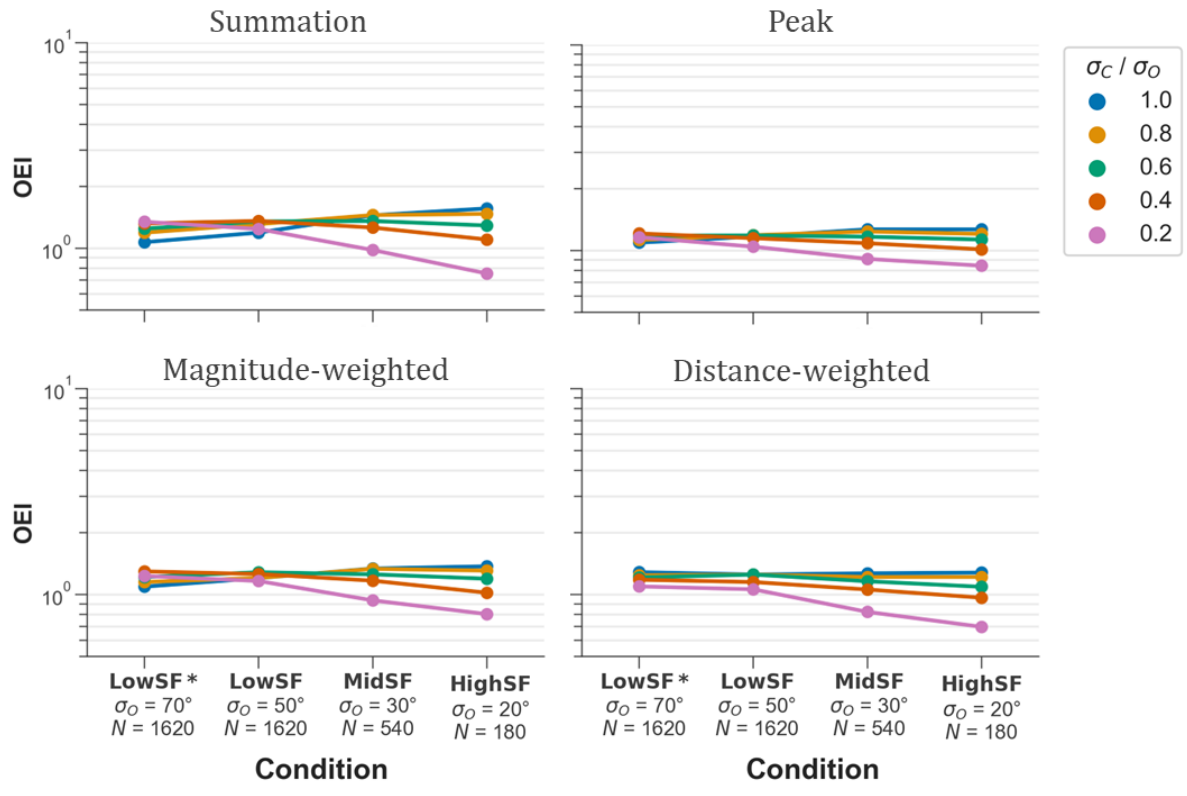

Figure 4.6. For each pooling method, OEI scores are plotted for each spatial frequency condition. The proportion of cardinal-tuned neurons was fixed at 0.7. The starred low spatial frequency condition had broadened orientation bandwidths. Coloured lines reflect the cardinal-orientation bandwidth, set as a fraction of the oblique-orientation bandwidth.

scores decreased with increasing spatial frequency, in stark disagreement with the behavioural empirical data.

Oblique response variability

In the presence of the same cardinal overrepresentation (the proportion of cardinal-tuned neurons was set to 0.7), with isotropic orientation bandwidths, the Fano factor for oblique-tuned neurons was set as a multiple (either 1, 2, 3, 4, or 5) of that for cardinal-tuned neurons. The Fano factor determined the variability of the trial-to-trial firing rates (see Section 3.). For the summation pooling method, increasing the scale of oblique noise had a negligible impact on OEI scores (Figure 4.7). In contrast, OEI scores were substantially

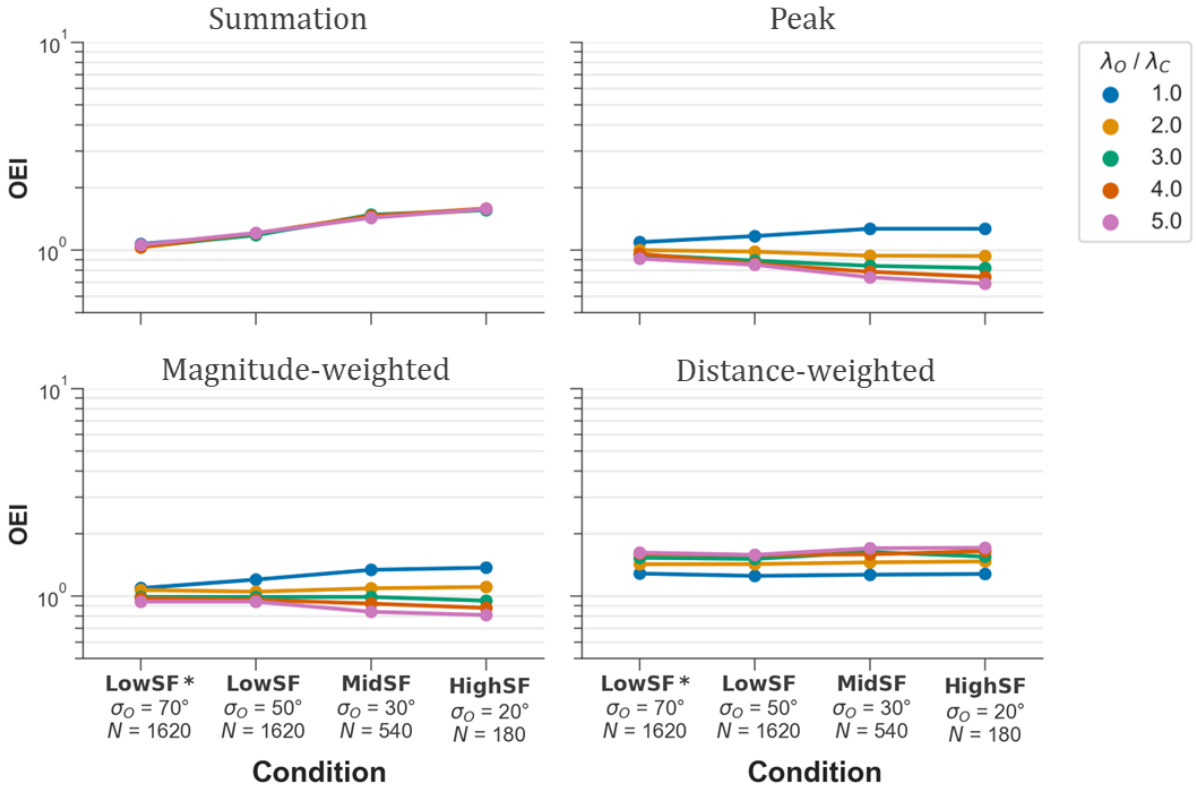

Figure 4.7. For each pooling method, OEI scores are plotted for each spatial frequency condition. The proportion of cardinal-tuned neurons was fixed at 0.7. The starred low spatial frequency condition had broadened orientation-tuning bandwidths. Coloured lines reflect the Fano factor for obliques, set as a multiple of the Fano factor for cardinals.

reduced at mid and high spatial frequencies for the 'peak' and 'magnitude-weighted' pooling methods, indicating that high levels of oblique-response variability improved the detection of the oblique orientation. For the distance-weighted pooling method, increasing the oblique-Fano factor resulted in larger OEI scores, that was invariant with respect to spatial frequency.

Thresholds

Contrast-detection thresholds were assessed whilst manipulating the extent of the cardinal overrepresentation (Figure 4.8). Despite narrowed orientation bandwidths and large reductions in the total number of model neurons with increasing spatial frequency, none of

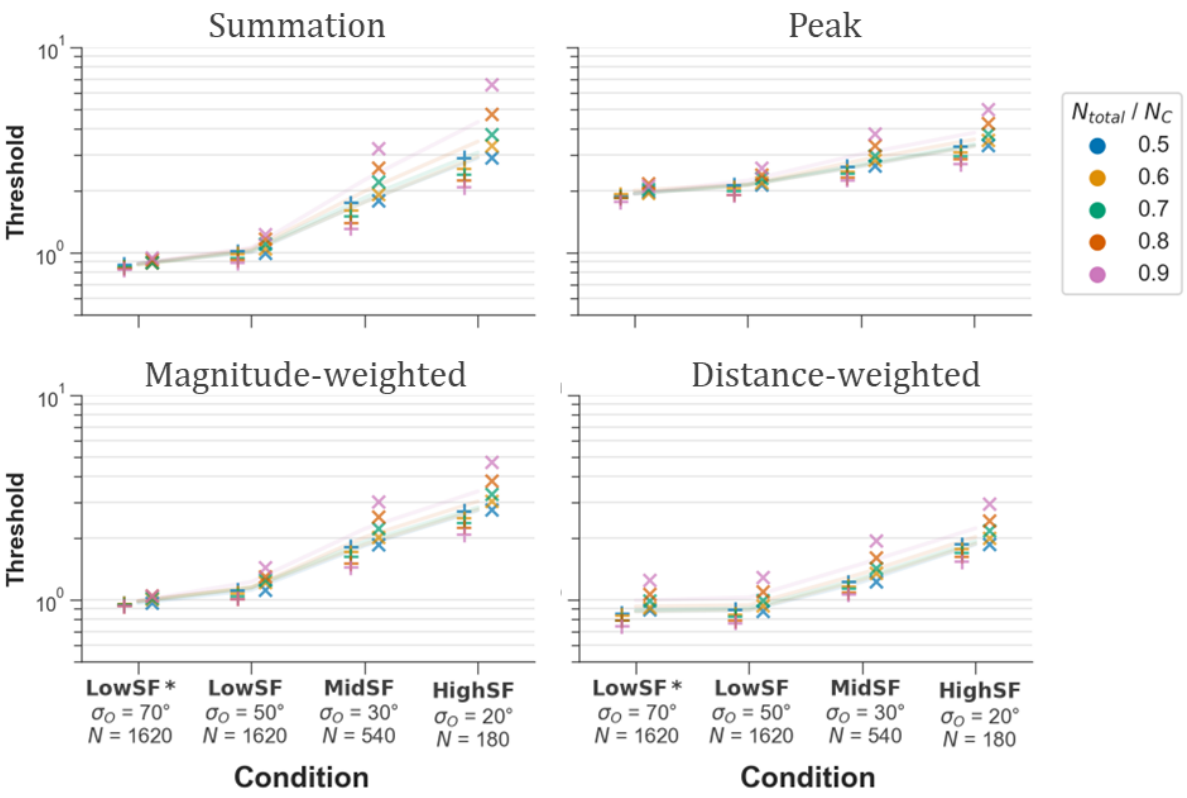

Figure 4.8. For each pooling method, contrast-detection thresholds for stimulus orientations of 0° (indicated by + symbols) and 45° (indicated by x symbols) are plotted for each spatial frequency condition. The starred low spatial frequency condition had broadened orientation-tuning bandwidths. Colours reflect the proportion of cardinal-tuned neurons in the model for a given simulation.

the tested pooling methods captured the over ten-fold changes in detection threshold (between low and high spatial frequencies) reported in the psychophysical experiment. Changes in detection threshold increases were largest for the summation pooling method. For an equal number of neurons tuned to cardinals and obliques (the blue datapoints in Figure 4.8), with roughly a three-fold increase between the low and high spatial frequency conditions.

4.2.5 Discussion

Overview

The behavioural oblique effect for contrast detection was found only at high spatial frequencies, consistent with previous research (Berkley et al., 1975; Campbell et al., 1966; Heeley & Timney, 1988; Long & Tuck, 1991; Mitchell et al., 1967; Pointer, 1996; Tootle & Berkley, 1983). Comparisons of the magnitude of the oblique effect with previous studies are difficult, either because the size of oblique effect was not explicitly quantified (Campbell et al., 1966; Heeley & Timney, 1988; Long & Tuck, 1991; Mitchell et al., 1967; Tootle & Berkley, 1983), or because data were provided from just a single participant thus rendering any generalisation unreliable (Berkley et al., 1975; Pointer, 1996). Indeed, the present work found discernible levels of inter-individual variation in the influence of spatial frequency on contrast-detection performance. Regardless, the present results are broadly consistent, at least qualitatively, with previous findings.

The summation pooling method, where the firing rates of all model neurons are summed with equal weights to form the response to a given stimulus, provided the strongest account of the behavioural data. The summation-pooling model demonstrated that a moderate cardinal overrepresentation (such that 70% of model neurons were tuned to cardinal

orientations) generated an oblique effect that increased with spatial frequency, and that approached the size of the average oblique effect observed in the behavioural experiment. This supports the classical explanation of the oblique effect, that the reduced sensitivity to oblique orientations results from an anisotropic distribution of cardinal-tuned and oblique-tuned neurons (B. Li et al., 2003; Sun et al., 2013). The extent of this cardinal overrepresentation is slightly larger than that reported neurophysiologically, with typical estimates ranging from 55 to 65% cardinal-tuned neurons. However, this could be modulated by inherent differences between other model parameters and the response characteristics of mechanisms in the human visual system. For example, additional simulations revealed that the oblique effect was greatly increased at high spatial frequencies when the exponent of the Naka-Rushton contrast-response function was uniformly reduced (Figure 4.9).

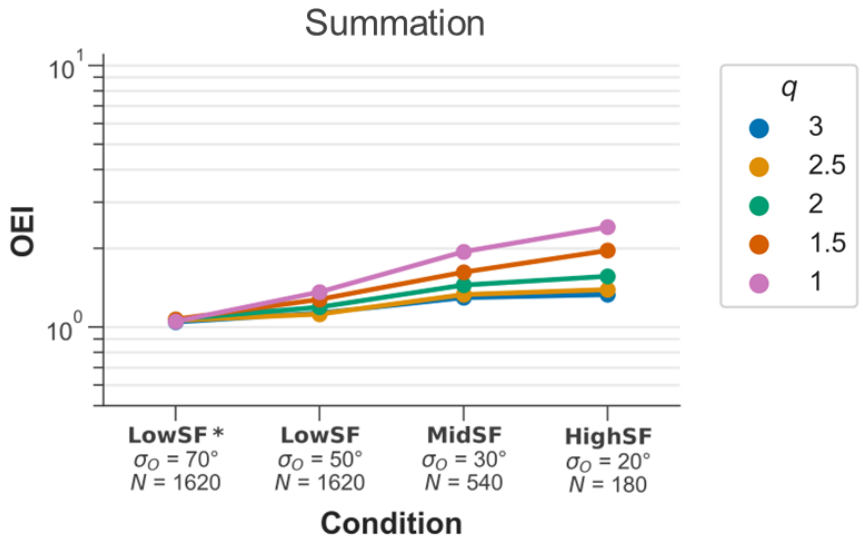

Figure 4.9. For the summation pooling method, OEI scores are plotted for each spatial frequency condition. The proportion of cardinal-tuned neurons was fixed at 0.7. The starred low spatial frequency condition had broadened orientation tuning bandwidths. Coloured lines reflect the exponent of the Naka-Rushton contrast response function.

Neural basis of the oblique effect for contrast detection

In model simulations, detection performance was impaired with increasing spatial frequency due to the uniform narrowing of orientation bandwidths, which reduced the extent of neural recruitment for a given stimulus orientation. The failure of the model to capture the scale of changes in contrast-detection thresholds observed behaviourally, associated with increasing spatial frequency, will be discussed subsequently in Section 4.5. The spatial frequency-dependency of the oblique effect arose in the model due to an interaction between orientation bandwidths and the proportion of cardinal-tuned neurons.

An overrepresentation of cardinal-tuned neurons effectively increased the signal-to-noise ratio (SNR) for cardinals relative to obliques, however this difference in the signal-to-noise ratio was diminished in the presence of broad, overlapping orientation-tuning curves in neurons selective for low spatial frequencies. Conversely, at high spatial frequencies, the narrowed orientation bandwidths of model neurons effectively increased this difference in the signal-to-noise ratio (in the presence of a cardinal overrepresentation), such that cardinal orientations were detected at lower contrasts than oblique orientations.

The oblique effect was only abolished at low spatial frequencies for a population of neurons with broader tuning bandwidths (70°) than typical estimates of the average tuning bandwidth in early visual cortex (~ 50°) (see Section 1.1.4). This required the assumption that, at near-threshold contrasts, subpopulations of neurons with broader tuning bandwidths will make a greater contribution to the detection of a visual stimulus. Future models could implement heterogeneous populations of orientation-selective neurons to investigate this claim. Although these results accommodate findings of a cardinal bias in early visual cortex that is invariant with spatial frequency (Fang et al., 2022; Sun et al., 2013), they do not rule out the possibility that the overrepresentation of cardinal-tuned neurons is accentuated at

higher spatial frequencies (B. Li et al., 2003).

In a subsample of three participants who performed additional observations at an intermediate spatial frequency, 8c/°, the size of the oblique effect for contrast detection did not increase progressively with spatial frequency. This contradicts findings that the oblique effect for contrast detection grows continuously in magnitude until the acuity limit is reached (Campbell et al., 1966; Pointer, 1996). Further investigation is required to quantify the exact relationship between the size of the oblique effect for contrast detection and spatial frequency, preferably over a larger range of spatial frequencies.

Other neuronal anisotropies

Introducing anisotropic tuning bandwidths into the model, such that cardinal-tuned neurons were more narrowly tuned than oblique-tuned neurons, abolished the spatial frequency-dependency of the oblique effect for contrast detection, and reduced its magnitude. This is consistent with the lack of neurophysiological evidence for anisotropic tuning bandwidths in macaque V1 or V2 neurons (G. Shen et al., 2014). The consequences of this finding for the oblique effect for orientation discrimination will be discussed in further detail in Section 4.5.

The scale of response variability for oblique-tuned neurons only contributed to the magnitude of the oblique effect when the distance-weighted pooling method was implemented in the model, such that firing rates were pooled from a subpopulation of neurons with orientation preferences within a restricted range (Andrei et al., 2019). However, this pooling method failed to account for the spatial frequency-dependency of the oblique effect. It is worth noting, however, that distance-weighted pooling could account for the oblique effect if the overrepresentation of cardinal-tuned neurons was restricted to higher spatial frequencies.

4.3 Orientation discrimination and spatial frequency

4.3.1 Introduction

The oblique effect for orientation discrimination has been demonstrated using a variety of stimuli, including sinusoidal gratings (Heeley & Timney, 1988), bars (Westheimer & Beard, 1998), and illusory contours (Westheimer, 2003a). Typically, orientation-discrimination thresholds for obliquely-orientated stimuli are two to three times larger than for cardinal orientations (Heeley et al., 1997; Heeley & Buchanan-Smith, 1992; Heeley & Timney, 1988; Westheimer, 2003a; Westheimer & Beard, 1998).

It has been reported that orientation-discrimination thresholds are invariant with respect to stimulus spatial frequency (Beaudot & Mullen, 2006; Heeley & Buchanan-Smith, 1990; Heeley & Timney, 1988; Matin et al., 1987), although there are suggestions that discrimination performance for oblique orientations becomes increasingly impaired at higher spatial frequencies (> 8c/°). However, the dependency of oblique-discrimination thresholds on spatial frequency tends to appear only at the group-level of analysis, and overlooks the fact that many individuals demonstrate an invariance to spatial frequency (Heeley & Timney, 1988; Matin et al., 1987). For decreasing spatial frequencies, under 1c/°, orientation-discrimination thresholds substantially increase (Burr & Wijesundra, 1991).

In the majority of previous studies which have investigated orientation discrimination as a function of stimulus spatial frequency, stimuli were presented at a fixed, absolute contrast across all spatial frequency conditions. The issue with using a fixed contrast is highlighted by substantial reductions in contrast sensitivity with increasing spatial frequency, which is accentuated for oblique orientations (see Section 4.2), and reports of a substantial impairment in orientation-discrimination performance for contrasts approaching the detection

threshold (Regan & Beverley, 1985; Webster et al., 1990). Therefore, to avoid this potential confound the present experiment equated the suprathreshold visibility of all stimuli by setting the stimulus contrast to a fixed multiple of the detection threshold for a particular condition. At low spatial frequencies (< 1c/°), matching the perceived contrast of stimuli successfully uncovered the modulation of orientation-discrimination performance by spatial frequency (Burr & Wijesundra, 1991), whereas this has not been explored for higher spatial frequencies.

Orientation-discrimination performance has been suggested to be determined, at least partially, by the slopes of the orientation-tuning curves of mechanisms which encode orientation (Beaudot & Mullen, 2006; Regan & Beverley, 1985). Anisotropic orientation bandwidths have therefore been proposed as an explanation of the oblique effect for orientation discrimination, whereby greater slopes of the tuning functions for cardinal-tuned mechanisms would result in an increased sensitivity to changes in orientation (Regan & Beverley, 1985). Indeed, the oblique effect for motion-direction discrimination was successfully modelled when cardinal-tuning bandwidths were half that of mechanisms tuned to oblique directions (Rokem & Silver, 2009). However, there is limited evidence for anisotropic orientation bandwidths from both psychophysical and neurophysiological work (see Sections 1.3 and 1.4). Additionally, the modelling work in Section 4.2 demonstrated that anisotropic tuning bandwidths did not contribute to the oblique effect for contrast detection.

Aims

The purpose of this experiment and the accompanying modelling work is to provide an account of the oblique effect for orientation discrimination at both low and high spatial frequencies, whilst controlling for stimulus visibility by setting the stimulus contrast across conditions to a fixed multiple of the contrast threshold (at least five times the detection threshold). The impact of neuronal anisotropies on model performance will be explored, in

manner analogous to that reported for the previous contrast-detection experiment (Section 4.2), with a view to assessing whether a unified model can account for the oblique effects for both contrast detection and orientation discrimination (see Section 4.5).

4.3.2 Methods

Participants

The same eight participants that completed the contrast-detection experiment (Section 4.2) also took part in the orientation-discrimination experiment. A subsample of three participants (P1, P5, P6) also performed additional measurements at an intermediate spatial frequency. Ethical guidelines were followed as described in Section 2.1.

Stimuli

Testing apparatus and stimulus parameters were identical to those described in Section 4.2.2, except for stimulus contrast which was set to a fixed multiple of the contrast threshold measured in corresponding orientation and spatial frequency conditions. The fixed multiple m was determined by dividing the maximum available contrast (nominally 100%) by the largest detection threshold of each participant, across all tested conditions (Table 4.2).

$$m = \frac{100}{\max T}$$

Equation 4.1

	P1	**P2**	**P3**	**P4**	**P5**	**P6**	**P7**	**P8**
m	24.6	6.42	6.75	3.69	25.7	4.92	16.4	15.8

Table 4.2. The multiple *m* of the contrast threshold used for each participant.

Design

Spatial frequency and orientation conditions were the same as those in Section 4.2.2. Orientation-discrimination thresholds were determined for each condition using a temporal two-alternative forced choice task (2AFC) with a 3-up 1-down adaptive staircase procedure (see Section 2.5). The chosen orientation condition defined the *standard* orientation, which was constant for each run of trials. The *comparison* orientation was defined by its orientation difference (determined by the staircase) from the standard orientation. The direction of this orientation difference, either clockwise or anticlockwise was randomised on each trial. Each run ended after ten reversals and the threshold was calculated as the arithmetic-mean orientation difference of the last five reversals. Participants completed a minimum of four runs in each condition. All runs were completed in a pseudorandom fashion. The 'oblique effect index' (OEI, see Section 2.8) scores quantified the size of the oblique effect, and the average OEI was given by the geometric-mean (gM) OEI score.

Procedure

On each trial, the standard and comparison stimuli were alternated across two sequential stimulus intervals. The order of presentation was randomised. Timings were the same as those in the contrast-detection experiment (Section 4.2.2). Participants judged which stimulus interval contained the orientation which was rotated more clockwise, using the 'F' and 'J' keys to refer to the first and second intervals, respectively. A central fixation spot was presented at the end of each trial until a valid keyboard response was collected. A response signalled the initiation of the next trial after a 500ms delay. No response feedback, as to the correctness of a given response, was given.

4.3.3 Results

A two-way repeated measures ANOVA revealed significant main effects of orientation ($F(3,21) = 15.34$, $p < .001$, $\eta^2_p = .687$) and spatial frequency ($F(1,7) = 5.95$, $p = .045$, $\eta^2_p = .459$) on orientation-discrimination thresholds. At both 2 and 16c/°, thresholds were significantly lower for horizontal (0°) and vertical (90°) than for the two obliques (-45 and 45°), and this was consistent across all eight participants (Figure 4.10). Discrimination thresholds for the -45° oblique were significantly higher at 16c/° than at 2c/°, but this

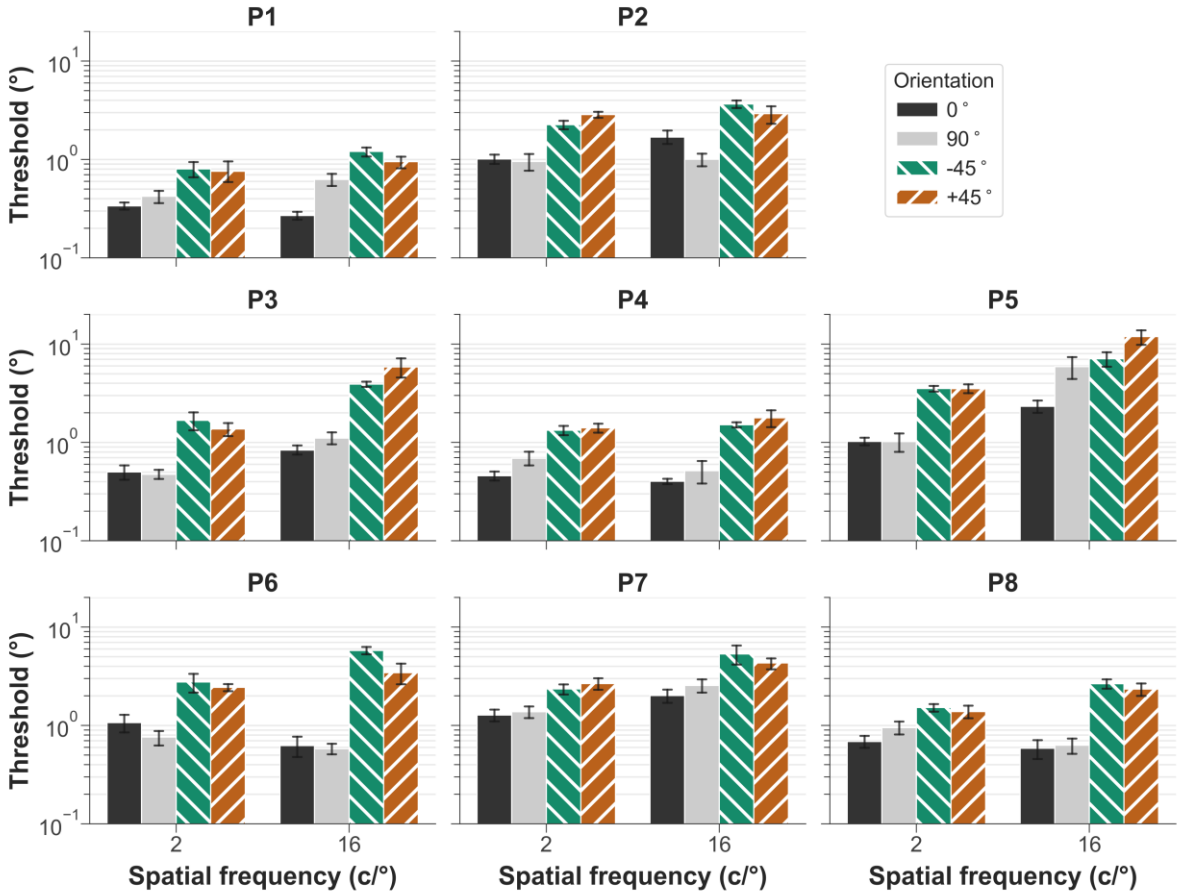

Figure 4.10. Orientation-discrimination thresholds plotted against spatial frequency for each participant. Error bars reflect the standard error (SE) of the mean threshold across runs. Cardinal thresholds were substantially lower than oblique thresholds in all participants.

difference did not reach significance for any other orientation. There were no significant differences between the two cardinal orientations, nor between the two obliques. Mean thresholds are shown in Figure 4.11.

A significant interaction between orientation and spatial frequency ($F(3,21) = 3.98$, $p = .022$) was found with a large effect size ($\eta^2_p = .362$), driven by four out of eight participants

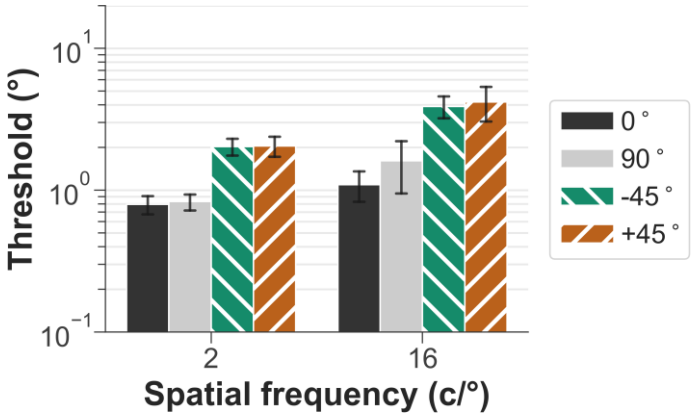

Figure 4.11. Mean orientation-discrimination thresholds are plotted against spatial frequency. Error bars reflect the standard error of the mean. At both spatial frequencies, thresholds were higher for the obliques (-45 and 45°) than for the cardinals (0 and 90°).

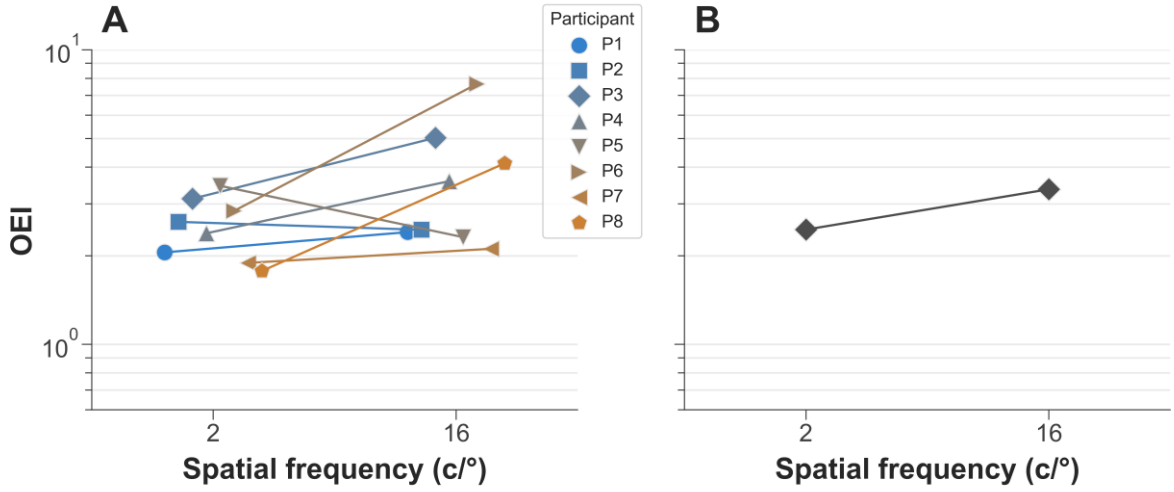

Figure 4.12. Individual oblique effect index (OEI) scores (*A*) and the geometric-mean OEI score (*B*) are plotted against spatial frequency.

with OEI scores substantially larger at 16c/° (gM = 3.36, SE = 0.55) than at 2c/° (gM = 2.45, SE = 0.20) (Figure 4.12). This difference was not found in the remaining four participants, who showed either a slight increase (P1, P4) or a negligible difference (P2) between OEI scores at 2 and 16c/°. Indeed, a paired samples t-test revealed no significant difference between OEI scores at 2 and 16c/°. The notably large OEI score of 7.66 for one participant (P7) at 16c/°, compared an OEI score of 2.83 at 2c/°, was driven by a reduction in cardinal thresholds and an increase in oblique thresholds.

A subsample of three participants (P1, P5, P6) performed the same orientation-discrimination task at an additional, intermediate spatial frequency (Figure 4.13). There was no consistent pattern in the OEI scores across spatial frequency conditions.

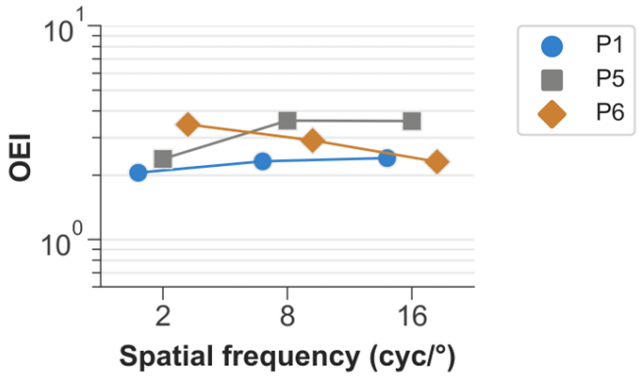

Figure 4.13. For each participant who performed the intermediate spatial frequency condition at 8 c/°, the oblique effect index (OEI) scores are plotted against spatial frequency.

4.3.4 Modelling

Design

Model performance was assessed on a simulated temporal orientation-discrimination 2AFC task (see Section 3.4.1), analogous to the behavioural task. Orientation anisotropies were implemented in a similar manner as those described for the contrast-detection experiment (Section 4.2). Model performance was assessed for each of the orientation decoders described in Section 3.2. Unless otherwise specified, model parameters were set to the 'default' values described in Section 3.5 and summarised in Table 4.1. For consistency with the findings of the previous contrast-detection experiment (Section 4.2), the default proportion of cardinal-tuned neurons was set to 0.7. For computational efficiency the model orientation-discrimination thresholds were measured for two stimulus orientations (0 and 45°). The 'oblique effect index' (OEI, see Section 2.8) scores quantified the magnitude of the oblique effect. The 'low', 'mid', and 'high' spatial frequency conditions were the same as those described for the contrast-detection experiment in Section 4.2. The modelling work aimed to reflect suprathreshold orientation-discrimination performance, therefore the stimulus contrast was set to 40%, corresponding to approximately 10 times the model-detection threshold in the high spatial frequency condition (see Section 4.2.4).

Overrepresentation

For the maximum-likelihood (ML) decoder, increasing the proportion of cardinal-tuned neurons (either 0.5, 0.6, 0.7, 0.8, or 0.9) generated a slight inverse oblique effect in the low spatial frequency condition, whereas OEI scores increased greatly at the highest spatial frequencies (Figure 4.14). Results were similar for the population-vector (PV) decoder, although the cardinal overrepresentation induced substantially larger OEI scores at mid to

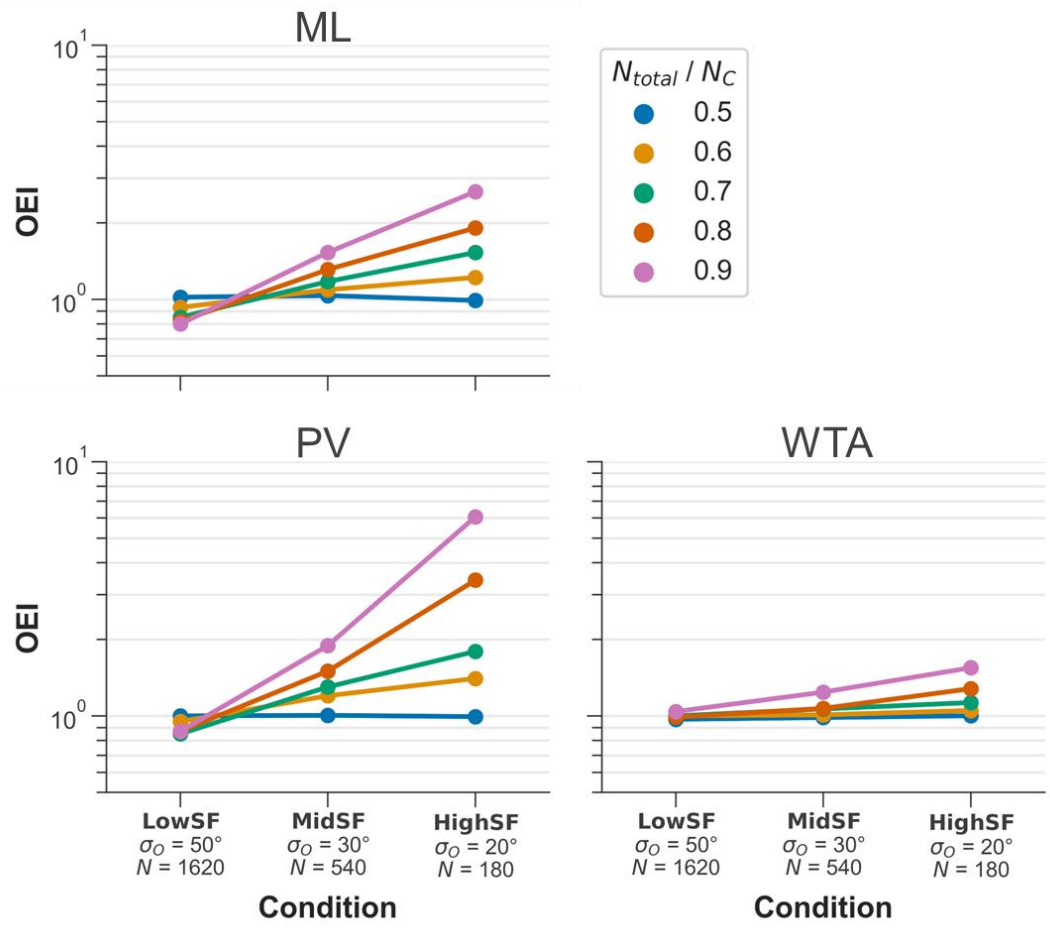

Figure 4.14. For the maximum-likelihood (ML), population-vector (PV) and winner-take-all (WTA) decoders, OEI scores are plotted for each spatial frequency condition. The starred low spatial frequency condition had broadened orientation-tuning bandwidths. Coloured lines reflect the proportion of cardinal-tuned neurons in the model.

high spatial frequencies, relative to the maximum-likelihood decoder. For the winner-take-all (WTA) decoder, OEI scores increased with spatial frequency but only in the presence of a considerable cardinal overrepresentation, such that the proportion of cardinal-tuned neurons was at least 0.8.

Tuning Anisotropy

Cardinal-orientation bandwidths were set as a fraction (either 1, 0.8, 0.6, 0.4, or 0.2) of the oblique-orientation bandwidths, with the proportion of cardinal-tuned neurons set to 0.7. For the maximum-likelihood and winner-take-all decoders, increasing the scale of the tuning anisotropy increased the magnitude of the oblique effect at all spatial frequencies (Figure 4.15). The magnitude of the oblique effect was largest for the winner-take-all decoder, and was mostly invariant to spatial frequency. In contrast, anisotropic orientation

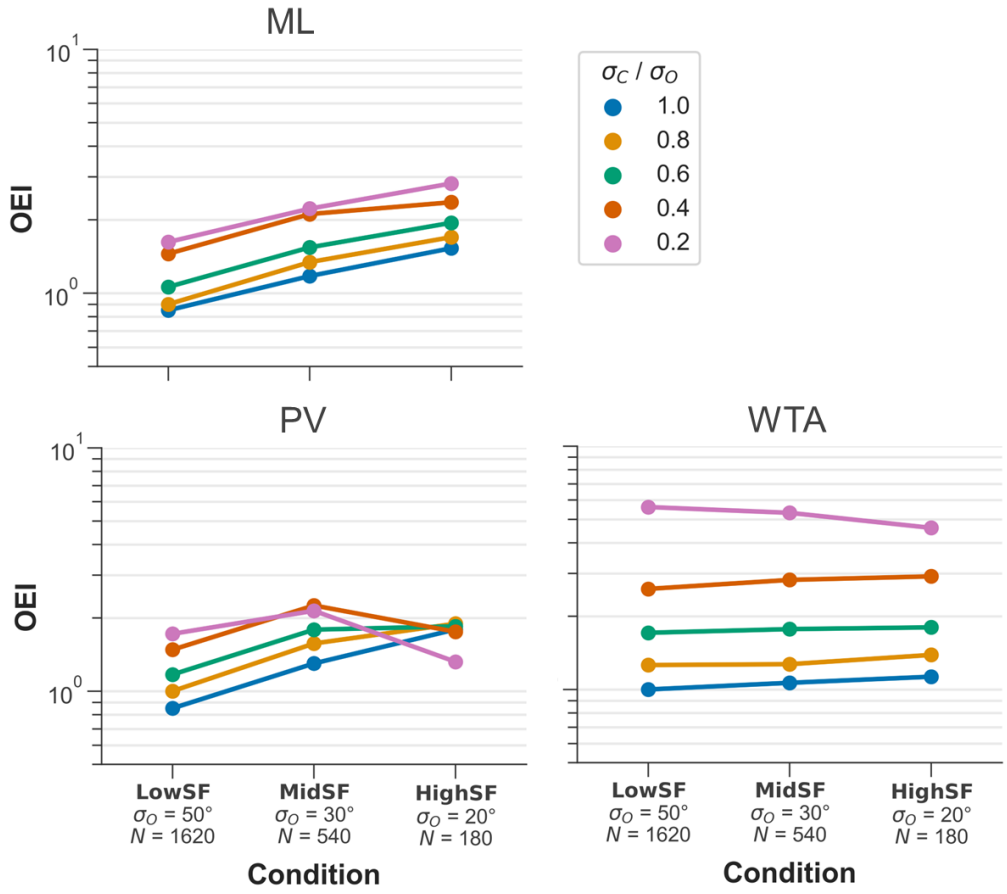

Figure 4.15. For the maximum-likelihood (ML), population-vector (PV) and winner-take-all (WTA) decoders, OEI scores are plotted for each spatial frequency condition. The proportion of cardinal-tuned neurons was fixed at 0.7. The starred low spatial frequency condition had broadened orientation-tuning bandwidths. Coloured lines reflect the cardinal bandwidth, set as a fraction of the oblique bandwidth.

bandwidths resulted in OEI scores for the population-vector decoder which increased at low spatial frequencies but substantially decreased for the highest spatial frequency condition.

Oblique noise

The Fano factor of oblique-tuned neurons was set as a multiple (either 1, 2, 3, 4, or 5) of that for cardinal-tuned neurons, with the proportion of cardinal-tuned neurons set to 0.7. To capture the size of the oblique effect for orientation discrimination, cardinal-orientation

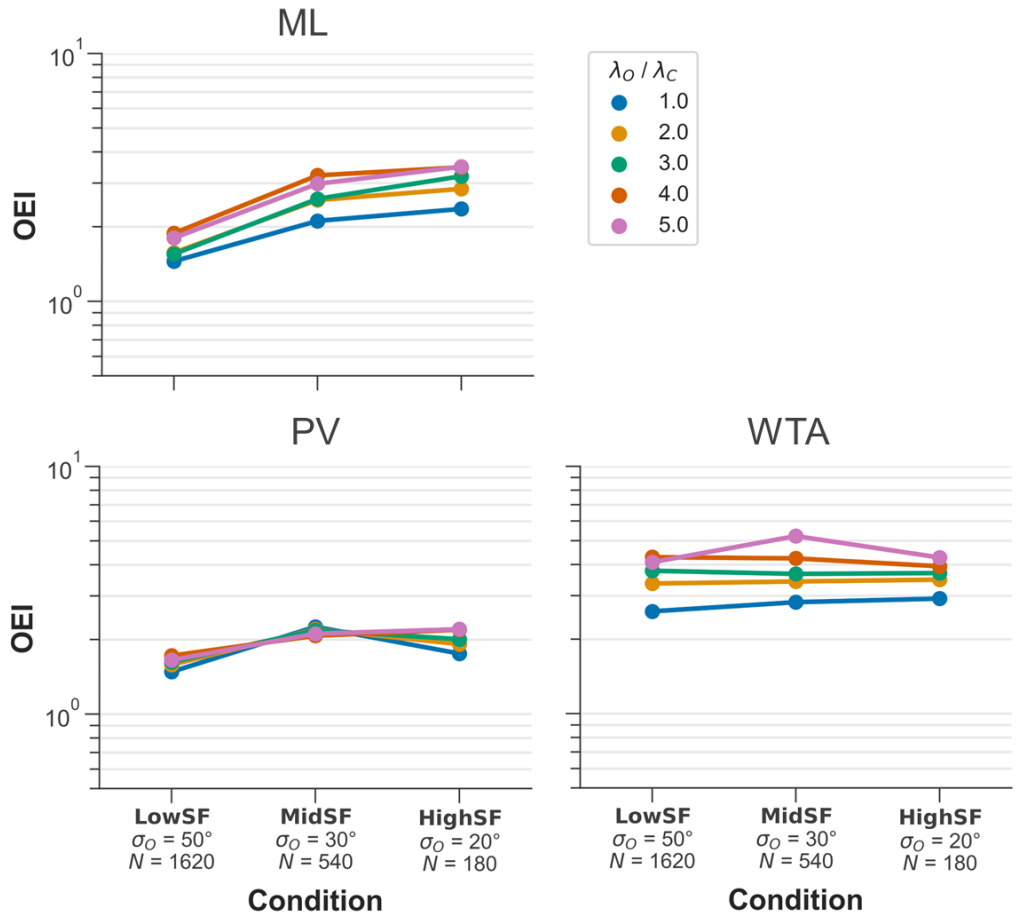

Figure 4.16. For the maximum-likelihood (ML), population-vector (PV) and winner-take-all (WTA) decoders, OEI scores are plotted for each spatial frequency condition. The proportion of cardinal-tuned neurons was fixed at 0.7, and the cardinal bandwidth was set to 0.4 times the oblique bandwidth. The starred low spatial frequency condition had broadened orientation-tuning bandwidths. Coloured lines reflect the Fano factor for oblique-tuned neurons, set as a multiple of the Fano factor for cardinal-tuned neurons.

bandwidths were set to 0.4 times the oblique-orientation bandwidth. For the maximum-likelihood and winner-take-all decoders, increases in response variability for oblique-tuned neurons resulted in moderate increases in OEI scores which were mostly uniform across spatial frequencies (Figure 4.16). In contrast, the oblique effect for the population-vector decoder was invariant with respect to anisotropic levels of response variability.

Thresholds

Orientation-discrimination thresholds were examined whilst varying the extent of anisotropic orientation bandwidths (Figure 4.17), with the proportion of cardinal-tuned neurons set to 0.7 and with an oblique-Fano factor of which was twice the cardinal-Fano factor. For the maximum-likelihood decoder, cardinal thresholds were mostly invariant to changes in spatial frequency, whereas oblique thresholds increased with spatial frequency. Thresholds for the population-vector decoder increased uniformly with spatial frequency, whereas moderate reductions in discrimination thresholds were found for the winner-take-all decoder under the same conditions. Orientation-discrimination thresholds for the winner-take-all decoder were roughly ten times larger than the thresholds for the maximum-likelihood decoder.

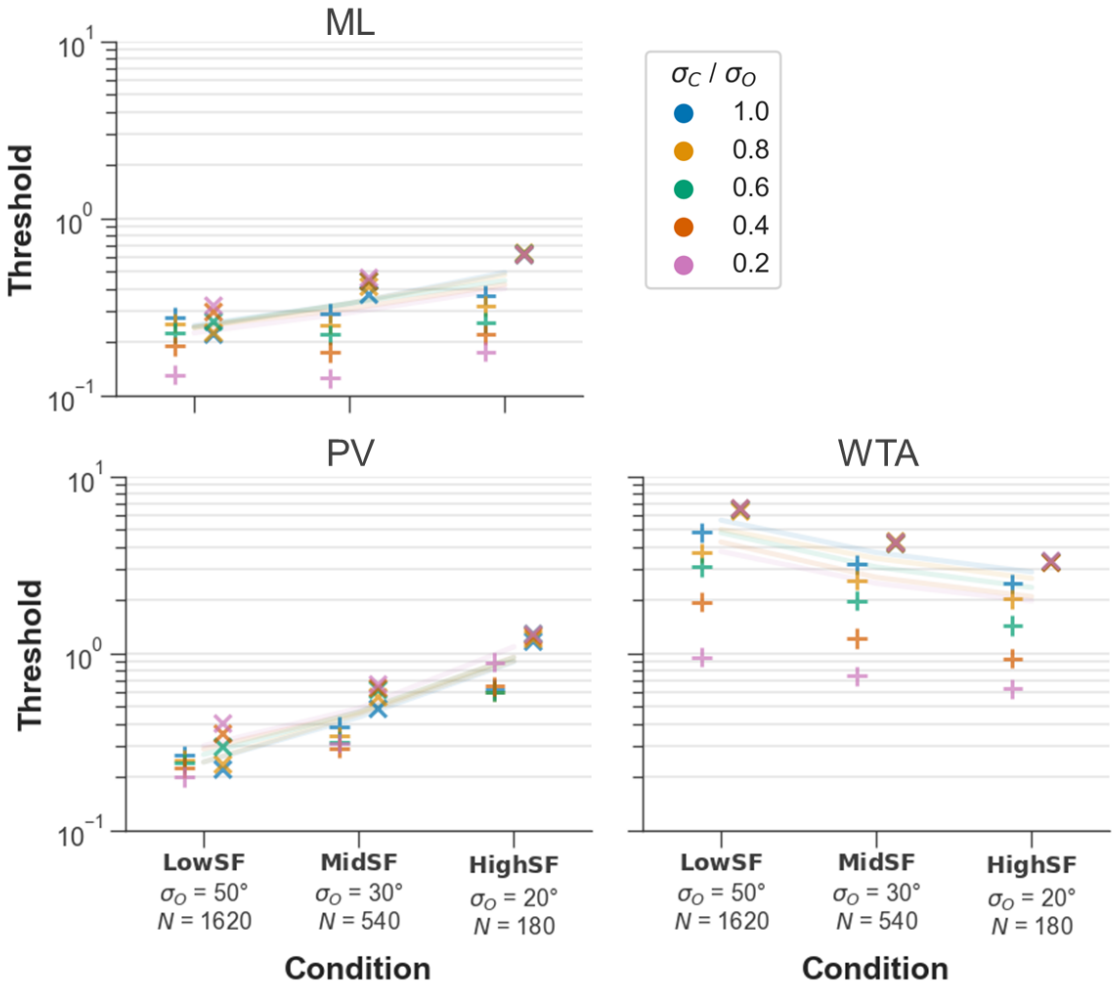

Figure 4.17. For the maximum-likelihood (ML), population-vector (PV) and winner-take-all (WTA) decoders, discrimination thresholds for stimulus orientations of 0° (+ symbols) and 45° (x symbols) are plotted for each spatial frequency condition. The proportion of cardinal neurons was 0.7, and the oblique Fano factor was double the cardinal-Fano factor. The starred low spatial frequency condition had broadened orientation bandwidths. Coloured lines reflect the cardinal bandwidth, set as a fraction of the oblique bandwidth.

4.3.5 Discussion

The behavioural experiment revealed that the oblique effect for orientation discrimination does not systematically vary with spatial frequency, supporting previous findings (Beaudot & Mullen, 2006; Heeley & Buchanan-Smith, 1990; Heeley & Timney, 1988; Matin et al., 1987). However, discrimination thresholds for oblique orientations were

found to increase as a function of spatial frequency for the vast majority of participants, although the extent of this effect varied greatly. This aligns with the group-level effects reported in previous work (Heeley & Buchanan-Smith, 1990; Heeley & Timney, 1988; Matin et al., 1987). Losses in performance at high spatial frequencies were unlikely to have resulted from impaired visibility because the stimulus contrast was set to a fixed multiple of the contrast threshold (at least five times). Future research should aim to measure orientation-discrimination performance for higher spatial frequencies than have been reported previously (> 20c/°), whilst ensuring to control for the perceived contrast of stimuli.

In the model, the size of the oblique effect for orientation discrimination was only captured in the presence of a substantial anisotropy in orientation-tuning bandwidths, such that cardinal bandwidths were approximately half of the oblique bandwidths. This is consistent with previous modelling work which found that the oblique effect for motion-direction discrimination was captured with a similar scale of anisotropy, in the tuning bandwidths of direction-selective neurons (Rokem & Silver, 2009). For neuronal populations with broader orientation bandwidths (50°), an overrepresentation of cardinal-tuned neurons and anisotropic levels of response variability were found to contribute only marginally to the oblique effect for orientation discrimination.

The oblique effect for orientation discrimination was best-captured by the winner-take-all decoder, such that moderate orientation anisotropies elicited large oblique effects, which were invariant with respect to spatial frequency. This conflicts with the view that discrimination performance is determined by the slopes of tuning curves (Beaudot & Mullen, 2006; Regan & Beverley, 1985). Instead, for the winner-take-all decoder, discrimination performance was determined primarily by the degree of overlap between the orientation-tuning curves of independent mechanisms. However, there is limited neurophysiological

evidence for anisotropic tuning bandwidths in V1 and V2 (see Section 1.4), and such an anisotropy was found to abolish the oblique effect in model simulations of contrast detection (see Section 4.2). Anisotropic orientation bandwidths may therefore emerge at a later stage in the visual pathways, in perceptual mechanisms which are possibly distinct from those serving contrast detection. This notion will be explored further in the general discussion of this Chapter (see Section 4.5).

4.4 Orientation discrimination and stimulus contrast

4.4.1 Introduction

At relatively low contrast levels, orientation-discrimination thresholds reportedly decrease with increasing stimulus contrast, before reaching asymptotic levels of performance at intermediate to high contrast levels, approximately 25 times the detection threshold (Regan & Beverley, 1985; Webster et al., 1990). This is unlikely to result from contrast-dependent changes in the spatial tuning properties of visual cortical neurons, because orientation selectivity is generally considered to be invariant with stimulus contrast (Albrecht & Hamilton, 1982; Bowne, 1990; Sclar et al., 1990; Skottun et al., 1987), at least for larger stimuli which extend beyond the classical receptive field into the extra-classical surround (Y.-J. Liu et al., 2015).

Contrast-dependent changes in orientation-discrimination performance can be extended over a wider contrast range by increasing the level of noise in the visual stimulus by, for example, implementing frame-by-frame orientation jitter (Mareschal & Shapley, 2004), using drifting gratings (Bowne, 1990), manipulating the stimulus-orientation bandwidth (Cass et al., 2009; Heeley et al., 1997), or by increasing the number of alternatives such as in a spatial 4AFC discrimination task (Reisbeck & Gegenfurtner, 1998). Therefore, the plateau in orientation-discrimination thresholds at intermediate contrasts may reflect a floor effect resulting from underlying levels of internal noise which inherently limit discrimination performance, which contrast-dependent increases in signal strength cannot overcome (Mareschal & Shapley, 2004). In the modelling work of the previous experiment, orientation-discrimination performance for the winner-take-all model was predominantly constrained by the orientation bandwidths of model neurons (see Section 4.3.4).

Oblique effect and contrast

The vast majority of previous research which measured the influence of stimulus contrast on orientation discrimination used a single cardinal orientation, therefore little is known about the modulation of the oblique effect by stimulus contrast. Although one study reported that there was no change in the size of the oblique effect with increasing contrast (Mareschal & Shapley, 2004), orientation-discrimination thresholds for the vertical orientation were compared with the pooled data of both the vertical and oblique orientations (for a single participant). Furthermore, visual inspection of their results indicates that the size of the oblique effect for orientation discrimination may have increased slightly between 4 and 20% contrast (see Figure 7 of Mareschal & Shapley, 2004).

One study reported that the oblique effect for orientation discrimination scales with stimulus contrast (Bloem & Ling, 2017b). Across a wide range of contrasts, they measured the proportion of correct discrimination judgements for a single, fixed orientation difference (equal to the discrimination threshold for obliques). Although they successfully ruled out a contrast-gain mechanism to account for their results, they reported that their results reflected increased levels of response gain for cardinal-tuned mechanisms. An alternative possibility, that has not yet been explored, is that the contrast-dependency of the oblique effect could emerge from the anisotropic response characteristics of orientation-selective mechanisms.

Aims

The purpose of this experiment was to investigate the influence of stimulus contrast on orientation-discrimination performance, with a view to informing a computational account of the oblique effect. The impact of neuronal anisotropies on model performance were explored whilst varying stimulus contrast, with model parameters guided by the preceding

work in this Chapter (see Sections 4.2 and 4.3).

4.4.2 Methods

Participants

Six participants took part in the present orientation-discrimination experiment, all with normal or corrected-to-normal vision. All but three participants (P1, P2, and P3) were naïve to the study aims. Ethical guidelines were followed as described in Section 2.1

Stimuli

The testing apparatus and stimulus parameters were the same as for the orientation-discrimination experiment described in Section 4.3.2, except the spatial frequency was 2c/°, and the stimulus contrast was varied across five levels of Michelson contrast (either 2.5, 5, 10, 20, or 40%). The lowest contrast condition, 2.5%, was roughly equivalent to five times the average contrast-detection threshold at 2c/° (see Section 4.2.4).

Design

For each run, the chosen contrast condition and orientation condition (either 0, 90, -45, or 45°) defined the corresponding parameters of the Gabor stimuli, which were constant for each run of trials. Orientation-discrimination thresholds were determined for each condition using a temporal two-alternative forced choice task (2AFC) with a 3-up 1-down adaptive staircase procedure (Section 2.5), whereby the orientation difference between the standard and comparison was determined by the staircase. The 'oblique effect index' (OEI, see Section 2.8) scores quantified the size of the oblique effect.

Procedure

Procedural details of the orientation-discrimination task were identical to those described in Section 4.4.2.

4.4.3 Results

A two-way repeated measures ANOVA found significant main effects of orientation ($F(3,21) = 44.8$, $p < .001$, $\eta^2_p = .865$) and contrast ($F(4,28) = 17.7$, $p < .001$, $\eta^2_p = .718$) on the measured orientation-discrimination thresholds. Consistent across all six participants, and for each contrast condition, pairwise comparisons revealed that thresholds were significantly lower for the cardinal orientations (0 and 90°) than for the obliques (-45 and 45°) (Figure

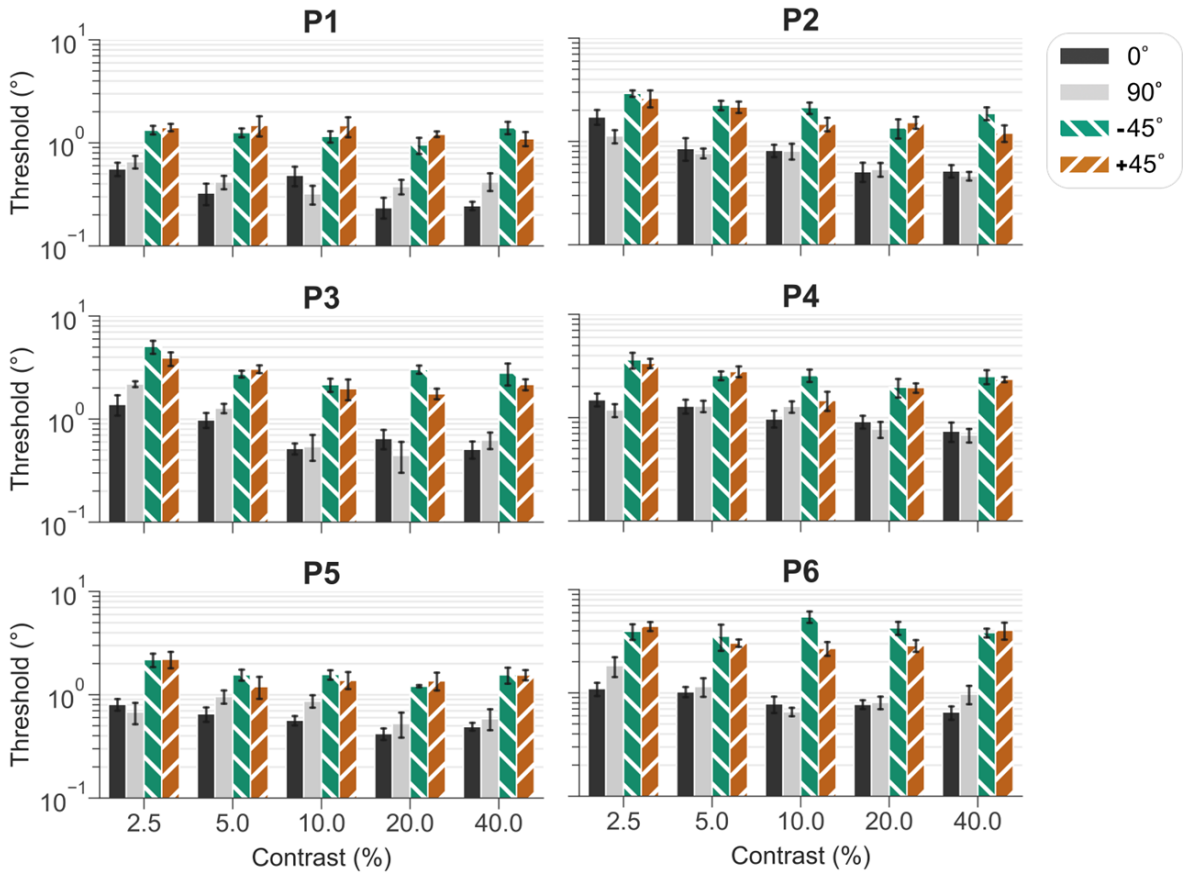

Figure 4.18. For each participant, orientation-discrimination thresholds are plotted against contrast, for horizontal (0°), vertical (90°), and the left (-45°) and right (45°) obliques.

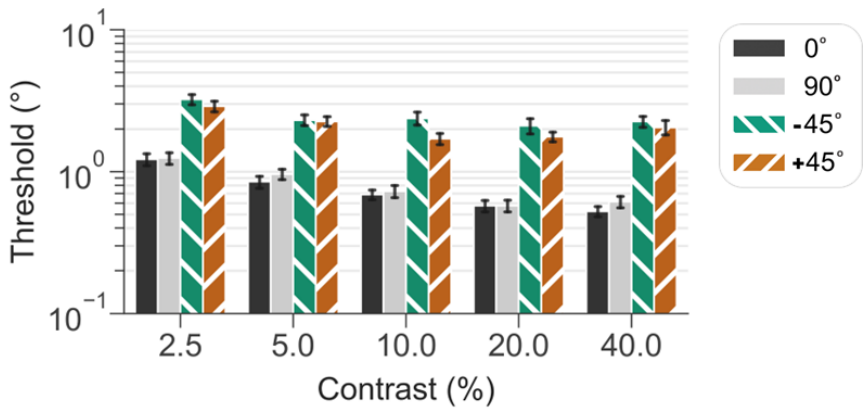

Figure 4.19. The mean orientation-discrimination thresholds across all six participants are plotted against contrast. Oblique thresholds reached asymptotic levels of performance at a lower contrast than cardinal thresholds.

4.18). There were no systematic differences in thresholds between horizontal and vertical, nor between the two oblique orientations. Mean thresholds are shown in Figure 4.19.

Although there was no significant interaction between orientation and contrast on discrimination thresholds, a one-way repeated measures ANOVA on the OEI scores revealed a significant main effect of contrast ($F(4,20) = 3.92$, $p = .017$) with a large effect size ($\eta^2_p = .439$). Consistent across all six participants (Figure 4.20), pairwise comparisons revealed that OEI scores at 40% contrast (gM = 3.68, SE = 0.28) were significantly higher than at 2.5% (gM = 2.50, SE = 0.15) or 5% contrast (gM = 2.55, SE = 0.15). In general, the increasing size of the oblique effect was driven by reductions in orientation-discrimination thresholds which occurred over a greater range of contrasts for the cardinal orientations than for the obliques (see Figure 4.18).

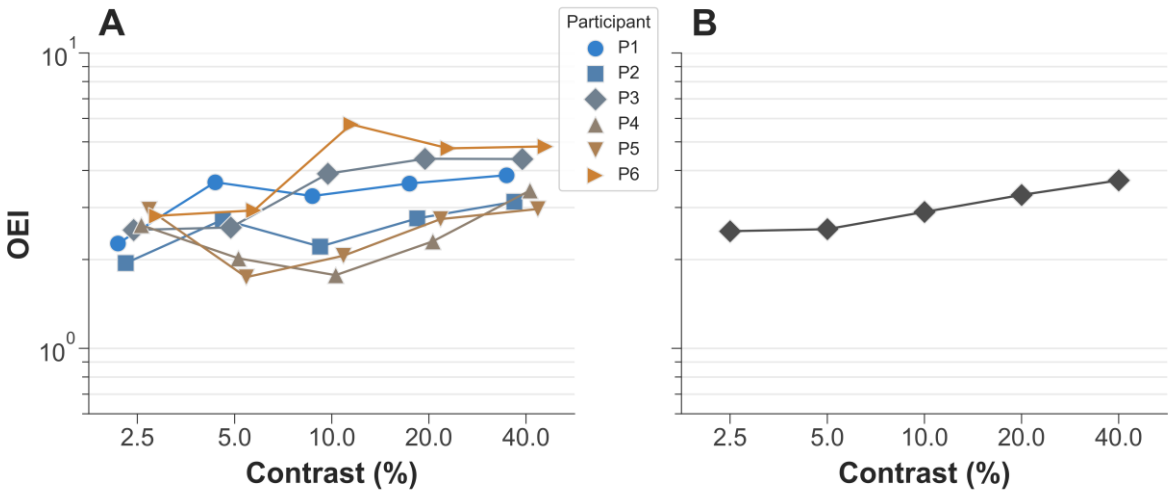

Figure 4.20. Individual oblique effect index (OEI) scores (*A*) and the geometric-mean OEI score (*B*) are plotted against stimulus contrast.

4.4.4 Modelling

Design

Model performance was assessed using a simulated temporal orientation-discrimination 2AFC task, analogous to the behavioural task (see Section 3.4.1). Unless otherwise specified, the 'default' model parameters were those defined in Section 3.5. Following the findings of Sections 4.2 and 4.3, orientation anisotropies were implemented by default for all model simulations, such that the proportion of cardinal-tuned neurons was set to 0.7, the cardinal-tuning bandwidth was set to 0.4 times the oblique-tuning bandwidth, and the oblique-Fano factor was set to 2 times that of the cardinal-Fano factor. Orientation-discrimination thresholds were measured for two standard orientations (either 0 or 45°) across six levels of stimulus contrast (either 2.5, 5, 10, 20, 40, or 80%). Just two standard orientations were tested for reasons of computational expediency, as there were no systematic differences between the two cardinal orientations nor the two obliques. The 'oblique effect

index' (OEI, see Section 2.8) quantified the magnitude of the oblique effect.

To align the model with the low spatial frequency condition described in the previous two experiments (Section 4.3.3), the oblique-orientation bandwidth was fixed at 50°. The default total number of neurons in this condition was reduced from 1620 to 540 to ease the computational overhead of numerous contrast conditions. The lowest contrast condition, 2.5%, was roughly equivalent to two times the contrast-detection threshold of the model.

Overrepresentation

Varying the proportion of cardinal-tuned neurons in the model (either 0.5, 0.6, 0.7, 0.8, or 0.9) had a substantial impact on the OEI scores for the maximum-likelihood and population-vector decoders at lower contrasts (Figure 4.21). For an equal number of cardinal oblique neurons, OEI scores for the maximum-likelihood decoder increased dramatically between 2.5 and 5% contrast before reaching asymptotic levels of performance at 20% contrast, whereas OEI scores for the population-vector and winner-take-all decoders scores increased gradually, and continuously, with increasing stimulus contrast over the entire range. For all decoders, the oblique effect was abolished at the lowest contrast tested (2.5%) in the absence of the cardinal overrepresentation. For the maximum-likelihood and population-vector decoders, increasing the proportion of cardinal-tuned neurons resulted in a substantial amplification of OEI scores at lower contrasts (< 20%), whereas OEI scores for the winner-take-all decoder were essentially invariant with respect to the proportion of cardinal-tuned neurons in the population.

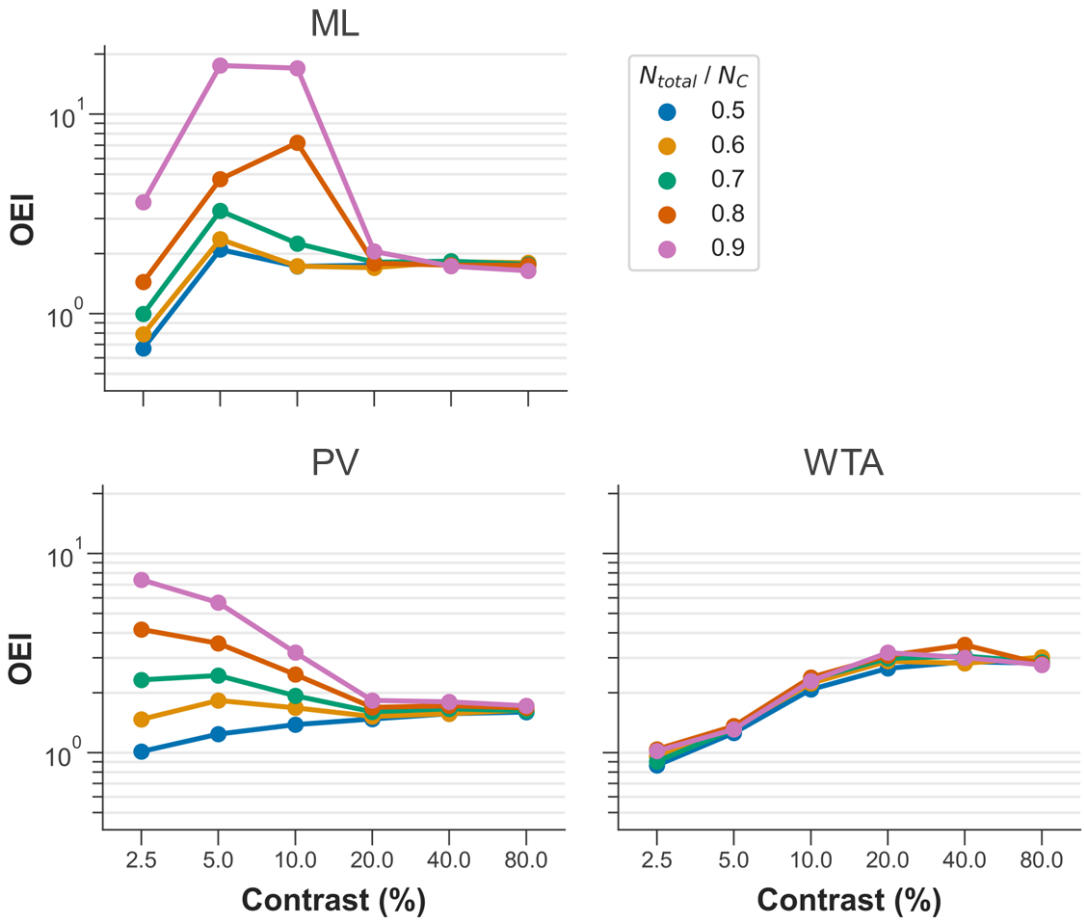

Figure 4.21. For the maximum-likelihood (ML), population-vector (PV) and winner-take-all (WTA) decoders, OEI scores are plotted against stimulus contrast. The cardinal bandwidth was fixed at 0.4 times the oblique bandwidth, and the oblique Fano factor was fixed at 2 times the cardinal Fano factor. Coloured lines reflect the proportion of cardinal-tuned neurons in the model. The y-axes were extended in this figure to account for the extreme OEI scores of the maximum-likelihood decoder.

Anisotropic tuning bandwidths

Variations in the extent of tuning anisotropy influenced the modulation of the oblique effect by contrast for all decoders (Figure 4.22). For the maximum-likelihood decoder, anisotropic tuning bandwidths increased the size of the oblique effect for orientation discrimination, which was accentuated at 5% contrast, whereas larger OEI scores were found

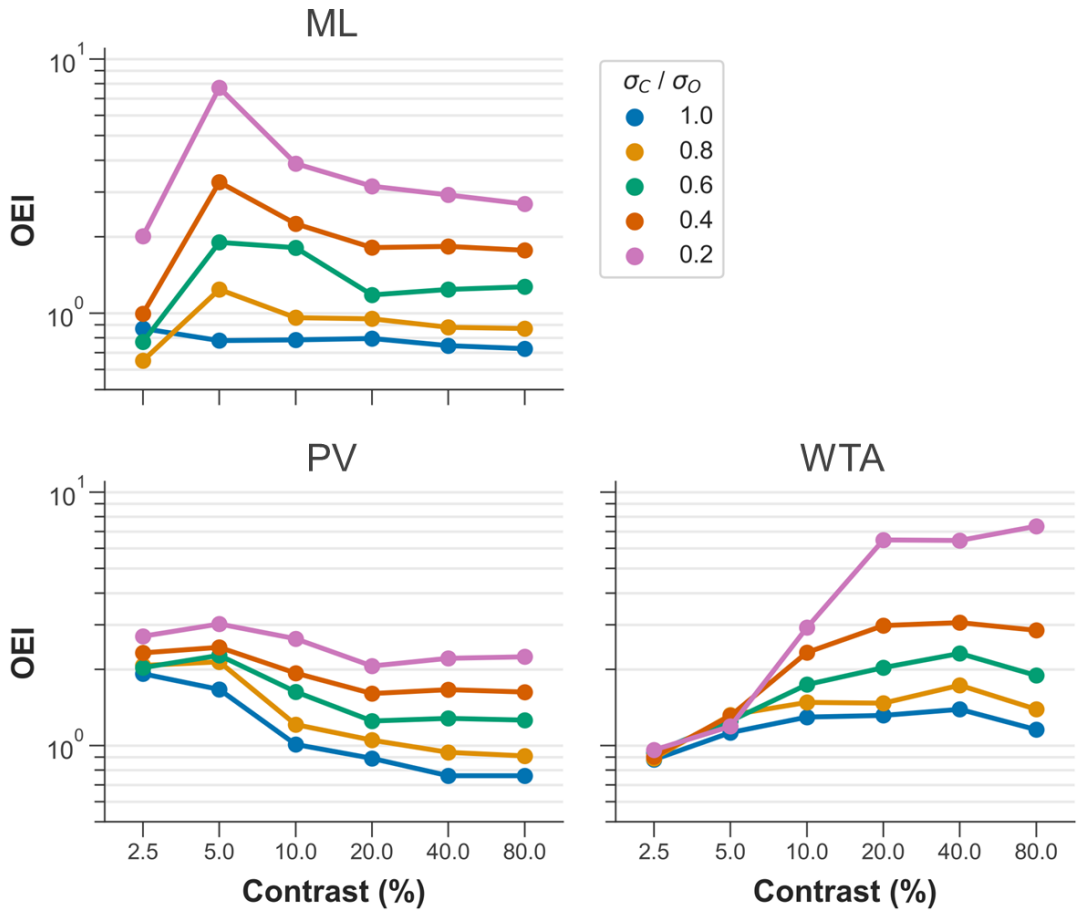

Figure 4.22. For the maximum-likelihood (ML), population-vector (PV) and winner-take-all (WTA) decoders, OEI scores are plotted against stimulus contrast. The cardinal bandwidth was fixed at 0.4 times the oblique bandwidth, and the oblique Fano factor was fixed at 2 times the cardinal Fano factor. Coloured lines reflect the cardinal bandwidth, set as a fraction of the oblique bandwidth.

3048 across all contrasts for the population decoder. For the winner-take-all decoder, the size of the
3049 oblique effect at low contrasts (2.5 and 5%) was not modulated by the presence of anisotropic
3050 tuning bandwidths, whereas OEI scores increased greatly before reaching asymptotic levels
3051 of performance at 20% contrast.

Oblique noise

Adjusting the Fano factor of oblique-tuned neurons did not strongly modulate the oblique effect for neither the maximum-likelihood nor the population-vector decoders (Figure 4.23). In contrast, for the winner-take-all decoder, increasing the scale of oblique noise resulted in smaller OEI scores at lower contrasts (< 20%) and larger OEI scores at the highest contrasts (> 20%).

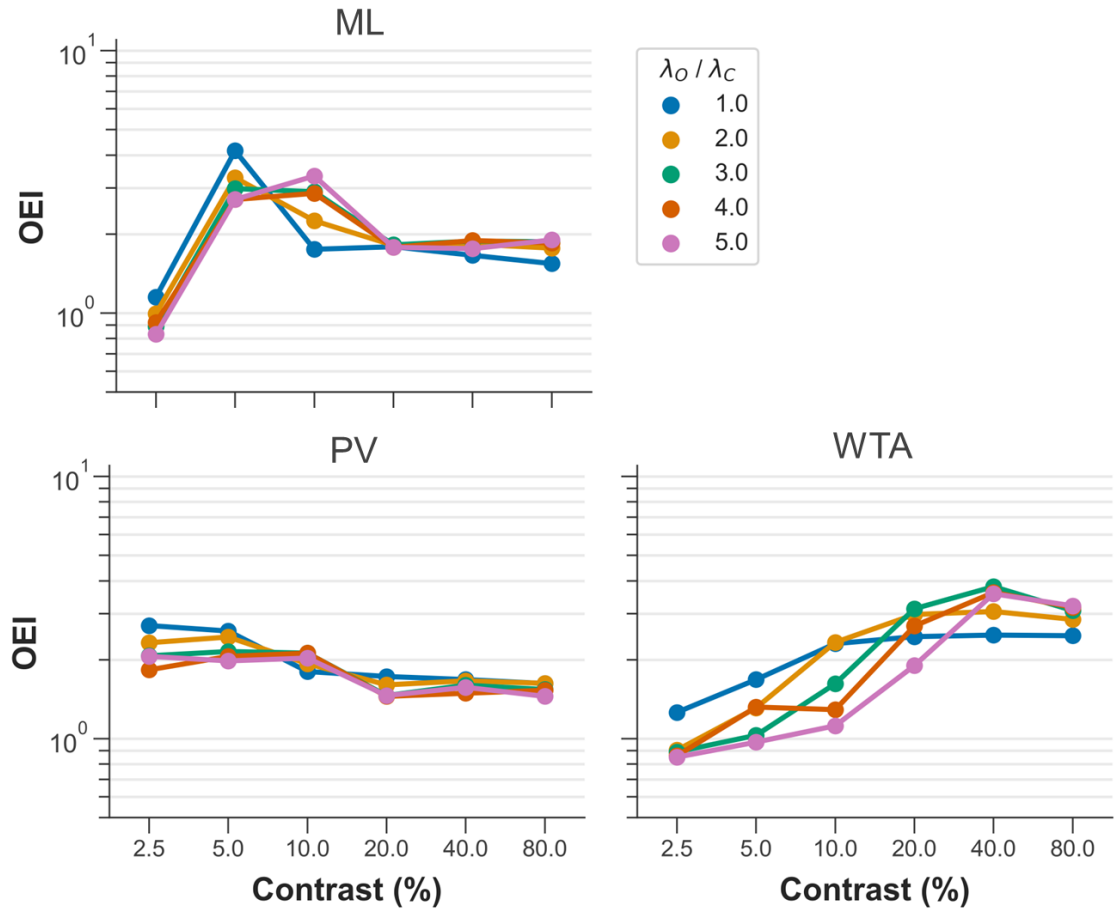

Figure 4.23. For the maximum-likelihood (ML), population-vector (PV) and winner-take-all (WTA) decoders, OEI scores are plotted against stimulus contrast. The proportion of cardinal-tuned neurons was fixed at 0.7, and the cardinal bandwidth was fixed at 0.4 times the oblique bandwidth. Coloured lines reflect the Fano factor for obliques, set as a multiple of the Fano factor for cardinals.

Thresholds

Orientation-discrimination thresholds were greatly reduced with increasing contrast for all decoders, although this effect was strongest for the maximum-likelihood decoder with a roughly ten-fold decrease in thresholds across the entire range of contrasts tested (Figure 4.24). Thresholds for the population-vector decoder decreased by roughly 80% across the

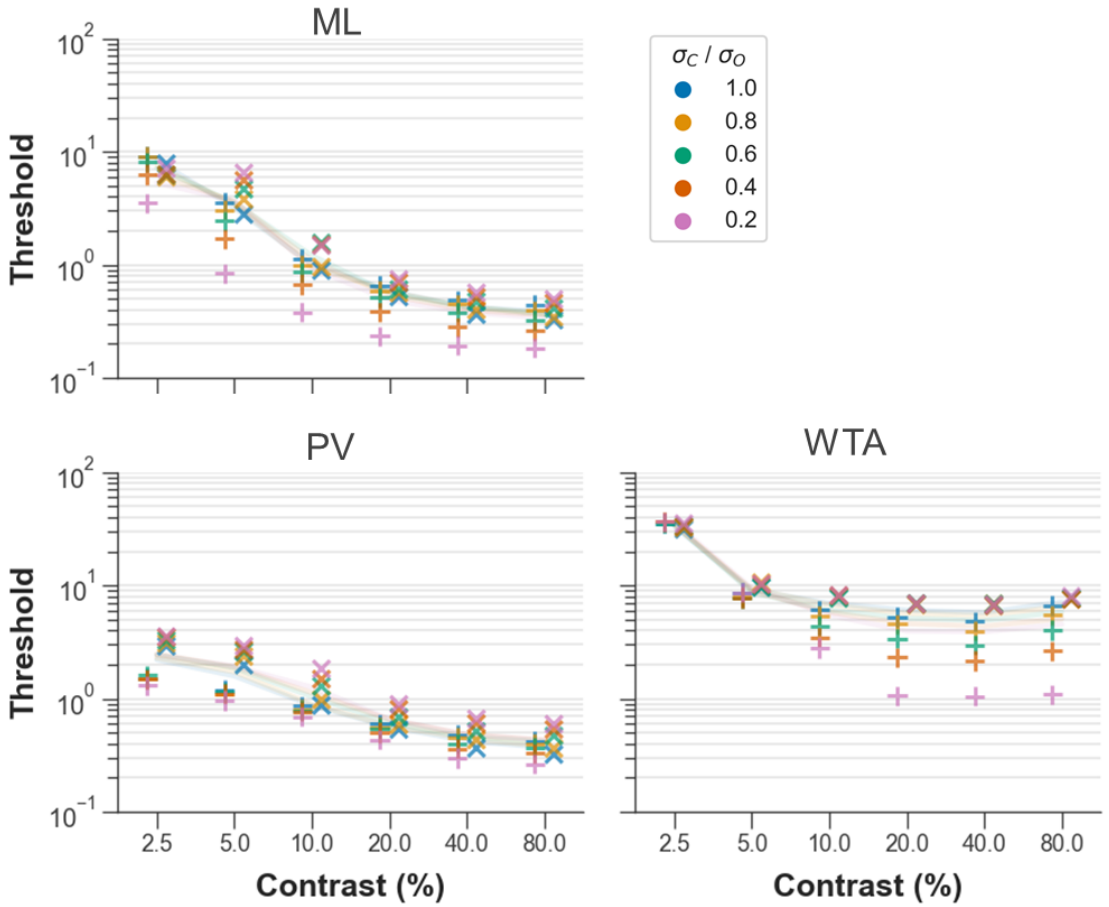

Figure 4.24. For the maximum-likelihood (ML), population-vector (PV) and winner-take-all (WTA) decoders, orientation-discrimination thresholds for stimulus orientations of 0° (indicated by + symbols) and 45° (indicated by x symbols) are plotted against stimulus contrast. The proportion of cardinal-tuned neurons was fixed at 0.7, the oblique Fano factor was fixed at 2 times the cardinal Fano factor. Colours reflect the cardinal bandwidth, set as a fraction of the oblique bandwidth.

same contrast range. For the winner-take-all decoder, threshold decreases were mostly restricted to between 2.5 and 5% contrast, whereas in the presence of anisotropic bandwidths, cardinal thresholds approached asymptotic levels of performance at a higher contrast (20%) than oblique thresholds (5%).

4.4.5 Discussion

Orientation-discrimination thresholds in the psychophysical experiment were found to decrease with increasing stimulus contrast before reaching asymptotic levels of performance at intermediate contrasts. For the cardinals, this contrast was approximately 20%, consistent with previous findings (Bowne, 1990; Regan & Beverley, 1985; Webster et al., 1990), although this contrast was approximately 5 or 10% for the obliques. Substantially larger improvements in orientation-discrimination performance with increasing contrast have been reported previously, however these occurred when the stimulus contrast ranged between two and four times the contrast-detection threshold (Webster et al., 1990). The lowest contrast used in the present experiment (2.5%) was approximately five times the average contrast-detection threshold, measured at a similar spatial frequency (2c/°) (see Section 4.2), which may account for the disparity with previous findings.

The size of the oblique effect for orientation discrimination was found to scale with stimulus contrast (Bloem & Ling, 2017b), driven by decreases in cardinal thresholds which reached asymptotic levels of performance at higher contrasts than oblique thresholds. Although non-monotonic variations in the influence of contrast on the size of the oblique effect were found for the majority of participants, it is difficult to conclude whether such variations were systematic or if they were simply due to measurement noise. It is unlikely that these findings reflect contrast-dependent changes in the response characteristics of

underlying neuronal mechanisms, because orientation selectivity is invariant with contrast for stimuli which extend beyond the classical receptive field into the extra-classical surround (Y.-J. Liu et al., 2015), such as those used in the present experiment.

The winner-take-all model captured the influence of contrast on orientation-discrimination performance, whereas the maximum-likelihood and population-vector models failed to consistently predict the increasing magnitude of the oblique effect with increasing contrast. These results are consistent with the findings of the previous experiment, in which the winner-take-all decoder captured the influence of spatial frequency on the oblique effect for orientation discrimination (see Section 4.3).

The plateau in orientation-discrimination thresholds at intermediate contrasts are suggested to reflect a floor effect (Mareschal & Shapley, 2004), resulting from some 'internal limit' (i.e., internal noise) which inherently limits discrimination performance. For the winner-take-all model, the contrast at which thresholds reached asymptotic levels of performance was determined primarily by the tuning bandwidths, and to a lesser extent the response variability, of model neurons. The behavioural finding of oblique-discrimination thresholds which plateau at lower stimulus contrasts than cardinal thresholds may therefore reflect the broadened orientation bandwidths of oblique-tuned mechanisms. Additional simulations revealed that the oblique effect for orientation discrimination could not be explained by simply increasing the response gain of cardinal-tuned mechanisms (Figure 4.25), which has been proposed previously (Bloem & Ling, 2017b).

The winner-take-all model predicted that the oblique effect for orientation discrimination should be greatly reduced or abolished at low contrasts, consistent with reports that the oblique effect scales with stimulus contrast (Bloem & Ling, 2017b). although this effect was not found in the psychophysical experiment. However, the winner-take-all model

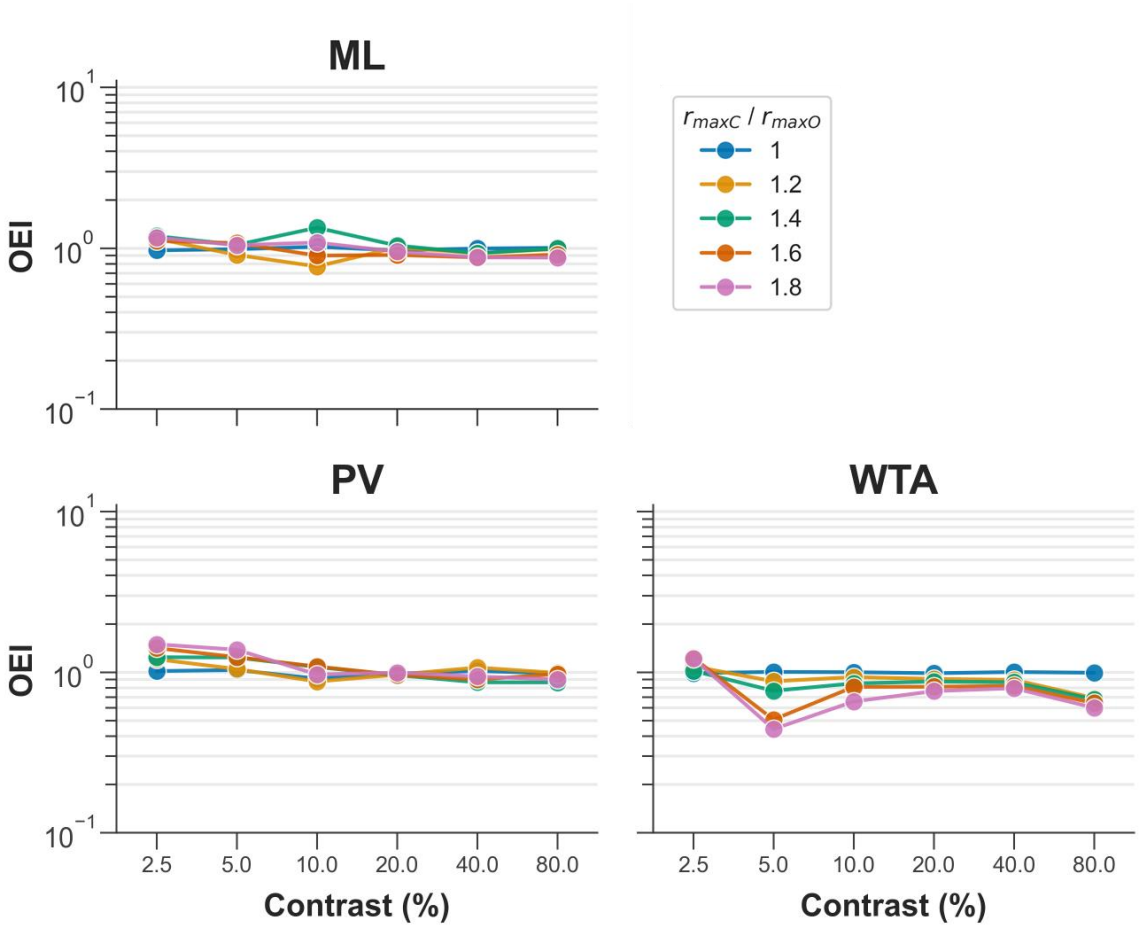

Figure *4.25.* For the maximum-likelihood (ML), population-vector (PV) and winner-take-all (WTA) decoders, OEI scores are plotted against stimulus contrast. The cardinal-maximum firing rate was set as a multiple (*coloured lines*) of the oblique-maximum firing rate. No other neuronal anisotropies were present.

successfully predicted large increases in orientation-discrimination thresholds at near-threshold contrasts (Webster et al., 1990), which were much lower than the contrasts used in the present experiment. A stimulus contrast of 2.5% corresponded to roughly double the contrast-detection threshold of the model (see Figure 4.8 in Section 4.2), whereas the same contrast corresponded to approximately five times the average detection threshold in the psychophysical experiment. Therefore, to fully test the predictions of the model, future research should measure the oblique effect for orientation discrimination over a wider range of stimulus contrasts, with contrast set at a multiple of the detection threshold.

4.5 Summary of findings

The commonly given explanation of the oblique effect is that there is an overrepresentation of cardinal-tuned neurons, relative to oblique-tuned neurons, in early visual cortical areas (see Sections 1.4 and 1.5). Modelling work revealed that this neuronal anisotropy was sufficient to account for the oblique effect for contrast detection, which emerged at relatively high spatial frequencies (see Section 4.2.4), but not to capture the magnitude of the oblique effect for orientation discrimination (see Sections 4.3 and 4.4). The oblique effect for orientation discrimination could only be reproduced when the orientation bandwidth of cardinal-tuned neurons was reduced to roughly half that of oblique-tuned neurons, consistent with previous modelling of the oblique effect for motion-direction discrimination (Rokem & Silver, 2009).

The presence of anisotropic orientation-tuning bandwidths resulted in a diminished oblique effect for contrast detection, that was invariant with respect to changes in spatial frequency, failing to capture the behavioural findings. This suggests that contrast detection and orientation discrimination may be served by distinct neural mechanisms, which may be independent of each other. This is consistent with the large body of evidence for an overrepresentation of cardinal-tuned neurons and the sparsity of neurophysiological and psychophysical evidence for anisotropic orientation bandwidths (see Sections 1.3, 1.4, and 1.5). Psychophysical estimates of orientation bandwidths, which tend to implement contrast-detection procedures (see Section 1.3.4), may reflect neural mechanisms which are separate from those which underlie orientation discrimination. This highlights a potentially fruitful avenue of research, in the comparison of orientation bandwidths for mechanisms of detection and discrimination. An alternative explanation is that orientation-selective mechanisms are shared for the two tasks, with anisotropic tuning bandwidths arising at higher contrasts.

However, orientation selectivity for larger stimuli which extend beyond the classical receptive field, as are used throughout this Chapter, is invariant with respect to changes in stimulus contrast (Y.-J. Liu et al., 2015).

The success of the summation pooling method, where information is pooled across the whole neuronal population, in capturing the oblique effect for contrast detection implicates orientation-decoding methods which integrate information in a similar manner. However, the maximum-likelihood and population-vector decoders failed to capture the oblique effect for orientation discrimination, especially as a function of contrast.

The winner-take-all model reproduced both the magnitude and spatial frequency-invariance of the oblique effect for orientation discrimination, and provided a particularly strong account of the influence of stimulus contrast on discrimination thresholds. This decoder was also robust to relatively large variations in the extent of cardinal overrepresentation. The predominant limiting factor on orientation-discrimination performance for the winner-take-all decoder model was the orientation bandwidth of individual mechanisms, which differs from the suggestion that discrimination performance is determined by the slopes of spatial tuning curves (Beaudot & Mullen, 2006; Regan & Beverley, 1985). The latter account stems from findings of moderate improvements in orientation-discrimination performance after adaptation to the stimulus orientation (Regan & Beverley, 1985). However, the orientation bandwidths of V1 neurons may be reduced after adaptation (C. A. Patterson et al., 2013; Wissig & Kohn, 2012), which improved orientation-discrimination performance for the winner-take-all model in the present study. However, orientation-discrimination thresholds are increased after adaptation to a stimulus that is rotated roughly 15° from the standard orientation (Regan & Beverley, 1985), which is harder to reconcile with the winner-take-all model. Although this could be partially attributed to

adaptation-induced shifts in the orientation preference of V1 neurons (C. A. Patterson et al., 2013; Wissig & Kohn, 2012), further investigation is required to understand the limiting factors on the precision of orientation encoding.

The model was unable to capture the scale of losses in contrast sensitivity observed behaviourally at high spatial frequencies, possibly due to the implementation of spatial frequency selectivity in the present model, where task performance at various nominal spatial frequencies was measured for independent model populations with distinct model parameters. Model populations in each spatial frequency condition were treated as independent from one another because they were assumed to have non-overlapping spatial frequency-tuning curves. This assumption is supported by findings that the detection of a grating is unimpaired by the simultaneous presentation of a mask grating of the same orientation, provided that the target and mask gratings differ sufficiently in spatial frequency (Sachs et al., 1971). Additionally, the average spatial frequency bandwidth of macaque V1 neurons is under 2 octaves (for preferred spatial frequencies above 2c/°), suggesting little overlap between the mechanisms in the 2 and 16c/° conditions tested behaviourally (De Valois, Albrecht, et al., 1982; Xing et al., 2004).

Spatial frequency-dependent changes in detection thresholds possibly could have been accounted for if model neurons were selective for both spatial frequency and orientation. Bandwidths for both parameters are known to decrease substantially with increasing preferred spatial frequency, thus generating potentially substantial reductions in visual sensitivity that were not captured by the present model (Y. Chen et al., 2020; De Valois, Albrecht, et al., 1982; H.-H. Yu et al., 2010). Such a scheme is plausible but it would be extremely computationally expensive to implement, although this may be an avenue worth pursuing in future research.

5. Psychophysical investigations of the orientation-selective mechanisms underlying perception

5.1 General introduction

Orientation-selective mechanisms (or 'orientation channels') are considered to reflect the collective activity of populations of neurons with similar preferred orientations (see Sections 1.2.5 and 1.3.4). Psychophysical investigations revealed the existence of multiple, independent orientation mechanisms by demonstrating their selectivity for specific features, such as orientation or spatial frequency (Graham, 1989). For example, contrast-detection thresholds for a Gabor stimulus are relatively unimpaired by the simultaneous presentation of a mask stimulus, provided that the two stimuli differ sufficiently in orientation (Phillips & Wilson, 1984) or spatial frequency (H. R. Wilson et al., 1983). Psychophysical estimates of orientation bandwidths are broadly similar to the bandwidths of orientation-selective neurons in V1 (Meese & Holmes, 2010), suggesting that mechanisms underlying perception may inherit their selectivities from neurons in earlier stages of the visual pathways. In support, inhibitory interactions between mechanisms, i.e., cross-orientation suppression, have been revealed through psychophysical investigations (Meese & Holmes, 2010), single-cell recordings (B. Li et al., 2006), and measurements of population-level activity in V1 (Brouwer & Heeger, 2011).

The classical explanation of the oblique effect is that the overrepresentation of cardinal-tuned neurons found neurophysiologically (see Section 1.4.2) favours visual performance for cardinal orientations relative to obliques orientations. Although this could account for the oblique effect for contrast detection, anisotropic numbers of mechanisms were not sufficient to explain the oblique effect for orientation discrimination (see Chapter 4).

Modelling work has found that the orientation bandwidth of cardinal-tuned mechanisms had to be approximately half that of oblique-tuned mechanisms in order to capture the size of the oblique effect for orientation discrimination (Chapter 4), or motion direction discrimination (Rokem & Silver, 2009). However, this contrasts with the wealth of single-cell investigations which report that orientation bandwidths are mostly isotropic in V1 and V2 (see Section 1.4.2. Therefore, the mechanisms underlying perception may not simply inherit the response characteristics of neurons in early visual cortex, and may be best-understood through psychophysical investigation.

The work in Chapter 4 indicates that response properties of orientation-selective mechanisms may be task-dependent, such that the oblique effect for contrast detection has a distinct neural basis from the oblique effect for orientation discrimination. However, psychophysical investigations have typically inferred the response characteristics of orientation-selective mechanisms from detection tasks (Graham, 1989). Therefore, the current understanding of the mechanisms underlying perception may reflect detection mechanisms only, rather than a general property of the visual system.

Section 5.2 explores whether there is a difference in the proportion of cardinal-tuned and oblique-tuned mechanisms which underlie perception. Section 5.3 investigates the orientation bandwidths of cardinal-tuned and oblique-tuned mechanisms, using contrast-detection and orientation-discrimination tasks. A summary of the experimental findings are presented in Section 5.4.

5.2 Estimating the number of cardinal and oblique mechanisms underlying perception

5.2.1 Introduction

The traditional explanation of the oblique effect is that there are more orientation-selective mechanisms which prefer cardinal orientations than oblique orientations. There is a large body of neurophysiological evidence for an overrepresentation of cardinal-tuned neurons in early visual cortex (see Section 1.4), which was confirmed as a feasible account of the oblique effect for contrast detection in Section 4.2. However, there are few psychophysical investigations of the relative number of cardinal-tuned and oblique-tuned mechanisms which underlie perception (see Section 1.3.4).

Direct measurements of the number of mechanisms underlying perception can be achieved using 'metamers', i.e., stimuli which are perceptually indistinguishable yet physically different (Cohen & Kappauf, 1982; J. Freeman & Simoncelli, 2011; Richards, 1979; Williams et al., 1991). To match the perception of a broadband stimulus composed of features uniformly sampled from a flat distribution, a stimulus containing a discrete number of narrowband inputs must elicit an equal response from all feature-selective mechanisms. Figure 5.1 provides an example of how metameric matches would be generated from orientation-selective mechanisms. For a system composed of three or more mechanisms, the minimum number of narrowband inputs that is sufficient to elicit a perceptual match with a

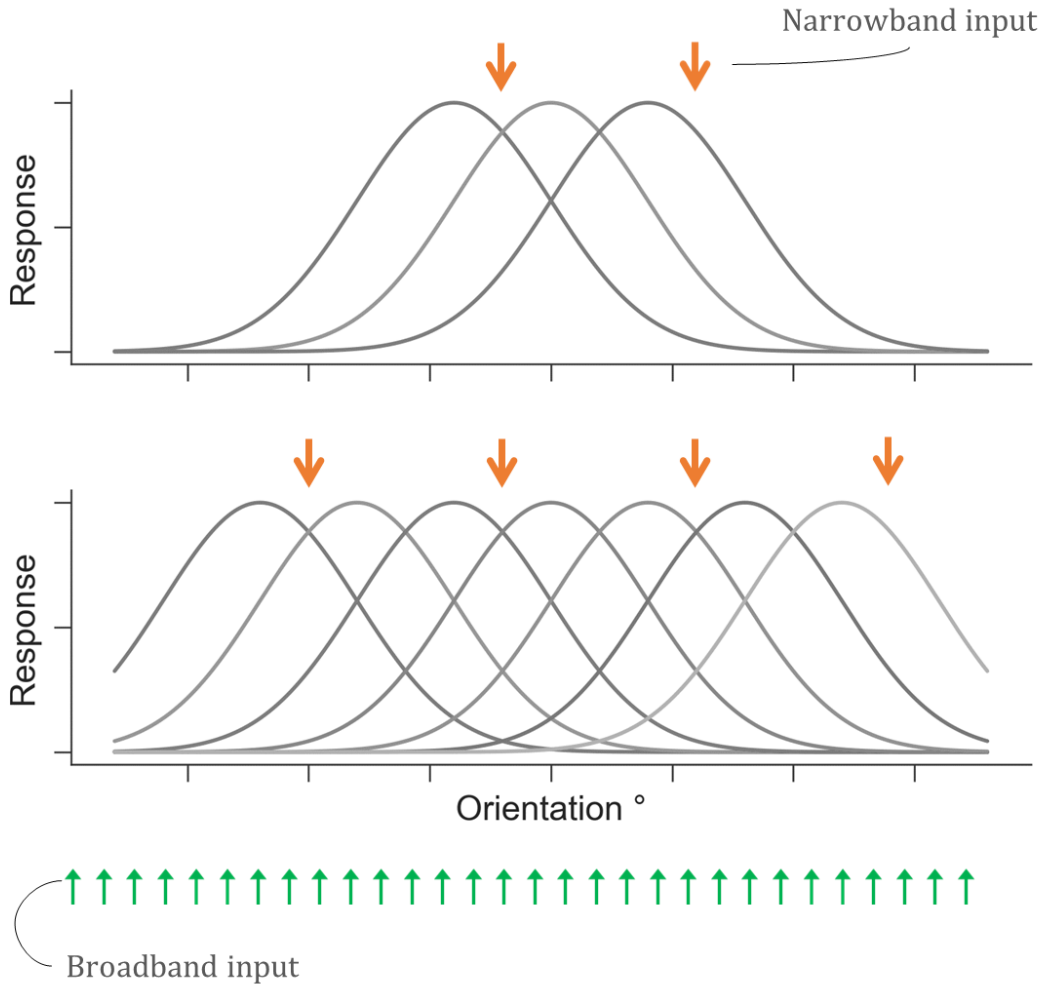

Figure 5.1. Examples of the minimum number of narrowband inputs (orange arrows) which generate identical filter responses to the broadband input (green arrows).

broadband stimulus is equal to the integer value of $N/2$, where N is the total number of mechanisms in the system. Crucially, this estimate is invariant with respect to the tuning bandwidths of individual mechanisms (Richards, 1979). Therefore, the minimum number of mechanisms in the system can be estimated psychophysically by measuring the smallest number of narrowband inputs which are perceptually indistinguishable from a broadband stimulus, multiplied by two, less 1 (Richards, 1979).

Assuming that perception is driven by the combined activity of multiple feature-selective mechanisms, metamers can be used to quantify the number of mechanisms which underlie various aspects of perception, including colour (Cohen & Kappauf, 1982), spatial

frequency and orientation (Richards, 1979), and motion (Williams et al., 1991). The field of colorimetry utilised metamers to estimate that there were at least three unique colour channels which served colour perception (Cohen & Kappauf, 1982; Richards, 1979). For motion perception, a field of moving dots which is broadband for motion direction (uniformly sampled from a 270° range of directions) is perceptually indistinguishable from field of dots moving in 9 unique directions (Williams et al., 1991). One previous study reported that as few as four superimposed orientations yielded a metameric match with a broadband stimulus composed of all possible orientations (Richards, 1979), however further details of this finding were not provided.

The present experiment aimed to estimate the minimum number of mechanisms which underlie orientation perception. To investigate whether there is an anisotropic number of cardinal-tuned and oblique-tuned mechanisms, orientations in both the discrete and broadband stimulus were uniformly sampled from a flat distribution, with a variable orientation range, which was centred on either the cardinal or oblique orientations.

5.2.2 Methods

Participants

Five participants took part in the metamers experiment, all with normal or corrected-to-normal vision. All but two participants (P1, P2) were naïve to the aims of the study. A subsample of two participants (P1, P2) performed an additional control experiment. Ethical guidelines were followed as described in Section 2.1.

Stimuli

The testing apparatus for the present experiment is described in Section 2.2. Monitor output was carefully linearised through photometric gamma correction (Section 2.3.1) and the

noisy-bit method provided precise control over the luminance resolution of the monitor (Section 2.3.2). The viewing distance was fixed at 60cm by means of a chinrest. Visual stimuli were arrays of 120 non-overlapping 'white' lines which were presented within a circular aperture that was 12° in diameter (see Section 2.4). Individual lines were formed by locally modulating the image luminance with an elongated, two-dimensional, Gaussian function with space constants of 0.17 x 0.01°, truncated at ± 0.50 x 0.03°. Unique line orientations were uniformly sampled from a flat distribution within a specified orientation range (either 15, 30, 60, or 90°) which was centred on the one of four standard orientations (either 0, 90, -45, or 45°). The *broadband stimulus* was composed of lines with no repeated orientations, whereas the *discrete stimulus* was composed of a discrete number of orientations (either 2, 3, 4, 5, or 6) which were repeated across the stimulus (Figure 5.2). The uniform

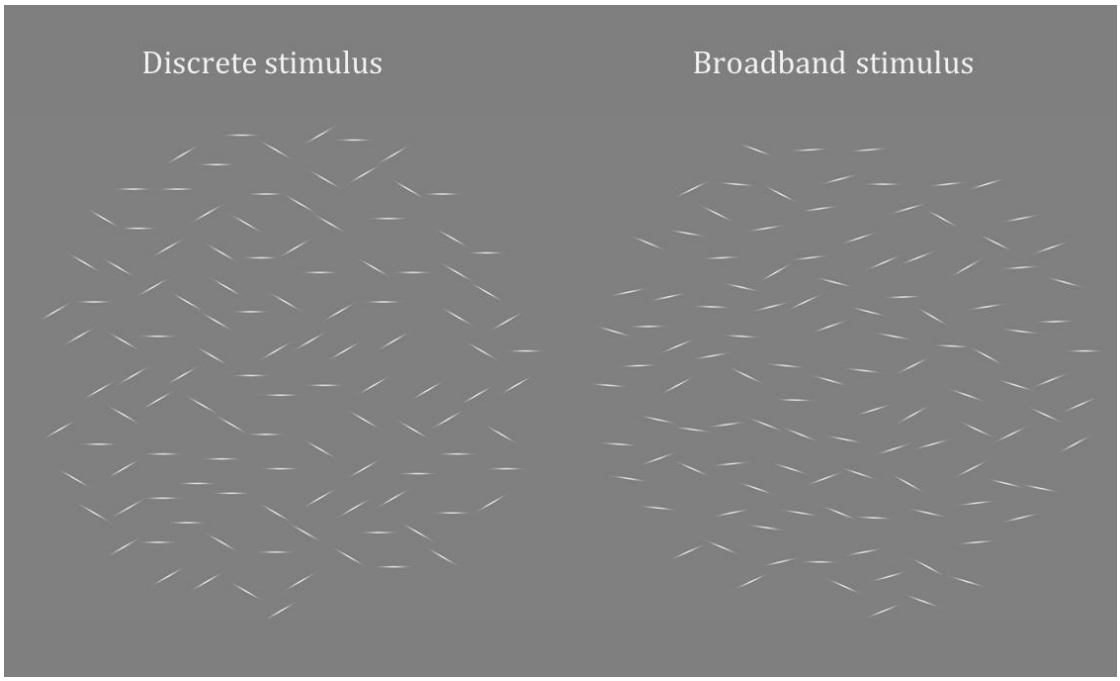

Figure 5.2. Example stimuli with a mean orientation θ of 0° and an orientation range of 60°. The 'discrete stimulus' (*left*) is composed of three unique orientations which are repeated across the stimulus, whereas all orientations in the 'broadband stimulus' (*right*) are unique.

spacing, S, between each orientation was determined by range of the orientation distribution, θ_{range}, and the number of unique orientations, N:

$$S = \frac{\theta_{range}}{N + 1}$$

Equation 5.1

Control experiment

A subsample of two participants (P1 and P2) performed an additional control experiment to confirm the generality of the findings, where the number of lines in the display and the line length were manipulated across three conditions. In the 'high-density' condition, stimulus parameters were identical to those described for the main experiment. Stimuli in the 'low-density' condition were composed of 60 lines which were of equal size to those in the high-density condition. Stimuli in the 'long-lines' condition were composed of 60 individual lines with Gaussian space-constants of 0.22 x 0.01°, truncated at ± 0.65 x 0.03°. In the 'low-density' and 'long-lines' conditions, the mid-points of lines were separated by a minimum distance of 1.3°. Orientations were sampled from an orientation range of either 15 or 30°, and the number of unique orientations in the discrete stimulus was set to 3.

Design

For each standard orientation and orientation range, the proportion of correct responses for each number of discrete orientations was measured, using a method of constant stimuli procedure (Section 2.6). Participants completed 200 trials in total for each condition, split into four runs of 50 trials. Stimulus parameters were constant throughout each run of trials. All runs were completed in a randomised fashion. Prior to formal data collection, participants completed one practice run in each condition, with feedback on the correctness of

their responses, to familiarise themselves with the experiment.

Procedure

Prior to each run, an example of both the discrete stimulus and the broadband stimulus were presented on screen to familiarise participants with the appearance of stimuli in the chosen condition. On each trial, the broadband stimulus and the discrete stimulus were each presented separately in one of two sequential 500ms stimulus intervals, which occurred before and after an 800ms interstimulus interval. The order of presentation was randomised. Participants judged whether the discrete stimulus was presented in the first or second interval by pressing the 'F' or 'J' key, respectively. A response signalled the initiation of the next trial after a 500ms delay. No response feedback, concerning the correctness of the participant's decision, was given.

Data analysis

The arithmetic-mean proportion of correct responses, p, was calculated for each condition, with the standard error (SE_p) given by:

$$SE_p = \sqrt{\frac{p(1-p)}{n}}$$

Equation 5.2

where n is the number of trials. The discrete stimulus was considered to be perceptually indistinguishable from the broadband stimulus if the proportion of correct responses did not significantly exceed chance performance. The statistical criterion for 'metamerism' was calculated to be 0.571, defined by the upper bound of the 95% confidence intervals for a binomial probability of 0.5, calculated using the Clopper-Pearson method (Clopper & Pearson, 1934). Although this criterion has been used previously (Williams et al., 1991), it is

important to acknowledge that it is at best an arbitrary choice. For instance, stimuli considered indistinguishable at one confidence level, might not be had a different statistical criterion been applied. Nonetheless, it is does allow the present results to be compared directly to those reported previously.

5.2.3 Results

Increasing the number of unique orientations in the discrete stimulus impaired the ability to discriminate it from the broadband stimulus. This was consistent for orientation ranges of 15, 30, (Figure 5.3), 60 and 90° (Figure 5.4). Increasing the orientation range improved task performance for all participants. For an orientation range of 15°, the proportion of correct responses for three out of five participants (P1, P2, and P3) approached the statistical criterion for metamerism with four unique orientations in the discrete stimulus. Of the remaining two participants, one (P5) approached this criterion with six unique orientations in the discrete stimulus, whereas the other (P4) performed substantially above chance level across all conditions. For an orientation range of 90°, only one participant (P3) reached this statistical criterion with six unique orientations in the discrete stimulus.

There were no systematic differences in performance between the cardinal and oblique mean orientations. Three out of five participants (P1, P2, and P3) showed impaired performance for obliques with just two unique orientations in the stimulus, for an orientation range of 15°, however this was not observed for larger numbers of unique orientations in the discrete stimulus. For an orientation range of 90°, three out of five participants (P1, P2, P5) demonstrated impaired discrimination performance for cardinal orientations relative to oblique orientations, which may be due to the presence of cardinal orientations at the extremes of the orientation distribution for oblique stimuli.

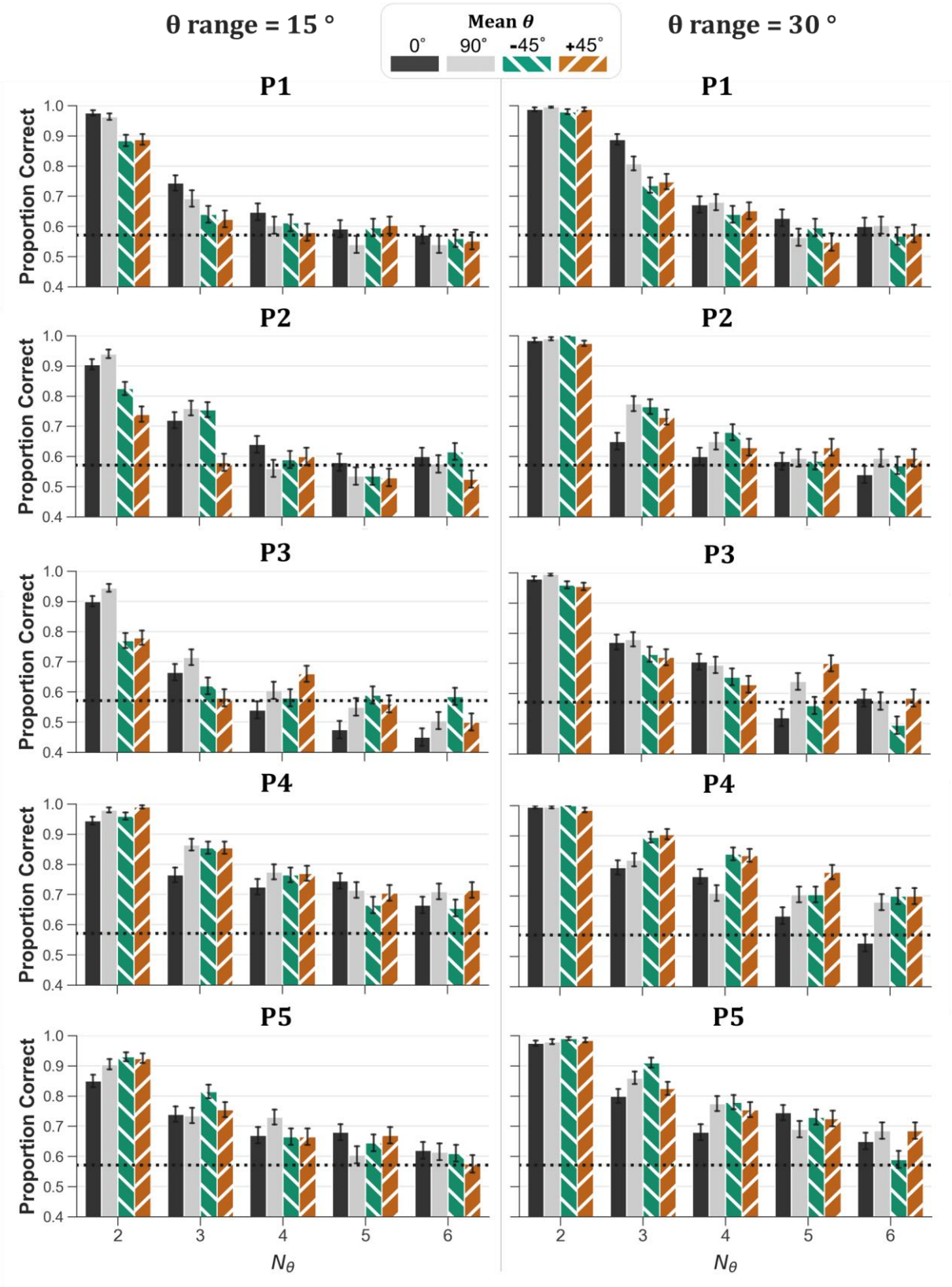

Figure 5.3. For each participant, the proportion correct for each mean orientation (either 0, 90, -45, or 45°) is plotted against the number of discrete orientations (N_θ). Data is shown for an orientation range of 15° (*left column*) and 30° (*right column*).

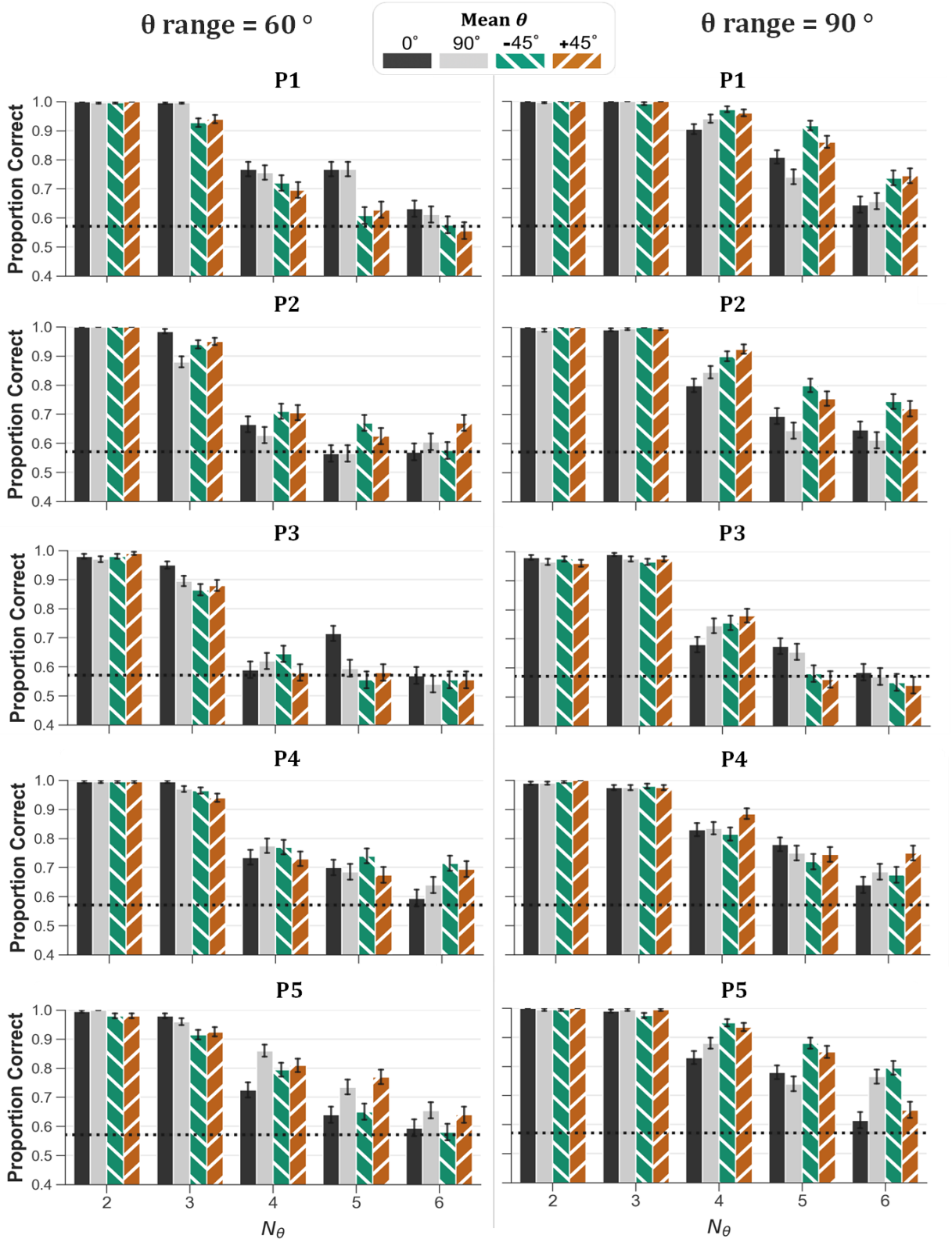

Figure 5.4. For each participant, the proportion correct for each mean orientation (either 0, 90, -45, or 45°) is plotted against the number of discrete orientations (N_θ). Data is shown for an orientation range of 60° (*left column*) and 90° (*right column*).

A subsample of two participants performed an additional control experiment which adjusted the total number of lines and varied the line length (Figure 5.5). Neither reducing the number of lines in the stimulus nor increasing the line length had a substantial impact on task performance for either participant.

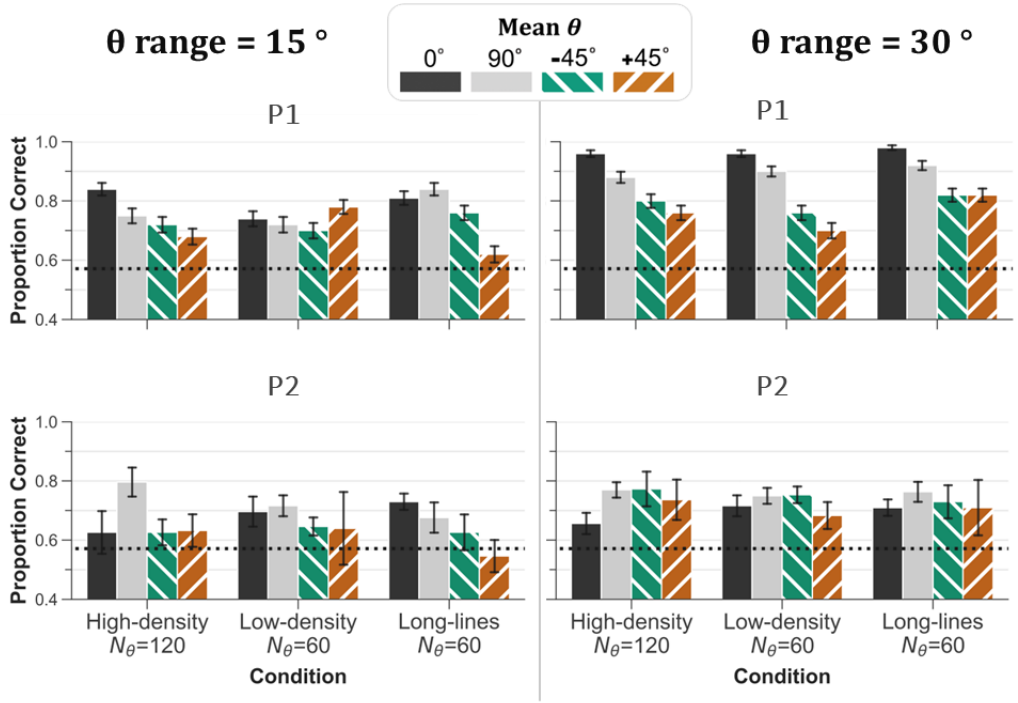

Figure 5.5. For a subsample of two participants, the proportion correct for each mean orientation (either 0, 90, -45, or 45°) is plotted for each tested condition. Data is shown for an orientation range of 15° (left column) and 30° (right column). The number of discrete orientations (N_θ) was set to 3.

5.2.4 Discussion

As expected from previous work (Richards, 1979; Williams et al., 1991), increasing the number of unique orientations in the discrete stimulus impaired the ability to discriminate between the discrete stimulus and the broadband stimulus. The minimum number of orientation-selective mechanisms underlying perception were estimated psychophysically by measuring the number of discrete orientations which were perceptually indistinguishable from the broadband stimulus, multiplied by two, less 1 (Richards, 1979). Discrimination performance did not reach the (arbitrary) significance threshold for 'metamerism', therefore only rough approximations of this number can be provided. A critical finding of the current study is that task performance was similar for stimuli with orientation distributions centred on either cardinal or oblique orientations, indicating that the overrepresentation of cardinal-tuned neurons which is found neurophysiologically (see Sections 1.4 and 1.5) is not reflected in the number of orientation-selective mechanisms which serve perception. Given the extent of individual variation in the distributions and response characteristics of visual cortical neurons (see Section 1.6.1), the robustness of perceptual mechanisms to such low-level inhomogeneities would promote a stable representation of the visual world that is similar across individuals.

Increasing the range of the orientation distributions improved task performance, such that approximately four unique orientations (7 mechanisms) were typically required to elicit metameric matches for an orientation range of 15°, whereas six unique orientations (11 mechanisms) were required to elicit metameric matches for an orientation range of 60°. This indicates that an increasing number of mechanisms are recruited for greater ranges of orientations, and that perception is not determined by a fixed number of mechanisms. However, despite a four-fold increase in the range of the orientation distribution (i.e., from 15

to 60°) the estimated minimum number of mechanisms only increased from approximately 7 to 11. The predominant limiting factor on task performance was the number of orientations in the discrete stimulus, rather than the range of the orientation distribution. Similar findings for orientation distributions centred on cardinals and obliques indicate that the mechanisms underlying perception may be flexible in terms of their preferred orientation.

These findings contradict a common assumption, that the orientation-selective mechanisms underlying perception have uniformly distributed orientation preferences (Ellemberg et al., 2006; Williams et al., 1991), such that there should be an even spacing between mechanisms regardless of the range of the distribution (Ellemberg et al., 2006; Watson & Robson, 1981). For example, one study reported that the number of direction-selective mechanisms scales with the range of the motion-direction distribution (Williams et al., 1991). However, the range of motion directions in their discrete stimulus was (according to the equation they provided) smaller for the discrete stimulus than for the broadband stimulus. Furthermore, they implemented much broader ranges (> 180°) than in the present experiment, which could be investigated in future research.

Performance often did not fall below the statistical criterion for metamerism, even with six unique orientations presented within a 15° range. This contradicts previous reports of four unique orientations, sampled across the full 180° range, being perceptually indistinguishable from a broadband stimulus (Richards, 1979). Task performance in the present experiment may have been facilitated by other visual cues which prevented the statistical criterion from being met, such as the identification of repeated orientations in the stimulus (i.e., numerosity judgements). This is exemplified by the inverse oblique effect which was observed for multiple participants for the 90° orientation range, which may reflect the presence of repeated cardinal orientations at the extremes of the orientation distribution

for oblique stimuli.

Short lines have a broadened stimulus-orientation bandwidth relative to long lines of equal width, as Fourier power is distributed over a range of adjacent orientations (see Section 1.3.3). However, the line stimuli used in the present experiment were at least twenty times as long as they were wide, an aspect ratio beyond which orientation-discrimination performance is reported to be invariant with line length (Heeley & Buchanan-Smith, 1998; Sally & Gurnsey, 2007). This was further demonstrated in the control experiment, whereby increasing the length of individual lines had little impact on task performance.

5.3 Estimating the orientation bandwidths of the mechanisms for detection and discrimination

5.3.1 Introduction

Modelling work in Chapter 4 revealed that the oblique effect for orientation discrimination was accounted for by anisotropic orientation bandwidths, such that cardinal-tuned mechanisms had orientation bandwidths which were roughly half that of oblique-tuned mechanisms (see Sections 4.3 and 4.4), in line with previous modelling work (Rokem & Silver, 2009). However, there is little neurophysiological evidence in early visual cortex (see Section 1.4), nor psychophysical evidence, for such an anisotropy.

Psychophysical estimates of orientation bandwidths have been derived from visual masking (Graham, 1989), where the target orientation is detected in the presence of a superimposed mask stimulus, with an orientation difference that is systematically varied relative to the target orientation (described in detail in Section 1.2.5). Masking is thought to elevate contrast-detection thresholds due to a diminished signal-to-noise ratio (SNR) of the mechanism at the target orientation, such that psychophysical bandwidth estimates from these data reflect the bandwidth of the underlying mechanism.

Psychophysical estimates of orientation bandwidth (full-width, half-max) in humans typically range from 30 to 60° in masking experiments (Blake & Holopigian, 1985; Campbell & Kulikowski, 1966; Phillips & Wilson, 1984; Thomas & Gille, 1979), which is broadly consistent with those recorded in orientation-selective neurons in early visual cortex (see Section 1.1.4). Although, an additional suppressive component which is isotropic, or possibly broadly tuned for orientation, can sometimes inflate these estimates (Meese & Holmes, 2010).

All previous psychophysical estimates of orientation bandwidth have been achieved by measuring detection performance whilst systematically adjusting the orientation of a singular mask stimulus. However, in these cases, detection of the target orientation may have been determined by the responses of orientation channels with orientation preferences adjacent to that of the target channel, which were less affected by the mask, i.e., 'off-channel looking' (see Section 1.2.5). Unaccounted for, this can lead to the underestimation of channel bandwidths (Serrano-Pedraza et al., 2013). Therefore, the present study implemented a 'dual masking' paradigm to estimate channel bandwidths, such that the target orientation was superimposed with two masks, which had orientations that are equidistant, in opposite directions, from the standard orientation (Hutchinson & Ledgeway, 2004; Serrano-Pedraza et al., 2013).

Orientation bandwidth estimates for cardinal and oblique stimuli have been compared previously for contrast-detection tasks, with the vast majority of findings indicating that there is no consistent difference in bandwidth between the two orientations (see Section 1.3.4). This is consistent with model simulations which revealed that anisotropic tuning bandwidths would abolish the oblique effect for contrast detection (see Section 4.2.4). However, it is unclear to what extent 'off-channel looking' may have influenced bandwidth estimates for the cardinal and oblique orientations.

The work in Chapter 4 revealed that a unified model could not account for the oblique effects for contrast detection and orientation discrimination, indicating that the mechanisms underlying detection may be distinct from those underlying discrimination. This predicts that the orientation-bandwidth estimates for a contrast-detection task may not be representative of the those for an orientation-discrimination task. Although visual masking does elevate orientation-discrimination thresholds (W. Li et al., 2000; Wehrhahn et al., 1996), the

orientation bandwidths of the underlying mechanisms have not been reported previously.

Aims

The present study aimed to evaluate previous psychophysical estimates of orientation bandwidths by implementing a dual-masking procedure in order to minimise the impact of 'off-channel looking'. Crucially, orientation-bandwidth estimates were generated separately for contrast detection and orientation discrimination. The modelling work in Chapter 4 generated three testable predictions. First, orientation bandwidths of detection mechanisms should be similar for cardinal and oblique orientations. Second, orientation bandwidths of discrimination mechanisms are anisotropic, such that cardinal bandwidths will be substantially narrower than oblique bandwidths. Finally, bandwidth estimates for detection may be broader than those for discrimination, at least for the cardinal orientations.

5.3.2 Methods

Participants

Four participants took part in the present experiment, all with normal or corrected-to-normal vision. Two participants (P3 and P4) were naïve to the aims of the study. Ethical guidelines were followed as described in Section 2.1.

Stimuli

The testing apparatus for the present experiment is the same as described in Section 2.2, except for the higher pixel resolution of 1400 x 1050. The viewing distance was fixed at 105cm by means of a chinrest, such that the size of each pixel was 0.0156 x 0.0156°. Monitor output was carefully linearised through photometric gamma correction (Section 2.3.1) and the

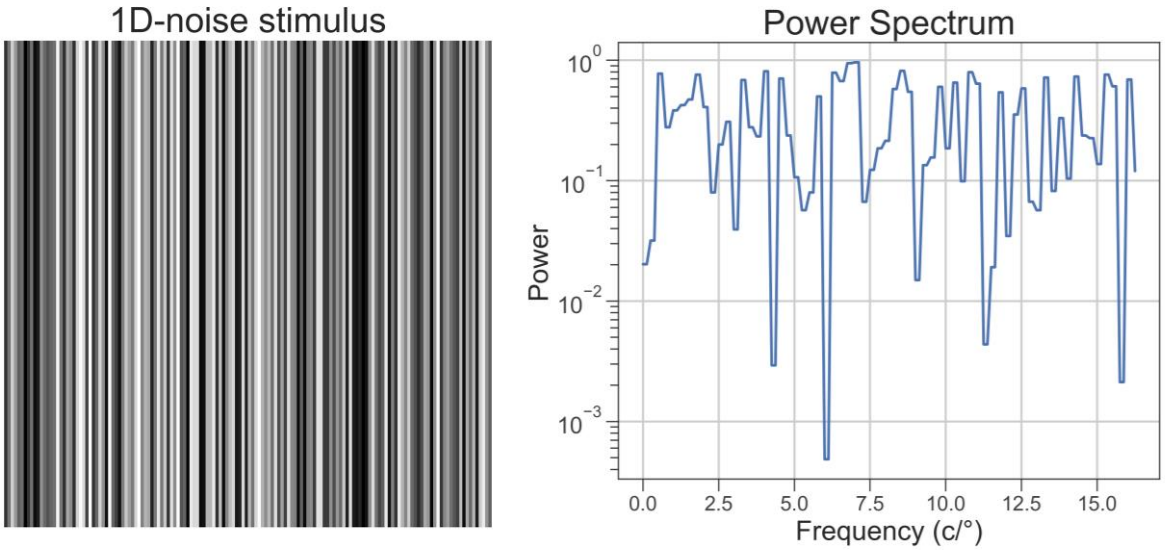

Figure 5.6. Example 1D-noise pattern (*left*) and its Fourier power spectrum along the x-direction (*right*).

noisy-bit method provided precise control over the luminance resolution of the display (see Section 2.3.2).

Visual stimuli were spatially 1D-noise stimuli (see Section 2.4) with a space-constant of 1.33°, truncated at ±4°. Luminance values of the 1D-noise distribution were sampled by pairs of adjacent pixels. Each 1D-noise stimulus was presented at a single orientation with a broadband spatial frequency spectrum (Figure 5.6). The maximum spatial frequency achievable was 16.04c/° The mask stimulus was composed of two, superimposed 1D-noise patterns, which were rotated by a variable distance either clockwise or anticlockwise from the standard orientation, θ_{std}:

$$\text{CLOCKWISE:} \quad \theta_{mask1} = \theta_{std} + \frac{\theta_{notch}}{2}$$

$$\text{ANTICLOCKWISE:} \quad \theta_{mask2} = \theta_{std} - \frac{\theta_{notch}}{2}$$

Equation 5.3

The orientation difference between the two mask components, θ_{notch}, will henceforth be termed the 'notch-width'. Each 1D-noise component of the mask stimulus had a Michelson contrast of 25%. The target stimulus was composed of a singular 1D-noise component, of variable contrast and orientation.

Contrast detection

For the contrast detection task, a two-alternative forced choice (2AFC) adaptive staircase procedure was implemented (Section 2.5), with the contrast of the target stimulus on each trial determined by the staircase-value. Detection thresholds for each run were taken as the arithmetic-mean staircase value of the last five reversals. The target stimulus was presented at one of four standard orientations (either 0, 90, -45, or 45°). The notch-width was either 0, 15, 30, 45, 60, 90, or 180°. For a notch-width of 180°, the two masking noise patterns had the same orientation, orthogonal to the standard orientation. 'Baseline' performance was defined by the threshold obtained in the 'no mask' condition, where the mask stimulus was absent. Stimulus parameters were constant for each block of trials. For a

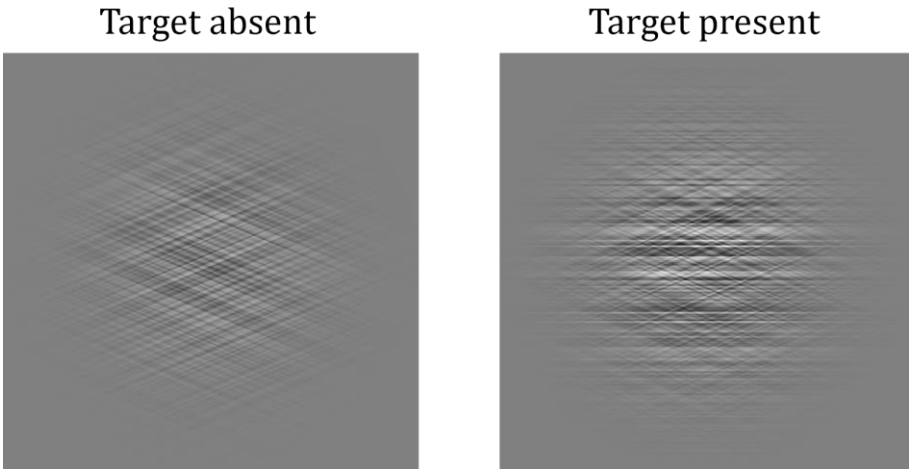

Figure 5.7. Example stimuli used in the detection task with two mask orientations separated by 45°, either in the absence (left) or presence (right) of the target orientation.

notch-width of 0°, the task was effectively a contrast-discrimination task, such that participants reported the higher contrast stimulus (perceived as more 'intense'). Participants completed at least two runs of trials for each condition, and data for each of the cardinal (0 and 90°) and oblique (-45 and 45°) conditions were pooled together. All runs were completed in a randomised fashion. Prior to each run, an example of each stimulus was presented on screen to familiarise participants with the appearance of stimuli in the chosen condition (Figure 5.7).

On each trial, the target stimulus was presented in one of two 300ms stimulus intervals, before and after a 500ms interstimulus interval. The mask stimulus was presented in both stimulus intervals except for the 'no mask' condition, in which it was absent. Participants judged in which interval the target stimulus was presented, using the 'F' or 'J' key to indicate the first and second stimulus interval, respectively. The order of presentation was randomised. A response signalled the initiation of the next trial after a 500ms delay. No response feedback, concerning the correctness of the participant's decision, was given.

Orientation discrimination

For the orientation-discrimination task, the orientation difference between the two target stimuli was defined by the staircase-value, $\Delta\theta$.

$$\theta_{target} = \theta_{std} \pm \frac{\Delta\theta}{2}$$

Equation 5.4

Where each target stimulus was presented either clockwise or anticlockwise from the standard orientation, θ_{std} (either 0, 90, -45, or 45°). The orientation of the target stimulus was

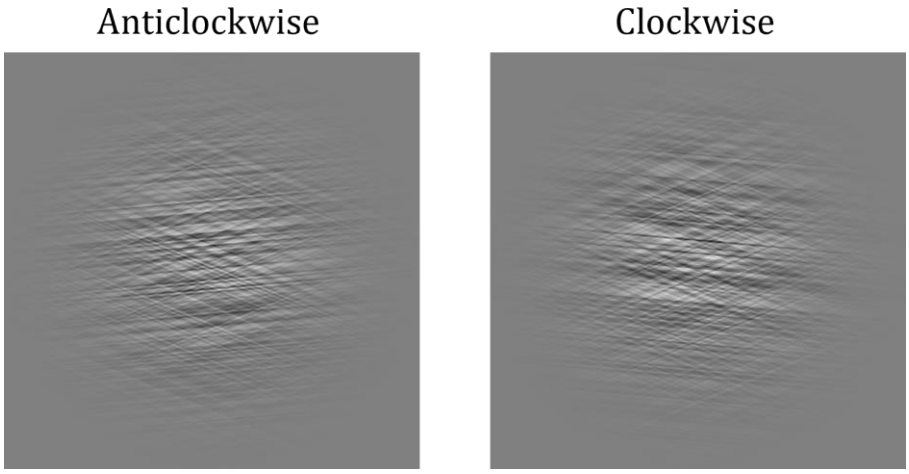

Figure 5.8. Example stimuli used in the discrimination task with two mask orientations separated by 45° in the presence of the target orientation, either rotated anticlockwise (left) or clockwise (right) equidistant from the standard orientation.

constrained such that it could not exceed the boundaries of the mask orientations, hence the 0° notch-width condition was excluded for the orientation-discrimination task. Instead, the notch-width was either 7.5, 15, 30, 45, 60, 90, or 180°. 'Baseline' performance was defined by the threshold obtained in the 'no mask' condition, where the mask stimulus was absent. Example stimuli are shown in Figure 5.8. The contrast of the target stimulus was fixed at 40%.

Procedural details for the orientation-discrimination task were the same as for the contrast-detection task, except that the target stimulus was presented in both stimulus intervals. Participants judged which target stimulus was rotated more clockwise, using the 'F' or 'J' keys to refer to the first and second intervals, respectively. The order of presentation was randomised.

Data analysis

Data for the cardinal condition were pooled from the horizontal and vertical orientations, and data for the oblique condition were pooled from the left and right oblique

orientations. Orientation bandwidths (full-width, half-max) were estimated independently for the contrast-detection and orientation-discrimination tasks, by fitting a Gaussian function to the measured thresholds (see Section 2.7).

The superimposition of grating stimuli meant that performance was potentially modulated by factors unrelated to the orientation selectivity of the target mechanism, such as cross-orientation suppression, reductions in the average local contrast, or the introduction of second-order visual information. Indeed, cross-orientation suppression (or some combination of these factors) has been demonstrated to inflate bandwidth estimates (Meese & Holmes, 2010). To reduce the impact of these factors on bandwidth estimates, the minimum value of the fitted function was set to the threshold measured in the 'no mask' condition.

For the contrast-detection task, the mean of the Gaussian function was set to 0°, and the standard deviation and maximum value were free parameters. Due to non-monotonic changes in discrimination performance as a function of the notch-width (i.e., the peak threshold elevation was shifted from 0°), the mean of the Gaussian function was a free parameter when fitting the discrimination data. To assess the reliability of findings, mean-bandwidth estimates were compared with those obtained by fitting a cosine function to the same data (see Section 2.7).

5.3.3 Results

Contrast detection

Contrast-detection thresholds decreased as a function of the difference between mask orientations, i.e., the 'notch-width' (Figure 5.9). Detection thresholds for a notch-width of 15° did not differ substantially from thresholds for a notch-width of 0°. Detection thresholds for a notch-width of 180°, for both cardinal and oblique orientations, were on average 41% larger

Orientation	P1	P2	P3	P4	Mean (SE)
Cardinal	76.5	80.9	76.3	59.6	73.3 (4.71)
Oblique	84.5	75.1	76.7	64.9	75.3 (4.03)

Table 5.1. Orientation bandwidth estimates (°) for cardinals and obliques on the detection task. See text for further details.

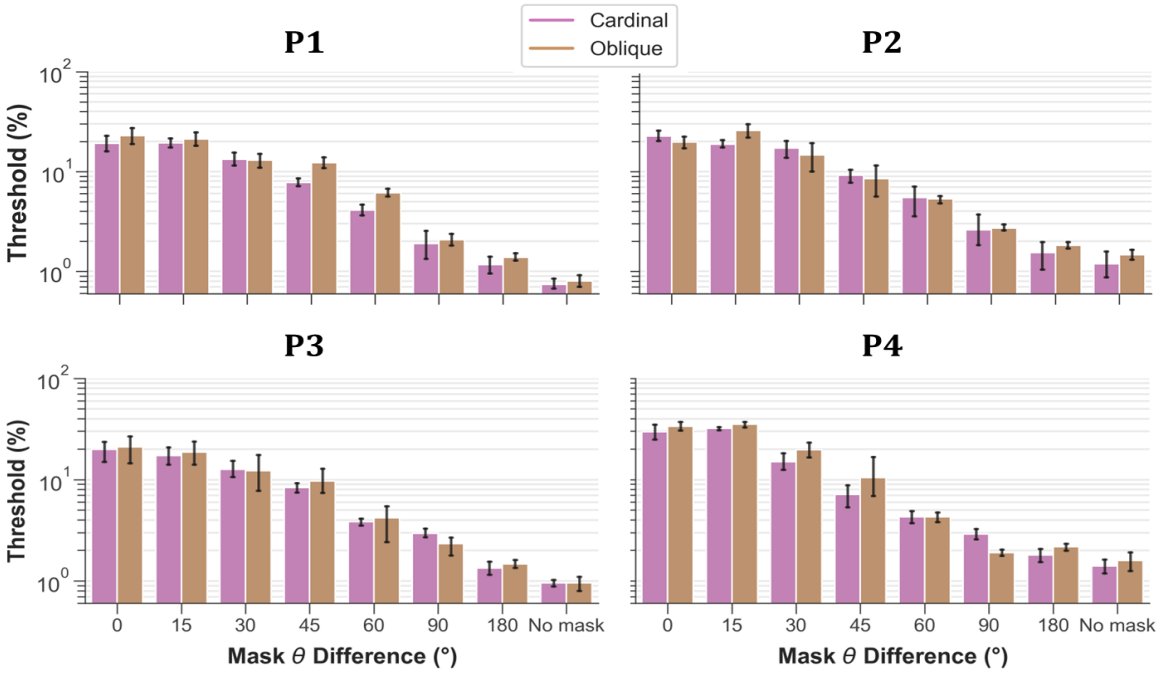

Figure 5.9. For each participant, contrast detection thresholds (%) for cardinals and obliques are plotted against the orientation difference between masks (i.e., 'notch-width'). The error bars represent the standard error of the mean.

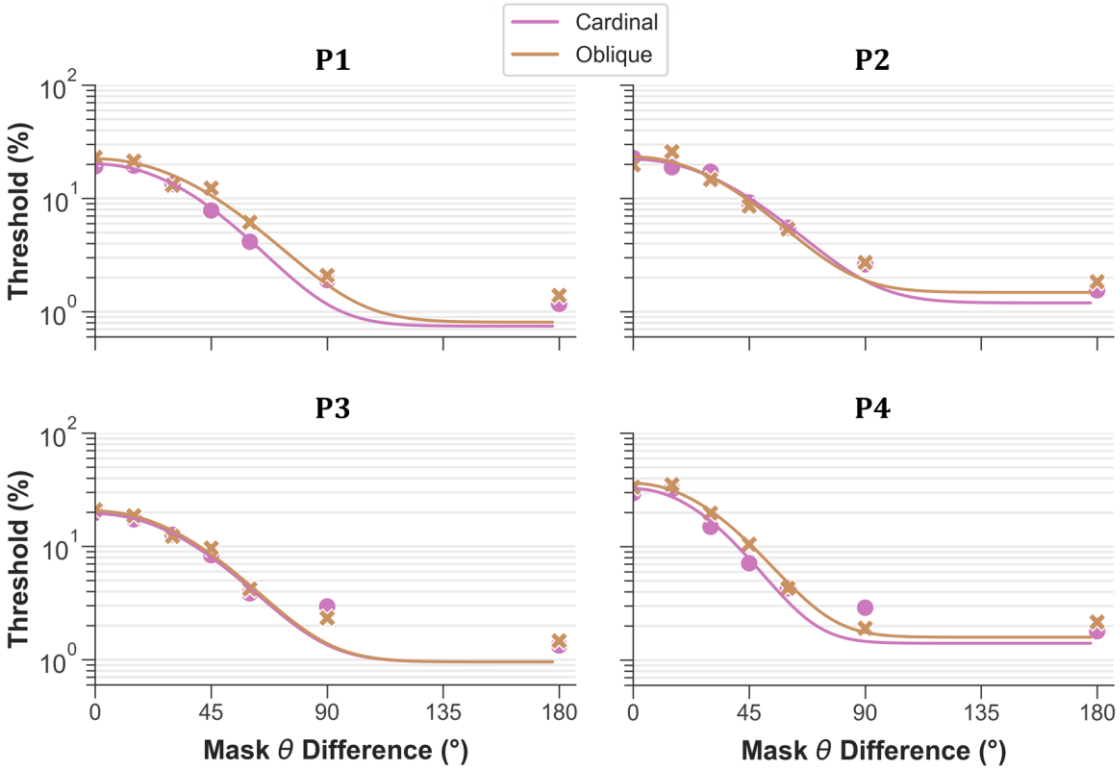

Figure 5.10. For each participant, a one-sided Gaussian function was fit to the contrast detection thresholds (%) as a function of the notch-width for cardinals and obliques. The minimum value of the Gaussian function was set to the baseline threshold, i.e., the detection threshold in the absence of the masks, whereas the peak was set to 0°.

than the baseline performance (in the absence of a mask stimulus).

For all participants, estimates of orientation bandwidth (Table 5.1) were similar for cardinal orientations (M = 73.3°, SE = 4.71°) and oblique (M = 75.3°, SE = 4.03°) orientations (Figure 5.10). When analysed independently, there were no consistent differences in the estimated bandwidths for the horizontal (M = 68.6°, SE = 5.26°) and vertical orientations (M = 78.2°, SE = 4.68°), nor between the left oblique (M = 75.6°, SE = 6.02°) and right oblique (M = 75.4°, SE = 2.49°). The reliability of mean-bandwidth estimates was demonstrated by similar findings when these data were fit with a cosine function, for cardinals (M = 73.7°, SE = 8.18°) and obliques (M = 74.1°, SE = 7.01°).

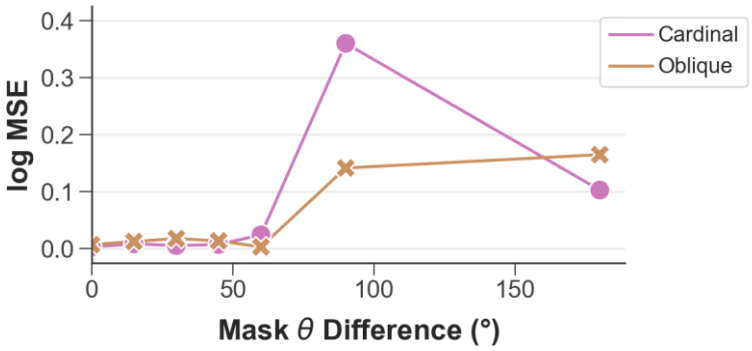

Figure 5.11. The logarithmic mean-square error (MSE) of the Gaussian function fitted to the contrast-detection thresholds.

The quality of the fit of the Gaussian distribution to the detection thresholds was quantified by the mean-squared-error (MSE) for each notch-width, calculated across all participants (Figure 5.11). The data were well-approximated by a Gaussian distribution for notch-widths at or below 60°. Large deviations were observed for notch-widths of 90 and 180° for both cardinal and oblique orientations. Cardinal detection thresholds for a notch-width of 90° greatly deviated from the fitted Gaussian in all four participants.

Orientation discrimination

Orientation-discrimination thresholds varied non-monotonically as a function of the notch-width (Figure 5.12), such that peak masking tended to occur for a notch-width of 15°. Discrimination thresholds for a notch-width of 7.5° were either lower than or equal to thresholds for a notch-width of 15°. For cardinal orientations, discrimination thresholds for a notch-width of 180° were on average 39% higher than baseline performance, whereas there was relatively little difference for oblique orientations.

Orientation	P1	P2	P3	P4	Mean (SE)
Cardinal	21.9	29.7	22.7	21.1	23.8 (1.98)
Oblique	43.7	29.6	66.4	68.7	52.1 (9.39)

Table 5.2. Orientation-bandwidth estimates (°) for cardinals and obliques on the orientation-discrimination task. See text for further details.

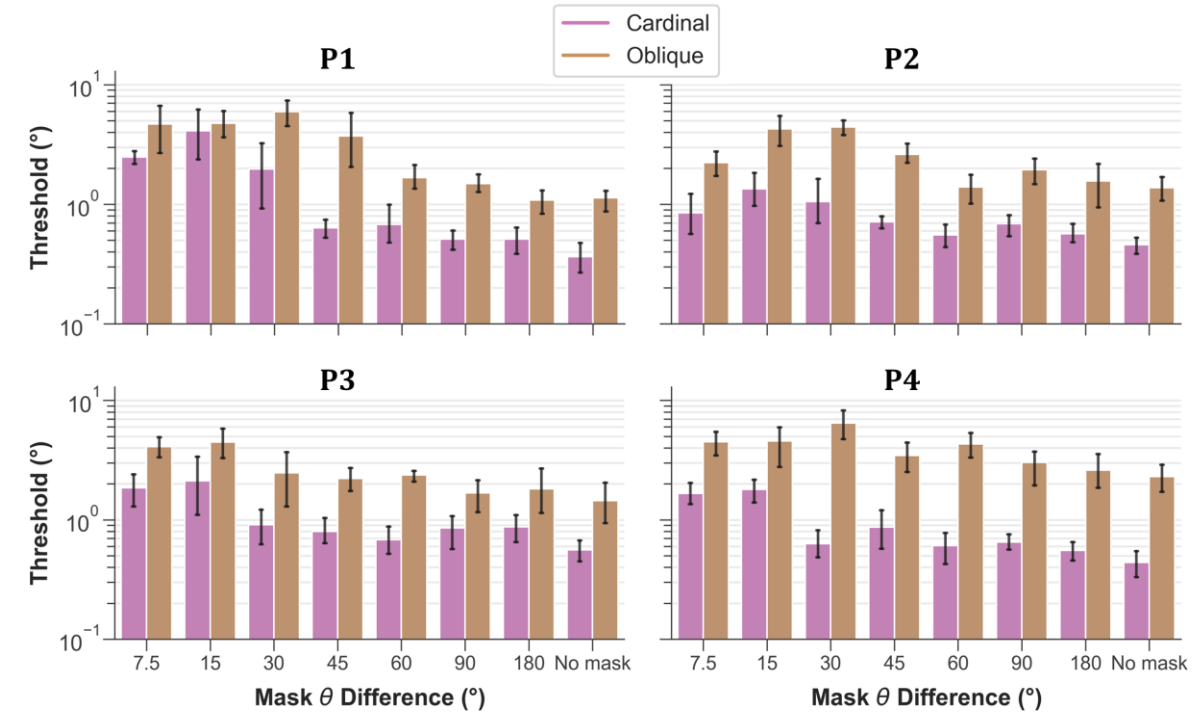

Figure 5.12. For each participant, orientation-discrimination thresholds (°) for cardinals and obliques are plotted against the orientation difference between masks (i.e., 'notch-width'). The error bars represent the standard error of the mean.

For three out of four participants, estimates of orientation bandwidth (Table 5.1) were markedly smaller for cardinal orientations (M = 23.8°, SE = 1.98°) than for oblique orientations (M = 52.1°, SE = 9.39°) (Figure 5.13). The remaining participant (P2) showed no difference between the bandwidth estimates for cardinal and oblique orientations. When analysed independently, there were no systematic differences in the estimated bandwidths for the horizontal (M = 23.7°, SE = 5.34°) and vertical orientations (M = 22.8°, SE = 4.56°), nor

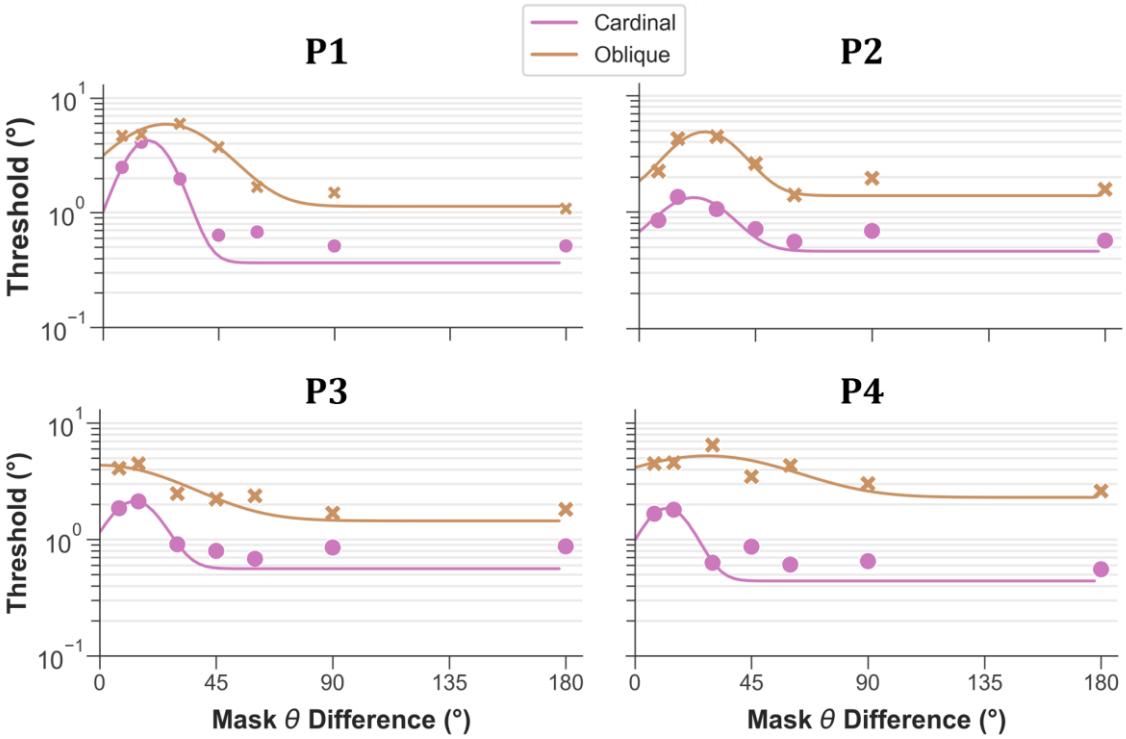

Figure 5.13. For each participant, a Gaussian function was fit to the discrimination thresholds (°) as a function of the notch-width. The minimum value of the Gaussian function was set to the baseline, i.e., the discrimination threshold in the absence of masking.

between the left oblique (M = 40.3°, SE = 18.4°) and right oblique (M = 36.3°, SE = 4.57°). Mean-bandwidth estimates were greatly elevated when data were fitted with a cosine function, although these were still roughly twice as large for cardinals (M = 36.5, SE = 7.24) relative to the obliques (M = 71.6, SE = 17.9).

The quality of the fit of the Gaussian distribution to the discrimination thresholds was quantified by the mean-squared-error (MSE) for each notch-width, calculated across all participants (Figure 5.14). The data were well-approximated by a Gaussian distribution for the oblique orientations, whereas larger deviations for cardinal orientations were observed for notch-widths at or above 45°.

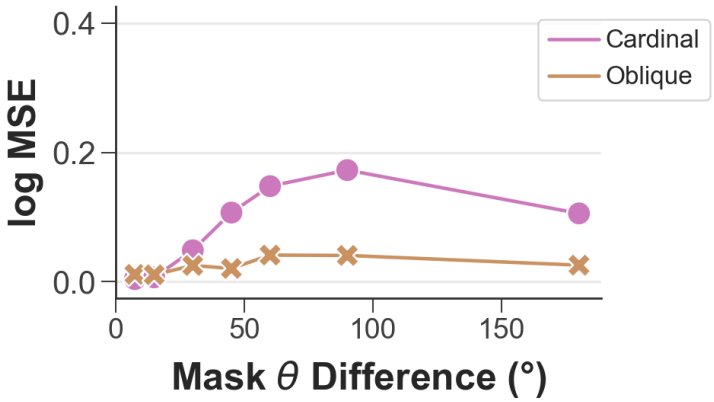

Figure 5.14. The logarithmic mean-square error (MSE) of the Gaussian function fitted to the orientation-discrimination thresholds.

5.3.4 Discussion

Detection

Psychophysical estimates of orientation bandwidth for detection mechanisms were not systematically different for cardinal and oblique orientations. This is generally consistent with previous research (Blake & Holopigian, 1985; Phillips & Wilson, 1984) and supports the assumption of isotropic bandwidths in the generation of the oblique effect for contrast detection (Section 4.2). Previous psychophysical work that reported anisotropic tuning bandwidths used samples of either one (Campbell & Kulikowski, 1966) or two participants (Thomas & Gille, 1979), with the extent of tuning anisotropy also varying greatly across participants. The lack of an oblique effect in the detection thresholds measured in the absence of a mask (the baseline) was expected due to the broadband spatial frequency content of the tested stimulus (Westheimer & Beard, 1998).

The full-bandwidth estimates of detection mechanisms were roughly 75°, which is far greater than previous estimates of approximately 60° (Blake & Holopigian, 1985; Phillips & Wilson, 1984), 40° (Meese & Holmes, 2010), and 30° (Campbell & Kulikowski, 1966;

Thomas & Gille, 1979). However, the use of a singular mask stimulus in these previous studies meant that detection of the target orientation may have been determined by the responses of mechanisms with similar orientation preferences which were less affected by the mask, i.e., 'off-channel looking' (see Section 1.3.4). Model simulations have revealed that off-channel looking can lead to the systematic underestimation of bandwidths in visual masking experiments. The 'dual-masking' paradigm used in the present experiment meant that detection of the target orientation could not be facilitated by off-channel looking (see Section 1.2.4, also see Hutchinson & Ledgeway, 2004), which may explain the broader tuning estimates relative to previous work. The estimated orientation bandwidths of detection mechanisms are consistent with the modelling work in Section 4.2, which found that the oblique effect for contrast detection was only abolished for more broadly tuned mechanisms with bandwidths of 70°.

There was a moderate elevation in detection thresholds in the presence of an orthogonally orientated mask stimulus (corresponding to a notch-width of 180°), relative to baseline performance, suggesting that the contribution of an additional, isotropic suppression component which has previously been suggested to inflate bandwidth estimates (Meese & Holmes, 2010). However, the impact of this additional suppressive component was addressed by fitting a Gaussian function with its minimum value set to the baseline threshold, measured in the absence of masking. Regardless, bandwidth estimates in the present study were still larger than those in previous studies which have implemented similar methods of bandwidth estimation (Blake & Holopigian, 1985; Phillips & Wilson, 1984; Thomas & Gille, 1979).

Discrimination

Orientation-discrimination thresholds were elevated for smaller notch-widths, consistent with previous findings (W. Li et al., 2000; Wehrhahn et al., 1996). The estimated

orientation bandwidth for cardinal-tuned discrimination mechanisms ranged between 22 and 30°, which is substantially smaller than the estimated bandwidths of detection mechanisms. This supports suggestions that the mechanisms underlying orientation discrimination are distinct from those underlying contrast detection, and that detection mechanisms are more broadly tuned for orientation (see Chapter 4). Additionally, these bandwidth estimates are smaller than the average orientation bandwidth of neurons in early visual cortex, ~ 50° (see Section 3.5.3).

Results suggested that the bandwidths of oblique-tuned discrimination mechanisms are approximately twice that of cardinal-tuned discrimination mechanisms. However, the present experiment cannot provide a precise estimate of the extent of this tuning anisotropy. The limited precision of orientation-tuning bandwidth estimates for oblique-tuned discrimination mechanisms was demonstrated by greater levels of inter-individual variation, estimates ranging from approximately 30 to 70°. Broader estimates of orientation tuning tended to occur in cases where the oblique thresholds were not substantially elevated by the masking stimuli. Additionally, the need for further investigation is highlighted by the absence of anisotropic tuning bandwidths for one participant. Considering the vast individual differences in threshold elevations for the discrimination task, future work should aim to standardise the masking strength across individual participants, prior to formal data collection. To achieve this in the discrimination task, the contrast of the target stimulus could be set at the detection threshold in the presence of 'dual masks' at a notch-width of 0°, for each participant.

Unlike for detection, maximum masking did not occur for the smallest notch-width on the orientation-discrimination task, indicating that masking-induced elevations of discrimination thresholds may not be directly related to the responsivity of mechanisms tuned

to the target orientation. Rather, bandwidth estimates may reflect changes in the responsivity of mechanisms that are selective for orientations which are slightly offset from the target orientation. This is consistent with the assumption that orientation-discrimination performance is constrained primarily by the tuning bandwidths (see Chapter 4) or the slopes (Regan & Beverley, 1985) of orientation-selective mechanisms with neighbouring orientation preferences. This may explain why discrimination performance tended to improve when the notch-width was reduced from 15 to 7.5, due to isolation of the targeted mechanism.

The current method assumes that masking-induced elevations in thresholds reflect reductions in the signal-to-noise ratio of the target mechanism, however superimposing 1D-noise patterns also introduces 'second-order' information into the stimulus. A potential limitation is that variations in stimulus orientation may have been signalled by changes in other visual features, such as the distribution of zero crossings in the superimposed stimulus (C. L. Baker & Mareschal, 2001; Dakin et al., 1999; Dakin & Watt, 1997), although the broadband spatial frequency information of the individual 1D-noise patterns will have reduced the regularity and salience of such second-order information (Dakin et al., 1999). To what extent the superimposition of target and mask stimuli impacted threshold and bandwidth estimates remains unclear. Therefore, to address this, future research could implement a temporal gap between the target and mask orientations (e.g., backwards masking) to ensure the absence of second-order information in the stimulus.

5.4 Summary of findings

The experimental work in the present Chapter revealed that there may be no difference in the number of cardinal-tuned and oblique-tuned mechanisms which serve orientation perception (Section 5.2), whereas orientation bandwidth estimates were narrower for cardinal-tuned discrimination mechanisms (Section 5.3). This supports the modelling work in Chapter 4, which demonstrated that the inclusion of anisotropic tuning bandwidths was necessary and sufficient to capture the oblique effect for orientation discrimination. For detection mechanisms, the estimated orientation tuning bandwidths were isotropic (Blake & Holopigian, 1985; Phillips & Wilson, 1984), consistent with demonstrations that anisotropic tuning bandwidths would abolish the oblique effect for contrast detection (Section 4.2).

The absence of an overrepresentation of cardinal-tuned mechanisms, which is necessary to elicit the oblique effect for contrast detection (Section 4.2), supports conclusions that the orientation-selective mechanisms which serve detection and discrimination are distinct from one another (see Chapter 4). Neurophysiological findings of an increased cardinal overrepresentation in higher visual areas, i.e., V4, relative to V1 (Fang et al., 2022; G. Shen et al., 2014), suggest that the mechanisms underlying perception are robust to variation at the level of individual neurons. Further empirical evidence for distinct detection and discrimination mechanisms comes from the absence of anisotropic tuning bandwidths for broadly tuned detection mechanisms, and their presence for narrowly tuned discrimination mechanisms. The present findings indicate that the oblique effects for contrast detection and orientation discrimination are generated by distinct neuronal anisotropies, challenging suggestions that the magnitude of the oblique effect simply scales with stimulus contrast (Bloem & Ling, 2017a). However, these conclusions are made with the assumption that the mechanisms underlying the perception of textures composed of multiple orientations (Section

4.2) are the same as those serving orientation discrimination using simpler (e.g. sinusoidal gratings) patterns (Section 4.3).

The broadened orientation bandwidths of detection mechanisms are not necessarily inconsistent with the contrast-invariance of orientation selectivity in early visual cortex (see Section 1.2). Rather, detection may be served by mechanisms that are independent of discrimination mechanisms, with wider orientation bandwidths than discrimination mechanisms, consistent with model predictions (see Section 4.2). Future research should explore whether the contrast-invariance of orientation-selectivity that is observed for individual neurons (Y.-J. Liu et al., 2015) extends to psychophysical estimates of tuning bandwidths for discrimination mechanisms.

Orientation discrimination (and possibly detection) may be achieved by a limited number of independently tuned orientation-selective mechanisms (Section 4.2), rather than the densely distributed pool of mechanisms which was implemented in the modelling work of Chapter 4. The minimum number of recruited mechanisms appears to be partially fixed, and partially driven by the range of orientations which are present (Section 4.2).

The estimated orientation bandwidths of detection mechanisms (~ 70°) and cardinal-tuned discrimination mechanisms (~ 25°) were very different from the average neurophysiological estimates in V1 (~ 50°). Therefore, the present findings indicate that the average response characteristics of individual neurons may not be representative of the mechanisms which underlie perception. Instead, subpopulations of neurons with different response properties could serve different visual functions, such as more broadly tuned neurons for detection, and more narrowly tuned neurons for discrimination. Alternatively, perceptual mechanisms may be robust to variations in the response properties of neuronal populations in early visual cortex, and may be instead determined by higher-level factors,

such as biases in the internal representation of orientation (see Section 1.3.5). This is supported by reports of ageing-related losses in contrast sensitivity that are not accompanied by losses in orientation-discrimination performance, nor by changes in psychophysical estimates of orientation bandwidth (Delahunt et al., 2008).

Psychophysical investigations of the mechanisms underlying perception may serve as a useful endpoint to understand the transformations of the response properties of individual neurons. Recent work has characterised the tuning properties of subpopulations of neurons in fMRI (Serences et al., 2009; Sun et al., 2013; Yacoub et al., 2008) which could reflect the activity of independent mechanisms (Brouwer & Heeger, 2011; Cowell et al., 2013). Future work could therefore characterise orientation-selectivity at various functional levels, from individual neurons to populations of neurons, and for psychophysical performance.

6. Investigating the contributions of cognitive factors to the oblique effect

6.1 General introduction

Cognitive factors

Orientation anisotropies in the responses of low-level visual mechanisms cannot fully account for the oblique effect (for review, see Section 1.3.5). For example, the oblique effect for orientation-discrimination is larger for illusory contours than for grating stimuli (Westheimer, 2003a), the oblique effect for orientation-discrimination does not follow retinal coordinates when the head is tilted by 45° (Buchanan-Smith & Heeley, 1993; Mikellidou et al., 2015), and larger errors are made when manually reproducing oblique orientations than cardinals in the absence of visual input, i.e., haptic perception (Gentaz et al., 2008). It has been proposed that there is an anisotropic cognitive component, independent from the encoding mechanisms of early visual cortex, which may account for these findings (Balikou et al., 2015; Heeley et al., 1997; Westheimer & Lavian, 2013).

Short-term memory

Anisotropic mechanisms in short-term visual memory may contribute to the magnitude of the oblique effect, such that representations of oblique orientations may decay faster than representations of cardinal orientations (Westheimer, 2003a). Indeed, the oblique effect for orientation-discrimination is reportedly larger on a temporal two-alternative forced choice (2AFC) task, with stimuli presented successively over a temporal delay, than on a spatial 2AFC task, with presented simultaneously in different spatial locations (Heeley & Buchanan-Smith, 1992; Westheimer, 2003a). However, the closely spaced stimulus

configurations in both of these previous studies may have generated tilt effects (where the simultaneous presentation of nearby orientations is known to alter the perceived orientation of the target orientation) which may have confounded their results (McMahon & MacLeod, 2003). Further details of these studies are provided in Section 1.3.5.

Dividing attention

Dividing attention between two spatial locations, as in the spatial 2AFC task, impairs performance for tasks that involve higher-order demands, such as the discrimination of conjunctions of features (e.g., letters or objects) which are encoded in higher visual areas (White et al., 2017). Conversely, dividing spatial attention does not impair the detection of simple visual features (Harrison et al., 2022; J. Moreland et al., 2017; J. C. Moreland & Boynton, 2020; Scharff et al., 2011; White et al., 2017). For example, dividing attention between two spatial locations impaired the discrimination of a 90° change in orientation, but not the simple detection of an oblique grating (J. Moreland et al., 2017). This is consistent with reports that modulating spatial attention (e.g., by presenting a visual cue which indicates the spatial location of the subsequently presented stimulus) increases the response gain of neuronal responses to a greater extent in higher visual areas (e.g., V4 and MT) than in primary visual cortex (for review, see Maunsell, 2015; also see Maunsell & Cook, 2002; O'Connor et al., 2002).

Dividing attention between stimuli in distinct spatial locations has been shown to induce an oblique effect in tasks that rely on cognitive functions (see Section 1.3.5), such as judgements of simultaneity (Kelly & Matthews, 2011). This suggests that the oblique effect, at least for higher-order visual tasks, may be generated by cognitive mechanisms which are greatly modulated by attention, such as those involved in memory-retrieval (J. Moreland et al., 2017). However, further research is required to establish the impact of divided attention

on the oblique effect for various psychophysical tasks, and the characterise the nature of these proposed (but generally poorly defined) cognitive mechanisms.

Probing cognitive mechanisms

In a single-interval orientation-discrimination task, in which observers discriminated the perceived orientation against their prior knowledge (i.e., the 'template') of the standard orientation, oblique thresholds were found to be approximately six times larger than cardinal thresholds (Buchanan-Smith & Heeley, 1993). This oblique effect is much larger than observed for typical, 2AFC orientation-discrimination tasks, where oblique thresholds are typically two to four times larger than cardinal thresholds (Buchanan-Smith & Heeley, 1993; also see Sections 4.3 and 4.4). The notably large oblique effect in the single-interval orientation-discrimination experiment may reflect the contribution of higher-order mechanisms, possibly related to the comparison of observers' prior knowledge of the standard orientation with the encoded visual orientation, which are not required in a typical, 2AFC orientation-discrimination task. Impaired oblique performance may reflect the imprecision of observers' internal representation of oblique orientations, relative to that of cardinals, possibly reflecting the predominance of cardinal orientations in the visual environment (Girshick et al., 2011). However, the extent to which prior knowledge can account for the larger oblique effect in the single-interval orientation-discrimination task (Buchanan-Smith & Heeley, 1993) requires further investigation.

Aims

The orientation-identification task in the present Chapter required observers to identify which of two stimuli were presented at the standard orientation, requiring the comparison of the encoded visual orientation with observers' internal representation (i.e.,

'template') of the standard orientation. Orientation-identification performance for cardinals and obliques may reflect the precision of observers' internal representations of these orientations. The initial behavioural experiments (see Sections 6.2 to 6.4) aimed to measure the oblique effect for orientation identification, and to probe the relative contributions of short-term memory and divided attention to identification performance (through comparison of the temporal and spatial tasks). The subsequent experiment compared orientation-identification and orientation-discrimination performance (see Section 6.5), and the accompanying modelling work explored the mechanisms underlying the oblique effect for orientation-identification (see Section 6.6). Specifically, the modelling work investigated whether the oblique effect for orientation identification could be explained solely by the low-level mechanisms which encode stimulus orientation, or whether an additional anisotropic component, independent of the encoding stage, is required.

6.2 Remote measurements of the oblique effect for orientation-identification

6.2.1 Overview

The aim of the present experiment was to measure the oblique effect for orientation-identification, which required observers to identify which of two stimuli were presented at the standard orientation. As described in Section 6.1, the oblique effect for a single-interval orientation-discrimination task was much larger (oblique thresholds were approximately six times larger than cardinal thresholds) than that found for typical, 2AFC orientation-discrimination tasks (Buchanan-Smith & Heeley, 1993). Both tasks involved the comparison between the encoded, visual orientation and observers' prior knowledge of the standard orientation, therefore the oblique effect for orientation identification was predicted to be of a similar size to that reported for the single-interval orientation-discrimination task.

To examine whether divided attention on the spatial 2AFC task impacted orientation-identification performance, performance was compared between spatial and temporal versions of the task (Heeley & Buchanan-Smith, 1992; Westheimer, 2003a; Westheimer & Lavian, 2013). Dividing attention between stimuli in distinct spatial locations has been shown to induce an oblique effect in tasks that rely on cognitive functions (see Section 1.3.5), such as judgements of simultaneity (Kelly & Matthews, 2011). Therefore, if the cognitive mechanisms serving orientation identification (such as the memory-retrieval of the standard orientation) are anisotropic, then the oblique effect for identification may be larger for the spatial task than the temporal task.

Author's note

Remote-testing methods were used in the present experiment due to testing restrictions caused by the impacts of the pandemic (see Covid Impact Statement).

6.2.2 Methods

Participants

Five participants took part in the remote, web-based experiment, all with normal or corrected-to-normal visual acuity. Participants were not screened for ocular pathology or visual dysfunction, but were instructed to wear appropriate refractive correction, if required. All but two participants (P1 and P2) were naïve to the aims of the study. Ethical guidelines were followed as described in Section 2.1.

Apparatus

Testing occurred remotely with participants running the experiment on their own devices (the particular devices used were not recorded). Consequently, monitor output was not corrected through photometric gamma correction, and the noisy-bit method was not implemented to precisely control the luminance resolution of the testing monitors (see Section 2.3). Participants were provided with instructions on how to install PsychoPy (Peirce et al., 2019) on their devices, and how to run the experiment. Participants were asked to sit in a dimly lit room with no visual distractions (e.g., flashing lights), place their device on a flat surface, set their screen brightness to its maximum, turn off any blue-light filters, and adjust the volume of their device to ensure that it was clearly audible. Prior to each run, participants were instructed to maintain a fixed viewing distance of 60cm (e.g., by cutting a piece of string to length and adjusting their seating position to ensure that the ends of the string, when

taut, just touched both the display and the bridge of the nose), and input the width, in cm, of the visible (active) portion of their visual display. Along with this information, the spatial resolution of each participant's monitor was retrieved, making it possible to standardise the size and spatial frequency of stimuli across different visual displays.

Stimuli

Visual stimuli were Gabor patterns (Section 2.4), composed of orientated, 2c/° sinusoidal luminance gratings presented within a spatial Gaussian window with a space-constant σ^2 of 1.33°, truncated at ±4°. The stimulus contrast was set to be 40% of the maximum available from the visual display.

Design

For each run, the chosen 'task' condition determined whether the temporal or spatial version of the two-alternative forced choice (2AFC), orientation-identification task would be completed. In the temporal task, the target and comparison stimuli were presented sequentially in a central location. In the spatial 2AFC task, the target and comparison stimuli were presented simultaneously, with their centre-points located 8° to the left or right of a central fixation spot.

An adaptive staircase procedure was implemented (see Section 2.5), such that the difference in orientation between the *comparison* orientation and the *standard* orientation (either 0, 90, -45, or 45°) was determined by the staircase. Each run ended after ten reversals and thresholds were calculated as the arithmetic-mean staircase value of the last five reversals. Participants completed a minimum of four runs in each condition. All runs were completed in a pseudorandom fashion. The 'oblique effect index' (OEI, see Section 2.8) scores quantified the magnitude of the oblique effect. The average OEI score was given by

the geometric-mean (gM).

Procedure

Prior to each run, an example image of a Gabor at the standard orientation was displayed to ensure that participants were familiar with the appearance of the standard stimulus. Written instructions explained that participants were required to identify which of two stimuli was presented at the standard orientation, and reminded participants to maintain their viewing distance at 60cm. Participants started the experiment when ready and the example standard orientation was removed from the screen.

In the temporal 2AFC task, the standard and comparison were presented in sequential, 300ms intervals at the centre of the screen, separated by a 500ms homogeneous blank field. Intervals were marked by distinct audible tones. Participants judged which interval contained the standard orientation using the 'F' and 'J' keys to refer to the first and second intervals, respectively. The order of presentation was randomised.

In the spatial 2AFC task, participants were twice reminded (prior to initiating each run) to maintain their fixation on a central spot throughout each run. Standard and comparison stimuli were presented simultaneously within a single, 300ms interval. Participants judged which spatial location the standard orientation appeared in, using the 'F' and 'J' keys to refer to the left and right locations, respectively. The order of locations was randomised. To aid central fixation, the fixation dot was ever-present, except for a 100ms period after each response to indicate that a valid keyboard response had been collected. In both the temporal and spatial tasks, a response signalled the initiation of the next trial after an 800ms delay. No response feedback, concerning the correctness of the participant's decision, was given.

6.2.3 Results

For the temporal 2AFC task, orientation-identification thresholds were substantially lower for horizontal (0°) and vertical (90°) orientations than for the obliques (-45 and 45°) (Figure 6.1). Similar results were obtained for the spatial 2AFC task, although thresholds for all orientations were higher than for the temporal 2AFC task. Mean thresholds are shown in Figure 6.2. For three out of five participants (P1, P2, and P3), OEI scores were higher on the spatial 2AFC task (gM = 8.40, SE = 0.75) than on the temporal 2AFC task (gM = 7.77, SE = 0.98) (Figure 6.3). However, the remaining two participants showed either no difference in OEI scores (P4) or a higher OEI score for the temporal task (P5).

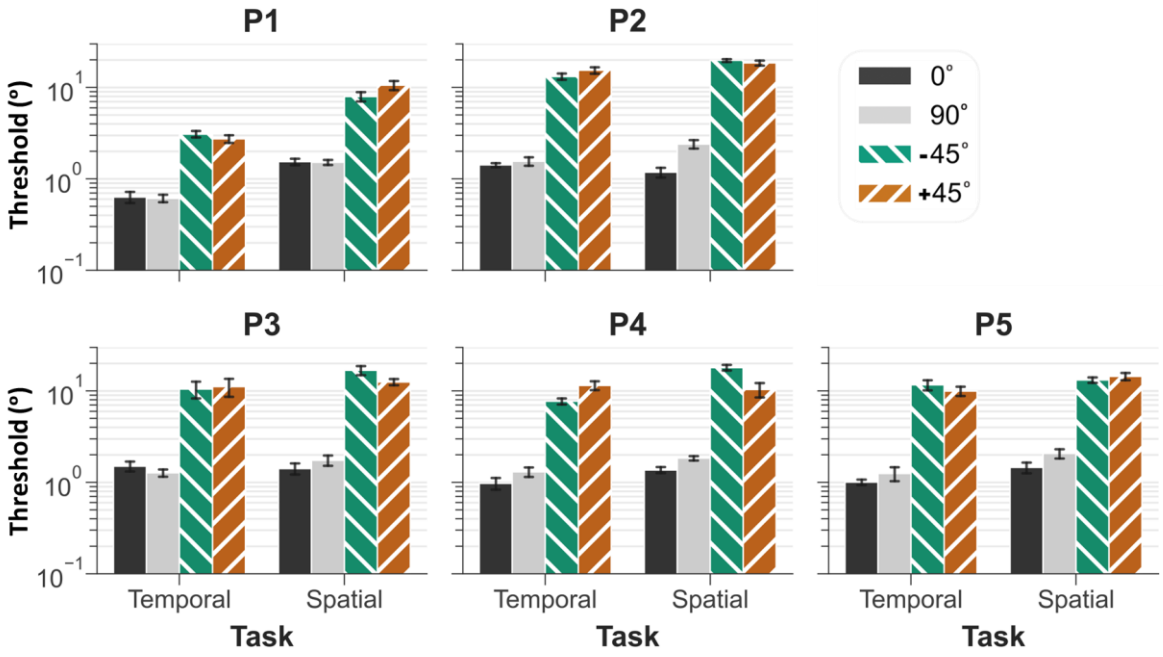

Figure 6.1. For each participant, orientation-identification thresholds are shown for the temporal and spatial 2AFC tasks. Error bars represent the bootstrapped standard error.

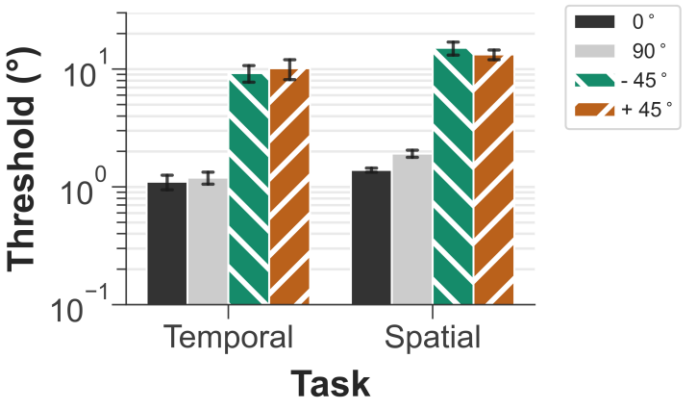

Figure 6.2. Mean orientation-identification thresholds are shown for the temporal and spatial 2AFC tasks. Error bars represent the standard error. Cardinal thresholds were much lower than oblique thresholds on both tasks.

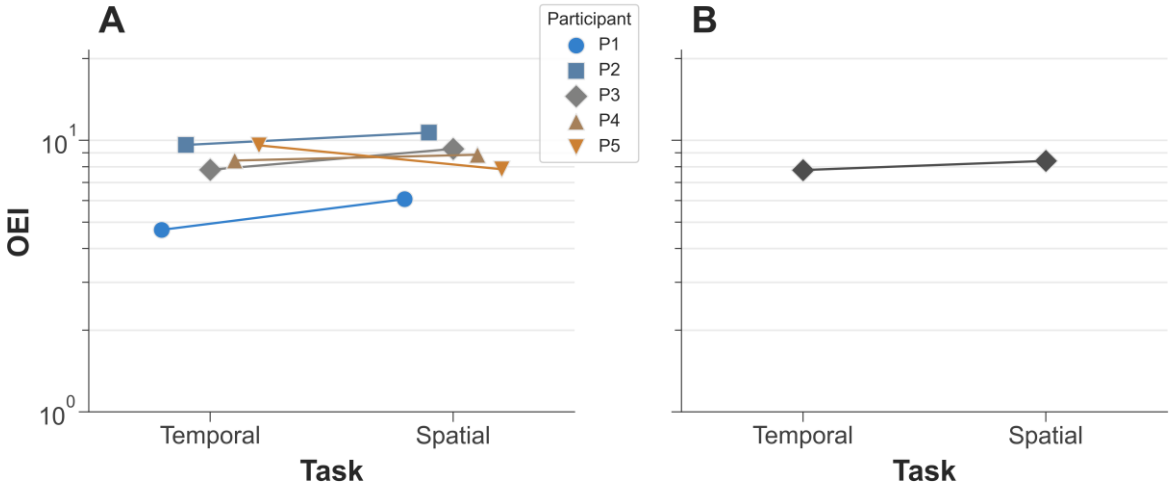

Figure 6.3. Individual oblique effect index (OEI) scores (*A*) and the geometric-mean OEI score (*B*) are shown for the temporal and spatial 2AFC tasks. OEI scores were larger on the spatial task than the temporal task in four out of five participants.

6.2.4 Summary

Large oblique effects were found for orientation identification, such that thresholds for oblique orientations were approximately eight times larger than for cardinal orientations.

This is much larger than previous reports of the oblique effect for orientation discrimination, where oblique thresholds are two to four times larger than cardinal thresholds (Heeley & Buchanan-Smith, 1992; Westheimer, 2003a; Westheimer & Beard, 1998; also see Sections 4.3 and 4.4). These results are consistent with the size of the oblique effect for a single-interval orientation-discrimination task (Buchanan-Smith & Heeley, 1993), which also relied on the comparison between the perceived orientation and observers' internal representation of the standard orientation.

There was no difference in the size of the oblique effect on the temporal and spatial tasks, although there was considerable inter-individual variation, with OEI scores ranging from approximately 5 to 10. However, this may reflect high levels of measurement noise due to the potential variability in remote-testing conditions (e.g., the presence of visual distractions), which could have obscured differences between the temporal and spatial versions of the experiment.

6.3 Lab-based measurements of the oblique effect for orientation identification

6.3.1 Overview

Differences in orientation-identification performance between the temporal and spatial tasks may have been obscured by the impacts of remote-testing (see Section 6.2). Therefore, the following experiment examined identification performance for both remote, web-based testing, and lab-based testing performed under strictly controlled laboratory conditions. In order to determine whether there was a memorial component to identification performance, due to the example of the standard stimulus which was presented prior to the initiation of each run, performance was tracked across the trials of individual runs.

6.3.2 Methods

Participants

20 participants, made up of a mixture of students and staff at the University of Nottingham and members of the general public, with a mean (SD) age of 25.3 (7.48) years were recruited to take part in the present experiment. Participants were not screened for ocular pathology or visual dysfunction, but were instructed to wear appropriate refractive correction, if required. Two out of 20 participants were excluded from subsequent data analyses as they failed to reach threshold performance levels of responding (i.e., at least 75% correct) in one or more conditions. One participant (P1) also took part in the previous remote-testing experiment (see Section 6.2). Counterbalancing of the order of testing meant that nine of 18 participants completed the web-based experiment first followed by the lab-based experiment, and the remaining nine completed the lab-based -experiment first followed by

the web-based experiment. Ethical guidelines were followed as described in Section 2.1.

Apparatus

The web-based experiment was designed in PsychoPy and run through Pavlovia, a web-based testing platform (Peirce et al., 2019), with custom JavaScript code. Participants used their own devices (the particular devices used were not recorded) and web-browsers to run the experiment. Testing conditions and experimental controls on the web-based experiment were implemented in the same manner as described in Section 6.2.

The lab-based experiment was analogous to the web-based experiment but took place under carefully controlled conditions at the University of Nottingham campus. The testing apparatus for the present experiment is described in Section 2.2. Monitor output was carefully linearised through photometric gamma correction, and the noisy-bit method provided precise control over the luminance resolution of the monitor (see Section 2.3). The viewing distance was fixed at 60cm by means of a chinrest.

Stimuli

Visual stimuli were Gabor patterns (Section 2.4) identical to those described in Section 6.2.2.

Design

Orientation-identification thresholds were determined for both the temporal and spatial two-alternative forced choice (2AFC) tasks, using the method of constant stimuli (see Section 2.6). There were four orientation conditions which set the value of the standard orientation (either 0, 90, -45, or 45°) which was constant for each run of trials. On each trial, the comparison orientation (which always differed from that of the standard) was chosen at

random from one of a predetermined set of seven levels based on the results of Section 6.2.2. Due to the substantial impairment in performance for oblique orientations relative to cardinals, the levels of orientation-offset between the standard and comparison were different for cardinal (0.71, 1.43, 2.14, 2.86, 3.57, 4.29, and 5.00°) and oblique orientations (3.57, 7.14, 10.70, 14.29, 17.80, 21.42, and 25.00°).

Each run comprised of ten repeats of the seven levels of orientation-offset, the sign of which (i.e., whether the comparison orientation was clockwise or anti-clockwise relative to the standard orientation) was randomised on each presentation. The proportion of correct responses for each level of orientation-offset was recorded. Participants were required to complete four runs (a total of 350 trials) on each orientation condition for each task. All runs were completed in a pseudorandom fashion. No response feedback, concerning the correctness of the participant's decision, was given.

Procedure

In the web-based experiment, participants initiated each run by clicking the relevant URL for each task. At the beginning of each run, participants were first presented with a dialogue box which prompted them to enter their participant identifier, monitor width (cm), and select their chosen standard orientation condition. The participants were also reminded to maintain their viewing distance at 60cm. Once this information was submitted, participants' browser windows were forced to full screen and written instructions explained that they were required to identify which of two stimuli was presented at the standard orientation. All other procedural details were identical to those described in Section 6.2, for both the web-based and lab-based experiments.

Data analysis

The proportion of correct responses for each level of orientation-offset was used to construct a psychometric function for each participant on each tested condition. A logistic curve was fit to the data to obtain the threshold (see Section 2.6), taken as the orientation-offset on the curve producing 75% correct responses. The 'oblique effect index' (OEI, see Section 2.8) scores quantified the magnitude of the oblique effect. The average OEI score was given by the geometric-mean (gM).

To test whether the oblique effect was larger for the spatial task than the temporal task, a one-tailed paired sampled t-test was used between OEI scores, for each of the lab-based and web-based experiments. The differences between OEI scores on the temporal and spatial tasks were confirmed not to violate the assumption of normality by Shapiro–Wilk tests.

The degree of agreement between web-based and lab-based thresholds was assessed for the temporal and spatial 2AFC tasks using Bland-Altman analyses (Bland & Altman, 1986, 1999). Due to a proportional relationship between variance and threshold magnitude, Bland-Altman analyses were performed on log-transformed thresholds and the limits of agreement were calculated on a log-scale (Bland & Altman, 1999). Consequently, difference scores were reported on a ratio scale (see Section 2.9).

6.3.3 Results

In the temporal and spatial versions of the web-based and lab-based experiments, orientation-identification thresholds were substantially lower for cardinal orientations relative to obliques (Figure 6.4). In the lab-based experiment, a one-tailed paired samples t-test revealed that OEI scores were significantly higher ($t(17) = 2.74$, $p < 0.01$) for the spatial task (gM = 7.44, SE = 0.35) than for the temporal task (gM = 6.32, SE = 0.49), with a moderate effect size (Cohen's $d = 0.44$). For the same participants in the web-based experiment, OEI scores were not significantly larger ($t(17) = 1.23$, $p = 0.12$) for the spatial 2AFC task (gM = 7.23, SE = 0.43) than for the temporal 2AFC task (gM = 6.53, SE = 0.47) (Figure 6.5).

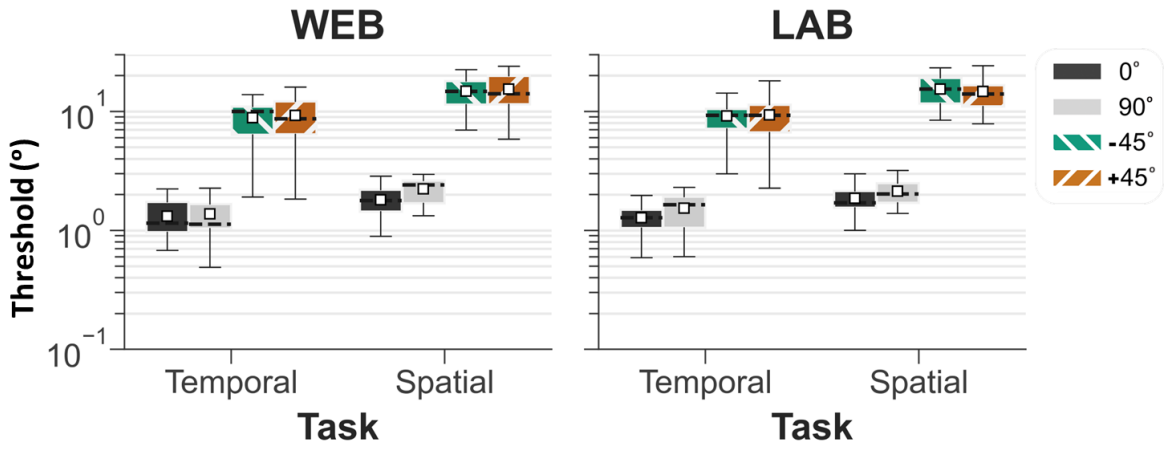

Figure 6.4. Boxplot showing the means (*white squares*), medians (*dotted lines*), and interquartile ranges (*boxes*) of thresholds for the web-based (*left*) and lab-based (*right*) orientation-identification experiments. Error bars represent the range.

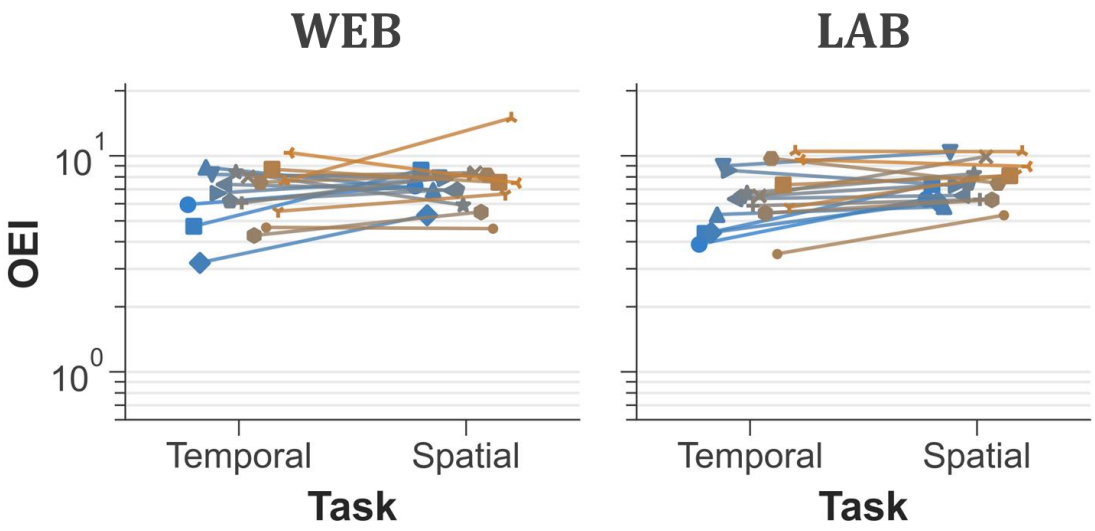

Figure 6.5. The oblique effect index (OEI) scores are given for the web-based (*top*) and lab-based (*bottom*) versions of the orientation-identification experiment. OEI scores for each participant are depicted by unique symbols and coloured lines.

4043

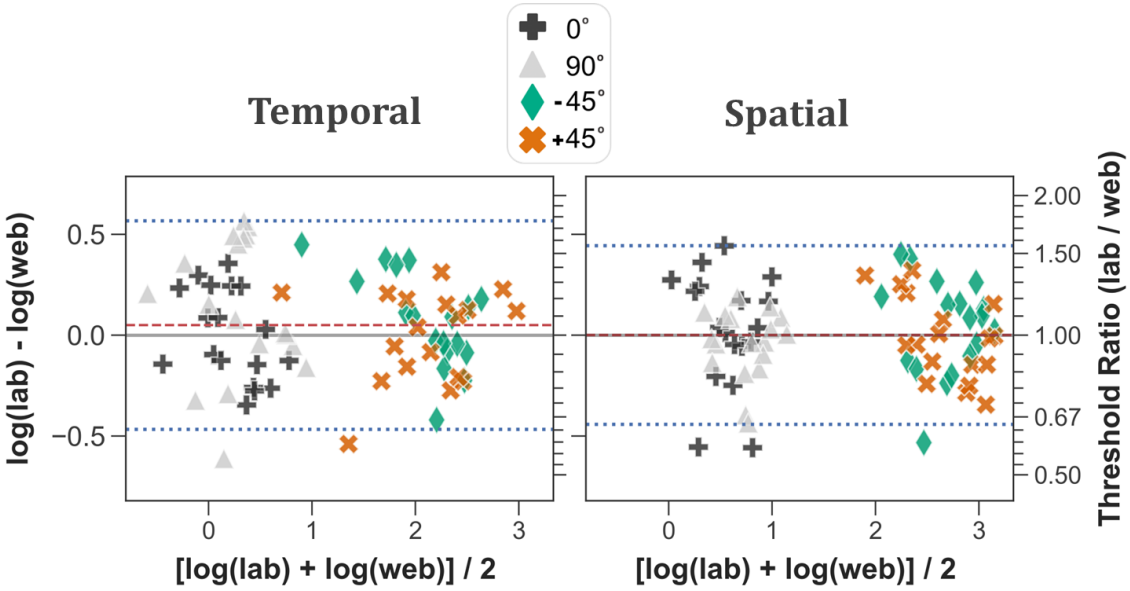

Figure 6.6. Bland-Altman plots of the log-transformed data for the spatial and temporal tasks. Differences between lab and web log-thresholds are plotted against the mean log-threshold. The mean difference (*red dashed line*), line of equality (*grey solid line*), and limits of agreement (*blue dotted lines*) are shown. The ratio scale (*right y-axis*) allows visualisation of the magnitude of difference between lab and web thresholds. There were high levels of agreement between the lab and web thresholds.

Variability in the differences between OEI scores, on the temporal and spatial tasks, was greater for the web-based experiment (SD = 2.45) than for the lab-based experiment (SD = 1.43). Despite this, Bland-Altman analyses revealed high levels of agreement between web-based and lab-based thresholds (Figure 6.6), with median 'absolute-ratio' scores (IQR) of 1.23 (0.25) and 1.16 (0.23) on the temporal and spatial 2AFC tasks, respectively.

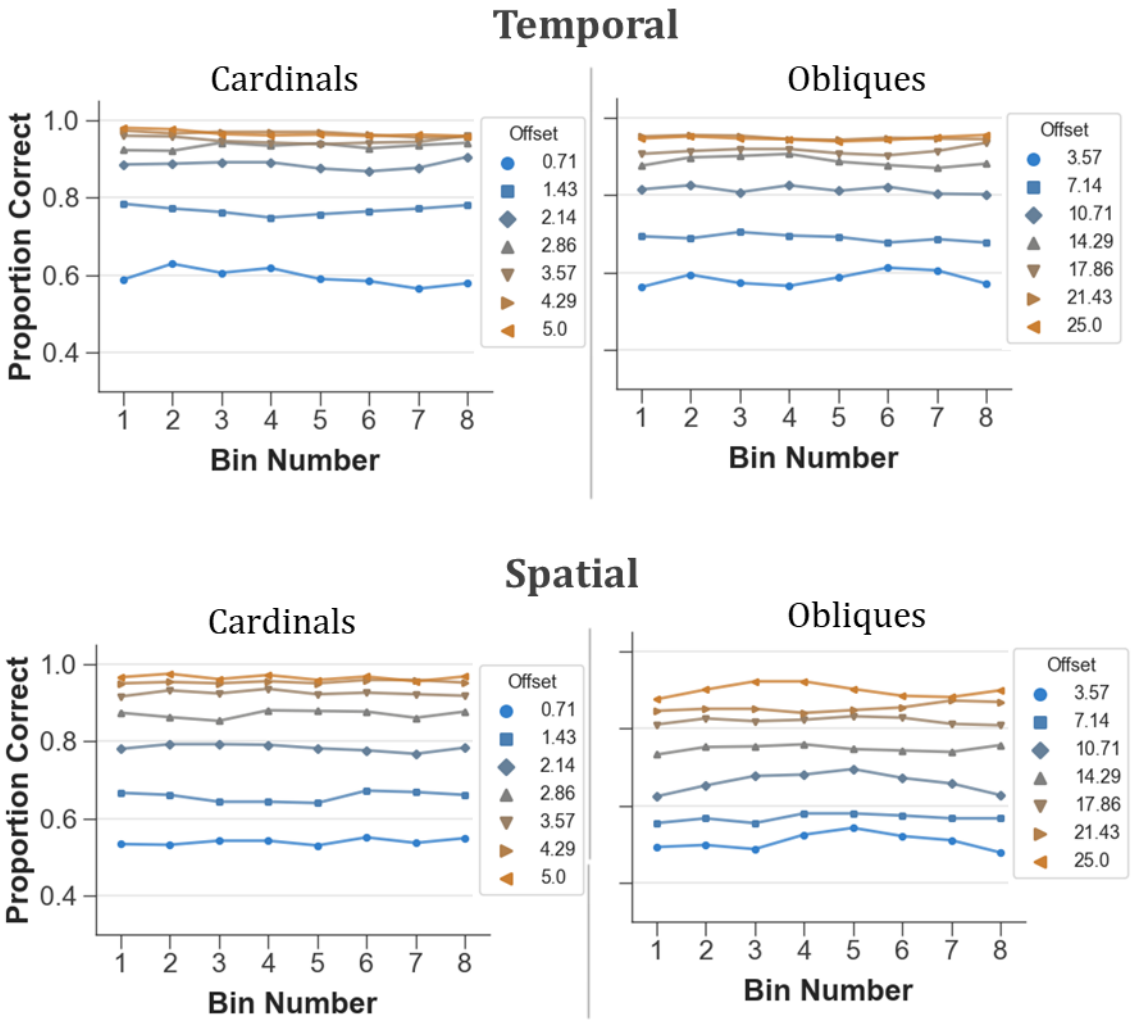

Figure 6.7. The mean proportion of correct responses for each level of orientation-offset were calculated in overlapping bins of three trials. For example, bin number 1 corresponds to trials 1, 2, and 3, bin number 2 corresponds to trials 2, 3, and 4, etc. Performance did not improve systematically over the course of a given run on either task.

The average performance for each level of orientation-offset, taken as the arithmetic-mean proportion correct in bins of three successive trials, did not change systematically throughout the course of a given run on the lab-based experiment (Figure 6.7). This was the case for both the temporal and spatial tasks, and for both cardinals and obliques, indicating that there was little influence of a memorial component relating to the presentation of the standard orientation prior to the commencement of each run. The magnitude of the oblique effect for identification did not change throughout the course of testing (Figure 6.8).

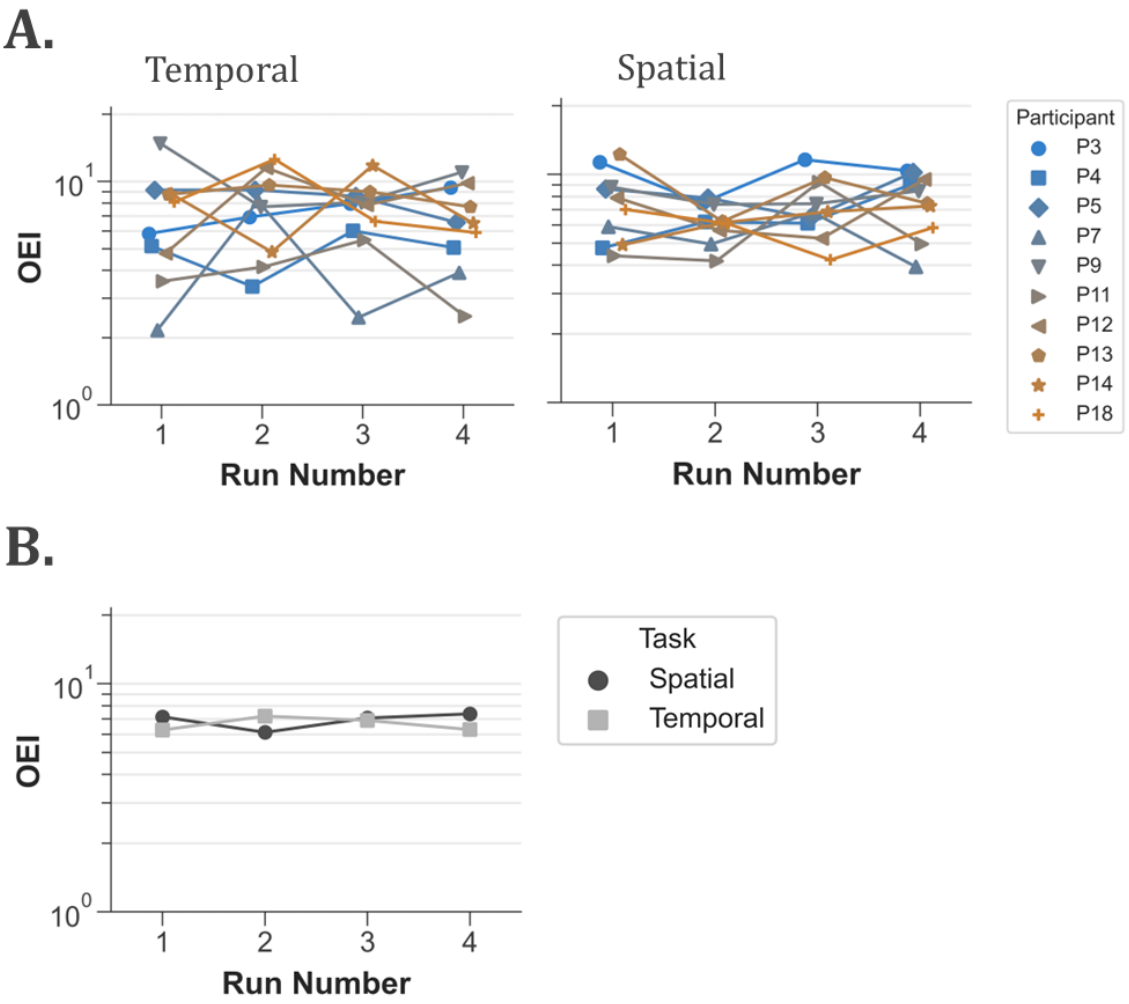

Figure 6.8. Each participant's OEI score (*A*) and the geometric-mean OEI score (*B*) for the temporal and spatial tasks were calculated separately for each individual run. The geometric-mean OEI score did not change during the course of testing.

6.3.4 Summary

Large oblique effects for the temporal and spatial tasks, of a similar magnitude to the previous experiment (see Section 6.2), were found for web-based and lab-based versions of the orientation-identification experiment. On the lab-based experiment, the oblique effect was found to be significantly larger for the spatial task than for the temporal task, consistent with reports that the oblique effect for visual-cognitive tasks increases when spatial attention is divided between two or more spatial locations (Balikou et al., 2015; Kelly & Matthews, 2011). On the identification task, increased attentional load on the spatial task may impact the mechanisms that compare the encoded visual stimulus with the memory of the standard, although there was no change in identification performance across a given run, indicating that this was not impacted by the presentation of the standard orientation prior to each run. Similarly, the size of the oblique effect for identification did not change across the course of testing, indicating the absence of learning effects which have been suggested to modulate the oblique effect (Westheimer & Lavian, 2013).

However, on the web-based experiment, the difference between OEI scores on the temporal and spatial tasks did not reach significance, despite high levels of agreement between the web-based and lab-based thresholds. The web-based testing protocol may therefore be unsuitable for capturing the effects of divided attention on the size of the oblique effect for orientation-identification. Whereas stimuli on the temporal task were presented centrally, stimuli on the spatial task were presented in the near-periphery, and it is unclear to what extent identification performance was impacted by the effects of eccentricity.

6.4 Examining the cognitive factors underlying the oblique effect for orientation identification

6.4.1 Overview

The relative impacts of stimulus eccentricity and spatial attention on identification performance, on the spatial task, are unclear. The following experiment therefore implemented a 'mixed' version of the orientation-identification task, whereby stimuli were presented in successive intervals, in alternating spatial locations. The temporal delay between intervals was the same as described for the temporal task, and the spatial positions were the same as described for the spatial task.

If identification performance is similar for the 'mixed' and spatial versions of the task, where stimuli are presented in the near-periphery, this would indicate that stimulus eccentricity impacts identification performance. Conversely, if identification performance is similar for the 'mixed' and temporal task, where stimuli are viewed successively in distinct temporal intervals, then this implicates the impacts of divided attention or short-term memory on performance.

6.4.2 Methods

Participants

Four participants took part in this experiment, all with normal or corrected-to-normal visual acuity. Participants were not screened for ocular pathology or visual dysfunction, but were instructed to wear appropriate refractive correction, if required. Two participants (P3 and P4) were naïve to the aims of the study, and the remaining two participants (P1 and P2) also took part in the previous experiment (Section 6.3).

Stimuli

The testing apparatus is as described in Section 2.2. Monitor output was carefully linearised through photometric gamma correction (Section 2.3.1) and the noisy-bit method provided precise control over the luminance resolution of the monitor (Section 2.3.2). Visual stimuli were Gabor patterns (Section 2.4) identical to those described in Sections 6.2.2 and 6.2.3.

Design

For each run, the chosen 'task' condition determined whether the temporal, spatial, or 'mixed' two-alternative forced choice (2AFC) task would be completed. The temporal and spatial 2AFC tasks were identical to those described previously (see Sections 6.2 and 6.3). In the 'mixed' 2AFC task, the *standard* and *comparison* stimuli were presented sequentially over a temporal delay, in alternating locations, 8° to the left or right a central fixation spot. The remainder of the screen was a homogenous, blank field. The standard orientation (either 0, 90, -45, or 45°) defined the orientation of the target stimulus for each run.

Orientation-identification thresholds were determined using the method of constant stimuli (see Section 2.6). To capture the typical performance range, the levels of orientation-offset were over a smaller range, for cardinal orientations (0.57, 1.14, 1.71, 2.29, 2.86, 3.43, and 4.00°), than in the previous experiment (see Section 6.3), whereas the levels of orientation-offset for the obliques were unchanged (3.57, 7.14, 10.70, 14.29, 17.80, 21.42, and 25.00°). Due to ceiling effects, one participant (P1) performed an additional orientation-offset level for the cardinals (0.36°) and the obliques (1.79°).

Procedure

Procedural details for the temporal and spatial 2AFC tasks were identical to those described for the lab-based experiment in Section 6.3. In the 'mixed' 2AFC task, the timings were the same as for the temporal task, and the locations of the standard and comparison stimuli were alternated between the same spatial locations as for the spatial task. Participants were twice reminded (prior to initiating each run) to maintain their fixation on a central spot throughout each run. Stimulus intervals were separated by a 500ms homogeneous, blank field. Stimulus intervals were marked by distinct audible tones. Participants judged in which stimulus interval the standard orientation appeared using the 'F' and 'J' keys to refer to the first and second intervals, respectively. The order of presentation and the order of locations were randomised. To aid central fixation, the fixation spot was ever-present, except for a 100ms period after each response to indicate that a valid keyboard response had been collected. In all three tasks, a response signalled the initiation of the next trial after an 800ms delay. No response feedback, concerning the correctness of the participant's decision, was given.

Data analysis

Thresholds were obtained as described in Section 6.3. The 'oblique effect index' (OEI, see Section 2.8) scores quantified the magnitude of the oblique effect. The average OEI score was given by the geometric-mean (gM).

6.4.3 Results

The oblique effect for orientation-identification was observed across all experimental conditions, such that oblique (-45 and 45°) thresholds were substantially lower than cardinal (0 and 90°) thresholds (Figure 6.9). All four participants showed larger identification thresholds for the spatial task relative to the temporal and 'mixed' tasks, which was consistent across all tested orientations. Mean thresholds are shown in Figure 6.10.

For all four participants, the magnitude of the oblique effect was larger for the spatial task (gM = 8.54, SE = 2.52) than for the temporal task (gM = 7.12, SE = 2.03). For two of

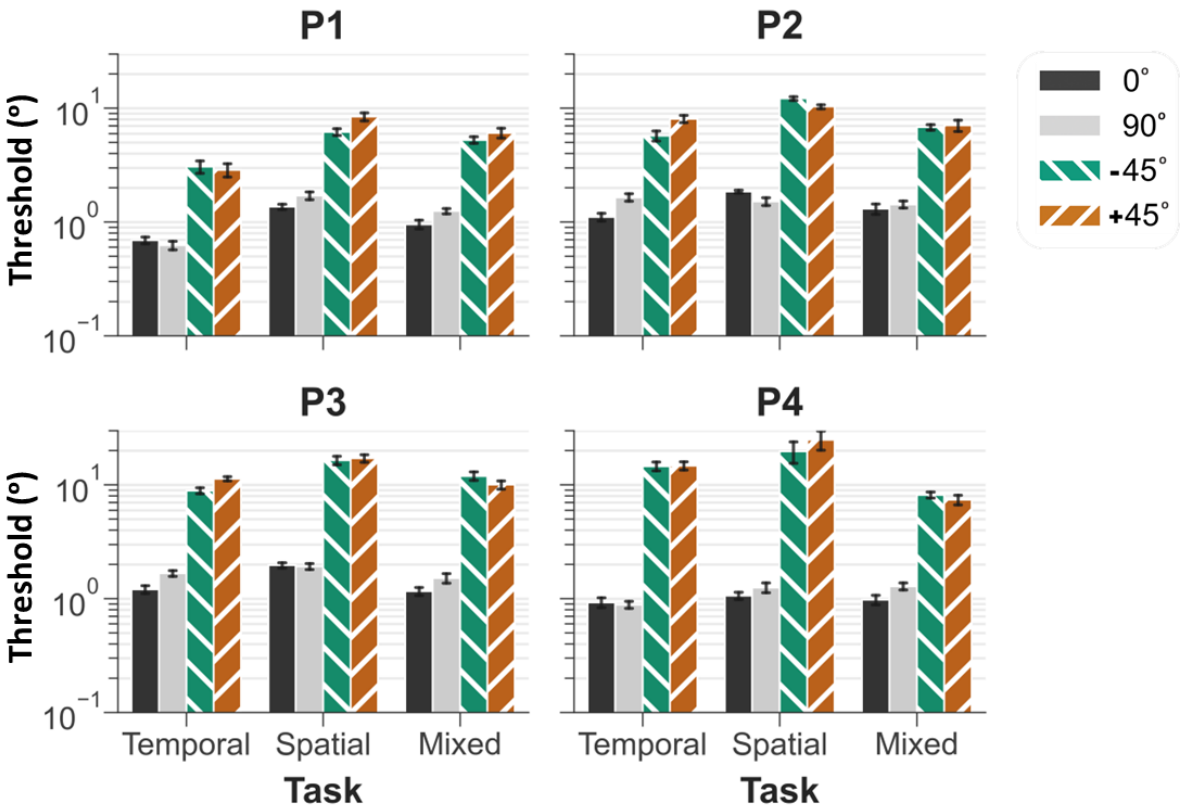

Figure 6.9. Orientation-identification thresholds for each participant on each of the temporal, spatial, and 'mixed' tasks. Error bars represent the bootstrapped standard error.

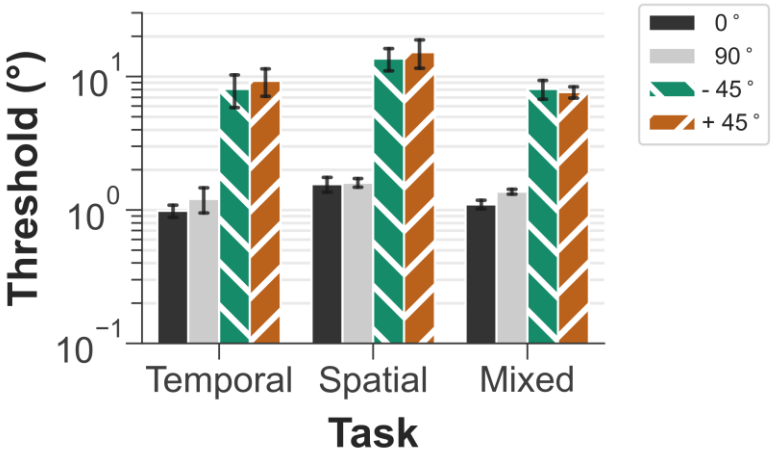

Figure 6.10. Mean orientation-identification thresholds are shown for the temporal, spatial and mixed 2AFC tasks. Error bars represent the standard error. Thresholds were higher on the spatial task relative to the temporal and mixed tasks.

four participants (P1 and P4), smaller oblique effects were found for the 'mixed' task (gM = 6.20, SE = 0.66) relative to the spatial task (Figure 6.11). Three out of four participants showed smaller oblique effects for the 'mixed' task relative to the temporal task.

Further inspection of the data from one participant (P4) revealed that they performed the temporal, spatial, and 'mixed' tasks in sequential order (rather than following instructions about randomisation), indicating that order effects (e.g., oblique learning) may have generated smaller oblique thresholds on the spatial and 'mixed' tasks relative to the temporal task. For the 'mixed' task, horizontal thresholds (M = 1.10°, SE = 0.08°) were lower than vertical thresholds (M = 1.37°, SE = 0.06°) for all four participants, however this effect was not found consistently on either of the temporal and spatial tasks.

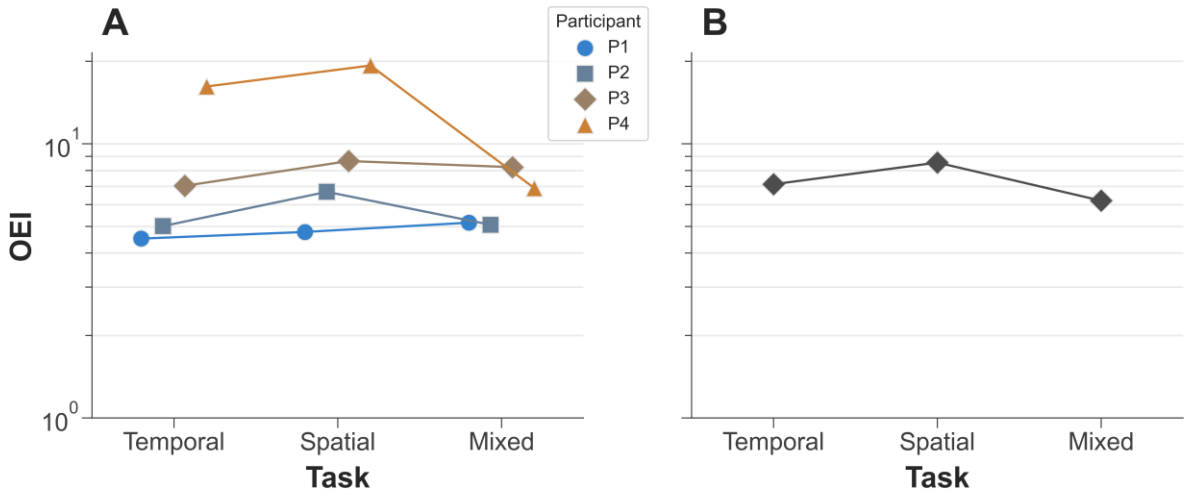

Figure 6.11. Individual oblique effect index (OEI) scores (*A*) and the geometric-mean OEI score (*B*) are shown for the temporal, spatial and mixed tasks. OEI scores were higher on the spatial task than on the temporal task in all participants.

6.4.4 Summary

The oblique effect for orientation-identification was larger for the spatial task than for the temporal task, consistent with previous findings (see Sections 6.2 and 6.3). Neither the oblique effect nor identification thresholds were systematically larger on the 'mixed' task relative to the temporal task, indicating that the difference between the temporal and spatial tasks cannot be attributed to the impacts of eccentricity on task performance. This is consistent with findings that the oblique effect for orientation discrimination is mostly invariant with respect to eccentricity, at least for line lengths of above 1° at eccentricities up to 9° (Westheimer, 2003b).

Although the group-level results indicate that the oblique effect on the spatial task was larger than on the 'mixed' task, two out of four participants did not show this effect. Therefore, results partially support the notion that divided attention induces the oblique effect for tasks with a cognitive component (i.e., memory-retrieval of the standard orientation) (see

Section 1.3.5), however the extent of this effect may be highly variable across individuals. Indeed, large individual differences are found for visual tasks which contain an attentional component, which may explain why this was not found for all tested participants. For example, contrast-detection thresholds are far more variable when attention is directed to a task-irrelevant orientation, than in the absence of attentional instructions (Bridwell et al., 2013). To understand the mechanisms of orientation identification, further investigation is required which directly compares visual performance for orientation-identification and orientation-discrimination tasks.

6.5 Comparing the oblique effects for orientation identification and discrimination

6.5.1 Overview

The oblique effect for orientation identification is larger, on average, on the spatial task than on the temporal and 'mixed' tasks (see Section 6.4). This is consistent with findings that, under conditions of divided attention, the oblique effect is induced for visual tasks with a cognitive component (see Section 1.3.5), such as judgements of simultaneity for grating stimuli (Kelly & Matthews, 2011). In the identification task, this cognitive component may reflect the retrieval of the standard orientation from participants' prior knowledge, similar to that required when manually reproducing an orientation from memory

If the impacts of divided attention on the oblique effect for identification reflects the modulation of anisotropic cognitive mechanisms, then the oblique effect on 'low-level' tasks should not be modulated by spatial attention, at least not the same extent as for identification. For instance, orientation discrimination involves the comparison of two visually encoded orientations, and does not necessitate the comparison with an internal 'template' of the standard orientation. Indeed, model simulations have revealed that the oblique effect for discrimination may be accounted for solely by anisotropic orientation bandwidths, in the mechanisms which encode orientation (see Sections 4.3 and 4.4).

Performance was assessed for temporal, spatial, and 'mixed' versions of orientation-identification and orientation-discrimination tasks. If similar sized oblique effects are found for the temporal, spatial, and 'mixed' versions of the orientation-discrimination task, this indicates that divided attention does not impact the size of the oblique effect for orientation-discrimination, and that identification relies on mechanisms which are independent from

those which determine discrimination performance. Conversely, if the oblique effect for discrimination is larger for the spatial task than for the temporal and 'mixed' tasks (as is found for identification), this indicates that discrimination and identification performance are determined by similar mechanisms.

Additionally, previous work has reported that the oblique effect for orientation-discrimination is larger for the stimuli presented successively over a temporal delay, than for stimuli presented simultaneously (Heeley & Buchanan-Smith, 1992; Westheimer, 2003a). This may reflect anisotropic storage mechanisms of visual short-term memory, such that representations of oblique orientations may decay faster than representations of cardinal orientations. If this is the case, then the oblique effect for discrimination should be larger on the temporal and 'mixed' tasks, than for the spatial task.

6.5.2 Methods

Participants

Six participants took part in the present experiment, three of whom (P1, P2, and P5) performed at least one of the previous orientation-identification experiments. Three participants were naïve to the aims of the study (P4, P5, and P6). Ethical guidelines were followed as described in Section 2.1.

Stimuli

The testing apparatus for the present experiment is as described in Section 2.2. Monitor output was carefully linearised through photometric gamma correction and the noisy-bit method provided precise control over the luminance resolution of the monitor (Section 2.3). Visual stimuli were Gabor patterns (Section 2.4) identical to those described for the previous experiments (see Sections 6.2, 6.3, and 6.4).

Design

For each run, the chosen 'task' condition determined whether the temporal, spatial, or 'mixed' versions of the two-alternative forced choice (2AFC) task would be completed. Thresholds were determined for the orientation-identification and orientation-discrimination tasks using the method of constant stimuli (see Section 2.6). To ensure that participants completed runs in a randomised fashion, the randomised order of conditions was automated. Interleaved runs on the identification and discrimination tasks were also completed in a randomised, automated fashion. A minimum of four runs were completed in each condition.

Orientation identification

The orientation-offsets for the identification task were taken from a reduced range compared to previous experiments, for both cardinals (0.4, 0.8, 1.2, 1.6, 2.0, 2.4, and 2.8°) and obliques (2, 4, 6, 8, 10, 12, 14, and 16°). Orientation-offsets were consistent across the temporal, spatial, and 'mixed' 2AFC tasks.

Orientation discrimination

Guided by previous findings (see Sections 4.3 and 4.4), the orientation-offsets for discrimination were smaller than those for identification, for both cardinals (0.3, 0.6, 0.9, 1.2, 1.5, 1.8, and 2.1°) and obliques (1, 2, 3, 4, 5, 6, and 7°). Orientation-offsets were consistent across the temporal, spatial, and 'mixed' 2AFC tasks.

Procedure

The procedural details of the temporal, spatial, and 'mixed' 2AFC tasks were identical to those described in Section 6.4, except for the inclusion of the orientation-discrimination task. In the discrimination task, participants judged which stimulus was rotated more

clockwise. No response feedback, concerning the correctness of the participant's decision, was given.

Data analysis

Thresholds for the orientation-discrimination and orientation-identification tasks were calculated as described in Sections 6.3 and 6.4. The 'oblique effect index' (OEI, see Section 2.8) scores quantified the magnitude of the oblique effect. The average OEI score was given by the geometric-mean (gM).

6.5.3 Results

In all six participants, the oblique effect was found for identification and discrimination in each of the temporal, spatial and mixed tasks, such that thresholds were substantially higher for the oblique orientations than the cardinal orientations (Figure 6.12). On average, thresholds on both the identification and discrimination task were smaller on the temporal task, than on the spatial or 'mixed' tasks (Figure 6.13).

To explore the impact of judgement (i.e., identification or discrimination) and task type (i.e., temporal, spatial, or mixed 2AFC) on the size of the oblique effect, a 2x3 repeated measures ANOVA was performed on the measured OEI scores. A significant main effect of judgement was found ($F(1,5) = 41.3$, $p < .001$, $\eta^2_p = .892$), and pairwise comparisons revealed that OEI scores were significantly higher on the identification task than on the discrimination task, for each of the temporal, spatial, and mixed tasks.

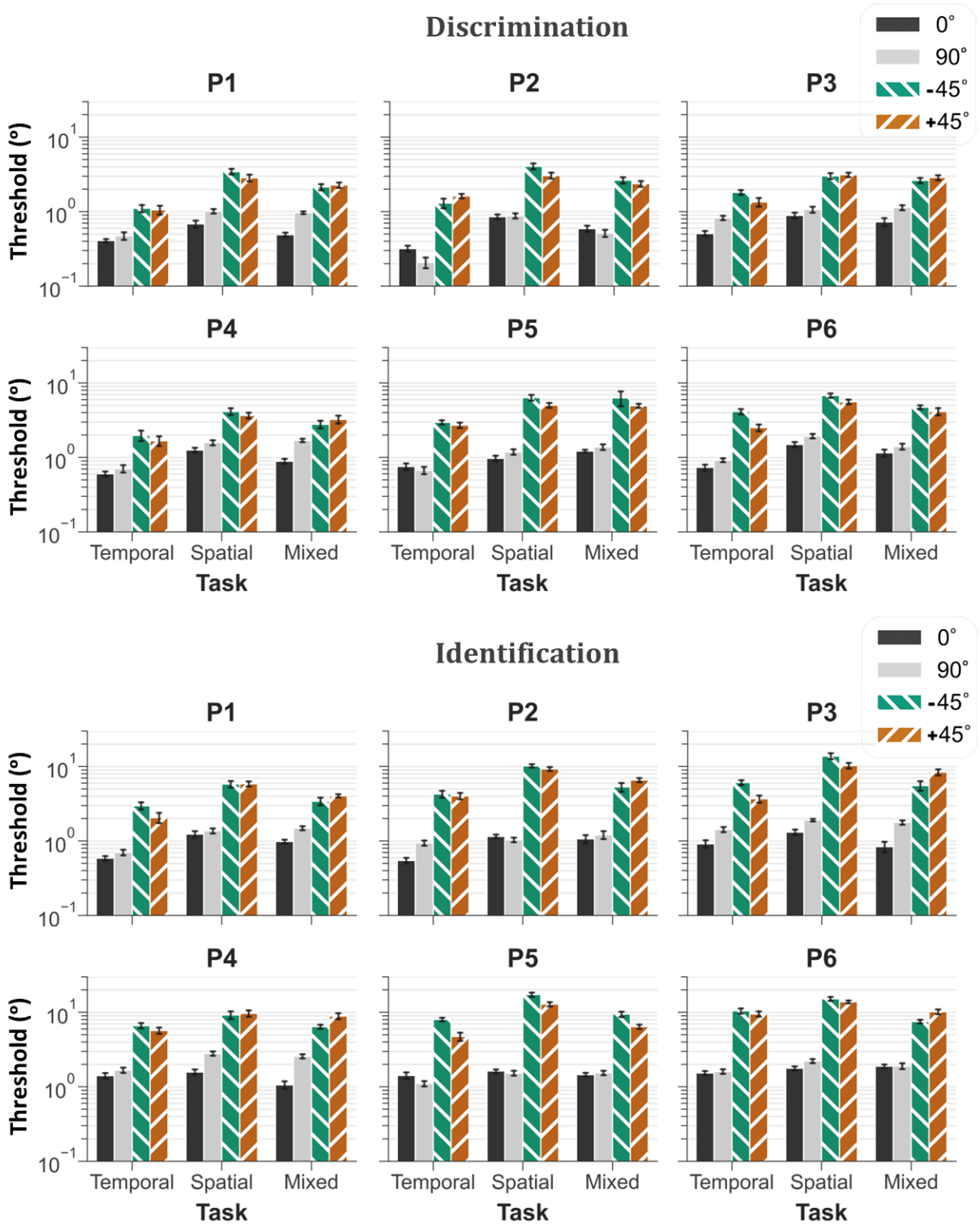

Figure 6.12. Orientation discrimination thresholds (*top*) and identification thresholds (*bottom*) for each participant on each of the temporal, spatial, and 'mixed' tasks. Error bars represent the bootstrapped standard error. Discrimination thresholds were lower than identification thresholds, especially for the obliques, and on the spatial task.

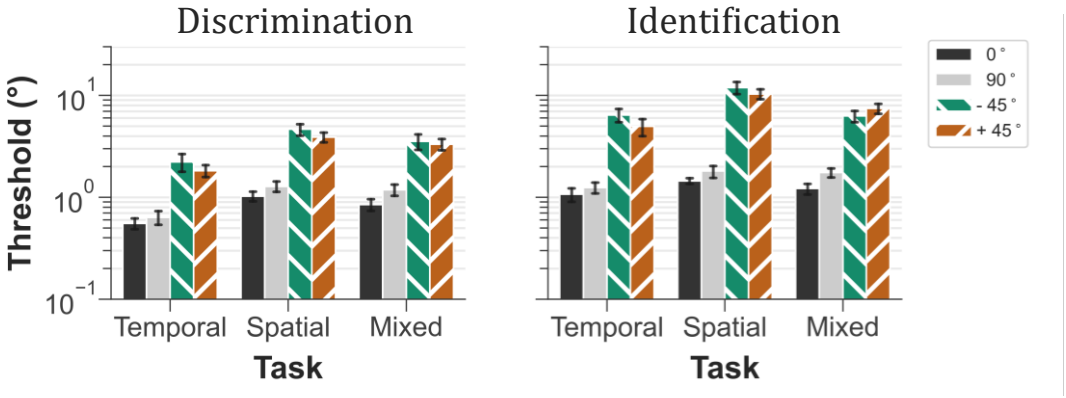

Figure 6.13. Mean thresholds for the orientation-discrimination and orientation-identification experiments, for each of the temporal, spatial and mixed 2AFC tasks. Error bars represent the standard error (SE). Identification thresholds were larger than discrimination thresholds, especially for the spatial task.

A significant interaction between judgement and task type was also found ($F(2,10) = 5.31$, $p = .017$) with a large effect size ($\eta^2_p = .558$). Pairwise comparisons revealed that OEI scores for identification were significantly larger on the spatial task (gM = 6.69, SE = 0.91) than on the temporal (gM = 4.76, SE = 0.37) or 'mixed' tasks (gM = 4.54, SE = 0.39), although the extent of this difference varied across participants (Figure 6.14). In contrast, for orientation-discrimination, there were no systematic differences between OEI scores on the temporal (gM = 3.36, SE = 0.45), spatial (gM = 3.69, SE = 0.32), or mixed (gM = 3.32, SE = 0.31) versions of the task.

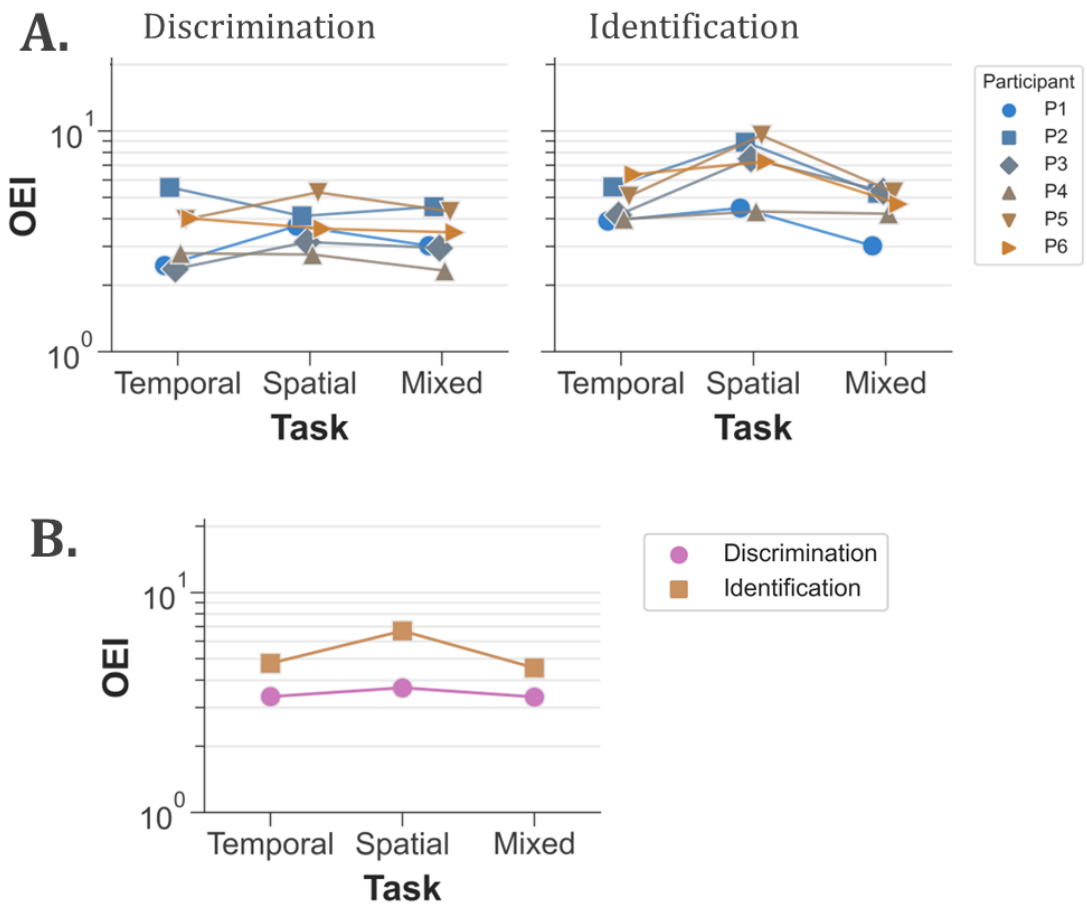

Figure 6.14. Oblique effect index (OEI) scores for each participant (*top*) and the geometric-mean OEI scores (*bottom*) for identification and discrimination. On average, OEI scores for identification were markedly higher on the spatial task than on the temporal or 'mixed' tasks, however this was not found for discrimination.

4275 The geometric-mean OEI score was tracked as a function of the run number (Figure
4276 6.15). On the temporal task, OEI (SE) scores for identification decreased from 5.95 (0.69) to
4277 3.96 (0.30) between the first and fourth run, whereas OEI scores for discrimination
4278 marginally decreased from 3.63 (0.63) to 3.34 (0.61). On the spatial and 'mixed' tasks, OEI
4279 scores did not change consistently for either of the identification and discrimination tasks.

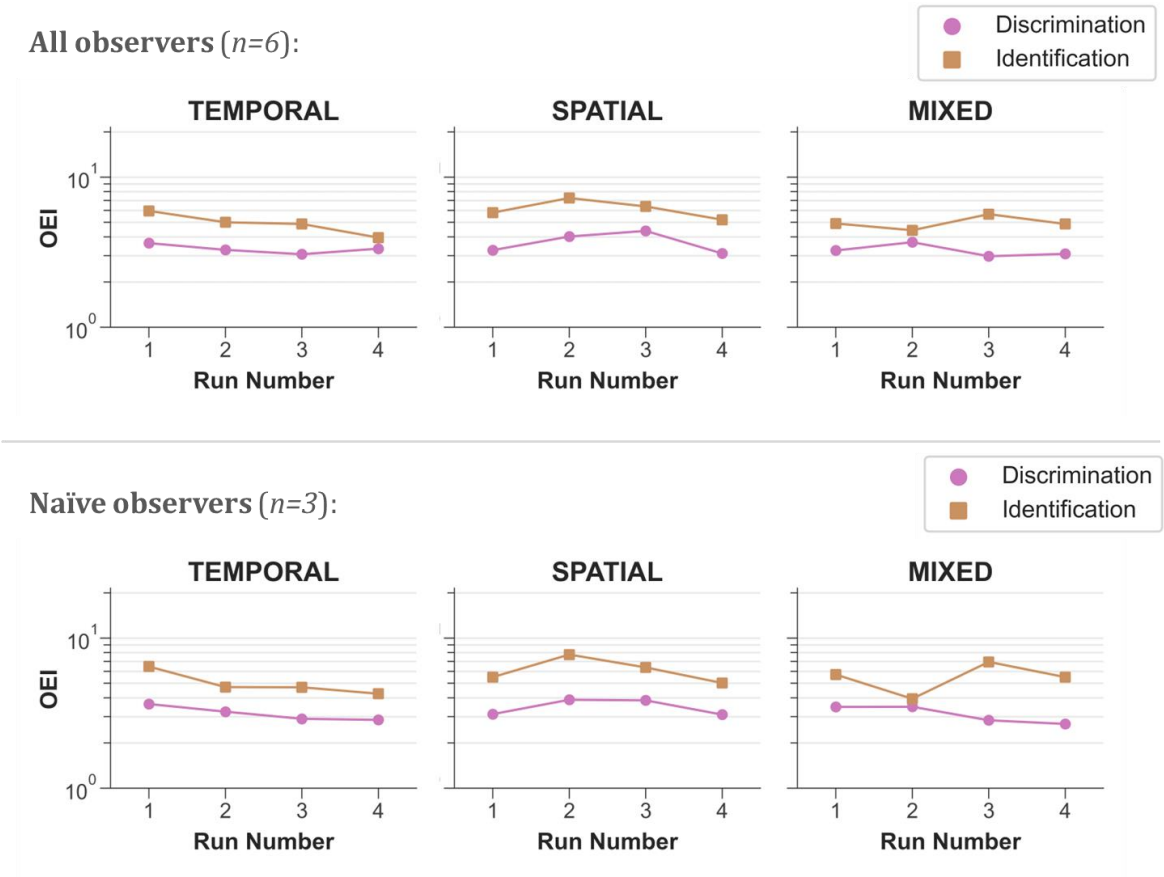

Figure 6.15. Geometric mean OEI scores for all participants (*A*) and a subsample of naïve observers (*B*) with no experience of either experiment. OEI scores were calculated for each run separately. In the majority of conditions, OEI scores did not change over the course of testing.

To explore whether prior experience with the orientation-identification task influenced these findings, the same analysis was performed on a subsample of three naïve observers (P3, P4, and P6), who had not performed either experiment previously. In this sample, the geometric-mean OEI (SE) scores for identification decreased from 6.46 (1.39) to 4.22 (0.30) between the first and fourth runs on the temporal task, whereas OEI scores for discrimination decreased from 3.57 (1.11) to 2.34 (0.38). There was no systematic change in OEI scores for the spatial task. On the 'mixed' task, the geometric-mean OEI scores for discrimination decreased from 3.35 (0.39) to 2.19 (0.63) between the first and fourth run.

6.5.4 Summary

The oblique effect for orientation identification was larger than that for orientation discrimination, across all of the temporal, spatial, and 'mixed' versions of the tasks, as expected from previous findings (see Sections 6.2 to 6.4). In the orientation-identification task, the perceived orientation (encoded in the firing rates of early visual cortical neurons) may be compared against observers' internal representation (or 'template') of the standard orientation. The larger oblique effect (and thresholds) for orientation identification relative to discrimination may therefore reflect an additional source of variance at this comparison stage.

In line with the findings of Section 6.4, the oblique effect for orientation identification was larger for the spatial task than for the temporal and 'mixed' tasks, although the extent of these differences varied greatly across participants. This is consistent with larger individual differences for visual tasks where visual attention is manipulated, relative to where is not (Bridwell et al., 2013). In contrast, the oblique effect for discrimination was similar in size across the same three tasks, indicating that divided attention in the spatial task did not modulate the size of the oblique effect for discrimination. Assuming that attentional modulation of the oblique effect reflects impacts on underlying cognitive mechanisms (see Section 1.3.5), these results indicate that orientation identification may rely on mechanisms which are independent from those which determine discrimination performance. However, further investigation is required work to test this hypothesis.

The oblique effect for identification in the present study, in which runs on the discrimination and identification tasks were interleaved, was much smaller than in previous experiments which involved runs only on the identification task (see Sections 6.2 to 6.4). Interleaving of runs on the identification and discrimination tasks may have refined observers' internal representations of the obliques, through repeated exposure to near-oblique

orientations on the discrimination task (where comparison orientations are much closer to the standard orientation than on the identification task). However, only three participants performed both of these testing protocols, indicating that further investigation is required to explore the generality of this finding.

There was no evidence of anisotropic storage mechanisms in visual short-term memory, which were predicted to generate larger oblique effects on the temporal and 'mixed' versions of the discrimination task (Westheimer, 2003a). Previous reports of a larger oblique effect in the temporal task than the spatial task (Heeley & Buchanan-Smith, 1992; Westheimer, 2003a) may have resulted from inappropriate stimulus-configurations in the spatial task (see Section 1.3.5).

6.6 Modelling the oblique effect for orientation identification

Overview

Model performance was assessed on simulated orientation-discrimination and orientation-identification tasks, analogous to those described for the behavioural experiments. The aim of the present modelling work was to provide an account of the oblique effect for orientation identification, which is much larger than that for discrimination. In Section 6.5, for the temporal 2AFC task, the geometric-mean 'oblique effect index' (OEI, see Section 2.8) score in the discrimination and identification tasks were 3.36 and 4.76, reflecting approximately a 40% difference between the two. However, it is important to note that in Sections 6.2 to 6.4, the geometric-mean OEI scores for identification on the temporal task ranged from 6.32 to 7.78.

The model for orientation identification was composed of two independent stages. First, the 'encoding stage' encoded the stimulus orientation in the firing rates of orientation-selective mechanisms, as described previously for orientation discrimination (see Sections 3.4.1). Secondly, the 'template stage' generated an estimate of the standard orientation from a separate population of orientation-selective mechanisms (this is a novel approximation of how participants' memory, or template, of the standard orientation may be represented in visual memory). Examination of the empirical, behavioural data revealed that identification performance was unchanged across the course of a given run (see Section 6.3), therefore the estimation of the standard orientation did not vary across trials. The model parameters of the 'template stage' were systematically varied, independently from the model parameter of the initial 'encoding stage'.

Orientation-identification

In the 'encoding stage', the model generated independent estimates of the standard orientation θ_{std} (either 0 or 45°) and the comparison orientation θ_{comp}. The comparison orientation was set to various levels of orientation difference (either clockwise or anticlockwise) from the standard orientation, as described for orientation-discrimination (see Section 3.4.1).

The neural population in the 'template stage' was independent from that of the 'encoding stage'. This population generated an estimate of the standard orientation, termed the 'template orientation' $\theta_{template}$. The model decided which of the two orientations decoded in the 'encoding stage' (θ_{std} and θ_{comp}) was closer to the template orientation:

$$D_{lvl} = \left|\theta_{std} - \theta_{template}\right| < \left|\theta_{comp} - \theta_{template}\right|$$

Equation 6.1

Where D_{lvl} is a binary array of the correct (1) and incorrect (0) responses for a given stimulus level θ_{lvl}. A psychometric function was constructed from the proportion of correct responses at each level of orientation difference. A logistic curve was fit to these data to calculate the identification threshold, defined as the orientation difference corresponding to 75% correct (see Section 2.6).

Fixed parameters

Unless otherwise specified, the 'default' parameter values for mechanisms in the 'encoding stage' and 'template stage' were set to those outlined in Table 6.1. The maximum likelihood (ML) or winner-take-all (WTA) versions of the model implemented the same decoder at the 'encoding stage' and at the 'template stage'. The population vector (PV) decoder

'Encoding stage'

Symbol	Cardinal Value	Oblique Value
N	90	90
σ_{ori}	25	50
λ_F	1	2
r_{max}	50	50

Table 6.1. Default model parameters for the 'encoding stage'. Other parameters were the same as those described in Section 3.5.

was demonstrated to be unable to account for the oblique effect for orientation-discrimination (see Chapter 4), therefore this decoder was omitted from the present work.

It was hypothesised that the large oblique effect for identification may result from a reduced number of mechanisms in the 'template stage', consistent with psychophysical findings that a limited number of mechanisms serve visual perception (see Section 5.3), despite dense populations of neurons being responsible for the initial encoding of visual features (see Section 1.2). Therefore, the number of mechanisms in the 'template stage' was varied between 4, 12, 20, 60, or 180, whereas this was fixed at 180 in the 'encoding stage'. To control for contrast-dependent changes in model performance (see Section 4.4), stimulus contrast was set to 40% in both the 'encoding stage' and the 'template stage'.

Anisotropic parameters

Model parameters were varied independently for cardinal-tuned and oblique-tuned mechanisms (see Section 3.6.1). Psychophysical investigations revealed no difference between the number of cardinal and oblique mechanisms underlying visual perception (see

Section 5.3), therefore the proportion of cardinal and oblique mechanisms was fixed at 0.5. Model simulations revealed that orientation bandwidths of cardinal mechanisms needed to be approximately half that of oblique mechanisms to generate the oblique effect for orientation-discrimination (see Sections 4.3 and 4.4), consistent with psychophysical bandwidth estimates for discrimination (see Section 5.3), therefore the 'default' cardinal bandwidth at the 'encoding stage' was set to 0.5 times the oblique bandwidth. For consistency with previous model simulations (see Sections 4.3 and 4.4), the 'default' Fano factor of oblique mechanisms was double that of cardinal mechanisms. Under these conditions, the OEI scores for discrimination (shown by dashed lines on each Figure) were approximately 1.3 and 2.2 for the maximum-likelihood and winner-take-all models, respectively.

Anisotropic tuning bandwidths

Model performance was assessed for various levels of anisotropic orientation bandwidths both the 'encoding stage' and 'template stage'. In the 'encoding stage', cardinal bandwidths were set as a fraction (0.5) of the oblique bandwidth. Independently, in the 'template stage', cardinal bandwidths were set as a fraction (1, 0.8, 0.6, 0.4, 0.2) of the oblique bandwidth (Figure 6.16).

For the maximum-likelihood and winner-take-all decoders, larger OEI scores for identification, relative to that for discrimination (shown by the dashed lines in Figure 6.16), were observed only when the extent of anisotropic orientation bandwidths in the 'template stage' was greater than in the 'encoding stage'. Conversely, OEI scores for identification were substantially lower than for discrimination when the anisotropy in the 'encoding stage' was greater than that in the 'template stage'. This interpretation was confirmed by additional simulations where, in the 'encoding stage', cardinal bandwidths were set to 0.25 times the oblique bandwidth (Figure 6.17). The following descriptions of results refer to the main

analysis, shown in Figure 6.16.

For the maximum likelihood decoder, the largest OEI scores occurred with 12 mechanisms in the 'template stage', and progressively smaller changes in OEI scores were found for larger numbers of mechanisms. OEI scores were greatly reduced with just 4 mechanisms. For 12 mechanisms with cardinal bandwidths set to either 0.4 or 0.2 times the oblique bandwidth in the 'template stage', the OEI scores for identification were 1.93 and 4.25, respectively.

For the winner-take-all decoder, OEI scores increased with an increasing number of mechanisms in the 'template stage', although the extent of these modulations were smaller than for the maximum-likelihood decoder. For 180 mechanisms with the cardinal bandwidths set to either 0.4 or 0.2 times the oblique bandwidth in the 'template stage', the OEI scores for identification were 2.72 and 3.10, respectively.

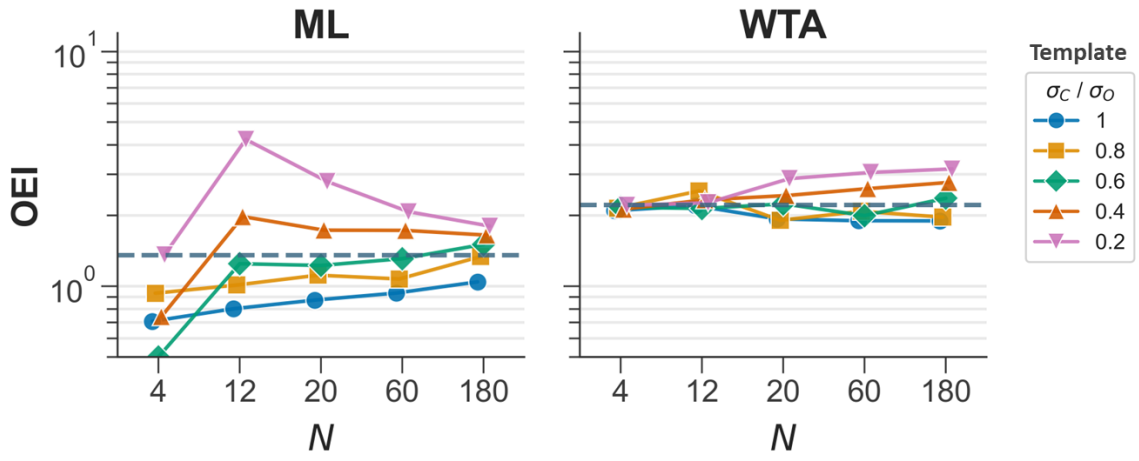

Figure 6.16. OEI scores for the maximum likelihood (ML) and winner-take-all (WTA) models. In the 'template stage', the number of mechanisms (*x-axis*) was varied, and the cardinal bandwidth was set as a fraction (*coloured lines*) of the oblique bandwidth. The OEI for discrimination is provided as a reference (*dashed line*).

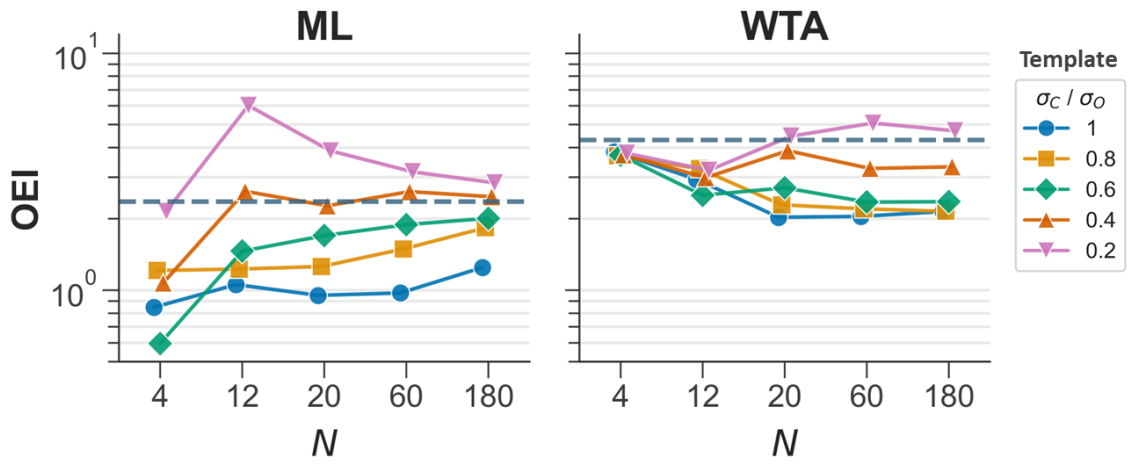

Figure 6.17. OEI scores for the maximum likelihood (ML) and winner-take-all (WTA) models. In the 'encoding stage', the cardinal bandwidth was 0.25 times the oblique bandwidth. All other model parameters were the same as in Figure 6.16. To generate a larger OEI score for identification, relative to discrimination (*dashed line*), the anisotropy in the 'template stage' was larger than in the 'encoding stage'

Thresholds

For the maximum-likelihood decoder, increasing the number of mechanisms in the 'template stage' generated smaller identification thresholds, and reduced the disparity between cardinal and oblique thresholds (Figure 6.18). In the presence of an extreme tuning anisotropy, such that cardinal bandwidths were 0.2 times the oblique bandwidth, cardinal performance was invariant with respect to the number of mechanisms. For the winner-take all model, oblique thresholds were mostly invariant to the total number of mechanisms in the 'template stage'. In the presence of anisotropic orientation bandwidths, cardinal thresholds decreased for larger numbers of mechanisms in the 'template stage'.

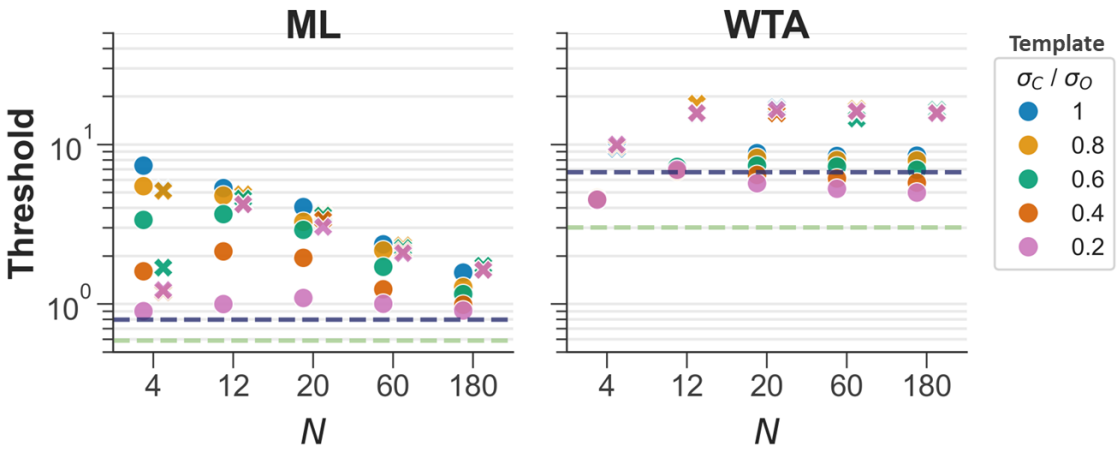

Figure 6.18. Identification thresholds for the maximum likelihood (ML) and winner-take-all (WTA) decoders. In the 'template stage', the number of mechanisms (*x-axis*) was varied, and the cardinal bandwidth was set as a fraction (*coloured lines*) of the oblique bandwidth. Discrimination thresholds are shown for the cardinal (*light dashed line*) and oblique (*dark dashed line*) stimulus orientation.

Anisotropic response variability

In the 'template stage', anisotropic levels of response variability were implemented by adjusting the Fano factor of oblique mechanisms, set as a multiple (either 1, 2, 4, 8, or 16) of the Fano factor of cardinal mechanisms, which was set to 1. To ensure that OEI scores for identification were larger than for discrimination, the cardinal bandwidth in the 'template stage' was set to 0.4 times the oblique bandwidth. For the maximum-likelihood model, with 12 or more mechanisms, extreme levels of anisotropic response variability (λo = 16) elicited only small increases in the OEI scores (Figure 6.19). For the winner-take-all model, with 60 or 180 mechanisms, lower levels of anisotropic response variability (λo = 2) caused a small increase in the OEI scores, whereas the oblique effect was almost abolished in the presence of extreme levels of anisotropic response variability (λo = 16).

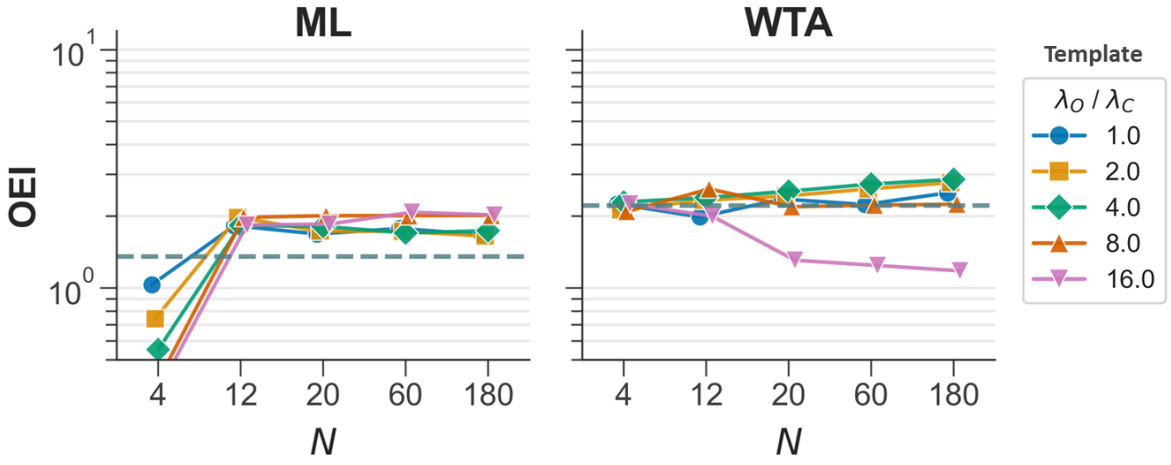

Figure 6.19. OEI scores for the maximum likelihood (ML) and winner-take-all (WTA) decoders. In the 'template stage', the number of mechanisms (*x-axis*) was varied, the oblique-Fano factor set as a multiple (*coloured lines*) of the cardinal-Fano factor, and the cardinal bandwidth was fixed at 0.4 times the oblique bandwidth. The OEI for discrimination is provided as a reference (*dashed line*).

Implementation of a prior

The prevalence of cardinal orientations in typical visual experience has been suggested to bias visual perception (Girshick et al., 2011), potentially by increasing the response gain of cardinal-tuned mechanisms (Bloem & Ling, 2017b). This was implemented in the 'template stage', by setting the cardinal-max firing rate as a multiple (either 1, 1.2, 1.4, 1.6, or 1.8) of the oblique-max firing rate (kept constant at 50 spikes/sec). To reiterate, anisotropic parameters changed gradually, according to a cosine distribution (see Section 3.6). Cardinal bandwidths in the 'template stage' were 0.4 times the oblique bandwidth in these initial simulations.

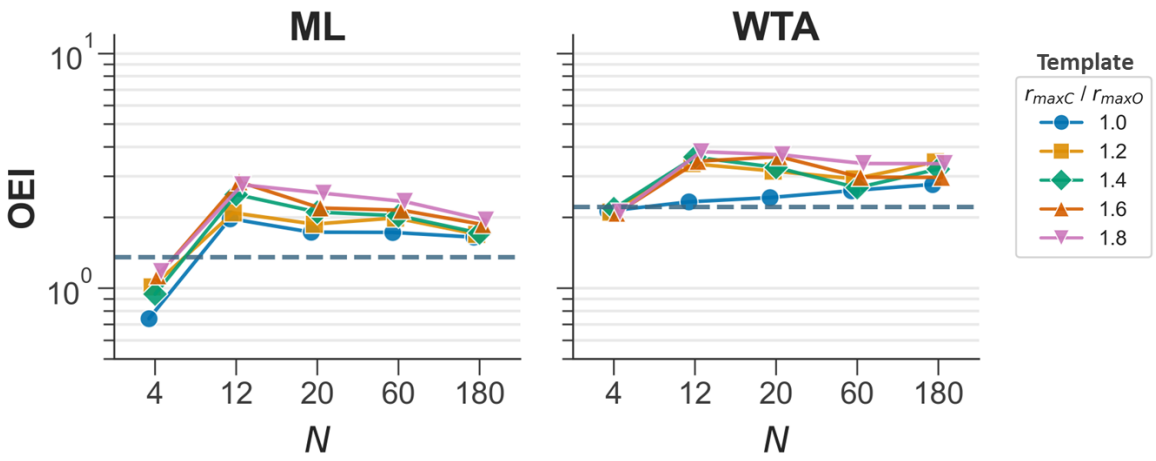

Figure 6.20. OEI scores for the maximum-likelihood (ML) and winner-take-all (WTA) decoders. In the 'template' stage, the number of mechanisms (*x-axis*) was varied, the cardinal-max firing rate was set as a multiple (*coloured lines*) of the oblique-max firing rate, and the cardinal bandwidth was fixed at 0.4 times the oblique bandwidth. The OEI for discrimination is provided as a reference (*dashed line*). A cardinal bias in response gain biases the estimate in the 'template stage' towards the cardinal orientations.

For the maximum-likelihood model, with between 12 and 60 mechanisms in the 'template stage', increasing the cardinal-max firing rate generated moderate increases in the OEI scores. For example, with the cardinal-max firing rate set to 1.4 times that for the obliques, the OEI score for identification was over double that for discrimination (shown by the dashed line in Figure 6.20). In contrast, this effect was greatly reduced with 180 mechanisms in the 'template stage'.

For the winner-take-all model, with 12 or 20 mechanisms in the 'template stage', small increases the cardinal responsivity generated large increases in OEI scores. With the cardinal-max firing rate set to 1.2 times the oblique max-firing rate , OEI scores were almost twice as high as compared to OEI scores for isotropic max firing rates. The impact of anisotropic max firing rates was greatly reduced with 60 or 180 mechanisms in the 'template stage', and absent with just four mechanisms.

Prior alone

Subsequent model simulations assessed whether anisotropic max firing rates could capture the larger oblique effect for identification, relative to that for discrimination, in the absence of anisotropic orientation bandwidths in the 'template stage'. In other words, cardinal bandwidths in the 'template stage' were equal to the oblique bandwidths, whilst the cardinal-max firing rate was set to a multiple of the oblique-max firing rate (Figure 6.21).

For the maximum-likelihood decoder, the absence of anisotropic orientation bandwidths in the 'template stage' elicited OEI scores for identification which were smaller than those for discrimination, even when the cardinal-max firing rate was 1.8 times the oblique-max firing rate. For the winner-take-all decoder, with 12 or more mechanisms in the 'template stage', a slight increase in the cardinal-response gain generated large increases in the OEI scores, similar to the results provided in Figure 6.20.

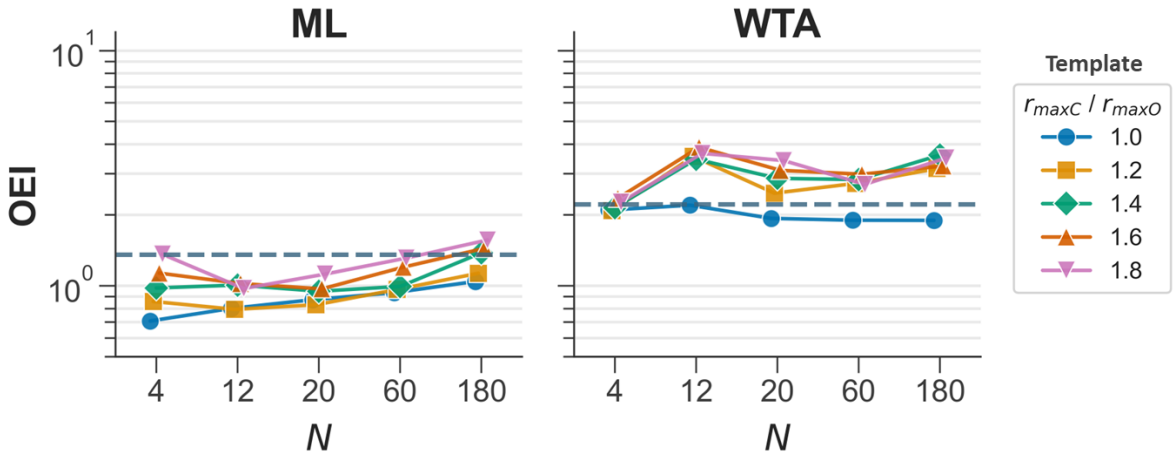

Figure 6.21. OEI scores for the maximum-likelihood (ML) and winner-take-all (WTA) decoders. All model parameters were the same as described in Figure 6.20, except in the 'template stage', the cardinal bandwidth was equal to the oblique bandwidth. The OEI for discrimination is provided as a reference (*dashed line*).

6.7 Summary of findings

Oblique effect for orientation identification

The aim of the present Chapter was to measure psychophysically the cognitive factors which have been suggested to contribute to the oblique effect (see Section 1.3.5). This was achieved by measuring performance on an orientation-identification task, for cardinal and oblique orientations. The identification task required observers to identify which of two stimuli were presented at the standard orientation, thus requiring the comparison of the perceived orientation against observers' prior knowledge of the standard orientation.

The oblique effect for orientation-identification was notably large, such that oblique thresholds were approximately 5 to 8 times larger than cardinal thresholds. This is consistent with a similarly large oblique effect which was reported for a single-interval orientation discrimination task, in which participants discriminated the visually encoded orientation against their internal representation of the standard orientation (Buchanan-Smith & Heeley, 1993). The oblique effect for orientation identification was far larger than has been reported for a variety of psychophysical tasks (for review, see Section 1.3), including contrast detection and orientation discrimination (see Chapter 4). For example, orientation-discrimination thresholds for the obliques are typically two to four times larger than for the cardinal orientations (see Sections 4.3, 4.4 and 6.5). The larger oblique effect for identification, relative to discrimination, was hypothesised to reflect an additional source of variance in a comparison stage, where the perceived orientation is compared against an internal representation of the remembered standard orientation (i.e., the 'template').

Modelling

Model simulations of orientation identification involved two independent stages. First, an initial 'encoding stage', where the stimulus orientation was encoded in a population of orientation-selective neurons. Second, the 'template stage' generated an estimate of the standard orientation from an independent population of orientation-selective neurons (considered to reflect the retrieval of orientation from memory). Consistent with initial predictions, the larger oblique effect for identification, relative to that for discrimination, could not be captured by anisotropies solely in the 'encoding stage', and instead required highly anisotropic mechanisms in the 'template stage' (see Section 6.6).

For the winner-take-all model, this required either extremely anisotropic tuning bandwidths, or the slightly increased response gain of cardinal mechanisms in the 'template stage'. For the maximum-likelihood model, this required extremely anisotropic bandwidths at both the 'encoding stage' and the 'template stage', alongside the increased responsivity of cardinal mechanisms in the 'template stage'. Increases in the response gain of cardinal mechanisms provides a solution for how prior knowledge may be integrated into the orientation-selective mechanisms serving identification judgements, such that estimates of the remembered standard orientation may be biased towards the cardinal axes. However, this contradicts findings that estimates of orientation are biased towards the oblique axes (see Section 1.3.5). Therefore, further investigation is required to test this prediction. Additionally, the present work could not distinguish between winner-take-all and maximum-likelihood models, therefore future work should aim to separate these decoding methods, possibly through measuring discrimination and identification performance on each task whilst varying low-level stimulus parameters, such as stimulus contrast (e.g., Section 4.4).

Divided attention

When tested under strictly controlled, laboratory conditions, the oblique effect for orientation identification was markedly larger for the spatial task than for the temporal task. This is consistent with reports that the oblique effect for visual tasks with a cognitive component increases when spatial attention is divided between two or more spatial locations (Balikou et al., 2015; Kelly & Matthews, 2011). For example, oblique biases in orientation-reproduction tasks (errors are biased towards the oblique axes), where participants manually reproduce a remembered orientation, are amplified when attention is divided between multiple visual orientations (Balikou et al., 2015). Despite clear differences at the group-level (i.e., the average oblique effect size), there were marked individual differences in the extent of the difference between the spatial task and the temporal and 'mixed' tasks. This is consistent with reports of larger individual differences in visual performance when visual attention is manipulated, relative to when is not. For example, contrast-detection thresholds are far more variable when attention is directed to a task-irrelevant orientation, than in the absence of attentional instructions (Bridwell et al., 2013).

Further research could expand on the present work, by examining performance under various levels of divided attention, for both the identification and discrimination tasks. For example, the oblique effect could be measured whilst adjusting the number of alternatives, on spatial 2AFC, 4AFC, and 6AFC tasks. Additionally, the impact of divided attention on performance could be modelled, for example, by decreasing the response gain of orientation-selective mechanisms in higher visual areas (for review, see Maunsell, 2015).

Visual short-term memory

There was little evidence for anisotropic mechanisms of short-term memory, such that

the oblique effect for orientation-discrimination was not larger for tasks where stimuli were presented successively over a temporal delay (i.e., the temporal and 'mixed' tasks), relative to the spatial task where stimuli were presented simultaneously. This contradicts previous findings (Heeley & Buchanan-Smith, 1992; Westheimer, 2003a), however these investigations used closely spaced stimulus configurations in their spatial 2AFC tasks, which may have been impacted by spatial interactions between visually encoded orientations (see Section 1.3.5). In contrast, the large spatial separation between the two stimuli in the present study (8° between the truncated edges of stimuli) make it unlikely for local orientation interactions, such as tilt-effects, which operate over very restricted spatial ranges (Schwartz et al., 2007), to have impacted measurements of the oblique effect. The oblique effect for discrimination was similar in magnitude across the temporal, spatial, and 'mixed' tasks, indicating that orientation discrimination may be less dependent on higher-level, cognitive mechanisms.

Oblique representations

On average, the magnitude of the oblique effect for identification was greatly reduced when runs on the identification task were interleaved with runs on the discrimination task (see Section 6.5), compared to experiments where only orientation-identification runs were performed (see Sections 6.2 to 6.4). Interleaving of runs on the identification and discrimination tasks may have refined observers' internal representations of the obliques, through repeated exposure to near-oblique orientations on the discrimination task (where comparison orientations were much closer to the standard orientation than on the identification task). This is consistent with the findings of perceptual learning studies which report greater learning effects for obliques than for cardinals (Jehee et al., 2012; Mayer, 1983; Vogels & Orban, 1985). However, only three participants performed both of the testing

protocols (i.e., interleaved identification and discrimination runs, and isolated identification run), therefore further investigation is required to explore the generality of this finding.

Individual differences

High levels of inter-individual variation were found in the size of the oblique effect for orientation-identification, with oblique effect index (OEI) scores ranging from approximately 3.5 to 10.5, compared with OEI scores for discrimination ranging from approximately 2.5 to 5.5. To investigate whether the oblique effect is a ubiquitous feature of the human visual system, and to gain further insight into the mechanisms of orientation-identification, individual differences should be examined in larger samples of participants.

7. Individual differences in the oblique effect

Authors note

To accommodate for the impacts of the pandemic, individual differences in the oblique effect were investigated using a web-based experiment (see Covid Impact Statement).

7.1 Introduction

Overview

An overwhelming body of evidence suggests that the oblique effect is a ubiquitous feature of the human visual system (see Section 1.3), although there is little research which has directly investigated this claim. Individual differences in the precision of orientation encoding have been noted previously (Dickinson et al., 2014; Edden et al., 2009; Vogels et al., 1984; see Section 1.6). For example, orientation-discrimination thresholds for an oblique standard orientation were shown to negatively correlate with the level of self-reported autistic traits in a sample of 94 participants, whereas this relationship was not found for cardinal discrimination thresholds (Dickinson et al., 2014). This indicates that the size of the oblique effect could be driven primarily by individual differences in oblique performance (e.g., Edden et al., 2009). However, further investigation is required to examine individual differences in the oblique effect for other demographics of participants.

Neuronal basis

There does not appear to be some 'general factor' which can predict individual differences in performance across various visual tasks (de-Wit & Wagemans, 2014; Mollon et al., 2017; Peterzell & Kennedy, 2016) Rather, individual differences reflect variability in the response characteristics of the mechanisms underlying specific visual functions (see Section

1.6). For example, higher resting levels of GABA in early visual cortex are associated with lowered orientation-discrimination thresholds, and a greatly reduced oblique effect (Edden et al., 2009). However, the notably large oblique effect for orientation-identification, relative to that for orientation-discrimination (see Section 6.5), could not be captured by anisotropies in the stimulus-driven, encoding mechanisms of a biologically inspired, population-coding model (see Section 6.6). Individual differences in orientation identification may instead reflect the joint contribution of low-level and cognitive mechanisms, which may be reflected in increased variability when attention is divided between two spatial locations (see Section 1.3.5).

Temporal versus spatial tasks

The work in Chapter 6 revealed that the oblique effect for orientation-identification, when measured under strictly controlled laboratory conditions, was significantly larger on a spatial 2AFC task (high attentional load) than on a temporal 2AFC task (low attentional load), suggesting that the oblique effect for identification may indeed be modulated by spatial attention (see Section 6.5). However, this difference did not reach statistical significance for participants who performed a web-based version of the same orientation-identification task (see Section 6.3). This was hypothesised to reflect an insensitivity of web-based testing to such an attentional effect. Therefore, the present experiment tested the generality of this hypothesis in a much larger sample of participants.

Reliability

To assess the reliability of findings, two large independent groups of participants performed the same orientation-identification experiment, one year apart. Substantial oblique effects for orientation identification were expected to be recorded in all tested participants,

across both groups, consistent with a large body of research which reports that task-based effects (typically cognitive tasks, e.g., Stroop) can be replicated using web-based methods (Crump et al., 2013; Sauter et al., 2020). Previous work has demonstrated that orientation-identification thresholds of individual observers are generally consistent across testing sessions (Leadbeater et al., 2023; see Section 6.3), however it is unclear whether group-level estimates of identification thresholds, oblique effect magnitude, and inter-individual variability, would vary substantially between two independent samples of participants. Comparing performance between two groups on an identical task eliminated any variation that could be attributed to methodological differences. For example, estimates of contrast sensitivity can vary dramatically between samples (D. H. Baker, 2013). For the web-based testing protocol to be considered as a useful tool to guide future research, then results should be consistent between independent groups of participants.

7.2 Methods

Participants

A total of 182 participants were recruited to take part in the orientation-identification experiment, all of whom were second-year undergraduate students in a 'Practical Methods' lab class, with a mean (SD) age of 20.1 (1.38) years. Participants comprised two independent cohorts of 90 and 92 participants who were tested on the same web-based task, one year apart. A total of 49 participants were excluded from formal data analyses as they completed fewer than four runs of trials on at least one tested condition, and one additional participant was excluded as they failed to reach threshold performance levels of responding (i.e., at least 75% correct) in one or more conditions. Of the 132 remaining participants, 63 were in the first group and 69 were in the second group. Participants were not screened for ocular

pathology or visual dysfunction but were instructed to wear appropriate refractive correction, if required. Ethical guidelines were followed as described in Section 2.1.

Apparatus

The apparatus used and the implementation of experimental controls were the same as described for the web-based experiment in Section 6.3.

Stimuli

Visual stimuli were the same as those described in Section 6.3. Stimuli were Gabor patterns (Section 2.4), composed of orientated 2c/° sinusoidal luminance gratings presented within a spatial Gaussian window with a space-constant σ^2 of 1.33°, truncated at ±4°. The stimulus contrast was set to be 40% of the maximum available from the visual display.

Design

The experimental conditions of the orientation-identification experiment were the same as those described in Section 6.3.

Procedure

Procedural details of the orientation-identification experiment were the same as those described in Section 6.3.

Data analysis

The proportion of correct responses for each level of orientation-offset was used to construct a psychometric function for each participant on each tested condition. A logistic curve was fit to the data to obtain the threshold (see Section 2.6), taken as the orientation-offset on the curve producing 75% correct responses. The oblique effect index (OEI, see

Section 2.8) quantified the magnitude of the oblique effect. To assess group-level effects, the geometric mean OEI score was calculated across participants. The variation in OEI scores was quantified by the interquartile range (IQR).

Bland-Altman analyses (see Section 2.9) assessed the agreement between measurements on the temporal and spatial tasks. Due to a proportional relationship between the variance and magnitude of difference scores for identification thresholds, Bland-Altman analyses were performed on log-transformed thresholds (Bland & Altman, 1999), and difference scores are reported on a ratio scale (see Section 2.9). No such relationship was found between the variance and magnitude of differences between OEI scores, hence these difference scores were reported in their original units.

The differences between OEI scores on the temporal and spatial tasks significantly deviated from a normal distribution, as demonstrated by Shapiro-Wilk tests, and were found to be significantly skewed. Therefore, a permutation test was conducted to investigate whether OEI scores on the temporal and spatial tasks were significantly different. A total of 1000 permutations were performed, shuffling the differences between paired observations.

7.3 Results

7.3.1 Within-groups

For the temporal and spatial versions of the orientation-identification task, identification thresholds were found to be substantially lower for the horizontal (0°) and vertical (90°) orientations than for the left (-45°) and right (45°) oblique orientations (Figure 7.1).

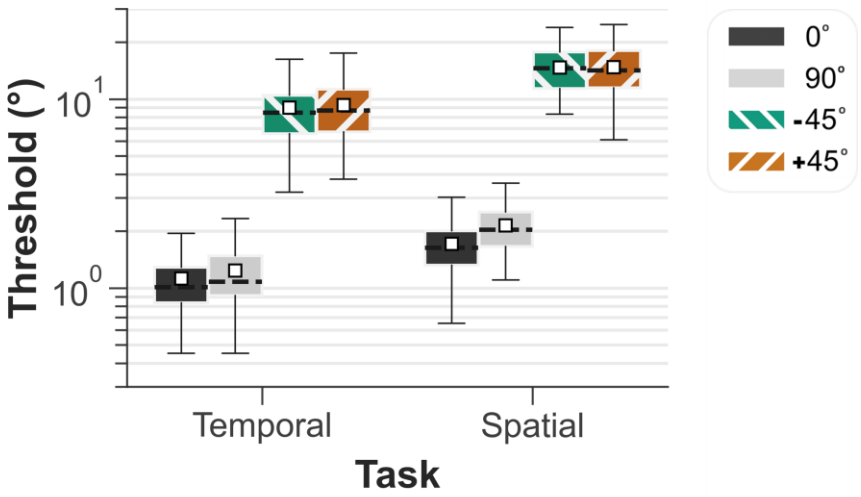

Figure 7.1. Boxplot showing the means (*white squares*), medians (*dotted line*), and interquartile ranges (*boxes*) of thresholds for all participants who completed the orientation-identification experiment (n = 132). Error bars represent the range.

4681

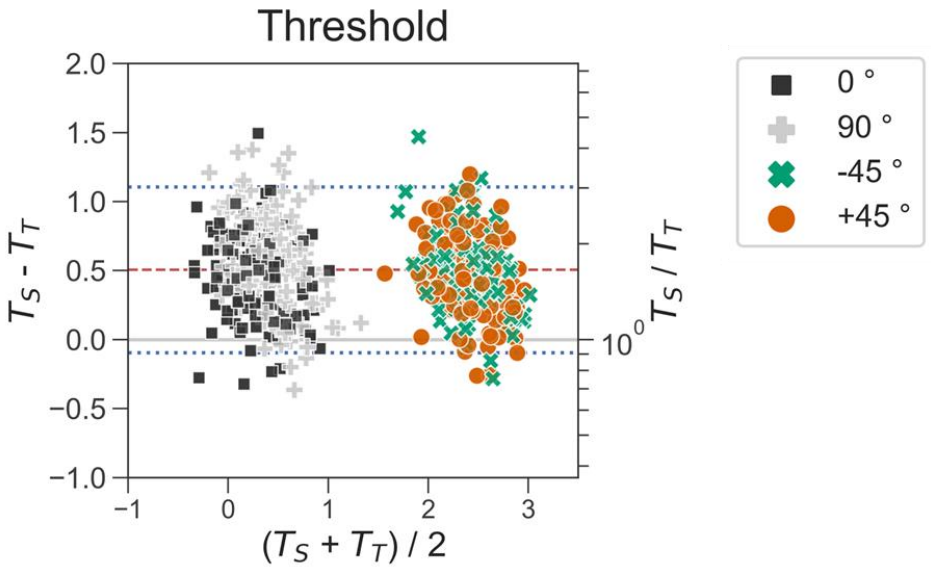

Figure 7.2. Bland-Altman plots on log-transformed identification thresholds. The differences between spatial and temporal log-thresholds are plotted against the mean log-threshold. The mean difference (*red dashed line*), line of equality (*grey solid line*) are shown. Limits of agreement (*blue dotted lines*) reflect the mean difference ± 1SD * 1.96. The ratio scale (*right y-axis*) allows visualisation of the magnitude of the difference between spatial and temporal thresholds.

Bland-Altman analysis was performed to assess the agreement between thresholds on the temporal and spatial tasks (Figure 7.2). A mean-difference ratio score (IQR) of 1.66 (0.63) demonstrated that thresholds on the spatial task were systematically higher than thresholds on the temporal task, although the extent of this difference varied across individual observers for each orientation condition. Indeed, many individuals showed similar levels of performance on the temporal and spatial tasks.

A large oblique effect was measured in every one of the 132 participants who completed the orientation-identification experiment, although the extent of this varied greatly across participants, with OEI scores ranging from 2.52 to 18.8 across both of the temporal and spatial tasks (Figure 7.3). Permutation tests revealed that there was no significant difference between the OEI scores on the temporal and spatial tasks ($p = 0.93$). The geometric-mean OEI (SE) scores for the temporal and spatial tasks were 7.78 (0.20) and 7.67 (0.18), respectively. This was consistent with previous estimates using a web-based testing

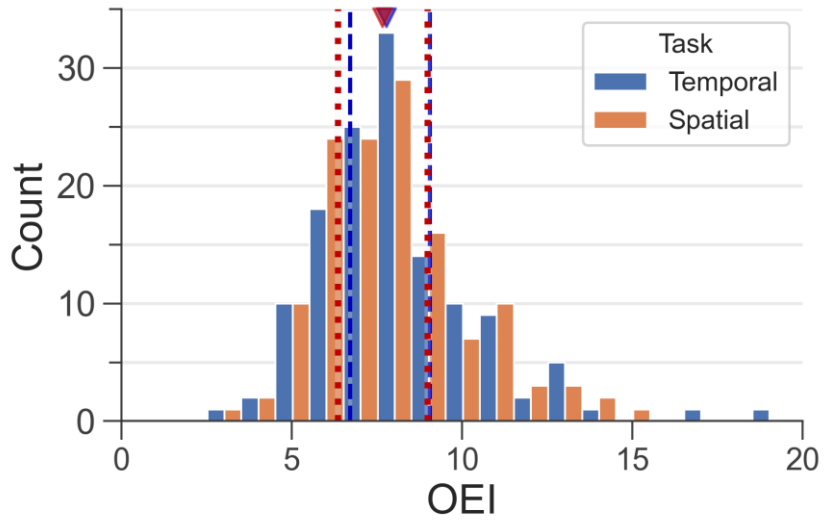

Figure 7.3. Histogram of oblique effect index (OEI) scores for all participants (n = 132). The geometric mean OEI scores are given for the temporal (*blue triangle*) and spatial tasks (*red triangle*). The bounds of the interquartile range are also given for the temporal (*blue dashed line*) and spatial tasks (*red dotted line*).

protocol (see Section 6.3). The interquartile range (IQR) of OEI scores on the temporal (2.34) and spatial tasks (2.63) indicated the presence of moderate inter-individual differences in the size of the oblique effect for orientation-identification.

Despite little difference between the mean OEI scores, Bland-Altman analysis revealed low levels of absolute agreement between the OEI scores on the temporal and spatial tasks (Figure 7.4), with the limits of agreement ranging from -4.04 to 5.64. However, a median absolute-difference score (IQR) of just 1.27 (1.72) indicated moderate levels of agreement in many participants.

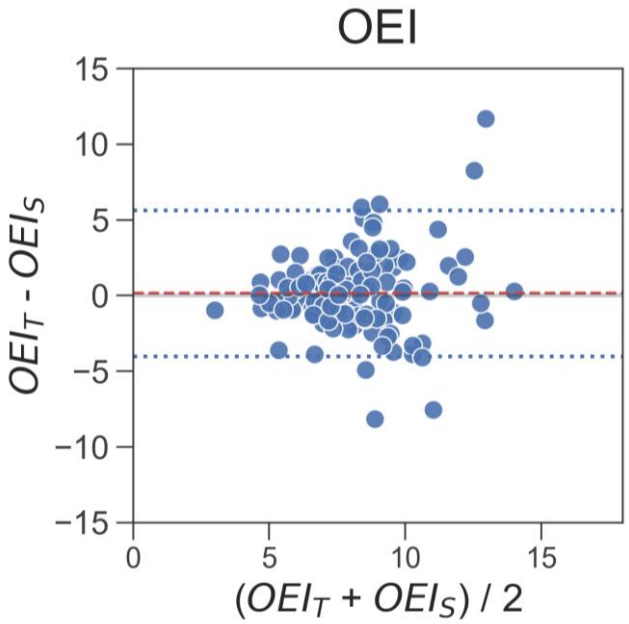

Figure 7.4. Bland–Altman plots of the 'oblique effect index' (OEI) scores. Differences between OEI scores on the spatial and temporal tasks are plotted against the mean. The mean difference (*red dashed line*) and line of equality (*grey solid line*) are shown. Limits of agreement (*blue dotted lines*) reflect the percentile range between 2.5 and 97.5%.

7.3.2 Between-groups comparisons

Group-level estimates of the arithmetic-mean orientation-identification thresholds were highly consistent between groups 1 and 2, for each tested orientation (Figure 7.5).

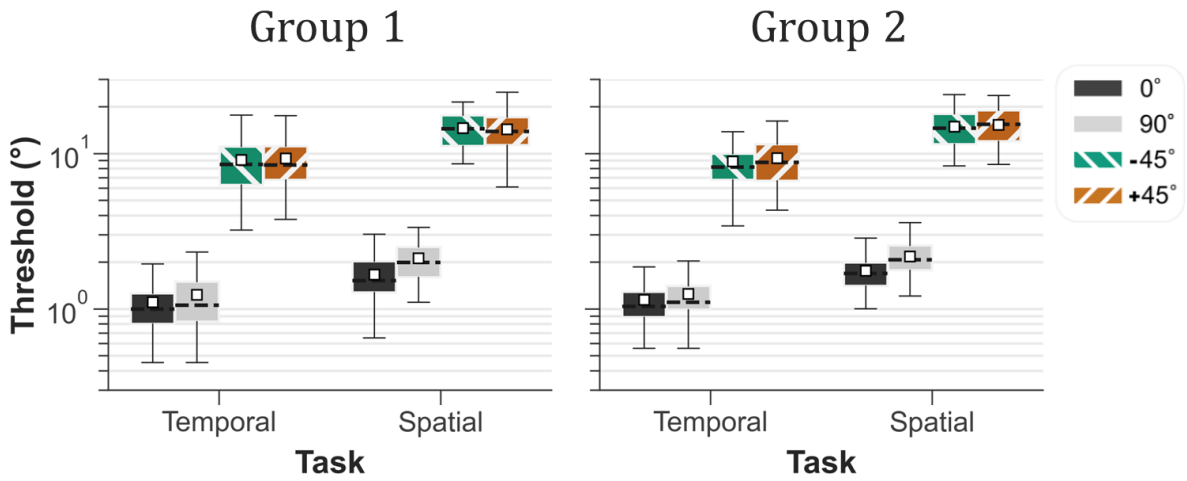

Figure 7.5. Boxplot showing the means (*white squares*), medians (*dotted line*), and interquartile ranges (*boxes*) of thresholds for each group of participants. Error bars represent the range. Estimates of the mean threshold were highly consistent between the two groups, for all tested orientations.

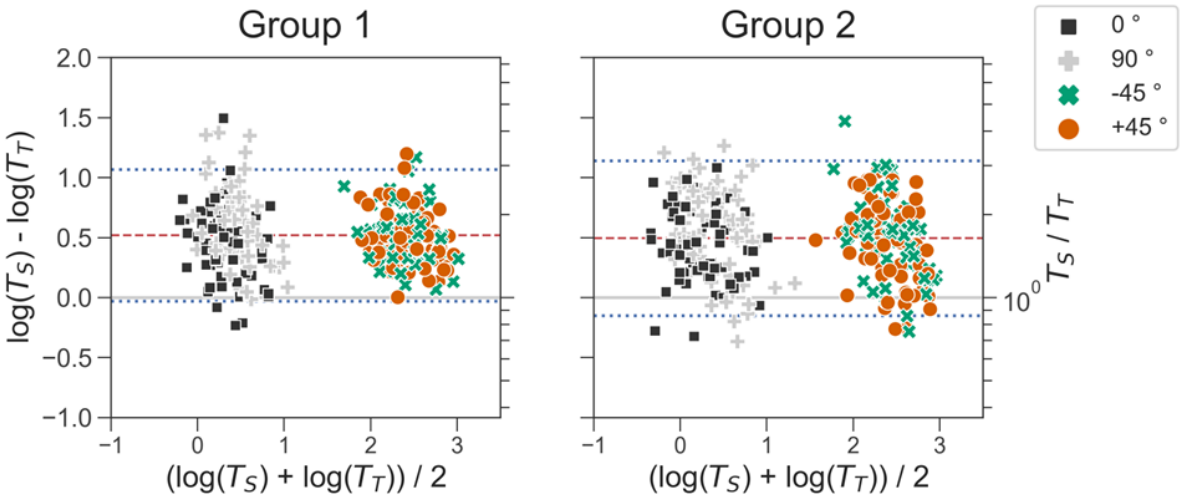

Figure 7.6. Bland-Altman plots of the log-transformed thresholds in group 1 (*left*) and group 2 (*right*). Figure details are the same as those described in Figure 7.2. Similar levels of individual agreement were shown in each group, however there was greater variability in the size of thresholds (*x-axis*) in group 2.

Orientation-identification thresholds were systematically larger on the spatial task than on the temporal task, with mean-difference ratio scores (IQR) of 1.68 (0.55) and 1.64 (0.71) in groups 1 and 2, respectively (Figure 7.6). There were also similar levels of inter-individual variation for groups 1 and 2.

The geometric-mean OEI scores were highly consistent between group 1 and group 2, for both the temporal and spatial versions of the task (Figure 7.7). However, the extent of individual differences in OEI scores varied substantially between groups, such that the

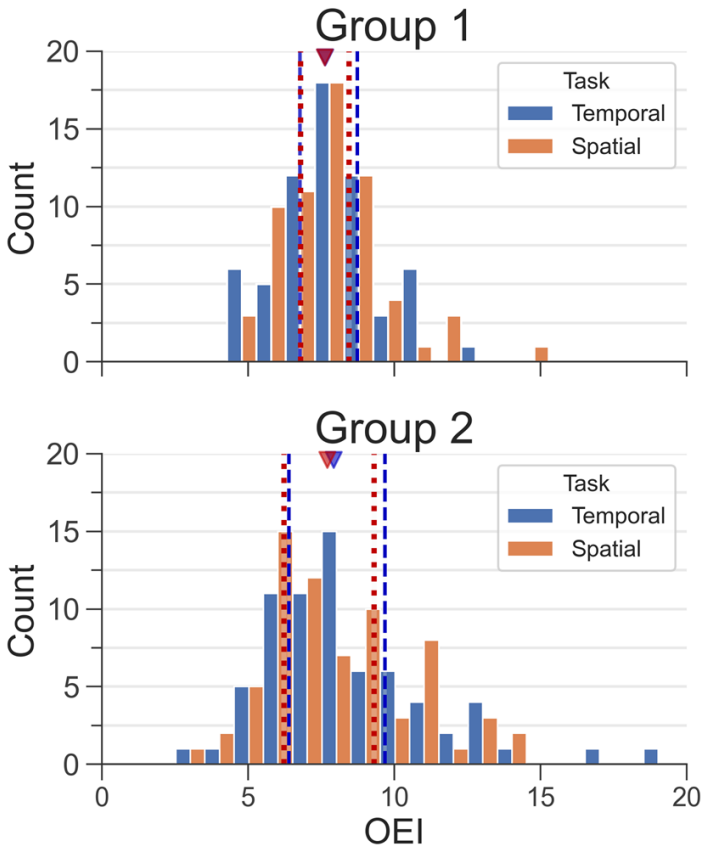

Figure 7.7. Histograms of 'oblique effect index' (OEI) scores for participants in group 1 (*top*) and group 2 (*bottom*). The geometric mean OEI scores are given for the temporal (*blue triangle*) and spatial tasks (*red triangle*). The bounds of the interquartile range (IQR) are also given for the temporal (*blue dashed line*) and spatial tasks (*red dotted line*). OEI scores were more variable in group 2 than group 1, despite similar geometric mean-OEI scores.

4714 interquartile ranges (IQR) of OEI scores on the temporal and spatial tasks were substantially
4715 smaller in group 1 (1.97 and 1.65) than in group 2 (3.28 and 3.01).

4716 Finally, the level of agreement for OEI scores measured on the temporal and spatial
4717 tasks was generally higher for group 1 than group 2 (Figure 7.8), with median absolute-
4718 difference scores (IQR) of 0.98 (1.70) and 1.41 (1.82), respectively. This indicates the
4719 presence of considerable measurement noise in the data of the second group.

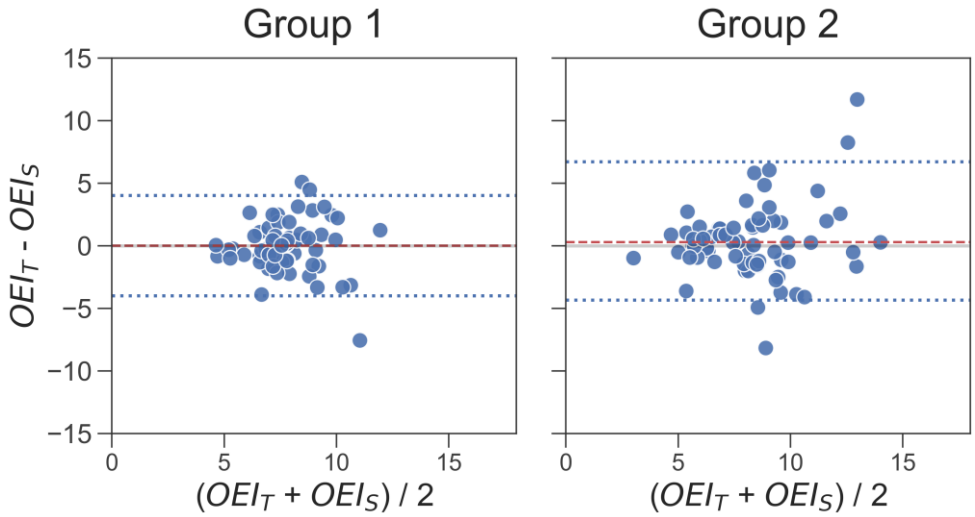

Figure 7.8. Bland–Altman plots of the 'oblique effect index' (OEI) scores for each participant in group 1 (left) and group 2 (right). Figure details are the same as those described in Figure 7.4. Despite similar mean OEI scores, limits of agreement were far greater in group 2 than in group 1, indicating substantial levels of measurement noise for this group.

7.4 Discussion

Individual differences in the oblique effect

The size of the oblique effect for orientation-identification varied between individual participants, such that the majority of 'oblique effect index' (OEI, see Section 2.8) scores ranged from approximately 6.5 to 9.0, across both temporal and spatial tasks. The size of these estimates is consistent with those reported previously for web-based and lab-based versions of the orientation-identification experiment (see Sections 6.2 to 6.4). Furthermore, every one of the 132 participants who completed the present experiment displayed an oblique effect, demonstrating that anisotropic orientation perception may be a ubiquitous feature of the human visual system.

Future work could compare individual differences in orientation-identification performance with estimates of individual differences for tasks which are predominantly reliant on low-level mechanisms (e.g., contrast detection and orientation discrimination). If orientation-identification performance is considerably more variable across individuals than for low-level tasks, such as orientation-discrimination, this could suggest an additional source of variance. For example, contrast-detection thresholds are far more variable when participants are instructed to attend to an orientation-offset from the standard orientation, than in the absence of attentional instructions (Bridwell et al., 2013). Additionally, the presence of an independent source of variance should also be reflected in the correlations of individual differences across difference tasks (for review, see Hammond & Buch, 2020; Mollon et al., 2017) Such work would benefit from using the same participants in all tested conditions.

Temporal versus spatial

The oblique effect was found not to be significantly larger on the spatial task than on

the temporal task, consistent with another experiment which also used remote, web-based methods to assess orientation-identification performance (see Section 6.3). However, under laboratory conditions with strict experimental controls, the oblique effect for orientation-identification was previously found to be significantly larger on the spatial task. It seems that web-based methods, with their inherent lack of precise control over viewing parameters and the testing environment (e.g., prone to visual distractions), may be ill-suited to capture this difference, especially if this is considered to reflect the attentional modulation of task performance. Indeed, after the systematic bias was accounted for, the poor agreement between the OEI scores of individual observers between the temporal and spatial tasks indicates the presence of substantial measurement noise in the web-based testing protocol. Future investigations of the oblique effect should therefore use lab-based methods, with strict experimental controls, to ensure that smaller effects of interest and individual differences can be reliably measured.

Between-groups reliability

Group-level measurements were highly consistent between the two independent groups of participants, including the means and interquartile ranges of orientation-identification thresholds, and the geometric-mean OEI score. This shows that testing two independent, but demographically very similar groups of participants (that is, both groups were predominantly female, well-educated adults in their early twenties), yields excellent reliability of group-level findings, despite considerable inter-individual variability. This validates and establishes the reliability of the web-based testing protocol for these purposes. Future research should explore whether similar levels of consistency are observed for a more diverse range of participants, including groups of participants who may interact with technology in a different manner to the present cohort of mostly young, healthy participants,

such as older participants or clinical groups. However, web-based methods may only be suitable to capture such group-level differences on the condition that sufficiently large sample sizes are recruited in order to offset the impacts of measurement noise, and the high percentage of participants who were excluded from further data analysis (~ 26%), due to not performing the instructed number of runs.

The extent of inter-individual variability in the size of the oblique effect was not consistent between the two groups of participants, in that the interquartile ranges of individual OEI scores were vastly greater in the second group than in the first group, for both the temporal and spatial tasks. Additionally, the agreement between OEI scores on the temporal and spatial tasks was far weaker in the second group, suggesting the presence of substantial measurement noise for the web-based testing protocol. These findings suggest that future investigations of individual differences in the oblique effect should measure visual performance under strictly controlled laboratory conditions, from sufficiently larger numbers of participants to offset the impacts of measurement noise.

8. General Discussion

8.1 Summary of main findings

The oblique effect, where task performance is improved for cardinal orientations relative to the obliques, was found to be a ubiquitous feature of the human visual system (see Chapter 7). The classical explanation of the oblique effect is that of an overrepresentation of cardinal-tuned neurons relative to oblique-tuned neurons (see Sections 1.3 to 1.5), however this account has not been examined systematically despite decades of research into the neural basis of the oblique effect (see Sections 1.3 to 1.5). Through a combination of psychophysical testing and computational modelling techniques, this thesis provides a thorough account of the neural mechanisms underlying the oblique effect in the human visual system. In this Section, the key findings of this thesis will be summarised, followed by a discussion of potential avenues for future research.

8.1.1 The oblique effect for contrast-detection

Consistent with the classical explanation of the oblique effect, the modelling of psychophysical data in Section 4.2 demonstrated that the oblique effect for contrast detection could indeed be generated by an overrepresentation of cardinal-tuned neurons. It had previously been unclear as to why the oblique effect for contrast-detection emerged only at relatively high spatial frequencies (see Sections 1.3 to 1.5), with initial suggestions of an overrepresentation of cardinal-tuned neurons that is restricted to neurons tuned to these spatial frequencies (B. Li et al., 2003). However, these findings are in conflict with the strong cardinal bias in neural activity which is observed at relatively low spatial frequencies (Roth et al., 2022; Sun et al., 2013).

The modelling work in Section 4.2 led to the novel explanation that the oblique effect for contrast-detection emerges only at relatively high spatial frequencies, due to the uniformly narrowed orientation bandwidths of neurons tuned to these spatial frequencies (Y. Chen et al., 2020; B. Li et al., 2003; G. Shen et al., 2014; Webster & De Valois, 1985). At high spatial frequencies, uniformly narrowed orientation bandwidths reduce the extent of neural recruitment for a given stimulus orientation, such that an overrepresentation of cardinal-tuned neurons effectively increases the signal-to-noise ratio (SNR) for cardinal orientations relative to oblique orientations. At lower spatial frequencies, this difference in the signal-to-noise ratio is diminished by the broadened orientation bandwidths of visual neurons, thus abolishing the oblique effect for contrast-detection. Psychophysical estimates of the orientation bandwidths of detection mechanisms, for stimuli with broadband spatial frequency information, were highly consistent with the model's predictions that bandwidths of approximately 70° (full-width half-max) were required to abolish the oblique effect for contrast-detection (see Sections 4.2 and 5.3).

8.1.2 The oblique effect for orientation-discrimination

Consistent with previous findings, the oblique effect for orientation-discrimination was substantially larger than that for contrast-detection. In contrast with the classical explanation of the oblique effect, the psychophysical and modelling work in Sections 4.3 and 4.4 demonstrated that a greater proportion of cardinal-tuned neurons was insufficient to account for the oblique effect for orientation-discrimination. This was consistent with the results of the metamerism experiment, of an equal number of cardinal-tuned and oblique-tuned mechanisms underlying orientation perception (see Section 5.2). Instead, the oblique effect for orientation-discrimination could only be captured by a model that included

anisotropic orientation bandwidths, such that the bandwidth of cardinal-tuned mechanisms was approximately half that of oblique-tuned mechanisms. The scale of this anisotropy was consistent with psychophysical estimates of the tuning bandwidths of discrimination mechanisms (see Section 5.3), and with previous modelling work which captured the behavioural oblique effect for motion direction-discrimination (Rokem & Silver, 2009).

It has previously been suggested that a deficit in the encoding of oblique orientations in visual short-term memory (Westheimer, 2003a) contributes to the oblique effect (see Section 1.3.5). The findings of Section 6.5 challenge this notion because the oblique effect for orientation-discrimination was not increased by the presence of a temporal delay between the standard and comparison stimuli (see Section 6.5). This apparent conflict with previous findings is likely to be due, at least in part, to differences in the stimulus configurations used when simultaneously presenting visual stimuli, as discussed in Section 1.3.5. The inclusion of a novel 'mixed' task in the current work, where stimuli were presented with a temporal delay in alternating spatial locations, controlled for any potential confounds due to eccentricity-dependent variations in discrimination performance across the visual field.

8.1.3 The oblique effect for orientation-identification

The orientation-identification task required participants to compare the perceived orientation against their prior knowledge of the standard orientation. The oblique effect for identification was found to be substantially larger than that for orientation-discrimination, such that identification thresholds were approximately five to eight times higher for oblique orientations than for cardinals (see Sections 6.4 and 6.5, and Chapter 7). The oblique effect for identification, but not discrimination, was increased when attention was divided between two spatial locations (see Sections 6.2 to 6.5). This suggests that the high-level, cognitive

demands of identification tasks are greater than those for discrimination tasks (Balikou et al., 2015; Essock, 1980; Heeley et al., 1997; Westheimer, 2003a).

The modelling work in Section 6.6 outlined a novel computational framework to account for the oblique effect for orientation identification. On each trial, the decision stage in the model compared the contents of the memory of the standard orientation with each encoded stimulus, in turn, to quantify its degree of similarity to the standard orientation. The larger oblique effect for identification relative to discrimination was captured only by anisotropies in the response characteristics (e.g., bandwidth, maximum firing rate) of the 'template stage', which generated the memory representation of the standard orientation. This is consistent with the notion that cognitive factors contribute to the oblique effect for orientation identification.

The size of the oblique effect for orientation identification was greatly reduced when runs were interleaved with an orientation-discrimination experiment, where comparison orientations are much closer to the standard orientation than on the identification task (see Section 6.5), compared to when identification runs were performed in isolation (see Sections 6.2 to 6.4, and Chapter 7). However, the size of the oblique effect for identification was generally unchanged across successive runs (see Section 6.5), indicating that visual experience may induce the near-instantaneous recalibration of the cognitive mechanisms responsible for generating the 'template' orientation.

8.1.4 Distinct mechanisms for detection and discrimination

The modelling work in Chapter 4 revealed that anisotropic orientation-tuning bandwidths were necessary to capture the oblique effect for orientation discrimination (see Sections 4.3 and 4.4), however such an anisotropy abolished the oblique effect for contrast

detection (see Section 4.2). Therefore, a single unified model could not account for the oblique effects found for both contrast detection and orientation discrimination, suggesting that these tasks may be served by functionally independent mechanisms. Model predictions were supported by the psychophysical work in Section 5.3, such that the orientation-bandwidth estimates of detection mechanisms were isotropic, whereas those of discrimination mechanisms were substantially narrower for the cardinal orientations than for the obliques. Most previous reports of psychophysically estimated orientation bandwidths have used contrast-detection tasks to provide insight into the mechanisms of perception (see Section 1.3.4). Crucially, the present findings challenge the generality of this approach and thus constrain the interpretation of such findings to detection mechanisms only.

8.1.5 The number of perceptual mechanisms

The 'metamers' procedure described in Section 5.2.2 quantifies the minimum number of orientation-selective mechanisms underlying perception, defined as the number of discrete inputs that is required to generate a percept that is indistinguishable from a broadband stimulus, multiplied by two, less 1 (Richards, 1979). It is often assumed that the orientation-selective mechanisms underlying perception are uniformly distributed across orientation-space (Ellemberg et al., 2006; Williams et al., 1991), however the minimum number of mechanisms did not increase proportionally with the range of orientations in the metamers task. For example, despite a four-fold increase in the orientation-range of the line elements in the display, from 15 to 60°, the estimated minimum number of mechanisms only increased from 7 to 11. Similar findings for orientation ranges centred on the cardinal and oblique axes indicates that the preferred orientations of perceptual mechanisms may not be uniformly spaced, and that the number of mechanisms is driven by the stimulus-input.

8.1.6 The computation of detection

Model simulations for contrast detection found that the 'summation' pooling method, where detection is determined by the pooled firing rates of the entire neural population, captured the size of the behavioural oblique effect in the presence of a biologically-plausible overrepresentation of cardinal-tuned neurons (see Sections 1.4 to 1.5). In contrast, the 'magnitude-weighted' and 'peak' pooling methods required much larger anisotropies to account for the behavioural oblique effect, such that 80 to 90% of the model's neurons needed to be tuned to the cardinal orientations. The 'distance-weighted' pooling method generated an oblique effect that was invariant with respect to spatial frequency, which strongly contradicts suggestions that firing rates may be pooled across a limited range of orientations (Andrei et al., 2019).

8.1.7 The computation of orientation perception

Model performance was assessed for various decoding algorithms (see Section 3.2), which generated the estimate of the stimulus orientation from the model firing rates. The winner-take-all (WTA) read-out algorithm was shown to best-capture the oblique effect for orientation discrimination, in that the measured oblique effect was invariant with respect to spatial frequency (see Section 4.3) and increased with stimulus contrast (see Section 4.4). Thresholds for this decoder were far higher than those estimated psychophysically, but the robustness of this decoder to variability in the response characteristics of model neurons could be beneficial considering the numerous noise sources of sensory encoding (Faisal et al., 2008). In contrast, the population-vector (PV) decoder was highly susceptible to variations in the response characteristics of model neurons and did not capture the behavioural data well.

To capture the size of the oblique effect for orientation discrimination, the maximum-

likelihood (ML) model required an extreme tuning anisotropy, such that cardinal bandwidths were 0.2 times the oblique bandwidths. This model could not capture the invariance of the oblique effect with respect to spatial frequency, nor the influence of contrast on orientation-discrimination performance. However, discrimination thresholds for the maximum-likelihood model were closer in magnitude to those observed psychophysically than for the winner-take-all model. Considering the high computational expense of likelihood computations, the maximum-likelihood model may be more suitable for a reduced number of orientation-selective mechanisms, such as those underlying perception (see Section 5.2).

It is entirely plausible that the visual system has simultaneous access to more than one type of orientation-decoding strategy and can flexibly adapt which it uses in any given situation to meet the prevailing stimuli and task demands. That is, it may exploit different solutions under different circumstances. This possibility has been the subject of much debate in other domains, such as motion processing (e.g., Rocchi et al., 2013), but there is still much uncertainty concerning the computations that govern human perception.

8.1.8 The reliability of web-based testing

The work in Chapter 7 demonstrated strong consistency between the population estimates of orientation-identification performance in two independent large samples of participants. This establishes the reliability of the web-based testing protocol for capturing orientation-identification performance in the tested population, which consisted of mostly young, university-educated students. In Section 6.3, the validity of the web-based testing protocol was demonstrated by strong individual agreement between orientation-identification thresholds measured using web- and lab-based methods. However, web-based testing was demonstrated to be not well suited for capturing the influence of spatial attention on the

oblique effect for orientation identification (see Section 6.3 and Chapter 7).

8.2 Unanswered questions

8.2.1 The independence of mechanisms for encoding and perception

The isotropic orientation-tuning bandwidths of detection mechanisms indicate a closer correspondence to the response characteristics of early visual cortical neurons than the anisotropic bandwidths of discrimination mechanisms (see Section 5.3). This is supported by reduced tuning bandwidth estimates for detection of relatively high spatial frequencies (S. J. Anderson et al., 1991; Phillips & Wilson, 1984; Snowden, 1992), which reflects the narrowed orientation bandwidths of V1 neurons tuned to these higher spatial frequencies (Y. Chen et al., 2020; B. Li et al., 2003; G. Shen et al., 2014; Webster & De Valois, 1985). However, these studies determined psychophysical bandwidth estimates using a test stimulus in the presence of a superimposed singular mask, leaving open the possibility that task performance may have been facilitated by neighbouring detection mechanisms, i.e., 'off-channel looking' (Hutchinson & Ledgeway, 2004). This is evidenced by much smaller bandwidth estimates than were reported for a 'dual-masking' paradigm which minimised off-channel looking (see Section 5.3). The precision of the bandwidth estimates in the 'dual-masking' experiment is further supported by their consistency with the model predictions for detection mechanisms, in that the oblique effect for contrast detection is only abolished for bandwidths of approximately 70° (see Section 4.2).

The finding that the mechanisms underlying discrimination may be distinct from those serving detection indicates that discrimination mechanisms could have response characteristics which are independent from those of early visual cortical neurons. Indeed, the anisotropic tuning bandwidths of discrimination mechanisms (see Section 5.3) has not been

reported in the neurophysiology literature (see Sections 1.4 and 1.5) but is required to account for the oblique effect for orientation discrimination (see Sections 4.3 and 4.4). Future work could estimate the bandwidths of discrimination mechanisms at low and high spatial frequencies. If the estimated bandwidths are independent of spatial frequency, this suggests that the response characteristics of these mechanisms may be distinct from those of the populations of neurons which encode visual orientation. This independence would support the suitability of the maximum-likelihood model for decoding orientation from these perceptual mechanisms, given that its precision is highly susceptible to low-level variability (see Section 4.3).

8.2.2 Predicting visual performance

It has been questioned whether the psychophysical estimates of orientation bandwidth truly reflect the response characteristics of the mechanisms underlying visual performance. For example, bandwidth estimates have been suggested to be overestimated due to the confounding influence of inhibitory interactions between mechanisms, i.e., cross-orientation suppression (Meese & Holmes, 2010). Indeed, visual masking induced threshold elevations in some observers which greatly deviated from the fitted Gaussian functions (see Section 5.3). To assess the validity of the visual masking experiment for measuring orientation bandwidths, future work could test whether individual differences in bandwidth estimates predict psychophysical performance in the absence of visual masking. For example, a re-examination of the data from Section 5.3 reveals a potential positive association between the measured threshold and estimated bandwidth for orientation discrimination. That is, the threshold versus bandwidth function appears to be reasonably approximated by a straight line, when plotted on log-linear axes, although this relationship is less clear for contrast

4987 detection (see Figure 8.1). Further data collection, from more experimental conditions or
4988 larger samples, is required to address the reliability of this finding. Accompanying modelling
4989 work could attempt to capture such individual variation by simulating orientation-
4990 discrimination performance whilst adjusting the orientation bandwidths of mechanisms.

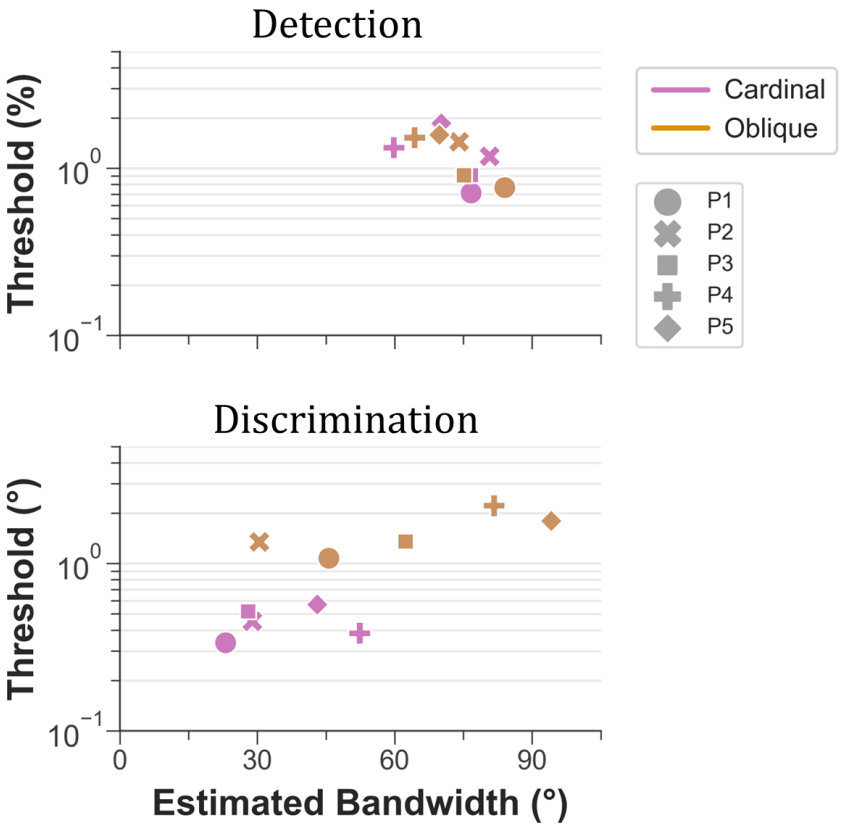

Figure 8.1. For each participant, the contrast-detection (*top*) and orientation-discrimination (*bottom*) thresholds are plotted against the orientation bandwidth estimate. Larger discrimination thresholds are associated with larger bandwidth estimates.

8.2.3 Investigating the mechanisms of contrast discrimination

Suprathreshold contrast discrimination may be served by the same mechanisms as contrast detection (Legge & Foley, 1980), distinct from the mechanisms of orientation discrimination or spatial frequency discrimination (Bowne, 1990). For example, previous modelling work has shown that contrast discrimination may be determined by the pooled firing rates from a population of orientation-selective neurons (Goris et al., 2009), in a manner not dissimilar from the modelling of contrast detection described in Section 4.2. The hypothesis that detection and contrast discrimination are served by the same mechanisms generates two key predictions. Firstly, there should be an oblique effect for contrast discrimination that arises only at relatively high spatial frequencies, typically above 8c/° in central vision (Pointer, 1996), which has not been investigated previously. Secondly, contrast-discrimination thresholds should greatly decrease with increasing spatial frequency, for which there is partial evidence (Legge, 1981). Accompanying modelling work should aim to generate a unified model to account for the psychophysical data on both tasks. Exploring whether different visual functions are served by functionally independent mechanisms provides crucial insight into the potential modularity of visual perception.

8.2.4 Quantifying the number of perceptual mechanisms

In the 'metamers' experiment, the minimum number of orientation-selective mechanisms underlying perception were estimated using spatial arrays of lines, with their orientations sampled from a defined orientation range (see Section 5.2). The data indicated that the minimum number of mechanisms did not increase proportionally with the range of orientations in the metamers task, suggesting that the mechanisms underlying perception are not uniformly distributed. Future work could examine how the estimated minimum number

of mechanisms scales with the orientation range, which should extend in increments beyond the ranges used in Section 5.2 (< 90°) to cover the full range of orientations. The non-uniformity in sampling suggests that orientations may be more densely sampled about the central tendency of the orientation range than more distal orientations. To test this, performance could be assessed by sampling discrete orientations from (say) a Gaussian distribution.

8.2.5 How is cognitive information integrated with sensory visual information?

The mechanisms underlying visual perception may not share the response characteristics of mechanisms responsible for the initial encoding of visual information (see Chapters 4 and 5). There is evidence to suggest that cognitive factors may influence these perceptual mechanisms (see Section 1.3.5 and Chapter 6). For example, the oblique effect for orientation discrimination may be reduced when stimuli are presented within an explicit visual reference frame (an obliquely orientated, unfilled square) which surrounds the stimulus (Westheimer & Lavian, 2013). Future work could measure orientation-discrimination performance in the presence and absence of such a visual reference frame, whilst varying the spatial separation between the stimulus and surrounding frame. If this effect is assumed to be cognitive in origin, then the oblique effect for orientation discrimination should be reduced even when the spatial separation between the central stimulus and visual reference frame is larger than the typical receptive field sizes of neurons in early visual cortex (J. Freeman & Simoncelli, 2011). Alternatively, such an effect may also be found for an illusory reference frame, similar to a Kaniza figure (Dienes & Trick, 2014), in the form of an illusory path between the visible corners of a visual reference frame.

The work in Section 6.5 indicated that there was an almost instantaneous recalibration of the cognitive mechanisms underlying the identification of visual orientation, when interleaving runs on orientation-identification and orientation discrimination tasks. Recent visual experience may therefore be integrated with encoded visual information to alter the response characteristics of perceptual mechanisms. To investigate this, psychophysical estimates of orientation bandwidths could be made before and after a training regime on an orientation-discrimination task, or in the presence and absence of an explicit visual reference frame.

Alternatively, the oblique effect for orientation discrimination has been demonstrated to follow a gravitational reference frame, such that thresholds are lowest for the physical horizontal and vertical, even when the head is tilted by 45° (Buchanan-Smith & Heeley, 1993; Mikellidou et al., 2015). To see whether vestibular information is integrated into the response characteristics of perceptual mechanisms, psychophysical bandwidth estimates could be made with the head tilted at angles of 0 and 45°, and whilst prone and facing upwards.

8.2.6 The role of attention in the oblique effect

The oblique effect for orientation identification was demonstrated to increase under conditions of high attentional load, with attention divided between two spatial locations to the left and right of central fixation, whereas this effect was not observed for orientation discrimination. The oblique effect for discrimination may also be influenced by cognitive factors, independent of those responsible for encoding visual orientation (Mikellidou et al., 2015; Westheimer & Lavian, 2013), suggesting that an attentional effect may be revealed for stronger manipulations of spatial attention. To manipulate attention, a spatial four-alternative

forced choice (4AFC) orientation-discrimination task could be implemented, potentially whilst directing attention to task-irrelevant stimulus features (e.g., Harrison et al., 2022; Moreland & Boynton, 2020). Indeed, such a design has been shown to generate an oblique effect for simultaneity judgements (Kelly & Matthews, 2011). If the oblique effect for orientation discrimination increases with attentional load, this would indicate that attentional mechanisms may serve to lessen the anisotropic perception of orientation.

8.2.7 Insight from individual differences

There may be distinct sources of the oblique effects for various visual tasks, including anisotropic tuning bandwidths for orientation discrimination (see Chapters 4 and 5) and cognitive factors for orientation identification (see Chapter 6). This is broadly consistent with previous suggestions of a 'Class 1' and 'Class 2' oblique effect, which are suggested to be driven by either low-level or cognitive factors, respectively (Balikou et al., 2015; Essock, 1980). The substantial individual differences in the size of the oblique effect (see Chapter 7) could be explored with accompanying modelling work in order to identify the main sources of inter-individual variation. To achieve this, the oblique effect could be quantified for various tasks by determining the best-fitting model parameters for each participant's data across experimental conditions.

8.2.8 The reliability of web-based methods in clinical populations

There is strong individual agreement between the orientation-identification thresholds measured with web-based and lab-based methods, demonstrating the reliability of the web-based testing protocol (see Section 6.3). Reliable web-based methods could improve the time and resource efficiency of clinical testing by increasing the frequency of assessments without increasing organisational demands for the clinician or patient. Common barriers that can

prevent patients from receiving treatment include cost, independent travel, and time commitments (Hartnett, 2005; Javitt & Aiello, 1996; Varano et al., 2015). Web-based methods would be especially useful in cases where performance on a psychophysical task is tracked over time, such as assessments of disease progression or treatment outcomes (Fu et al., 2017; Ogata et al., 2019; Y.-Z. Wang et al., 2013). Performance on a global 'orientation-discrimination' task (Bedell et al., 2009), similar to the orientation-identification experiment described in Chapter 6, is associated with the active inflammation status of patients with age-related macular degeneration (ARMD), and is closely related to the severity of structural changes due to accumulated retinal fluid (Fu et al., 2017). However, certain collectives of participants (e.g., clinical populations, older people) may interact with technology in a different manner to the sample of healthy, mainly younger participants tested in Section 6.3. Therefore, agreement between web-based and lab-based measurements must first be demonstrated in clinical populations before developing web-based tasks for clinical settings.

8.3 Concluding remarks

The work in this thesis challenges the classical view that the oblique effect is generated solely by an overrepresentation of cardinal-tuned mechanisms which serve visual perception. Through a series of psychophysical experiments and complementary modelling work, this theory has been demonstrated to be insufficient to explain how humans perceive orientated edges in the world. The oblique effect may not be a unitary phenomenon, such that oblique effects measured for different visual tasks may be generated by different subpopulations of orientation-selective mechanisms, each with their own distinctive pattern of inhomogeneities or orientation anisotropies. These populations may vary in terms of their distribution or response characteristics, and may be differentially susceptible to higher-level cognitive influences. Finally, the ubiquity of the oblique effect in the human visual system indicates that it should be a benchmark feature for any models of orientation perception. Modelling the oblique effect across different visual tasks and experimental conditions may contribute greatly to the understanding of how edges, object boundaries and contours are initially processed by the visual system. This is important because extracting the local orientation information from an image, is a fundamental first step for more complex perceptual operations such as shape encoding and object recognition.

9. References

Abbott, L. F., & Dayan, P. (1999). The Effect of Correlated Variability on the Accuracy of a Population Code. *Neural Computation*, *11*(1), 91–101. https://doi.org/10.1162/089976699300016827

Adorján, P., Levitt, J. B., Lund, J. S., & Obermayer, K. (1999). A model for the intracortical origin of orientation preference and tuning in macaque striate cortex. *Visual Neuroscience*, *16*(2), 303–318. https://doi.org/10.1017/S0952523899162114

Albrecht, D. G., & Hamilton, D. B. (1982). Striate cortex of monkey and cat: Contrast response function. *Journal of Neurophysiology*, *48*(1), 217–237. https://doi.org/10.1152/jn.1982.48.1.217

Allard, R., & Faubert, J. (2008). The noisy-bit method for digital displays: Converting a 256 luminance resolution into a continuous resolution. *Behavior Research Methods*, *40*(3), 735–743. https://doi.org/10.3758/BRM.40.3.735

Altavini, T. S., Conde-Ocazionez, S. A., Eriksson, D., Wunderle, T., & Schmidt, K. E. (2017). Selective interhemispheric circuits account for a cardinal bias in spontaneous activity within early visual areas. *NeuroImage*, *146*, 971–982. https://doi.org/10.1016/j.neuroimage.2016.09.048

Amir, Y., Harel, M., & Malach, R. (1993). Cortical Hierarchy Reflected in the Organization of Intrinsic Connections in Macaque Monkey Visual-Cortex. *Journal of Comparative Neurology*, *334*(1), 19–46. https://doi.org/10.1002/cne.903340103

Anderson, R. S., Evans, D. W., & Thibos, L. N. (1996). Effect of window size on detection acuity and resolution acuity for sinusoidal gratings in central and peripheral vision. *Journal of the Optical Society of America A*, *13*(4), 697. https://doi.org/10.1364/JOSAA.13.000697

Anderson, S. J., Mullen, K. T., & Hess, R. F. (1991). Human peripheral spatial resolution for achromatic and chromatic stimuli: Limits imposed by optical and retinal factors. *The Journal of Physiology*, *442*(1), 47–64. https://doi.org/10.1113/jphysiol.1991.sp018781

Andrade, M. J. O. de, Neto, A. C., Oliveira, A. R. de, Santana, J. B., & Santos, N. A. dos. (2018). Daily variation of visual sensitivity to luminance contrast: Effects of time of measurement and circadian typology. *Chronobiology International*, *35*(7), 996–1007. https://doi.org/10.1080/07420528.2018.1450753

Andrei, A. R., Pojoga, S., Janz, R., & Dragoi, V. (2019). Integration of cortical population signals for visual perception. *Nature Communications*, *10*(1), 3832. https://doi.org/10.1038/s41467-019-11736-2

Angelucci, A., Bijanzadeh, M., Nurminen, L., Federer, F., Merlin, S., & Bressloff, P. C. (2017). Circuits and Mechanisms for Surround Modulation in Visual Cortex. *Annual Review of Neuroscience*, *40*(1), 425–451. https://doi.org/10.1146/annurev-neuro-072116-031418

Angelucci, A., & Bressloff, P. C. (2006). Contribution of feedforward, lateral and feedback connections to the classical receptive field center and extra-classical receptive field surround of primate V1 neurons. In *Progress in Brain Research* (Vol. 154, pp. 93–120). Elsevier. https://doi.org/10.1016/S0079-6123(06)54005-1

Anzai, A., Bearse, M. A., Freeman, R. D., & Cai, D. (1995). Contrast coding by cells in the cat's striate cortex: Monocular *vs.* binocular detection. *Visual Neuroscience*, *12*(1), 77–93. https://doi.org/10.1017/S0952523800007331

Appelle, S. (1972). Perception and discrimination as a function of stimulus orientation: The 'oblique effect' in man and animals. *Psychological Bulletin*, *78*(4), 266–278. https://doi.org/10.1037/h0033117

Arakawa, K., Tobimatsu, S., Kurita-Tashima, S., Nakayama, M., Kira, J.-I., & Kato, M. (2000). Effects of stimulus orientation on spatial frequency function of the visual evoked potential. *Experimental Brain Research*, *131*(1), 121–125. https://doi.org/10.1007/s002219900274

Baker, C. L., & Mareschal, I. (2001). Chapter 12 Processing of second-order stimuli in the visual cortex. In *Progress in Brain Research* (Vol. 134, pp. 171–191). Elsevier. https://doi.org/10.1016/S0079-6123(01)34013-X

Baker, D. H. (2013). What Is the Primary Cause of Individual Differences in Contrast Sensitivity? *PLoS ONE*, *8*(7), e69536. https://doi.org/10.1371/journal.pone.0069536

Baker, D. H., & Meese, T. S. (2012). Zero-dimensional noise: The best mask you never saw. *Journal of Vision*, *12*(10), 20–20. https://doi.org/10.1167/12.10.20

Balaram, P., Young, N. A., & Kaas, J. H. (2014). Histological features of layers and sublayers in cortical visual areas V1 and V2 of chimpanzees, macaque monkeys, and humans. *Eye and Brain*, *2014*(6 Suppl 1), 5–18. https://doi.org/10.2147/EB.S51814

Baldwin, A. S., Baker, D. H., & Hess, R. F. (2016). What Do Contrast Threshold Equivalent Noise Studies Actually Measure? Noise vs. Nonlinearity in Different Masking Paradigms. *PLoS ONE*, *11*(3), e0150942. https://doi.org/10.1371/journal.pone.0150942

Balikou, P., Gourtzelidis, P., Mantas, A., Moutoussis, K., Evdokimidis, I., & Smyrnis, N. (2015). Independent sources of anisotropy in visual orientation representation: A visual and a cognitive oblique effect. *Experimental Brain Research*, *233*(11), 3097–3108. https://doi.org/10.1007/s00221-015-4379-5

Barbur, J. L., & Stockman, A. (2010). Photopic, Mesopic and Scotopic Vision and Changes in Visual Performance. In *Encyclopedia of the Eye* (pp. 323–331). Elsevier.

https://doi.org/10.1016/B978-0-12-374203-2.00233-5

Barlow, H. (1961). Possible Principles Underlying the Transformations of Sensory Messages. *Sensory Communication*, *1*. https://doi.org/10.7551/mitpress/9780262518420.003.0013

Barlow, H. B., Blakemore, C., & Pettigrew, J. D. (1967). The neural mechanism of binocular depth discrimination. *The Journal of Physiology*, *193*(2), 327–342. https://doi.org/10.1113/jphysiol.1967.sp008360

Bastos, A. M., Vezoli, J., Bosman, C. A., Schoffelen, J.-M., Oostenveld, R., Dowdall, J. R., De Weerd, P., Kennedy, H., & Fries, P. (2015). Visual Areas Exert Feedforward and Feedback Influences through Distinct Frequency Channels. *Neuron*, *85*(2), 390–401. https://doi.org/10.1016/j.neuron.2014.12.018

Battaglini, P. P., Galletti, C., & Fattori, P. (1993). Functional properties of neurons in area V1 of awake macaque monkeys: Peripheral versus central visual field representation. *Archives Italiennes De Biologie*, *131*(4), 303–315.

Bauer, J. A., Owens, D. A., Thomas, J., & Held, R. (1979). Monkeys Show an Oblique Effect. *Perception*, *8*(3), 247–253. https://doi.org/10.1068/p080247

Bauer, R., & Jordan, W. (1993). Different anisotropies for texture and grating stimuli in the visual map of cat striate cortex. *Vision Research*, *33*(11), 1447–1450. https://doi.org/10.1016/0042-6989(93)90138-m

Beaudot, W. H. A., & Mullen, K. T. (2006). Orientation discrimination in human vision: Psychophysics and modeling. *Vision Research*, *46*(1–2), 26–46. https://doi.org/10.1016/j.visres.2005.10.016

Bedell, H. E., Tong, J., Woo, S. Y., House, J. R., & Nguyen, T. (2009). Orientation Discrimination with Macular Changes Associated with Early AMD. *Optometry and*

Vision Science, *86*(5), 485–491. https://doi.org/10.1097/OPX.0b013e31819fa6e2

Belmore, S. C., & Shevell, S. K. (2008). Very-long-term chromatic adaptation: Test of gain theory and a new method. *Visual Neuroscience*, *25*(3), 411–414. https://doi.org/10.1017/S0952523808080450

Ben-Yishai, R., Bar-Or, R. L., & Sompolinsky, H. (1995). Theory of orientation tuning in visual cortex. *Proceedings of the National Academy of Sciences*, *92*(9), 3844–3848. https://doi.org/10.1073/pnas.92.9.3844

Ben-Yishai, R., Hansel, D., & Sompolinsky, H. (1997). Traveling Waves and the Processing of Weakly Tuned Inputs in a Cortical Network Module. *Journal of Computational Neuroscience*, *4*(1), 57–77. https://doi.org/10.1023/A:1008816611284

Berens, P., Ecker, A. S., Gerwinn, S., Tolias, A. S., & Bethge, M. (2011). Reassessing optimal neural population codes with neurometric functions. *Proceedings of the National Academy of Sciences*, *108*(11), 4423–4428. https://doi.org/10.1073/pnas.1015904108

Bergmann, J., Pilatus, U., Genç, E., Kohler, A., Singer, W., & Pearson, J. (2016). V1 surface size predicts GABA concentration in medial occipital cortex. *NeuroImage*, *124*, 654–662. https://doi.org/10.1016/j.neuroimage.2015.09.036

Berkley, A., Kitterle, F., & Watkins, D. (1975). *Grating visibility as a function of orientations and retinal eccentricity*. 6. https://doi.org/10.1016/0042-6989(75)90213-8

Bishop, P. O., Coombs, J. S., & Henry, G. H. (1973). Receptive fields of simple cells in the cat striate cortex. *The Journal of Physiology*, *231*(1), 31–60. https://doi.org/10.1113/jphysiol.1973.sp010218

Bisti, S., & Maffei, L. (1974). Behavioural contrast sensitivity of the cat in various visual meridians. *The Journal of Physiology*, *241*(1), 201–210. https://doi.org/10.1113/jphysiol.1974.sp010649

5233 Blake, R., & Holopigian, K. (1985). *Orientation selectivity in cats and humans assessed by*
5234 *masking*. 8. https://doi.org/10.1016/0042-6989(85)90224-x
5235 Blakemore, C., & Nachmias, J. (1971). The orientation specificity of two visual after-effects.
5236 *The Journal of Physiology*, *213*(1), 157–174.
5237 https://doi.org/10.1113/jphysiol.1971.sp009374
5238 Blakemore, C., Nachmias, J., & Sutton, P. (1970). The perceived spatial frequency shift:
5239 Evidence for frequency-selective neurones in the human brain. *The Journal of*
5240 *Physiology*, *210*(3), 727–750. https://doi.org/10.1113/jphysiol.1970.sp009238
5241 Bland, M. J., & Altman, D. G. (1986). Statistical methods for assessing agreement between
5242 two methods of clinical measurement. *The Lancet*, *327*(8476), 307–310.
5243 https://doi.org/10.1016/S0140-6736(86)90837-8
5244 Bland, M. J., & Altman, D. G. (1999). Measuring agreement in method comparison studies.
5245 *Statistical Methods in Medical Research*, *8*(2), 135–160.
5246 https://doi.org/10.1177/096228029900800204
5247 Bloem, I. M., & Ling, S. (2017a). Attentional modulation interacts with orientation
5248 anisotropies in contrast perception. *Journal of Vision*, *17*(11), 6.
5249 https://doi.org/10.1167/17.11.6
5250 Bloem, I. M., & Ling, S. (2017b). Attentional modulation interacts with orientation
5251 anisotropies in contrast perception. *Journal of Vision*, *17*(11), 6.
5252 https://doi.org/10.1167/17.11.6
5253 Bockisch, C. J., & Haslwanter, T. (2001). Three-dimensional eye position during static roll
5254 and pitch in humans. *Vision Research*, *41*(16), 2127–2137.
5255 https://doi.org/10.1016/s0042-6989(01)00094-3
5256 Boltz, R. L., Harwerth, R. S., & Smith, E. L. (1979). Orientation Anisotropy of Visual Stimuli

in Rhesus Monkey: A Behavioral Study. *Science*, *205*(4405), 511–513. https://doi.org/10.1126/science.109923

Bonhoeffer, T., & Grinvald, A. (1991). Iso-orientation domains in cat visual cortex are arranged in pinwheel-like patterns. *Nature*, *353*(6343), 429–431. https://doi.org/10.1038/353429a0

Borst, A., & Theunissen, F. E. (1999). Information theory and neural coding. *Nature Neuroscience*, *2*(11), 947–957. https://doi.org/10.1038/14731

Borwein, B. (1981). The Retinal Receptor: A Description. In J. M. Enoch & F. L. Tobey (Eds.), *Vertebrate Photoreceptor Optics* (Vol. 23, pp. 11–81). Springer Berlin Heidelberg. https://doi.org/10.1007/978-3-540-38507-3_2

Bosten, J. M., Goodbourn, P. T., Bargary, G., Verhallen, R. J., Lawrance-Owen, A. J., Hogg, R. E., & Mollon, J. D. (2017). An exploratory factor analysis of visual performance in a large population. *Vision Research*, *141*, 303–316. https://doi.org/10.1016/j.visres.2017.02.005

Bowmaker, J. K. (1984). Microspectrophotometry of vertebrate photoreceptors. *Vision Research*, *24*(11), 1641–1650. https://doi.org/10.1016/0042-6989(84)90322-5

Bowne, S. F. (1990). Contrast discrimination cannot explain spatial frequency, orientation or temporal frequency discrimination. *Vision Research*, *30*(3), 449–461. https://doi.org/10.1016/0042-6989(90)90086-Z

Braddick, O., Campbell, F. W., & Atkinson, J. (1978). Channels in Vision: Basic Aspects. In R. Held, H. W. Leibowitz, & H.-L. Teuber (Eds.), *Perception* (pp. 3–38). Springer Berlin Heidelberg. https://doi.org/10.1007/978-3-642-46354-9_1

Bridwell, D. A., Hecker, E. A., Serences, J. T., & Srinivasan, R. (2013). Individual differences in attention strategies during detection, fine discrimination, and coarse discrimination.

Journal of Neurophysiology, *110*(3), 784–794. https://doi.org/10.1152/jn.00520.2012

Briggs, F., Mangun, G. R., & Usrey, W. M. (2013). Attention enhances synaptic efficacy and the signal-to-noise ratio in neural circuits. *Nature*, *499*(7459), 476–480. https://doi.org/10.1038/nature12276

Brouwer, G. J., & Heeger, D. J. (2011). Cross-orientation suppression in human visual cortex. *Journal of Neurophysiology*, *106*(5), 2108–2119. https://doi.org/10.1152/jn.00540.2011

Buchanan-Smith, H. M., & Heeley, D. W. (1993). Anisotropic Axes in Orientation Perception are Not Retinotopically Mapped. *Perception*, *22*(12), 1389–1402. https://doi.org/10.1068/p221389

Budd, J. M. L. (1998). Extrastriate feedback to primary visual cortex in primates: A quantitative analysis of connectivity. *Proceedings of the Royal Society of London. Series B: Biological Sciences*, *265*(1400), 1037–1044. https://doi.org/10.1098/rspb.1998.0396

Buffalo, E. A., Fries, P., Landman, R., Buschman, T. J., & Desimone, R. (2011). Laminar differences in gamma and alpha coherence in the ventral stream. *Proceedings of the National Academy of Sciences*, *108*(27), 11262–11267. https://doi.org/10.1073/pnas.1011284108

Burr, D. C., & Wijesundra, S.-A. (1991). Orientation discrimination depends on spatial frequency. *Vision Research*, *31*(7–8), 1449–1452. https://doi.org/10.1016/0042-6989(91)90064-C

Butler, R., Mierzwinski, G. W., Bernier, P. M., Descoteaux, M., Gilbert, G., & Whittingstall, K. (2020). Neurophysiological basis of contrast dependent BOLD orientation tuning. *NeuroImage*, *206*, 116323. https://doi.org/10.1016/j.neuroimage.2019.116323

5305 Caelli, T., Brettel, H., Rentschler, I., & Hilz, R. (1983). *Discrimination thresholds in the two-*
5306 *dimensional spatial frequency domain*. 5.
5307 Callaway, E. M. (1998). Local circuits in primary visual cortex of the macaque monkey.
5308 *Annual Review of Neuroscience*, *21*(1), 47–74.
5309 https://doi.org/10.1146/annurev.neuro.21.1.47
5310 Campbell, F. W., Cleland, B. G., Cooper, G. F., & Enroth-Cugell, C. (1968). The angular
5311 selectivity of visual cortical cells to moving gratings. *The Journal of Physiology*,
5312 *198*(1), 237–250. https://doi.org/10.1113/jphysiol.1968.sp008604
5313 Campbell, F. W., & Kulikowski, J. J. (1966). Orientational selectivity of the human visual
5314 system. *The Journal of Physiology*, *187*(2), 437–445.
5315 https://doi.org/10.1113/jphysiol.1966.sp008101
5316 Campbell, F. W., Kulikowski, J. J., & Levinson, J. (1966). The effect of orientation on the
5317 visual resolution of gratings. *The Journal of Physiology*, *187*(2), 427–436.
5318 https://doi.org/10.1113/jphysiol.1966.sp008100
5319 Campbell, F. W., & Robson, J. G. (1968). Application of Fourier analysis to the visibility of
5320 gratings. *The Journal of Physiology*, *197*(3), 551–566.
5321 https://doi.org/10.1113/jphysiol.1968.sp008574
5322 Carandini, M., & Ferster, D. (2000). Membrane Potential and Firing Rate in Cat Primary
5323 Visual Cortex. *The Journal of Neuroscience*, *20*(1), 470–484.
5324 https://doi.org/10.1523/JNEUROSCI.20-01-00470.2000
5325 Carandini, M., Heeger, D. J., & Movshon, J. A. (1997). Linearity and Normalization in
5326 Simple Cells of the Macaque Primary Visual Cortex. *The Journal of Neuroscience*,
5327 *17*(21), 8621–8644. https://doi.org/10.1523/JNEUROSCI.17-21-08621.1997
5328 Carandini, M., Heeger, D. J., & Senn, W. (2002). A Synaptic Explanation of Suppression in

Visual Cortex. *The Journal of Neuroscience*, *22*(22), 10053–10065. https://doi.org/10.1523/JNEUROSCI.22-22-10053.2002

Carrasco, M. (2014). *Attention Alters Appearance*. *7*(3), 79–106. https://doi.org/10.1038/nn1194

Cass, J., Stuit, S., Bex, P., & Alais, D. (2009). Orientation bandwidths are invariant across spatiotemporal frequency after isotropic components are removed. *Journal of Vision*, *9*(12), 17–17. https://doi.org/10.1167/9.12.17

Celebrini, S., Thorpe, S., Trotter, Y., & Imbert, M. (1993). Dynamics of orientation coding in area VI of the awake primate. *Visual Neuroscience*, *10*(5), 811–825. https://doi.org/10.1017/S0952523800006052

Chan, D., Rajsic, J., & Pratt, J. (2017). Go-getters and procrastinators: Investigating individual differences in visual cognition across university semesters. *Vision Research*, *141*, 317–324. https://doi.org/10.1016/j.visres.2016.09.007

Chapman, B., & Bonhoeffer, T. (1998). Overrepresentation of horizontal and vertical orientation preferences in developing ferret area 17. *Proceedings of the National Academy of Sciences of the United States of America*, *95*(5), 2609–2614. https://doi.org/10.1073/pnas.95.5.2609

Chapman, R. W., Danko, G., Rizzo, C., Egan, R. W., Mauser, P. J., & Kreutner, W. (1991). Prejunctional GABA-B inhibition of cholinergic, neurally-mediated airway contractions in guinea-pigs. *Pulmonary Pharmacology*, *4*(4), 218–224. https://doi.org/10.1016/0952-0600(91)90014-T

Chen, S., & Levi, D. M. (1996). Meridional Anisotropy in the Discrimination of Parallel and Perpendicular Lines—Effect of Body Tilt. *Perception*, *25*(6), 633–649. https://doi.org/10.1068/p250633

Chen, Y., Ko, H., Zemelman, B. V., Seidemann, E., & Nauhaus, I. (2020). Uniform spatial pooling explains topographic organization and deviation from receptive-field scale invariance in primate V1. *Nature Communications*, *11*(1), 6390. https://doi.org/10.1038/s41467-020-19954-9

Choi, S.-Y., Borghuis, B., Rea, R., Levitan, E. S., Sterling, P., & Kramer, R. H. (2005). Encoding Light Intensity by the Cone Photoreceptor Synapse. *Neuron*, *48*(4), 555–562. https://doi.org/10.1016/j.neuron.2005.09.011

Chui, T. Y., Song, H., & Burns, S. A. (2008). Adaptive-optics imaging of human cone photoreceptor distribution. *Journal of the Optical Society of America A*, *25*(12), 3021. https://doi.org/10.1364/JOSAA.25.003021

Chung, S., & Ferster, D. (1998). Strength and Orientation Tuning of the Thalamic Input to Simple Cells Revealed by Electrically Evoked Cortical Suppression. *Neuron*, *20*(6), 1177–1189. https://doi.org/10.1016/S0896-6273(00)80498-5

Clopper, C. J., & Pearson, E. S. (1934). The use of confidence or fiducial limits illustrataed in the case of the binomial. *Biometrika*, *26*(4), 404–413. https://doi.org/10.2307/2331986

Cohen, J. B., & Kappauf, W. E. (1982). Metameric Color Stimuli, Fundamental Metamers, and Wyszecki's Metameric Blacks. *The American Journal of Psychology*, *95*(4), 537. https://doi.org/10.2307/1422186

Cook, P. B., & McReynolds, J. S. (1998). Lateral inhibition in the inner retina is important for spatial tuning of ganglion cells. *Nature Neuroscience*, *1*(8), 714–719. https://doi.org/10.1038/3714

Coppola, D. M., & White, L. E. (2004). Visual experience promotes the isotropic representation of orientation preference. *Visual Neuroscience*, *21*(1), 39–51. https://doi.org/10.1017/S0952523804041045

Coppola, D. M., White, L. E., Fitzpatrick, D., & Purves, D. (1998). Unequal representation of cardinal and oblique contours in ferret visual cortex. *Proceedings of the National Academy of Sciences*, *95*(5), 2621–2623. https://doi.org/10.1073/pnas.95.5.2621

Coppola, David. M., Purves, H. R., McCoy, A. N., & Purves, D. (1998). The distribution of oriented contours in the real world. *Proceedings of the National Academy of Sciences*, *95*(7), 4002–4006. https://doi.org/10.1073/pnas.95.7.4002

Corbett, J. E., & Carrasco, M. (2011). Visual performance fields: Frames of reference. *PLoS ONE*, *6*(9). https://doi.org/10.1371/journal.pone.0024470

Cowell, R., Huber, D., & Serences, J. (2013). A novel method for fMRI analysis: Inferring neural mechanisms from voxel tuning. *Journal of Vision*, *13*(9), 116–116. https://doi.org/10.1167/13.9.116

Cronin, B., Stevenson, I. H., Sur, M., & Körding, K. P. (2010). Hierarchical Bayesian Modeling and Markov Chain Monte Carlo Sampling for Tuning-Curve Analysis. *Journal of Neurophysiology*, *103*(1), 591–602. https://doi.org/10.1152/jn.00379.2009

Crump, M. J. C., McDonnell, J. V., & Gureckis, T. M. (2013). Evaluating Amazon's Mechanical Turk as a Tool for Experimental Behavioral Research. *PLoS ONE*, *8*(3), e57410. https://doi.org/10.1371/journal.pone.0057410

Curcio, C. A., Sloan, K. R., Kalina, R. E., & Hendrickson, A. E. (1990). Human photoreceptor topography. *The Journal of Comparative Neurology*, *292*(4), 497–523. https://doi.org/10.1002/cne.902920402

Daffner, K. R., Scinto, L. F., Calvo, V., Faust, R., Mesulam, M. M., West, W. C., & Holcomb, P. J. (2000). The influence of stimulus deviance on electrophysiologic and behavioral responses to novel events. *Journal of Cognitive Neuroscience*, *12*(3), 393–406. https://doi.org/10.1162/089892900562219

Dakin, S. C., Mareschal, I., & Bex, P. J. (2005). An oblique effect for local motion: Psychophysics and natural movie statistics. *Journal of Vision*, *5*(10), 878–878. https://doi.org/10.1167/5.10.9

Dakin, S. C., & Watt, R. J. (1997). The computation of orientation statistics from visual texture. *Vision Research*, *37*(22), 3181–3192. https://doi.org/10.1016/S0042-6989(97)00133-8

Dakin, S. C., Williams, C. B., & Hess, R. F. (1999). The interaction of first- and second-order cues to orientation. *Vision Research*, *39*(17), 2867–2884. https://doi.org/10.1016/S0042-6989(98)00307-1

Daugman, J. G. (1984). Spatial visual channels in the fourier plane. *Vision Research*, *24*(9), 891–910. https://doi.org/10.1016/0042-6989(84)90065-8

Davey, M. P., & Zanker, J. M. (1998). Detecting the orientation of short lines in the periphery. *Australian and New Zealand Journal of Ophthalmology*, *26*, S104–S107. https://doi.org/10.1111/j.1442-9071.1998.tb01354.x

de la Rocha, J., Doiron, B., Shea-Brown, E., Josić, K., & Reyes, A. (2007). Correlation between neural spike trains increases with firing rate. *Nature*, *448*(7155), 802–806. https://doi.org/10.1038/nature06028

De Valois, R. L., Albrecht, D. G., & Thorell, L. G. (1982). Spatial frequency selectivity of cells in macaque visual cortex. *Vision Research*, *22*(5), 545–559. https://doi.org/10.1016/0042-6989(82)90113-4

De Valois, R. L., & De Valois, K. K. (1990). *Spatial Vision*. Oxford University Press, Incorporated.

De Valois, R. L., Jacobs, G. H., & Jones, A. E. (1962). Effects of Increments and Decrements of Light on Neural Discharge Rate. *Science*, *136*(3520), 986–988.

https://doi.org/10.1126/science.136.3520.986

De Valois, R. L., Morgan, H., & Snodderly, D. M. (1974). Psychophysical studies of monkey Vision-III. Spatial luminance contrast sensitivity tests of macaque and human observers. *Vision Research*, *14*(1), 75–81. https://doi.org/10.1016/0042-6989(74)90118-7

De Valois, R. L., William Yund, E., & Hepler, N. (1982). The orientation and direction selectivity of cells in macaque visual cortex. *Vision Research*, *22*(5), 531–544. https://doi.org/10.1016/0042-6989(82)90112-2

De Weerd, P., Vandenbussche, E., & Orban, G. A. (1990). Bar orientation discrimination in the cat. *Visual Neuroscience*, *4*(3), 257–268. https://doi.org/10.1017/S0952523800003394

de-Wit, L., & Wagemans, J. (2014). *Individual Differences in Local and Global Perceptual Organization* (J. Wagemans, Ed.). Oxford University Press. https://doi.org/10.1093/oxfordhb/9780199686858.013.028

DeAngelis, G. C., Robson, J. G., Ohzawa, I., & Freeman, R. D. (1992). Organization of suppression in receptive fields of neurons in cat visual cortex. *Journal of Neurophysiology*, *68*(1), 144–163. https://doi.org/10.1152/jn.1992.68.1.144

Delahunt, P. B., Hardy, J. L., & Werner, J. S. (2008). The effect of senescence on orientation discrimination and mechanism tuning. *Journal of Vision*, *8*(3), 1–9. https://doi.org/10.1167/8.3.5

Deneve, S., Latham, P. E., & Pouget, A. (1999). Reading population codes: A neural implementation of ideal observers. *Nature Neuroscience*, *2*(8), 740–745. https://doi.org/10.1038/11205

Deubel, H., & Elsner, T. (1986). Threshold perception and saccadic eye movements.

Biological Cybernetics, *54*(6), 351–358. https://doi.org/10.1007/BF00355540

DeWeese, M. R., Hromádka, T., & Zador, A. M. (2005). Reliability and Representational Bandwidth in the Auditory Cortex. *Neuron*, *48*(3), 479–488. https://doi.org/10.1016/j.neuron.2005.10.016

Di Russo, F., Pitzalis, S., Spitoni, G., Aprile, T., Patria, F., Spinelli, D., & Hillyard, S. A. (2005). Identification of the neural sources of the pattern-reversal VEP. *NeuroImage*, *24*(3), 874–886. https://doi.org/10.1016/j.neuroimage.2004.09.029

Dickinson, A., Jones, M., & Milne, E. (2014). Oblique Orientation Discrimination Thresholds Are Superior in Those with a High Level of Autistic Traits. *Journal of Autism and Developmental Disorders*, *44*(11), 2844–2850. https://doi.org/10.1007/s10803-014-2147-1

Dienes, N., & Trick, L. (2014). Tracking Illusory Contour Figures. *Journal of Vision*, *14*(10), 348. https://doi.org/10.1167/14.10.348

DiMattina, C. (2016). Comparing models of contrast gain using psychophysical experiments. *Journal of Vision*, *16*(9), 1. https://doi.org/10.1167/16.9.1

Dosher, B., & Lu, Z.-L. (2017). Visual Perceptual Learning and Models. *Annual Review of Vision Science*, *3*(1), 343–363. https://doi.org/10.1146/annurev-vision-102016-061249

Douglas, R. J., & Martin, K. A. C. (2007). Mapping the Matrix: The Ways of Neocortex. *Neuron*, *56*(2), 226–238. https://doi.org/10.1016/j.neuron.2007.10.017

Dumoulin, S. O., & Wandell, B. A. (2008). Population receptive field estimates in human visual cortex. *NeuroImage*, *39*(2), 647–660. https://doi.org/10.1016/j.neuroimage.2007.09.034

Ecker, A. S., Berens, P., Cotton, R. J., Subramaniyan, M., Denfield, G. H., Cadwell, C. R., Smirnakis, S. M., Bethge, M., & Tolias, A. S. (2014). State Dependence of Noise

Correlations in Macaque Primary Visual Cortex. *Neuron*, *82*(1), 235–248. https://doi.org/10.1016/j.neuron.2014.02.006

Edden, R. A. E., Muthukumaraswamy, S. D., Freeman, T. C. A., & Singh, K. D. (2009). Orientation discrimination performance is predicted by GABA concentration and gamma oscillation frequency in human primary visual cortex. *Journal of Neuroscience*, *29*(50), 15721–15726. https://doi.org/10.1523/JNEUROSCI.4426-09.2009

Eisen-Enosh, A., Farah, N., Burgansky-Eliash, Z., Polat, U., & Mandel, Y. (2017). Evaluation of Critical Flicker-Fusion Frequency Measurement Methods for the Investigation of Visual Temporal Resolution. *Scientific Reports*, *7*(1), Article 1. https://doi.org/10.1038/s41598-017-15034-z

Ellemberg, D., Allen, H. A., & Hess, R. F. (2006). Second-order spatial frequency and orientation channels in human vision. *Vision Research*, *46*(17), 2798–2803. https://doi.org/10.1016/j.visres.2006.01.028

El-Shamayleh, Y., Kumbhani, R. D., Dhruv, N. T., & Movshon, J. A. (2013). Visual Response Properties of V1 Neurons Projecting to V2 in Macaque. *Journal of Neuroscience*, *33*(42), 16594–16605. https://doi.org/10.1523/JNEUROSCI.2753-13.2013

Emery, K. J., Volbrecht, V. J., Peterzell, D. H., & Webster, M. A. (2017). Variations in normal color vision. VI. Factors underlying individual differences in hue scaling and their implications for models of color appearance. *Vision Research*, *141*, 51–65. https://doi.org/10.1016/j.visres.2016.12.006

Engbert, R. (2006). Microsaccades: A microcosm for research on oculomotor control, attention, and visual perception. In *Progress in Brain Research* (Vol. 154, pp. 177–192). Elsevier. https://doi.org/10.1016/S0079-6123(06)54009-9

Essock, E. A. (1980). The oblique effect of stimulus identification considered with respect to two classes of oblique effects. *Perception*, *9*(1), 37–46. https://doi.org/10.1068/p090037

Eysel, U. T., Crook, J. M., & Machemer, H. F. (1990). GABA-induced remote inactivation reveals cross-orientation inhibition in the cat striate cortex. *Experimental Brain Research*, *80*(3). https://doi.org/10.1007/BF00228003

Fain, G. L., Matthews, H. R., Cornwall, M. C., & Koutalos, Y. (2001). Adaptation in Vertebrate Photoreceptors. *Physiological Reviews*, *81*(1), 117–151. https://doi.org/10.1152/physrev.2001.81.1.117

Faisal, A., Selen, L., P. J., & Wolpert, D. M. (2008). Noise in the nervous system. *Psychological Review*, *73*(3), 242–247. https://doi.org/10.1037/h0023240

Fang, C., Cai, X., & Lu, H. D. (2022). Orientation anisotropies in macaque visual areas. *Proceedings of the National Academy of Sciences*, *119*(15), e2113407119. https://doi.org/10.1073/pnas.2113407119

Felleman, D. J., & Van Essen, D. C. (1991). Distributed hierarchical processing in the primate cerebral cortex. *Cerebral Cortex (New York, N.Y.: 1991)*, *1*(1), 1–47. https://doi.org/10.1093/cercor/1.1.1-a

Ferster, D. (1981). A comparison of binocular depth mechanisms in areas 17 and 18 of the cat visual cortex. *The Journal of Physiology*, *311*(1), 623–655. https://doi.org/10.1113/jphysiol.1981.sp013608

Ferster, D., Chung, S., & Wheat, H. (1996). Orientation selectivity of thalamic input to simple cells of cat visual cortex. *Nature*, *380*(6571), 249–252. https://doi.org/10.1038/380249a0

Finlay, B. L., Schiller, P. H., & Volman, S. F. (1976). Meridional differences in orientation

sensitivity in monkey striate cortex. *Brain Research*, *105*(2), 350–352. https://doi.org/10.1016/0006-8993(76)90433-9

Finn, I. M., Priebe, N. J., & Ferster, D. (2007). The Emergence of Contrast-Invariant Orientation Tuning in Simple Cells of Cat Visual Cortex. *Neuron*, *54*(1), 137–152. https://doi.org/10.1016/j.neuron.2007.02.029

Flaxman, S. R., Bourne, R. R. A., Resnikoff, S., Ackland, P., Braithwaite, T., Cicinelli, M. V., Das, A., Jonas, J. B., Keeffe, J., Kempen, J. H., Leasher, J., Limburg, H., Naidoo, K., Pesudovs, K., Silvester, A., Stevens, G. A., Tahhan, N., Wong, T. Y., & Taylor, H. R. (2017). Global causes of blindness and distance vision impairment 1990-2020: A systematic review and meta-analysis. *Lancet Global Health*, *5*(12), E1221–E1234. https://doi.org/10.1016/S2214-109X(17)30393-5

Foi, A., Trimeche, M., Katkovnik, V., & Egiazarian, K. (2008). Practical Poissonian-Gaussian Noise Modeling and Fitting for Single-Image Raw-Data. *IEEE Transactions on Image Processing*, *17*(10), 1737–1754. https://doi.org/10.1109/TIP.2008.2001399

Franssen, L., Coppens, J. E., & van den Berg, T. (2006). Compensation comparison method for assessment of retinal straylight. *Investigative Ophthalmology & Visual Science*, *47*(2), 768–776. https://doi.org/10.1167/iovs.05-0690

Freeman, J., Brouwer, G. J., Heeger, D. J., & Merriam, E. P. (2011). Orientation Decoding Depends on Maps, Not Columns. *Journal of Neuroscience*, *31*(13), 4792–4804. https://doi.org/10.1523/JNEUROSCI.5160-10.2011

Freeman, J., & Simoncelli, E. P. (2011). Metamers of the ventral stream. *Nature Neuroscience*, *14*(9), 1195–1201. https://doi.org/10.1038/nn.2889

Freeman, R. D., & Thibos, L. N. (1975). Visual evoked responses in humans with abnormal visual experience. *The Journal of Physiology*, *247*(3), 711–724.

https://doi.org/10.1113/jphysiol.1975.sp010953

Freeman, T. C. B., Durand, S., Kiper, D. C., & Carandini, M. (2002). Suppression without Inhibition in Visual Cortex. *Neuron*, *35*(4), 759–771. https://doi.org/10.1016/S0896-6273(02)00819-X

Frégnac, Y., & Bathellier, B. (2015). Cortical Correlates of Low-Level Perception: From Neural Circuits to Percepts. *Neuron*, *88*(1), 110–126. https://doi.org/10.1016/j.neuron.2015.09.041

Frien, A., Eckhorn, R., Bauer, R., Woelbern, T., & Gabriel, A. (2000). Fast oscillations display sharper orientation tuning than slower components of the same recordings in striate cortex of the awake monkey. *The European Journal of Neuroscience*, *12*(4), 1453–1465. https://doi.org/10.1046/j.1460-9568.2000.00025.x

Fries, W. (1981). The projection from the lateral geniculate nucleus to the prestriate cortex of the macaque monkey. *Proceedings of the Royal Society of London. Series B, Biological Sciences*, *213*(1190), 73–86. https://doi.org/10.1098/rspb.1981.0054

Friston, K. (2005). A theory of cortical responses. *Philosophical Transactions of the Royal Society B: Biological Sciences*, *360*(1456), 815–836. https://doi.org/10.1098/rstb.2005.1622

Frost, B. J., & Kaminer, J. J. (1975). The Orientation Anisotropy and Orientation Constancy: A Visual Evoked Potential Study. *Perception*, *4*(1), 51–58. https://doi.org/10.1068/p040051

Frostig, R. D., & Chen-Bee, C. H. (2009). Visualizing Adult Cortical Plasticity Using Intrinsic Signal Optical Imaging. In R. D. Frostig (Ed.), *In Vivo Optical Imaging of Brain Function* (2nd ed.). CRC Press/Taylor & Francis. http://www.ncbi.nlm.nih.gov/books/NBK20227/

Fu, H., Zhang, B., Tong, J., Bedell, H., Zhang, H., Yang, Y., Nie, C., Luo, Y., & Liu, X. (2017). Relationships of orientation discrimination threshold and visual acuity with macular lesions in age-related macular degeneration. *PLoS ONE*, *12*(9), e0185070. https://doi.org/10.1371/journal.pone.0185070

Furmanski, C. S., & Engel, S. A. (2000). An oblique effect in human primary visual cortex. *Nature Neuroscience*, *3*(6), 535–536. https://doi.org/10.1038/75702

Furmanski, C. S., Schluppeck, D., & Engel, S. A. (2004). Learning Strengthens the Response of Primary Visual Cortex to Simple Patterns. *Current Biology*, *14*(7), 573–578. https://doi.org/10.1016/j.cub.2004.03.032

Gaeta, H., Friedman, D., & Hunt, G. (2003). Stimulus characteristics and task category dissociate the anterior and posterior aspects of the novelty P3. *Psychophysiology*, *40*(2), 198–208. https://doi.org/10.1111/1469-8986.00022

Gardner, J. L., Anzai, A., Ohzawa, I., & Freeman, R. D. (1999). Linear and nonlinear contributions to orientation tuning of simple cells in the cat's striate cortex. *Visual Neuroscience*, *16*(6), 1115–1121. https://doi.org/10.1017/s0952523899166112

Gattass, R., Galkin, T. W., Desimone, R., & Ungerleider, L. G. (2014). Subcortical connections of area V4 in the macaque. *Journal of Comparative Neurology*, *522*(8), 1941–1965. https://doi.org/10.1002/cne.23513

Geisler, W. S., & Albrecht, D. G. (1997). Visual cortex neurons in monkeys and cats: Detection, discrimination, and identification. *Visual Neuroscience*, *14*(5), 897–919. https://doi.org/10.1017/S0952523800011627

Gentaz, E., Baud-Bovy, G., & Luyat, M. (2008). The haptic perception of spatial orientations. *Experimental Brain Research*, *187*(3), 331–348. https://doi.org/10.1007/s00221-008-1382-0

5593 Georgopoulos, A. P., Schwartz, A. B., & Kettner, R. E. (1986). Neuronal Population Coding
5594 of Movement Direction. *Science*, *233*(4771), 1416–1419.
5595 https://doi.org/10.1126/science.3749885
5596 Ghodrati, M., Khaligh-Razavi, S.-M., & Lehky, S. R. (2017). Towards building a more
5597 complex view of the lateral geniculate nucleus: Recent advances in understanding its
5598 role. *Progress in Neurobiology*, *156*, 214–255.
5599 https://doi.org/10.1016/j.pneurobio.2017.06.002
5600 Giavarina, D. (2015). Understanding Bland Altman analysis. *Biochemia Medica*, *25*(2), 141–
5601 151. https://doi.org/10.11613/BM.2015.015
5602 Gilbert, C. D., & Wiesel, T. N. (1990). The influence of contextual stimuli on the orientation
5603 selectivity of cells in primary visual cortex of the cat. *Vision Research*, *30*(11), 1689–
5604 1701. https://doi.org/10.1016/0042-6989(90)90153-C
5605 Girshick, A. R., Landy, M. S., & Simoncelli, E. P. (2011). Cardinal rules: Visual orientation
5606 perception reflects knowledge of environmental statistics. *Nature Neuroscience*,
5607 *14*(7), 926–932. https://doi.org/10.1038/nn.2831
5608 Goodale, M. A., & Milner, A. D. (1992). Separate visual pathways for perception and action.
5609 *Trends in Neurosciences*, *15*(1), 20–25. https://doi.org/10.1016/0166-2236(92)90344-
5610 8
5611 Goodchild, A. K., Ghosh, K. K., & Martin, P. R. (1996). Comparison of photoreceptor spatial
5612 density and ganglion cell morphology in the retina of human, macaque monkey, cat,
5613 and the marmoset Callithrix jacchus. *The Journal of Comparative Neurology*, *366*(1),
5614 55–75. https://doi.org/10.1002/(SICI)1096-9861(19960226)366:1<55::AID-
5615 CNE5>3.0.CO;2-J
5616 Goris, R. L. T., Putzeys, T., Wagemans, J., & Wichmann, F. A. (2013). A neural population

model for visual pattern detection. *Psychological Review*, *120*(3), 472–496. https://doi.org/10.1037/a0033136

Goris, R. L. T., Simoncelli, E. P., & Movshon, J. A. (2015). Origin and Function of Tuning Diversity in Macaque Visual Cortex. *Neuron*, *88*(4), 819–831. https://doi.org/10.1016/j.neuron.2015.10.009

Goris, R. L. T., Wichmann, F. A., & Henning, G. B. (2009). A neurophysiologically plausible population code model for human contrast discrimination. *Journal of Vision*, *9*(7), 15–15. https://doi.org/10.1167/9.7.15

Grabska-Barwińska, A., Distler, C., Hoffmann, K. P., & Jancke, D. (2009). Contrast independence of cardinal preference: Stable oblique effect in orientation maps of ferret visual cortex. *European Journal of Neuroscience*, *29*(6), 1258–1270. https://doi.org/10.1111/j.1460-9568.2009.06656.x

Graham, N. (1977). Visual detection of aperiodic spatial stimuli by probability summation among narrowband channels. *Vision Research*, *17*(5), 637–652. https://doi.org/10.1016/0042-6989(77)90140-7

Graham, N. (1989). *Visual Pattern Analyzers*. Oxford University Press. https://doi.org/10.1093/acprof:oso/9780195051544.001.0001

Green, D. M. (1964). Consistency of auditory detection judgements. *Psychological Review*, *71*, 392–407. https://doi.org/10.1037/h0044520

Gresh, J., Goletz, P. W., Crouch, R. K., & Rohrer, B. (2003). Structure–function analysis of rods and cones in juvenile, adult, and aged C57BL/6 and Balb/c mice. *Visual Neuroscience*, *20*(2), 211–220. https://doi.org/10.1017/S0952523803202108

Grinvald, A., Shoham, D., Shmuel, A., Glaser, D., Vanzetta, I., Shtoyerman, E., Slovin, H., Wijnbergen, C., Hildesheim, R., & Arieli, A. (1999). In-vivo Optical Imaging of

Cortical Architecture and Dynamics. In U. Windhorst & H. Johansson (Eds.), *Modern Techniques in Neuroscience Research* (pp. 893–969). Springer Berlin Heidelberg. https://doi.org/10.1007/978-3-642-58552-4_34

Grünert, U., & Martin, P. R. (2020). Cell types and cell circuits in human and non-human primate retina. *Progress in Retinal and Eye Research*, *78*, 100844. https://doi.org/10.1016/j.preteyeres.2020.100844

Grzeczkowski, L., Clarke, A. M., Francis, G., Mast, F. W., & Herzog, M. H. (2017). About individual differences in vision. *Vision Research*, *141*, 282–292. https://doi.org/10.1016/j.visres.2016.10.006

Gur, M., Beylin, A., & Snodderly, D. M. (1997). Response Variability of Neurons in Primary Visual Cortex (V1) of Alert Monkeys. *The Journal of Neuroscience*, *17*(8), 2914–2920. https://doi.org/10.1523/JNEUROSCI.17-08-02914.1997

Gur, M., & Snodderly, D. M. (2006). High Response Reliability of Neurons in Primary Visual Cortex (V1) of Alert, Trained Monkeys. *Cerebral Cortex*, *16*(6), 888–895. https://doi.org/10.1093/cercor/bhj032

Hammond, B. R., & Buch, J. (2020). Individual differences in visual function. *Experimental Eye Research*, *199*, 108186. https://doi.org/10.1016/j.exer.2020.108186

Hammond, B. R., Fletcher, L. M., & Elliott, J. G. (2013). Glare disability, photostress recovery, and chromatic contrast: Relation to macular pigment and serum lutein and zeaxanthin. *Investigative Ophthalmology & Visual Science*, *54*(1), 476–481. https://doi.org/10.1167/iovs.12-10411

Hammond, B. R., Renzi, L. M., Sachak, S., & Brint, S. F. (2010). Contralateral comparison of blue-filtering and non-blue-filtering intraocular lenses: Glare disability, heterochromatic contrast, and photostress recovery. *Clinical Ophthalmology*

(Auckland, N.Z.), *4*, 1465–1473. https://doi.org/10.2147/OPTH.S15102

Hammond, P. (1973). Contrasts in spatial organization of receptive fields at geniculate and retinal levels: Centre surround and outer surround. *The Journal of Physiology*, *228*(1), 115–137. https://doi.org/10.1113/jphysiol.1973.sp010076

Hammond, P., & Pomfrett, C. J. D. (1990). Influence of spatial frequency on tuning and bias for orientation and direction in the cat's striate cortex. *Vision Research*, *30*(3), 359–369. https://doi.org/10.1016/0042-6989(90)90078-Y

Hand, P. J. (1981). The 2-Deoxyglucose Method. In L. Heimer & M. J. Robards (Eds.), *Neuroanatomical Tract-Tracing Methods* (pp. 511–538). Springer US. https://doi.org/10.1007/978-1-4613-3189-6_15

Hansel, D., & Sompolinsky, H. (1996). Chaos and synchrony in a model of a hypercolumn in visual cortex. *Journal of Computational Neuroscience*, *3*(1), 7–34. https://doi.org/10.1007/BF00158335

Hansen, B. C., & Essock, E. A. (2004). A horizontal bias in human visual processing orientation and its correspondence to the structural components of natural scenes. *Journal of Vision*, *4*(12), 1044–1060. https://doi.org/10.1167/4.12.5

Hansen, B. C., & Essock, E. A. (2006). Anisotropic local contrast normalization: The role of stimulus orientation and spatial frequency bandwidths in the oblique and horizontal effect perceptual anisotropies. *Vision Research*, *46*(26), 4398–4415. https://doi.org/10.1016/j.visres.2006.07.016

Harrison, A., Ling, S., & Foster, J. (2022). Divided attention impairs detection of simple visual features. *Journal of Vision*, *22*(14), 3293. https://doi.org/10.1167/jov.22.14.3293

Hartnett, M. E. (2005). Perceived Barriers to Diabetic Eye Care: Qualitative Study of Patients

and Physicians. *Archives of Ophthalmology*, *123*(3), 387. https://doi.org/10.1001/archopht.123.3.387

Haun, A. M., & Essock, E. A. (2010). Contrast sensitivity for oriented patterns in 1/f noise: Contrast response and the horizontal effect. *Journal of Vision*, *10*(10), 1–1. https://doi.org/10.1167/10.10.1

Hawkins, A. S., Szlyk, J. P., Ardickas, Z., Alexander, K. R., & Wilensky, J. T. (2003). Comparison of Contrast Sensitivity, Visual Acuity, and Humphrey Visual Field Testing in Patients with Glaucoma: *Journal of Glaucoma*, *12*(2), 134–138. https://doi.org/10.1097/00061198-200304000-00008

Hecht, S., Shlaer, S., & Pirenne, M. H. (1942). Energy, Quanta, and Vision. *Journal of General Physiology*, *25*(6), 819–840. https://doi.org/10.1085/jgp.25.6.819

Hedges, V. (2022). *Introduction to neuroscience* (Open edition). Michigan State University Libraries.

Heeger, D. J. (1992). Normalization of cell responses in cat striate cortex. *Visual Neuroscience*, *9*(2), 181–197. https://doi.org/10.1017/S0952523800009640

Heeley, D. W., & Buchanan-Smith, H. M. (1990). Recognition of stimulus orientation. *Vision Research*, *30*(10), 1429–1437. https://doi.org/10.1016/0042-6989(90)90024-F

Heeley, D. W., & Buchanan-Smith, H. M. (1992). Orientation Acuity Estimated With Simultaneous and Successive Procedures. *Spatial Vision*, *6*(1), 1–10. https://doi.org/10.1163/156856892X00028

Heeley, D. W., & Buchanan-Smith, H. M. (1998). The influence of stimulus shape on orientation acuity. *Experimental Brain Research*, *120*(2), 217–222. https://doi.org/10.1007/s002210050395

Heeley, D. W., Buchanan-Smith, H. M., Cromwell, J. A., & Wright, J. S. (1997). The oblique

5713 effect in orientation acuity. *Vision Research*, *37*(2), 235–242.
5714 https://doi.org/10.1016/S0042-6989(96)00097-1
5715 Heeley, D. W., & Timney, B. (1988). Meridional anisotropies of orientation discrimination for
5716 sine wave gratings. *Vision Research*, *28*(2), 337–344. https://doi.org/10.1016/0042-
5717 6989(88)90162-9
5718 Heeley, D. W., & Timney, B. (1989). Spatial frequency discrimination at different
5719 orientations. *Vision Research*, *29*(9), 1221–1228. https://doi.org/10.1016/0042-
5720 6989(89)90068-0
5721 Heggelund, P., & Albus, K. (1978). Orientation selectivity of single cells in striate cortex of
5722 cat: The shape of orientation tuning curves. *Vision Research*, *18*(8), 1067–1071.
5723 https://doi.org/10.1016/0042-6989(78)90037-8
5724 Heinrich, S. P., Aertsen, A., & Bach, M. (2008). Oblique effects beyond low-level visual
5725 processing. *Vision Research*, *48*(6), 809–818.
5726 https://doi.org/10.1016/j.visres.2007.12.012
5727 Henderson, M., & Serences, J. T. (2021). Biased orientation representations can be explained
5728 by experience with nonuniform training set statistics. *Journal of Vision*, *21*(8), 10.
5729 https://doi.org/10.1167/jov.21.8.10
5730 Henry, G. H., Dreher, B., & Bishop, P. O. (1974). Orientation specificity of cells in cat striate
5731 cortex. *Journal of Neurophysiology*, *37*(6), 1394–1409.
5732 https://doi.org/10.1152/jn.1974.37.6.1394
5733 Higgins, G. C., & Stultz, K. (1950). *Variation of Visual Acuity with Various Test-Object*
5734 *Orientations and Viewing Conditions*. 3.
5735 Himmelberg, M. M., Winawer, J., & Carrasco, M. (2022). Linking individual differences in
5736 human primary visual cortex to contrast sensitivity around the visual field. *Nature*

Communications, *13*(1), 3309. https://doi.org/10.1038/s41467-022-31041-9

Hirsch, J. A., Martinez, L. M., Pillai, C., Alonso, J.-M., Wang, Q., & Sommer, F. T. (2003). Functionally distinct inhibitory neurons at the first stage of visual cortical processing. *Nature Neuroscience*, *6*(12), 1300–1308. https://doi.org/10.1038/nn1152

Howard, I. P., & Templeton, W. B. (1966). *Human spatial orientation* (p. 533). John Wiley & Sons.

Hoy, J. L., & Niell, C. M. (2015). Layer-Specific Refinement of Visual Cortex Function after Eye Opening in the Awake Mouse. *The Journal of Neuroscience*, *35*(8), 3370–3383. https://doi.org/10.1523/JNEUROSCI.3174-14.2015

Hu, J. M., Song, X. M., Wang, Q., & Roe, A. W. (2020). Curvature domains in V4 of macaque monkey. *eLife*, *9*, e57261. https://doi.org/10.7554/eLife.57261

Huang, L., Shou, T., Chen, X., Yu, H., Sun, C., & Liang, Z. (2006). Slab-like functional architecture of higher order cortical area 21a showing oblique effect of orientation preference in the cat. *NeuroImage*, *32*(3), 1365–1374. https://doi.org/10.1016/j.neuroimage.2006.05.007

Huang, L., Song, Y., Li, J., Zhen, Z., Yang, Z., & Liu, J. (2014). Individual differences in cortical face selectivity predict behavioral performance in face recognition. *Frontiers in Human Neuroscience*, *8*. https://doi.org/10.3389/fnhum.2014.00483

Hubel, D. H. (1982). Exploration of the primary visual cortex, 1955–78. *Nature*, *299*(5883), 515–524. https://doi.org/10.1038/299515a0

Hubel, D. H., & Wiesel, T. N. (1959). Receptive fields of single neurones in the cat's striate cortex. *The Journal of Physiology*, *148*(3), 574–591. https://doi.org/10.1113/jphysiol.1959.sp006308

Hubel, D. H., & Wiesel, T. N. (1962). Receptive fields, binocular interaction and functional

architecture in the cat's visual cortex. *The Journal of Physiology*, *160*(1), 106–154. https://doi.org/10.1113/jphysiol.1962.sp006837

Hubel, D. H., & Wiesel, T. N. (1967). Cortical and callosal connections concerned with the vertical meridian of visual fields in the cat. *Journal of Neurophysiology*, *30*(6), 1561–1573. https://doi.org/10.1152/jn.1967.30.6.1561

Hubel, D. H., & Wiesel, T. N. (1968). Receptive fields and functional architecture of monkey striate cortex. *The Journal of Physiology*, *195*(1), 215–243. https://doi.org/10.1113/jphysiol.1968.sp008455

Hubel, D. H., & Wiesel, T. N. (1970). The period of susceptibility to the physiological effects of unilateral eye closure in kittens. *The Journal of Physiology*, *206*(2), 419–436. https://doi.org/10.1113/jphysiol.1970.sp009022

Hubel, D. H., & Wiesel, T. N. (1974). Sequence regularity and geometry of orientation columns in the monkey striate cortex. *The Journal of Comparative Neurology*, *158*(3), 267–293. https://doi.org/10.1002/cne.901580304

Hubel, Wiesel, & LeVay. (1977). Plasticity of ocular dominance columns in monkey striate cortex. *Philosophical Transactions of the Royal Society of London. B, Biological Sciences*, *278*(961), 377–409. https://doi.org/10.1098/rstb.1977.0050

Hübener, M., & Bonhoeffer, T. (2002). Optical Imaging of Functional Architecture in Cat Primary Visual Cortex. In *The Cat Primary Visual Cortex* (pp. 131–iii). Elsevier. https://doi.org/10.1016/B978-012552104-8/50003-1

Hübener, M., Shoham, D., Grinvald, A., & Bonhoeffer, T. (1997). Spatial Relationships among Three Columnar Systems in Cat Area 17. *The Journal of Neuroscience*, *17*(23), 9270–9284. https://doi.org/10.1523/JNEUROSCI.17-23-09270.1997

Hughes, A. (1975). A quantitative analysis of the cat retinal ganglion cell topography. *Journal*

of Comparative Neurology, *163*(1), 107–128. https://doi.org/10.1002/cne.901630107

Hutchinson, C. V., & Ledgeway, T. (2004). Spatial frequency selective masking of first-order and second-order motion in the absence of off-frequency `looking'. *Vision Research*, *44*(13), 1499–1510. https://doi.org/10.1016/j.visres.2004.01.014

Ibbotson, M., & Jung, Y. J. (2020). Origins of Functional Organization in the Visual Cortex. *Frontiers in Systems Neuroscience*, *14*, 10. https://doi.org/10.3389/fnsys.2020.00010

Ingram, N. T., Sampath, A. P., & Fain, G. L. (2016). Why are rods more sensitive than cones?: Why are rods more sensitive than cones? *The Journal of Physiology*, *594*(19), 5415–5426. https://doi.org/10.1113/JP272556

Issa, N. P., Trepel, C., & Stryker, M. P. (2000). Spatial Frequency Maps in Cat Visual Cortex. *The Journal of Neuroscience*, *20*(22), 8504–8514. https://doi.org/10.1523/JNEUROSCI.20-22-08504.2000

Jastrow, J. (1892). Studies from the University of Wisconsin: On the Judgment of Angles and Positions of Lines. *The American Journal of Psychology*, *5*(2), 214. https://doi.org/10.2307/1410867

Javitt, J. C., & Aiello, L. P. (1996). Cost-Effectiveness of Detecting and Treating Diabetic Retinopathy. *Annals of Internal Medicine*, *124*(1), 164–169. https://doi.org/10.7326/0003-4819-124-1_part_2-199601011-00017

Jazayeri, M., & Movshon, J. A. (2006). Optimal representation of sensory information by neural populations. *Nature Neuroscience*, *9*(5), 690–696. https://doi.org/10.1038/nn1691

Jehee, J. F. M., Ling, S., Swisher, J. D., Van Bergen, R. S., & Tong, F. (2012). Perceptual Learning Selectively Refines Orientation Representations in Early Visual Cortex. *The Journal of Neuroscience*, *32*(47), 16747–16753.

https://doi.org/10.1523/JNEUROSCI.6112-11.2012

Jonas, J. B., Gusek, G. C., & Fernández, M. C. (1991). Correlation of the Blind Spot Size to the Area of the Optic Disk and Parapapillary Atrophy. *American Journal of Ophthalmology*, *111*(5), 559–565. https://doi.org/10.1016/S0002-9394(14)73698-0

Jones, D., Westall, C., Averbeck, K., & Abdolell, M. (2003). Visual acuity assessment: A comparison of two tests for measuring children's vision. *Ophthalmic and Physiological Optics*, *23*(6), 541–546. https://doi.org/10.1046/j.1475-1313.2003.00150.x

Jones, J. P., & Palmer, L. A. (1987). An evaluation of the two-dimensional Gabor filter model of simple receptive fields in cat striate cortex. *Journal of Neurophysiology*, *58*(6), 1233–1258. https://doi.org/10.1152/jn.1987.58.6.1233

Jones, J. P., Stepnoski, A., & Palmer, L. A. (1987). The two-dimensional spectral structure of simple receptive fields in cat striate cortex. *Journal of Neurophysiology*, *58*(6), 1212–1232. https://doi.org/10.1152/jn.1987.58.6.1212

Ju, N.-S., Guan, S.-C., Tao, L., Tang, S.-M., & Yu, C. (2021). Orientation Tuning and End-stopping in Macaque V1 Studied with Two-photon Calcium Imaging. *Cerebral Cortex*, *31*(4), 2085–2097. https://doi.org/10.1093/cercor/bhaa346

Kalia, M., & Whitteridge, D. (1973). The visual areas in the splenial sulcus of the cat. *The Journal of Physiology*, *232*(2), 275–283. https://doi.org/10.1113/jphysiol.1973.sp010269

Kamitani, Y., & Tong, F. (2005). Decoding the visual and subjective contents of the human brain. *Nature Neuroscience*, *8*(5), 679–685. https://doi.org/10.1038/nn1444

Kandel, E. R., Koester, J., Mack, S., & Siegelbaum, S. (Eds.). (2021). *Principles of neural science* (Sixth edition). McGraw Hill.

Kaspiris-Rousellis, C., Siettos, C. I., Evdokimidis, I., & Smyrnis, N. (2017). Reaching to virtual targets: The oblique effect reloaded in 3-D. *Neuroscience*, *343*, 128–139. https://doi.org/10.1016/j.neuroscience.2016.11.039

Kastner, S., Schneider, K. A., & Wunderlich, K. (2006). Beyond a relay nucleus: Neuroimaging views on the human LGN. *Progress in Brain Research*, *155*, 125–143. https://doi.org/10.1016/S0079-6123(06)55008-3

Katz, L. C., & Shatz, C. J. (1996). Synaptic Activity and the Construction of Cortical Circuits. *Science*, *274*(5290), 1133–1138. https://doi.org/10.1126/science.274.5290.1133

Keil, M. S., & Cristóbal, G. (2000). Separating the chaff from the wheat: Possible origins of the oblique effect. *Journal of the Optical Society of America A*, *17*(4), 697. https://doi.org/10.1364/JOSAA.17.000697

Kelly, J. G., & Matthews, N. (2011). Attentional oblique effect when judging simultaneity. *Journal of Vision*, *11*(6), 1–15. https://doi.org/10.1167/11.6.10

Kennedy, H., & Orban, G. A. (1979). Preferences for horizontal or vertical orientation in cat visual cortical neurones [proceedings]. *The Journal of Physiology*, *296*, 61P-62P.

Kirchhoff, B. A., & Buckner, R. L. (2006). Functional-Anatomic Correlates of Individual Differences in Memory. *Neuron*, *51*(2), 263–274. https://doi.org/10.1016/j.neuron.2006.06.006

Klein, M., & Birch, D. G. (2009). Psychophysical assessment of low visual function in patients with retinal degenerative diseases (RDDs) with the Diagnosys full-field stimulus threshold (D-FST). *Documenta Ophthalmologica*, *119*(3), 217–224. https://doi.org/10.1007/s10633-009-9204-7

Koch, E., Jin, J., Alonso, J. M., & Zaidi, Q. (2016). Functional implications of orientation

maps in primary visual cortex. *Nature Communications*, *7*(1), 13529. https://doi.org/10.1038/ncomms13529

Koelewijn, L., Dumont, J. R., Muthukumaraswamy, S. D., Rich, A. N., & Singh, K. D. (2011). Induced and evoked neural correlates of orientation selectivity in human visual cortex. *NeuroImage*, *54*(4), 2983–2993. https://doi.org/10.1016/j.neuroimage.2010.11.045

Kritzer, M., Cowey, A., & Somogyi, P. (1992). Patterns of Interlaminar and Intralaminar Gabaergic Connections Distinguish Striate (v1) and Extrastriate (v2, V4) Visual Cortices and Their Functionally Specialized Subdivisions in the Rhesus-Monkey. *Journal of Neuroscience*, *12*(11), 4545–4564.

Krubitzer, L. (2007). The magnificent compromise: Cortical field evolution in mammals. *Neuron*, *56*(2), 201–208. https://doi.org/10.1016/j.neuron.2007.10.002

Krukowski, A. E., & Stone, L. S. (2005). Expansion of direction space around the cardinal axes revealed by smooth pursuit eye movements. *Neuron*, *45*(2), 315–323. https://doi.org/10.1016/j.neuron.2005.01.005

Kukkonen, H., Rovamo, J., Tiippana, K., & Näsänen, R. (1993). Michelson contrast, RMS contrast and energy of various spatial stimuli at threshold. *Vision Research*, *33*(10), 1431–1436. https://doi.org/10.1016/0042-6989(93)90049-3

Kulikowski, J. J., Abadi, R., & King-Smith, P. E. (1973). Orientational selectivity of grating and line detectors in human vision. *Vision Research*, *13*(8), 1479–1486. https://doi.org/10.1016/0042-6989(73)90007-2

Kulikowski, J. J., & Tolhurst, D. J. (1973). Psychophysical evidence for sustained and transient detectors in human vision. *The Journal of Physiology*, *232*(1), 149–162. https://doi.org/10.1113/jphysiol.1973.sp010261

Lagnado, L. (2002). Signal Amplification: Let's Turn Down The Lights. *Current Biology*, *12*(6), R215–R217. https://doi.org/10.1016/S0960-9822(02)00754-6

Lamb, T., & Pugh, E. (1992). A Quantitative Account of the Activation Steps Involved in Phototransduction in Amphibian Photoreceptors. *Journal of Physiology*, *449*, 719–758. https://doi.org/10.1113/jphysiol.1992.sp019111

Lampl, I., Anderson, J. S., Gillespie, D. C., & Ferster, D. (2001). Prediction of Orientation Selectivity from Receptive Field Architecture in Simple Cells of Cat Visual Cortex. *Neuron*, *30*(1), 263–274. https://doi.org/10.1016/S0896-6273(01)00278-1

Law, M. I., Zahs, K. R., & Stryker, M. P. (1988). Organization of primary visual cortex (area 17) in the ferret. *Journal of Comparative Neurology*, *278*(2), 157–180. https://doi.org/10.1002/cne.902780202

Leadbeater, R. J., McGraw, P., & Ledgeway, T. (2023). Assessing the reliability of web-based measurements of visual function. *Behavior Research Methods*. https://doi.org/10.3758/s13428-022-02057-2

Lee, B. B., Martin, P. R., & Grünert, U. (2010). Retinal connectivity and primate vision. *Progress in Retinal and Eye Research*, *29*(6), 622–639. https://doi.org/10.1016/j.preteyeres.2010.08.004

Lee, C., Rohrer, W. H., & Sparks, D. L. (1988). Population coding of saccadic eye movements by neurons in the superior colliculus. *Nature*, *332*(6162), 357–360. https://doi.org/10.1038/332357a0

Lee, S.-H., Kwan, A. C., Zhang, S., Phoumthipphavong, V., Flannery, J. G., Masmanidis, S. C., Taniguchi, H., Huang, Z. J., Zhang, F., Boyden, E. S., Deisseroth, K., & Dan, Y. (2012). Activation of specific interneurons improves V1 feature selectivity and visual perception. *Nature*, *488*(7411), 379–383. https://doi.org/10.1038/nature11312

5905 Legge, G. E. (1981). A power law for contrast discrimination. *Vision Research*, *21*(4), 457–
5906 467. https://doi.org/10.1016/0042-6989(81)90092-4
5907 Legge, G. E., & Foley, J. M. (1980). Contrast masking in human vision. *Journal of the*
5908 *Optical Society of America*, *70*(12), 1458. https://doi.org/10.1364/JOSA.70.001458
5909 LeVay, S., & Voigt, T. (1988). Ocular dominance and disparity coding in cat visual cortex.
5910 *Visual Neuroscience*, *1*(4), 395–414. https://doi.org/10.1017/S0952523800004168
5911 Leventhal, A. G. (1983). Relationship between preferred orientation and receptive field
5912 position of neurons in cat striate cortex. *Journal of Comparative Neurology*, *220*(4),
5913 476–483. https://doi.org/10.1002/cne.902200409
5914 Leventhal, A. G., & Hirsch, H. V. (1977). Effects of early experience upon orientation
5915 sensitivity and binocularity of neurons in visual cortex of cats. *Proceedings of the*
5916 *National Academy of Sciences of the United States of America*, *74*(3), 1272–1276.
5917 https://doi.org/10.1073/pnas.74.3.1272
5918 Levitt, H. (1971). Transformed Up-Down Methods in Psychoacoustics. *The Journal of the*
5919 *Acoustical Society of America*, *49*(2B), 467–477. https://doi.org/10.1121/1.1912375
5920 Levitt, J. B., Kiper, D. C., & Movshon, J. A. (1994). Receptive fields and functional
5921 architecture of macaque V2. *Journal of Neurophysiology*, *71*(6), 2517–2542.
5922 https://doi.org/10.1152/jn.1994.71.6.2517
5923 Li, B., Peterson, M. R., & Freeman, R. D. (2003). Oblique effect: A neural basis in the visual
5924 cortex. *Journal of Neurophysiology*, *90*(1), 204–217.
5925 https://doi.org/10.1152/jn.00954.2002
5926 Li, B., Thompson, J. K., Duong, T., Peterson, M. R., & Freeman, R. D. (2006). Origins of
5927 Cross-Orientation Suppression in the Visual Cortex. *Journal of Neurophysiology*,
5928 *96*(4), 1755–1764. https://doi.org/10.1152/jn.00425.2006

Li, W., Thier, P., & Wehrhahn, C. (2000). Contextual Influence on Orientation Discrimination of Humans and Responses of Neurons in V1 of Alert Monkeys. *Journal of Neurophysiology*, *83*(2), 941–954. https://doi.org/10.1152/jn.2000.83.2.941

Liang, Z., Shen, W., & Shou, T. (2007). Enhancement of oblique effect in the cat's primary visual cortex via orientation preference shifting induced by excitatory feedback from higher-order cortical area 21a. *Neuroscience*, *145*(1), 377–383. https://doi.org/10.1016/j.neuroscience.2006.11.051

Linden, D. E. J. (2005). The p300: Where in the brain is it produced and what does it tell us? *The Neuroscientist: A Review Journal Bringing Neurobiology, Neurology and Psychiatry*, *11*(6), 563–576. https://doi.org/10.1177/1073858405280524

Liu, G. B., & Pettigrew, J. D. (2003). Orientation mosaic in barn owl's visual Wulst revealed by optical imaging: Comparison with cat and monkey striate and extra-striate areas. *Brain Research*, *961*(1), 153–158. https://doi.org/10.1016/s0006-8993(02)03747-2

Liu, Y.-J., Hashemi-Nezhad, M., & Lyon, D. C. (2015). Contrast invariance of orientation tuning in cat primary visual cortex neurons depends on stimulus size: Contrast invariance in V1 depends on stimulus size. *The Journal of Physiology*, *593*(19), 4485–4498. https://doi.org/10.1113/JP271180

Liu, Z., Gaska, J. P., Jacobson, L. D., & Pollen, D. A. (1992). Interneuronal interaction between members of quadrature phase and anti-phase pairs in the cat's visual cortex. *Vision Research*, *32*(7), 1193–1198. https://doi.org/10.1016/0042-6989(92)90213-3

Logothetis, N. K., Pauls, J., Augath, M., Trinath, T., & Oeltermann, A. (2001). Neurophysiological investigation of the basis of the fMRI signal. *Nature*, *412*(6843), 150–157. https://doi.org/10.1038/35084005

Lombardo, M., & Lombardo, G. (2010). Wave aberration of human eyes and new descriptors

of image optical quality and visual performance. *Journal of Cataract and Refractive Surgery*, *36*(2), 313–331. https://doi.org/10.1016/j.jcrs.2009.09.026

Long, G. M., & Tuck, J. P. (1991). Comparison of Contrast Sensitivity Functions across Three Orientations: Implications for Theory and Testing. *Perception*, *20*(3), 373–380. https://doi.org/10.1068/p200373

Lu, H. D., Chen, G., Cai, J., & Roe, A. W. (2017). Intrinsic signal optical imaging of visual brain activity: Tracking of fast cortical dynamics. *NeuroImage*, *148*, 160–168. https://doi.org/10.1016/j.neuroimage.2017.01.006

Lu, H. D., Chen, G., Tanigawa, H., & Roe, A. W. (2010). A motion direction map in macaque V2. *Neuron*, *68*(5), 1002–1013. https://doi.org/10.1016/j.neuron.2010.11.020

Lu, T., Liang, L., & Wang, X. (2001). Temporal and rate representations of time-varying signals in the auditory cortex of awake primates. *Nature Neuroscience*, *4*(11), 1131–1138. https://doi.org/10.1038/nn737

Lu, Y., Yin, J., Chen, Z., Gong, H., Liu, Y., Qian, L., Li, X., Liu, R., Andolina, I. M., & Wang, W. (2018). Revealing Detail along the Visual Hierarchy: Neural Clustering Preserves Acuity from V1 to V4. *Neuron*, *98*(2), 417-428.e3. https://doi.org/10.1016/j.neuron.2018.03.009

Lu, Z.-L., & Dosher, B. A. (2008). Characterizing observers using external noise and observer models: Assessing internal representations with external noise. *Psychological Review*, *115*(1), 44–82. https://doi.org/10.1037/0033-295X.115.1.44

Lund, J. S. (1973). Organization of neurons in the visual cortex, area 17, of the monkey (Macaca mulatta). *The Journal of Comparative Neurology*, *147*(4), 455–495. https://doi.org/10.1002/cne.901470404

Lund, J. S., Lund, R. D., Hendrickson, A. E., Bunt, A. H., & Fuchs, A. F. (1975). The origin

of efferent pathways from the primary visual cortex, area 17, of the macaque monkey as shown by retrograde transport of horseradish peroxidase. *Journal of Comparative Neurology*, *164*(3), 287–303. https://doi.org/10.1002/cne.901640303

Lund, N. J., & MacKay, D. M. (1983). Sleep and the McCollough effect. *Vision Research*, *23*(9), 903–906. https://doi.org/10.1016/0042-6989(83)90059-7

Luo, D.-G., Xue, T., & Yau, K.-W. (2008). How vision begins: An odyssey. *Proceedings of the National Academy of Sciences*, *105*(29), 9855–9862. https://doi.org/10.1073/pnas.0708405105

Lupión Durán, T., García-Ben, A., Rodríguez Méndez, V., Gálvez Alcázar, L., García-Ben, E., & García-Campos, J. M. (2021). Study of visual acuity and contrast sensitivity in diabetic patients with and without non-proliferative diabetic retinopathy. *International Ophthalmology*. https://doi.org/10.1007/s10792-021-01930-x

Lyakhovetskii, V., Chetverikov, A., Zelenskaya, I., Tomilovskaya, E., & Karpinskaia, V. (2023). Perception of length and orientation in dry immersion. *Frontiers in Neural Circuits*, *17*, 1157228. https://doi.org/10.3389/fncir.2023.1157228

Lyon, D. C., & Rabideau, C. (2012). Lack of robust LGN label following transneuronal rabies virus injections into macaque area V4. *The Journal of Comparative Neurology*, *520*(11), 2500–2511. https://doi.org/10.1002/cne.23050

Mackintosh, J., & Sutherland, N. S. (1963). Visual discrimination by the goldfish: The orientation of rectangles. *Animal Behaviour*, *11*(1), 135–141. https://doi.org/10.1016/0003-3472(63)90021-6

Maffei, L., & Campbell, F. W. (1970). Neurophysiological Localization of the Vertical and Horizontal Visual Coordinates in Man. *Science*, *167*(3917), 386–387. https://doi.org/10.1126/science.167.3917.386

6001 Mahroo, O. A. (2023). Visual electrophysiology and “the potential of the potentials”. *Eye*,
6002 *37*(12), Article 12. https://doi.org/10.1038/s41433-023-02491-2
6003 Maloney, R. T., & Clifford, C. W. G. (2015). Orientation anisotropies in human primary
6004 visual cortex depend on contrast. *NeuroImage*, *119*, 129–145.
6005 https://doi.org/10.1016/j.neuroimage.2015.06.034
6006 Mangel, S. C. (1991). Analysis of the horizontal cell contribution to the receptive field
6007 surround of ganglion cells in the rabbit retina. *The Journal of Physiology*, *442*(1),
6008 211–234. https://doi.org/10.1113/jphysiol.1991.sp018790
6009 Mannion, D. J., McDonald, J. S., & Clifford, C. W. G. (2010). Orientation Anisotropies in
6010 Human Visual Cortex. *Journal of Neurophysiology*, *103*(6), 3465–3471.
6011 https://doi.org/10.1152/jn.00190.2010
6012 Mansfield, R. J. (1974). Neural basis of orientation perception in primate vision. *Science*,
6013 *186*(4169), 1133–1135. https://doi.org/10.1126/science.186.4169.1133
6014 Mareschal, I., & Shapley, R. M. (2004). Effects of contrast and size on orientation
6015 discrimination. *Vision Research*, *44*(1), 57–67.
6016 https://doi.org/10.1016/j.visres.2003.07.009
6017 Mariño, J., Schummers, J., Lyon, D. C., Schwabe, L., Beck, O., Wiesing, P., Obermayer, K.,
6018 & Sur, M. (2005). Invariant computations in local cortical networks with balanced
6019 excitation and inhibition. *Nature Neuroscience*, *8*(2), 194–201.
6020 https://doi.org/10.1038/nn1391
6021 Markov, N. T., Misery, P., Falchier, A., Lamy, C., Vezoli, J., Quilodran, R., Gariel, M. A.,
6022 Giroud, P., Ercsey-Ravasz, M., Pilaz, L. J., Huissoud, C., Barone, P., Dehay, C.,
6023 Toroczkai, Z., Van Essen, D. C., Kennedy, H., & Knoblauch, K. (2011). Weight
6024 Consistency Specifies Regularities of Macaque Cortical Networks. *Cerebral Cortex*

(New York, NY), *21*(6), 1254–1272. https://doi.org/10.1093/cercor/bhq201

Martinez, L. M., & Alonso, J.-M. (2003). Complex Receptive Fields in Primary Visual Cortex. *The Neuroscientist*, *9*(5), 317–331. https://doi.org/10.1177/1073858403252732

Martinez, L. M., Wang, Q., Clay Reid, R., Pillai, C., Alonso, J.-M., Sommer, F. T., & Hirsch, J. A. (2005). Receptive field structure varies with layer in the primary visual cortex. *Nature Neuroscience*, *8*(3), 372–379. https://doi.org/10.1038/nn1404

Masland, R. H. (2012). The Neuronal Organization of the Retina. *Neuron*, *76*(2), 266–280. https://doi.org/10.1016/j.neuron.2012.10.002

Matin, E., Rubsamen, C., & Vannata, D. (1987). Orientation discrimination as a function of orientation and spatial frequency. *Perception & Psychophysics*, *41*(4), 303–307. https://doi.org/10.3758/BF03208230

Matthews, N., & Qian, N. (1999). Axis-of-motion affects direction discrimination, not speed discrimination. *Vision Research*, *39*(13), 2205–2211. https://doi.org/10.1016/S0042-6989(98)00300-9

Maunsell, J. H. R. (2015). Neuronal Mechanisms of Visual Attention. *Annual Review of Vision Science*, *1*(1), 373–391. https://doi.org/10.1146/annurev-vision-082114-035431

Maunsell, J. H., & van Essen, D. C. (1983). The connections of the middle temporal visual area (MT) and their relationship to a cortical hierarchy in the macaque monkey. *The Journal of Neuroscience: The Official Journal of the Society for Neuroscience*, *3*(12), 2563–2586. https://doi.org/10.1523/JNEUROSCI.03-12-02563.1983

May, K. A., & Solomon, J. A. (2015a). Connecting psychophysical performance to neuronal response properties I: Discrimination of suprathreshold stimuli. *Journal of Vision*, *15*(6), 8. https://doi.org/10.1167/15.6.8

6049 May, K. A., & Solomon, J. A. (2015b). Connecting psychophysical performance to neuronal
6050 response properties II: Contrast decoding and detection. *Journal of Vision*, *15*(6), 9.
6051 https://doi.org/10.1167/15.6.9
6052 Mayer, M. J. (1983). Practice improves adults' sensitivity to diagonals. *Vision Research*,
6053 *23*(5), 547–550. https://doi.org/10.1016/0042-6989(83)90130-X
6054 Mazade, R., & Alonso, J. M. (2017). Thalamocortical processing in vision. *Visual*
6055 *Neuroscience*, *34*, E007. https://doi.org/10.1017/S0952523817000049
6056 Mazurek, M., Kager, M., & Van Hooser, S. D. (2014). Robust quantification of orientation
6057 selectivity and direction selectivity. *Frontiers in Neural Circuits*, *8*.
6058 https://doi.org/10.3389/fncir.2014.00092
6059 McAlinden, C., Khadka, J., & Pesudovs, K. (2011). Statistical methods for conducting
6060 agreement (comparison of clinical tests) and precision (repeatability or
6061 reproducibility) studies in optometry and ophthalmology. *Ophthalmic and*
6062 *Physiological Optics*, *31*(4), 330–338. https://doi.org/10.1111/j.1475-
6063 1313.2011.00851.x
6064 McDonald, J. S., Mannion, D. J., & Clifford, C. W. G. (2012). Gain control in the response of
6065 human visual cortex to plaids. *Journal of Neurophysiology*, *107*(9), 2570–2580.
6066 https://doi.org/10.1152/jn.00616.2011
6067 McGovern, D. P., Walsh, K. S., Bell, J., & Newell, F. N. (2017). Individual differences in
6068 context-dependent effects reveal common mechanisms underlying the direction
6069 aftereffect and direction repulsion. *Vision Research*, *141*, 109–116.
6070 https://doi.org/10.1016/j.visres.2016.08.009
6071 McIlwain, J. T. (1977). Orientation of slit pupil and visual streak in the eye of the cat. *Journal*
6072 *of Comparative Neurology*, *175*(3), 337–344. https://doi.org/10.1002/cne.901750307

6073 McLaughlin, D., Shapley, R., Shelley, M., & Wielaard, D. J. (2000). A neuronal network
6074 model of macaque primary visual cortex (V1): Orientation selectivity and dynamics in
6075 the input layer 4Cα. *Proceedings of the National Academy of Sciences*, *97*(14), 8087–
6076 8092. https://doi.org/10.1073/pnas.110135097
6077 McMahon, M. J., & MacLeod, D. I. A. (2003). The origin of the oblique effect examined with
6078 pattern adaptation and masking. *Journal of Vision*, *3*(3), 230–239.
6079 https://doi.org/10.1167/3.3.4
6080 Meese, T. S., & Holmes, D. J. (2010). Orientation masking and cross-orientation suppression
6081 (XOS): Implications for estimates of filter bandwidth. *Journal of Vision*, *10*(12), 9–9.
6082 https://doi.org/10.1167/10.12.9
6083 Meinhardt, G., Meinhardt-Injac, B., & Persike, M. (2019). Orientation-invariance of
6084 individual differences in three face processing tasks. *Royal Society Open Science*,
6085 *6*(1), 181350. https://doi.org/10.1098/rsos.181350
6086 Mejias, J. F., Murray, J. D., Kennedy, H., & Wang, X.-J. (2016). Feedforward and feedback
6087 frequency-dependent interactions in a large-scale laminar network of the primate
6088 cortex. *Science Advances*, *2*(11), e1601335. https://doi.org/10.1126/sciadv.1601335
6089 Merbs, S., & Nathans, J. (1992). Absorption-Spectra of Human Cone Pigments. *Nature*,
6090 *356*(6368), 433–435. https://doi.org/10.1038/356433a0
6091 Metha, A. B., Vingrys, A. J., & Badcock, D. R. (1993). Calibration of a color monitor for
6092 visual psychophysics. *Behavior Research Methods, Instruments, & Computers*, *25*(3),
6093 371–383. https://doi.org/10.3758/BF03204528
6094 Michalareas, G., Vezoli, J., van Pelt, S., Schoffelen, J.-M., Kennedy, H., & Fries, P. (2016).
6095 Alpha-Beta and Gamma Rhythms Subserve Feedback and Feedforward Influences
6096 among Human Visual Cortical Areas. *Neuron*, *89*(2), 384–397.

https://doi.org/10.1016/j.neuron.2015.12.018

Michel, C. M., & Brunet, D. (2019). EEG Source Imaging: A Practical Review of the Analysis Steps. *Frontiers in Neurology*, *10*, 325. https://doi.org/10.3389/fneur.2019.00325

Mikellidou, K., Cicchini, G. M., Thompson, P. G., & Burr, D. C. (2015). The oblique effect is both allocentric and egocentric. *Journal of Vision*, *15*(8), 24. https://doi.org/10.1167/15.8.24

Mikhailova, E. S., Gerasimenko, N. Yu., Krylova, M. A., Izyurov, I. V., & Slavutskaya, A. V. (2015). Mechanisms of orientation sensitivity of human visual system: Part II. Neural patterns of early processing of information about line orientation. *Human Physiology*, *41*(3), 229–241. https://doi.org/10.1134/S0362119715030111

Miller, J. P., Jacobs, G. A., & Theunissen, F. E. (1991). Representation of sensory information in the cricket cercal sensory system. I. Response properties of the primary interneurons. *Journal of Neurophysiology*, *66*(5), 1680–1689. https://doi.org/10.1152/jn.1991.66.5.1680

Milner, A. D., & Goodale, M. A. (2008). Two visual systems re-viewed. *Neuropsychologia*, *46*(3), 774–785. https://doi.org/10.1016/j.neuropsychologia.2007.10.005

Mitchell, D. E., Freeman, R. D., & Westheimer, G. (1967). Effect of Orientation on the Modulation Sensitivity for Interference Fringes on the Retina*. *Journal of the Optical Society of America*, *57*(2), 246. https://doi.org/10.1364/JOSA.57.000246

Mohan, Y. S., Jayakumar, J., Lloyd, E. K. J., Levichkina, E., & Vidyasagar, T. R. (2019). Diversity of Feature Selectivity in Macaque Visual Cortex Arising from a Limited Number of Broadly Tuned Input Channels. *Cerebral Cortex*, *29*(12), 5255–5268. https://doi.org/10.1093/cercor/bhz063

Mollon, J. D., & Baker, M. R. (1995). The use of CRT displays in research on colour vision. In B. Drum, A. J. Adams, C. R. Cavonius, S. J. Dain, G. Haegerstrom-Portnoy, K. Kitahara, K. Knoblauch, A. Kurtenbach, B. B. Lee, J. Mollon, J. D. Moreland, J. Pokorny, L. T. Sharpe, H. A. Sperling, W. H. Swanson, & E. Zrenner (Eds.), *Colour Vision Deficiencies XII* (Vol. 57, pp. 423–444). Springer Netherlands. https://doi.org/10.1007/978-94-011-0507-1_51

Mollon, J. D., Bosten, J. M., Peterzell, D. H., & Webster, M. A. (2017). Individual differences in visual science: What can be learned and what is good experimental practice? *Vision Research*, *141*, 4–15. https://doi.org/10.1016/j.visres.2017.11.001

Monier, C., Chavane, F., Baudot, P., Graham, L. J., & Frégnac, Y. (2003). Orientation and direction selectivity of synaptic inputs in visual cortical neurons: A diversity of combinations produces spike tuning. *Neuron*, *37*(4), 663–680. https://doi.org/10.1016/s0896-6273(03)00064-3

Moreland, J. C., & Boynton, G. M. (2020). *Divided attention for feature-based selection in visual cortex* (p. 2020.01.27.922047). bioRxiv. https://doi.org/10.1101/2020.01.27.922047

Moreland, J., Palmer, J., & Boynton, G. (2017). Divided attention effects are larger for change detection than for simple detection. *Journal of Vision*, *17*(10), 963. https://doi.org/10.1167/17.10.963

Morrone, M. C., Burr, D. C., & Maffei, L. (1982). Functional implications of cross-orientation inhibition of cortical visual cells. I. Neurophysiological evidence. *Proceedings of the Royal Society of London. Series B, Biological Sciences*, *216*(1204), 335–354. https://doi.org/10.1098/rspb.1982.0078

Morrone, M. C., Burr, D. C., & Speed, H. D. (1987). Cross-orientation inhibition in cat is

GABA mediated. *Experimental Brain Research*, *67*(3). https://doi.org/10.1007/BF00247294

Moskowitz, A., & Sokol, S. (1985). Effect of stimulus orientation on the latency and amplitude of the VEP. *Investigative Ophthalmology & Visual Science*, *26*(2), 246–248.

Movshon, J. A., & Blakemore, C. (1973). Orientation Specificity and Spatial Selectivity in Human Vision. *Perception*, *2*(1), 53–60. https://doi.org/10.1068/p020053

Murgas, K. A., Wilson, A. M., Michael, V., & Glickfeld, L. L. (2020). Unique Spatial Integration in Mouse Primary Visual Cortex and Higher Visual Areas. *The Journal of Neuroscience*, *40*(9), 1862–1873. https://doi.org/10.1523/JNEUROSCI.1997-19.2020

Muthukumaraswamy, S. D. (2013). High-frequency brain activity and muscle artifacts in MEG/EEG: A review and recommendations. *Frontiers in Human Neuroscience*, *7*(MAR), 1–11. https://doi.org/10.3389/fnhum.2013.00138

Nachmias, J. (1960). Meridional Variations in Visual Acuity and Eye Movements during Fixation*. *Journal of the Optical Society of America*, *50*(6), 569. https://doi.org/10.1364/JOSA.50.000569

Naka, K. I., & Rushton, W. A. H. (1966). S-potentials from luminosity units in the retina of fish (Cyprinidae). *The Journal of Physiology*, *185*(3), 587–599. https://doi.org/10.1113/jphysiol.1966.sp008003

Nandy, A. S., Sharpee, T. O., Reynolds, J. H., & Mitchell, J. F. (2013). The Fine Structure of Shape Tuning in Area V4. *Neuron*, *78*(6), 1102–1115. https://doi.org/10.1016/j.neuron.2013.04.016

Nasr, S., & Tootell, R. B. H. (2012). A cardinal orientation bias in scene-selective visual cortex. *Journal of Neuroscience*, *32*(43), 14921–14926.

https://doi.org/10.1523/JNEUROSCI.2036-12.2012

Nauhaus, I., Benucci, A., Carandini, M., & Ringach, D. L. (2008). Neuronal selectivity and local map structure in visual cortex. *Bone*. https://doi.org/10.1038/jid.2014.371

Neisser, U. (1967). *Cognitive psychology*. Prentice Hall.

Nelson, J. I., Kato, H., & Bishop, P. O. (1977). Discrimination of orientation and position disparities by binocularly activated neurons in cat straite cortex. *Journal of Neurophysiology*, *40*(2), 260–283. https://doi.org/10.1152/jn.1977.40.2.260

Nelson, S. (1991a). Temporal interactions in the cat visual system. I. Orientation- selective suppression in the visual cortex. *The Journal of Neuroscience*, *11*(2), 344–356. https://doi.org/10.1523/JNEUROSCI.11-02-00344.1991

Nelson, S. (1991b). Temporal interactions in the cat visual system. II. Suppressive and facilitatory effects in the lateral geniculate nucleus. *The Journal of Neuroscience*, *11*(2), 357–368. https://doi.org/10.1523/JNEUROSCI.11-02-00357.1991

Noda, H., Freeman, R. B., Gies, B., & Creutzfeldt, O. D. (1971). Neuronal responses in the visual cortex of awake cats to stationary and moving targets. *Experimental Brain Research*, *12*(4), 389–405. https://doi.org/10.1007/BF00234494

Normann, R. A., & Werblin, F. S. (1974). Control of Retinal Sensitivity. *Journal of General Physiology*, *63*(1), 37–61. https://doi.org/10.1085/jgp.63.1.37

O'Connor, D. H., Fukui, M. M., Pinsk, M. A., & Kastner, S. (2002). Attention modulates responses in the human lateral geniculate nucleus. *Nature Neuroscience*, *5*(11), 1203–1209. https://doi.org/10.1038/nn957

Ogata, N. G., Boer, E. R., Daga, F. B., Jammal, A. A., Stringham, J. M., & Medeiros, F. A. (2019). Visual Crowding in Glaucoma. *Investigative Ophthalmology & Visual Science*, *60*(2), 538–543. https://doi.org/10.1167/iovs.18-25150

6193 Ohki, K., Chung, S., Ch'ng, Y. H., Kara, P., & Reid, R. C. (2005). Functional imaging with
6194 cellular resolution reveals precise micro-architecture in visual cortex. *Nature*,
6195 *433*(7026), 597–603. https://doi.org/10.1038/nature03274
6196 Ohki, K., Chung, S., Kara, P., Hübener, M., Bonhoeffer, T., & Reid, R. C. (2006). Highly
6197 ordered arrangement of single neurons in orientation pinwheels. *Nature*, *442*(7105),
6198 925–928. https://doi.org/10.1038/nature05019
6199 Orban, G. A., & Kennedy, H. (1981). The influence of eccentricity on receptive field types
6200 and orientation selectivity in areas 17 and 18 of the cat. *Brain Research*, *208*(1), 203–
6201 208. https://doi.org/10.1016/0006-8993(81)90633-8
6202 Orban, G. A., Vandenbussche, E., & Vogels, R. (1984a). Human Orientation Discrimination
6203 Tested With Long Stimuli. *Vision Research*.
6204 Orban, G. A., Vandenbussche, E., & Vogels, R. (1984b). *Meridional Variations and Other*
6205 *Properties Suggesting That Acuity and Orientation Discrimination Rely on Different*
6206 *Neuronal Mechanisms*. *4*(March 1983). https://doi.org/10.1016/0275-5408(84)90058-
6207 9
6208 Orban, G., Vandenbussche, E., Rufin Vogels, & Vogels, R. (1984). Human orientation
6209 discrimination tested with long stimuli. *Vision Research*, *24*(2), 121–128.
6210 https://doi.org/10.1016/0042-6989(84)90097-x
6211 Otero-Millan, J., Troncoso, X. G., Macknik, S. L., Serrano-Pedraza, I., & Martinez-Conde, S.
6212 (2008). Saccades and microsaccades during visual fixation, exploration, and search:
6213 Foundations for a common saccadic generator. *Journal of Vision*, *8*(14), 21–21.
6214 https://doi.org/10.1167/8.14.21
6215 Pantazis, D., Fang, M., Qin, S., Mohsenzadeh, Y., Li, Q., & Cichy, R. M. (2018). Decoding
6216 the orientation of contrast edges from MEG evoked and induced responses.

NeuroImage, *180*, 267–279. https://doi.org/10.1016/j.neuroimage.2017.07.022

Parker, A. J. (2007). Binocular depth perception and the cerebral cortex. *Nature Reviews Neuroscience*, *8*(5), 379–391. https://doi.org/10.1038/nrn2131

Parker, A. J. (2016). Vision in our three-dimensional world. *Philosophical Transactions of the Royal Society B: Biological Sciences*, *371*(1697), 20150251. https://doi.org/10.1098/rstb.2015.0251

Parriss, J. R. (1964). A Technique for Testing the Cat's Discrimination of Differently Oriented Rectangles. *Nature*, *202*(4934), 771–773. https://doi.org/10.1038/202771a0

Pasik, P., Pasik, T., Hamori, J., & Szentagothai, J. (1973). Golgi type II interneurons in the neuronal circuit of the monkey lateral geniculate nucleus. *Experimental Brain Research*, *17*(1). https://doi.org/10.1007/BF00234561

Patterson, C. A., Wissig, S. C., & Kohn, A. (2013). Distinct Effects of Brief and Prolonged Adaptation on Orientation Tuning in Primary Visual Cortex. *The Journal of Neuroscience*, *33*(2), 532–543. https://doi.org/10.1523/JNEUROSCI.3345-12.2013

Patterson, R. D., & Nimmo-Smith, I. (1980). Off-frequency listening and auditory-filter asymmetry. *The Journal of the Acoustical Society of America*, *67*(1), 229–245. https://doi.org/10.1121/1.383732

Peirce, J., Gray, J. R., Simpson, S., MacAskill, M., Höchenberger, R., Sogo, H., Kastman, E., & Lindeløv, J. K. (2019). PsychoPy2: Experiments in behavior made easy. *Behavior Research Methods*, *51*(1), 195–203. https://doi.org/10.3758/s13428-018-01193-y

Pelli, D. G., & Bex, P. (2013). Measuring contrast sensitivity. *Vision Research*, *90*, 10–14. https://doi.org/10.1016/j.visres.2013.04.015

Perrett, D. I., Smith, P. A., Potter, D. D., Mistlin, A. J., Head, A. S., Milner, A. D., & Jeeves, M. A. (1985). Visual cells in the temporal cortex sensitive to face view and gaze

6241 direction. *Proceedings of the Royal Society of London. Series B, Biological Sciences*,
6242 *223*(1232), 293–317. https://doi.org/10.1098/rspb.1985.0003
6243 Peterzell, D. H., & Kennedy, J. F. (2016). Discovering Sensory Processes Using Individual
6244 Differences: A Review and Factor Analytic Manifesto. *Electronic Imaging*, *28*(16), 1–
6245 11. https://doi.org/10.2352/ISSN.2470-1173.2016.16.HVEI-112
6246 Petro, L. S., Vizioli, L., & Muckli, L. (2014). Contributions of cortical feedback to sensory
6247 processing in primary visual cortex. *Frontiers in Psychology*, *5*.
6248 https://doi.org/10.3389/fpsyg.2014.01223
6249 Pettigrew, J. D., Nikara, T., & Bishop, P. O. (1968). Binocular interaction on single units in
6250 cat striate cortex: Simultaneous stimulation by single moving slit with receptive fields
6251 in correspondence. *Experimental Brain Research*, *6*(4), 391–410.
6252 https://doi.org/10.1007/BF00233186
6253 Pettine, W. W., Steinmetz, N. A., & Moore, T. (2019). Laminar segregation of sensory coding
6254 and behavioral readout in macaque V4. *Proceedings of the National Academy of*
6255 *Sciences of the United States of America*, *116*(29), 14749–14754.
6256 https://doi.org/10.1073/pnas.1819398116
6257 Pewsey, A., Lewis, T., & Jones, M. C. (2007). The wrapped family of circular distributions.
6258 *Australian & New Zealand Journal of Statistics*, *49*(1), 79–91.
6259 https://doi.org/10.1111/j.1467-842X.2006.00465.x
6260 Phillips, G. C., & Wilson, H. R. (1984). Orientation bandwidths of spatial mechanisms
6261 measured by masking. *Journal of the Optical Society of America A*, *1*(2), 226.
6262 https://doi.org/10.1364/JOSAA.1.000226
6263 Pilz, K. S., Äijälä, J. M., & Manassi, M. (2020). Selective age-related changes in orientation
6264 perception. *Journal of Vision*, *20*(13), 13. https://doi.org/10.1167/jov.20.13.13

Pilz, K. S., & Papadaki, D. (2019). An advantage for horizontal motion direction discrimination. *Vision Research*, *158*, 164–172. https://doi.org/10.1016/j.visres.2019.03.005

Poggio, G. F., Doty, R. W., & Talbot, W. H. (1977). Foveal striate cortex of behaving monkey: Single-neuron responses to square-wave gratings during fixation of gaze. *Journal of Neurophysiology*, *40*(6), 1369–1391. https://doi.org/10.1152/jn.1977.40.6.1369

Poggio, G., Gonzalez, F., & Krause, F. (1988). Stereoscopic mechanisms in monkey visual cortex: Binocular correlation and disparity selectivity. *The Journal of Neuroscience*, *8*(12), 4531–4550. https://doi.org/10.1523/JNEUROSCI.08-12-04531.1988

Pointer, J. S. (1996). Evidence of a Global Oblique Effect in Human Extrafoveal Vision. *Perception*, *25*(5), 523–530. https://doi.org/10.1068/p250523

Poletti, M., & Rucci, M. (2016). A compact field guide to the study of microsaccades: Challenges and functions. *Vision Research*, *118*, 83–97. https://doi.org/10.1016/j.visres.2015.01.018

Pollen, D. A., & Ronner, S. F. (1981). Phase Relationships Between Adjacent Simple Cells in the Visual Cortex. *Science*, *212*(4501), 1409–1411. https://doi.org/10.1126/science.7233231

Pollen, D. A., & Ronner, S. F. (1983). Visual cortical neurons as localized spatial frequency filters. *IEEE Transactions on Systems, Man, and Cybernetics*, *SMC-13*(5), 907–916. https://doi.org/10.1109/TSMC.1983.6313086

Ponulak, F., & Kasinski, A. (2011). Introduction to spiking neural networks: Information processing, learning and applications. *Acta Neurobiologiae Experimentalis*, *71*(4), 409–433. https://doi.org/10.55782/ane-2011-1862

Pouget, A., Dayan, P., & Zemel, R. (2000). Information processing with population codes. *Nature Reviews Neuroscience*, *1*(2), 125–132. https://doi.org/10.1038/35039062

Priebe, N. J. (2016). Mechanisms of Orientation Selectivity in the Primary Visual Cortex. *Annual Review of Vision Science*, *2*(1), 85–107. https://doi.org/10.1146/annurev-vision-111815-114456

Priebe, N. J., & Ferster, D. (2008). Inhibition, Spike Threshold, and Stimulus Selectivity in Primary Visual Cortex. *Neuron*, *57*(4), 482–497. https://doi.org/10.1016/j.neuron.2008.02.005

Priebe, N. J., Mechler, F., Carandini, M., & Ferster, D. (2004). The contribution of spike threshold to the dichotomy of cortical simple and complex cells. *Nature Neuroscience*, *7*(10), 1113–1122. https://doi.org/10.1038/nn1310

Prince, S. J. D., Pointon, A. D., Cumming, B. G., & Parker, A. J. (2002). Quantitative analysis of the responses of V1 neurons to horizontal disparity in dynamic random-dot stereograms. *Journal of Neurophysiology*, *87*(1), 191–208. https://doi.org/10.1152/jn.00465.2000

Proverbio, A. M., Esposito, P., & Zani, A. (2002). Early involvement of the temporal area in attentional selection of grating orientation: An ERP study. *Cognitive Brain Research*, *13*(1), 139–151. https://doi.org/10.1016/S0926-6410(01)00103-3

Quick, R. F. (1974). A vector-magnitude model of contrast detection. *Kybernetik*, *16*(2), 65–67. https://doi.org/10.1007/BF00271628

Raiguel, S., Vogels, R., Mysore, S. G., & Orban, G. A. (2006). Learning to See the Difference Specifically Alters the Most Informative V4 Neurons. *Journal of Neuroscience*, *26*(24), 6589–6602. https://doi.org/10.1523/JNEUROSCI.0457-06.2006

Read, J. C. A. (2015). The place of human psychophysics in modern neuroscience.

Neuroscience, *296*, 116–129. https://doi.org/10.1016/j.neuroscience.2014.05.036

Read, J. C. A., & Cumming, B. G. (2004). Ocular Dominance Predicts Neither Strength Nor Class of Disparity Selectivity With Random-Dot Stimuli in Primate V1. *Journal of Neurophysiology*, *91*(3), 1271–1281. https://doi.org/10.1152/jn.00588.2003

Regan, D., & Beverley, K. I. (1985). Postadaptation orientation discrimination. *Journal of the Optical Society of America A*, *2*(2), 147–147. https://doi.org/10.1364/josaa.2.000147

Reid, R. C., & Alonso, J.-M. (1995). Specificity of monosynaptic connections from thalamus to visual cortex. *Nature*, *378*(6554), 281–284. https://doi.org/10.1038/378281a0

Reisbeck, T. E., & Gegenfurtner, K. R. (1998). Effects of contrast and temporal frequency on orientation discrimination for luminance and isoluminant stimuli. *Vision Research*, *38*(8), 1105–1117. https://doi.org/10.1016/S0042-6989(97)00240-X

Ribot, J., Tanaka, S., O'Hashi, K., & Ajima, A. (2008). Anisotropy in the representation of direction preferences in cat area 18. *European Journal of Neuroscience*, *27*(10), 2773–2780. https://doi.org/10.1111/j.1460-9568.2008.06219.x

Richards, W. (1979). Quantifying sensory channels: Generalizing colorimetry to orientation and texture, touch, and tones. *Sensory Processes*, *3*(3), 207–229.

Rieke, F., & Baylor, D. A. (1998). Single-photon detection by rod cells of the retina. *Reviews of Modern Physics*, *70*(3), 1027–1036. https://doi.org/10.1103/RevModPhys.70.1027

Rieke, F., Warland, D., Ruyter van Steveninck, R. R. de, & Bialek, W. S. (1999). *Spikes: Exploring the neural code* (First MIT Press paperback edition). The MIT Press.

Ringach, D. L. (2002). Spatial Structure and Symmetry of Simple-Cell Receptive Fields in Macaque Primary Visual Cortex. *Journal of Neurophysiology*, *88*(1), 455–463. https://doi.org/10.1152/jn.2002.88.1.455

Ringach, D. L., Hawken, M. J., & Shapley, R. (1997). Dynamics of orientation tuning in

macaque primary visual cortex. *Nature*, *387*(6630), 281–284. https://doi.org/10.1038/387281a0

Ringach, D. L., Shapley, R. M., & Hawken, M. J. (2002). Orientation Selectivity in Macaque V1: Diversity and Laminar Dependence. *The Journal of Neuroscience*, *22*(13), 5639–5651. https://doi.org/10.1523/JNEUROSCI.22-13-05639.2002

Rocchi, F., Ledgeway, T., & Webb, B. S. (2013). Visual motion integration is mediated by directional ambiguities in local motion signals. *Frontiers in Computational Neuroscience*, *7*(NOV), 1–9. https://doi.org/10.3389/fncom.2013.00167

Roe, A. W., Fritsches, K., & Pettigrew, J. D. (2005). Optical imaging of functional organization of V1 and V2 in marmoset visual cortex. *The Anatomical Record. Part A, Discoveries in Molecular, Cellular, and Evolutionary Biology*, *287*(2), 1213–1225. https://doi.org/10.1002/ar.a.20248

Rokem, A., & Silver, M. A. (2009). A model of encoding and decoding in V1 and MT accounts for motion perception anisotropies in the human visual system. *Brain Research*, *1299*, 3–16. https://doi.org/10.1016/j.brainres.2009.07.005

Rolfs, M. (2009). Microsaccades: Small steps on a long way. *Vision Research*, *49*(20), 2415–2441. https://doi.org/10.1016/j.visres.2009.08.010

Rose, D., & Blakemore, C. (1974). An analysis of orientation selectivity in the cat's visual cortex. *Experimental Brain Research*, *20*(1). https://doi.org/10.1007/BF00239014

Roth, Z. N., Heeger, D. J., & Merriam, E. P. (2018). Stimulus vignetting and orientation selectivity in human visual cortex. *eLife*, *7*, e37241. https://doi.org/10.7554/eLife.37241

Roth, Z. N., Kay, K., & Merriam, E. P. (2022). Natural scene sampling reveals reliable coarse-scale orientation tuning in human V1. *Nature Communications*, *13*(1), 6469.

https://doi.org/10.1038/s41467-022-34134-7

Rovamo, J., & Virsu, V. (1979). An estimation and application of the human cortical magnification factor. *Experimental Brain Research*, *37*(3). https://doi.org/10.1007/BF00236819

Rovamo, J., Virsu, V., Laurinen, P., & Hyvärinen, L. (1982). *Resolution of gratings oriented along and across meridians in peripheral vision*. *23*(5), 5.

Rubin, G. S. (1993). Comparison of Acuity, Contrast Sensitivity, and Disability Glare Before and After Cataract Surgery. *Archives of Ophthalmology*, *111*(1), 56. https://doi.org/10.1001/archopht.1993.01090010060027

Rushton, W. A. H. (1972). Review Lecture. Pigments and signals in colour vision. *The Journal of Physiology*, *220*(3), 1–31. https://doi.org/10.1113/jphysiol.1972.sp009719

Saarinen, J., & Levi, D. M. (1994). *Orientation Anisotropy in Vernier Acuity*.

Sachs, M. B., Nachmias, J., & Robson, J. G. (1971). Spatial-Frequency Channels in Human Vision. *Journal of the Optical Society of America*, *61*(9), 1176. https://doi.org/10.1364/JOSA.61.001176

Sadagopan, S., & Ferster, D. (2012). Feedforward Origins of Response Variability Underlying Contrast Invariant Orientation Tuning in Cat Visual Cortex. *Neuron*, *74*(5), 911–923. https://doi.org/10.1016/j.neuron.2012.05.007

Salinas, E., & Abbott, L. F. (1994). Vector reconstruction from firing rates. *Journal of Computational Neuroscience*, *1*(1–2), 89–107. https://doi.org/10.1007/BF00962720

Sally, S. L., & Gurnsey, R. (2007). Foveal and extra-foveal orientation discrimination. *Experimental Brain Research*, *183*(3), 351–360. https://doi.org/10.1007/s00221-007-1048-3

Samaey, C., Wagemans, J., & Moors, P. (2020). Individual differences in processing

orientation and proximity as emergent features. *Vision Research*, *169*, 12–24. https://doi.org/10.1016/j.visres.2020.02.002

Samonds, J. M., & Bonds, A. B. (2005). Gamma oscillation maintains stimulus structure-dependent synchronization in cat visual cortex. *Journal of Neurophysiology*, *93*(1), 223–236. https://doi.org/10.1152/jn.00548.2004

Sasaki, Y., Rajimehr, R., Kim, B. W., Ekstrom, L. B., Vanduffel, W., & Tootell, R. B. H. (2006). The Radial Bias: A Different Slant on Visual Orientation Sensitivity in Human and Nonhuman Primates. *Neuron*, *51*(5), 661–670. https://doi.org/10.1016/j.neuron.2006.07.021

Saul, A. B., & Humphrey, A. L. (1992). Temporal-frequency tuning of direction selectivity in cat visual cortex. *Visual Neuroscience*, *8*(4), 365–372. https://doi.org/10.1017/S0952523800005101

Sauter, M., Draschkow, D., & Mack, W. (2020). Building, Hosting and Recruiting: A Brief Introduction to Running Behavioral Experiments Online. *Brain Sciences*, *10*(4), 251. https://doi.org/10.3390/brainsci10040251

Scharff, A., Palmer, J., & Moore, C. M. (2011). Extending the simultaneous-sequential paradigm to measure perceptual capacity for features and words. *Journal of Experimental Psychology: Human Perception and Performance*, *37*(3), 813–833. https://doi.org/10.1037/a0021440

Schenk, T., & McIntosh, R. D. (2010). Do we have independent visual streams for perception and action? *Cognitive Neuroscience*, *1*(1), 52–62. https://doi.org/10.1080/17588920903388950

Schiller, P. H., Finlay, B. L., & Volman, S. F. (1976a). Quantitative studies of single-cell properties in monkey striate cortex. I. Spatiotemporal organization of receptive fields.

Journal of Neurophysiology, *39*(6), 1288–1319. https://doi.org/10.1152/jn.1976.39.6.1288

Schiller, P. H., Finlay, B. L., & Volman, S. F. (1976b). Quantitative studies of single-cell properties in monkey striate cortex. II. Orientation specificity and ocular dominance. *Journal of Neurophysiology*, *39*(6), 1320–1333. https://doi.org/10.1152/jn.1976.39.6.1320

Schoups, A., Vogels, R., Qian, N., & Orban, G. A. (2001). Practising orientation identification improves orientation coding in V1 neurons. *Nature*, *412*(6846), 549–553.

Schummers, J. (2007). Dynamics of orientation tuning in cat V1 neurons depend on location within layers and orientation maps. *Frontiers in Neuroscience*, *1*(1), 145–159. https://doi.org/10.3389/neuro.01.1.1.011.2007

Schummers, J., Mariño, J., & Sur, M. (2002). Synaptic Integration by V1 Neurons Depends on Location within the Orientation Map. *Neuron*, *36*(5), 969–978. https://doi.org/10.1016/S0896-6273(02)01012-7

Schummers, J., Sharma, J., & Sur, M. (2005). Bottom-up and top-down dynamics in visual cortex. In *Progress in Brain Research* (Vol. 149, pp. 65–81). Elsevier. https://doi.org/10.1016/S0079-6123(05)49006-8

Schwartz, O., Hsu, A., & Dayan, P. (2007). Space and time in visual context. *Nature Reviews Neuroscience*, *8*(7), 522–535. https://doi.org/10.1038/nrn2155

Schwarzkopf, D. S., Anderson, E. J., De Haas, B., White, S. J., & Rees, G. (2014). Larger Extrastriate Population Receptive Fields in Autism Spectrum Disorders. *The Journal of Neuroscience*, *34*(7), 2713–2724. https://doi.org/10.1523/JNEUROSCI.4416-13.2014

Sclar, G., Maunsell, J. H. R., & Lennie, P. (1990). Coding of image contrast in central visual

pathways of the macaque monkey. *Vision Research*, *30*(1), 1–10. https://doi.org/10.1016/0042-6989(90)90123-3

Sengpiel, F., Stawinski, P., & Bonhoeffer, T. (1999). Influence of experience on orientation maps in cat visual cortex. *Nature Neuroscience*, *2*(8), 727–732. https://doi.org/10.1038/11192

Serences, J., Saproo, S., Scolari, M., Ho, T., & Muftuler, L. (2009). Estimating the influence of attention on population codes in human visual cortex using voxel-based tuning functions. *NeuroImage*, *44*(1), 223–231. https://doi.org/10.1016/j.neuroimage.2008.07.043

Serrano-Pedraza, I., Sierra-Vázquez, V., & Derrington, A. M. (2013). Power spectrum model of visual masking: Simulations and empirical data. *Journal of the Optical Society of America A*, *30*(6), 1119. https://doi.org/10.1364/JOSAA.30.001119

Shadlen, M., Britten, K., Newsome, W., & Movshon, J. (1996). A computational analysis of the relationship between neuronal and behavioral responses to visual motion. *The Journal of Neuroscience*, *16*(4), 1486–1510. https://doi.org/10.1523/JNEUROSCI.16-04-01486.1996

Shavit, A. Y., Li, W., & Matin, L. (2013). Individual Differences in Perceived Elevation and Verticality: Evidence of a Common Visual Process. *Multisensory Research*, *26*(3), 205–239. https://doi.org/10.1163/22134808-00002413

Shen, G., Tao, X., Zhang, B., Smith, E. L., & Chino, Y. M. (2014). Oblique effect in visual area 2 of macaque monkeys. *Journal of Vision*, *14*(2), 1–16. https://doi.org/10.1167/14.2.3

Shen, W., Liang, Z., & Shou, T. (2008). Weakened feedback abolishes neural oblique effect evoked by pseudo-natural visual stimuli in area 17 of the cat. *Neuroscience Letters*,

437(1), 65–70. https://doi.org/10.1016/j.neulet.2008.03.054

Shepherd, A. J. (2020). Tracking the Migraine Cycle Using Visual Tasks. *Vision*, *4*(2), 23. https://doi.org/10.3390/vision4020023

Sillito, A. M. (1975). The effectiveness of bicuculline as an antagonist of GABA and visually evoked inhibition in the cat's striate cortex. *The Journal of Physiology*, *250*(2), 287–304. https://doi.org/10.1113/jphysiol.1975.sp011055

Singer, W. (1977). Control of thalamic transmission by corticofugal and ascending reticular pathways in the visual system. *Physiological Reviews*, *57*(3), 386–420. https://doi.org/10.1152/physrev.1977.57.3.386

Skottun, B. C., Bradley, A., Sclar, G., Ohzawa, I., & Freeman, R. D. (1987). The effects of contrast on visual orientation and spatial frequency discrimination: A comparison of single cells and behavior. *Journal of Neurophysiology*, *57*(3), 773–786. https://doi.org/10.1152/jn.1987.57.3.773

Skottun, B. C., De Valois, R. L., Grosof, D. H., Movshon, J. A., Albrecht, D. G., & Bonds, A. B. (1991). Classifying simple and complex cells on the basis of response modulation. *Vision Research*, *31*(7–8), 1078–1086. https://doi.org/10.1016/0042-6989(91)90033-2

Smith, A. T. (2001). Estimating Receptive Field Size from fMRI Data in Human Striate and Extrastriate Visual Cortex. *Cerebral Cortex*, *11*(12), 1182–1190. https://doi.org/10.1093/cercor/11.12.1182

Smith, M. A., Bair, W., & Movshon, J. A. (2006). Dynamics of suppression in macaque primary visual cortex. *The Journal of Neuroscience: The Official Journal of the Society for Neuroscience*, *26*(18), 4826–4834. https://doi.org/10.1523/JNEUROSCI.5542-06.2006

Smyrnis, N., Mantas, A., & Evdokimidis, I. (2014). Two independent sources of anisotropy in

the visual representation of direction in 2-D space. *Experimental Brain Research*, *232*(7), 2317–2324. https://doi.org/10.1007/s00221-014-3928-7

Snowden, R. J. (1992). Orientation bandwidth: The effect of spatial and temporal frequency. *Vision Research*, *32*(10), 1965–1974. https://doi.org/10.1016/0042-6989(92)90056-O

Sokoloff, L., Reivich, M., Kennedy, C., Des Rosiers, M. H., Patlak, C. S., Pettigrew, K. D., Sakurada, O., & Shinohara, M. (1977). The [14C]deoxyglucose method for the measurement of local cerebral glucose utilization: Theory, procedure, and normal values in the conscious and anesthetized albino rat. *Journal of Neurochemistry*, *28*(5), 897–916. https://doi.org/10.1111/j.1471-4159.1977.tb10649.x

Solomon, S. G., & Rosa, M. G. P. (2014). A simpler primate brain: The visual system of the marmoset monkey. *Frontiers in Neural Circuits*, *8*. https://doi.org/10.3389/fncir.2014.00096

Somers, D., Nelson, S., & Sur, M. (1995). An emergent model of orientation selectivity in cat visual cortical simple cells. *The Journal of Neuroscience*, *15*(8), 5448–5465. https://doi.org/10.1523/JNEUROSCI.15-08-05448.1995

Sompolinsky, H., Golomb, D., & Kleinfeld, D. (1990). Global processing of visual stimuli in a neural network of coupled oscillators. *Proceedings of the National Academy of Sciences*, *87*(18), 7200–7204. https://doi.org/10.1073/pnas.87.18.7200

Sompolinsky, H., & Shapley, R. (1997). New perspectives on the mechanisms for orientation selectivity. *Current Opinion in Neurobiology*, *7*(4), 514–522. https://doi.org/10.1016/S0959-4388(97)80031-1

Stimberg, M., Wimmer, K., Martin, R., Schwabe, L., Mariño, J., Schummers, J., Lyon, D. C., Sur, M., & Obermayer, K. (2009). The operating regime of local computations in primary visual cortex. *Cerebral Cortex (New York, N.Y.: 1991)*, *19*(9), 2166–2180.

https://doi.org/10.1093/cercor/bhn240

Stone, J. (1978). The number and distribution of ganglion cells in the cat's retina. *Journal of Comparative Neurology*, *180*(4), 753–771. https://doi.org/10.1002/cne.901800407

Strasburger, H. (2022). On the cortical mapping function – Visual space, cortical space, and crowding. *Vision Research*, *194*, 107972. https://doi.org/10.1016/j.visres.2021.107972

Stringham, J. M., & Hammond, B. R. (2008). Macular pigment and visual performance under glare conditions. *Optometry and Vision Science: Official Publication of the American Academy of Optometry*, *85*(2), 82–88. https://doi.org/10.1097/OPX.0b013e318162266e

Stromeyer, C. F., & Klein, S. (1975). Evidence against narrow-band spatial frequency channels in human vision: The detectability of frequency modulated gratings. *Vision Research*, *15*(8–9), 899-IN1. https://doi.org/10.1016/0042-6989(75)90229-1

Sun, P., Gardner, J. L., Costagli, M., Ueno, K., Allen Waggoner, R., Tanaka, K., & Cheng, K. (2013). Demonstration of tuning to stimulus orientation in the human visual cortex: A high-resolution fMRI study with a novel continuous and periodic stimulation paradigm. *Cerebral Cortex*, *23*(7), 1618–1629. https://doi.org/10.1093/cercor/bhs149

Sutherland, N. S. (1957). Visual discrimination of orientation by octopus. *British Journal of Psychology*, *48*(1), 55–71. https://doi.org/10.1111/j.2044-8295.1957.tb00599.x

Swindale, N. V. (1998). Orientation tuning curves: Empirical description and estimation of parameters. *Biological Cybernetics*, *78*(1), 45–56. https://doi.org/10.1007/s004220050411

Swisher, J. D., Gatenby, J. C., Gore, J. C., Wolfe, B. A., Moon, C.-H., Kim, S.-G., & Tong, F. (2010). Multiscale Pattern Analysis of Orientation-Selective Activity in the Primary Visual Cortex. *The Journal of Neuroscience*, *30*(1), 325–330.

https://doi.org/10.1523/JNEUROSCI.4811-09.2010

Takács, E., Sulykos, I., Czigler, I., Barkaszi, I., & Balázs, L. (2013). Oblique effect in visual mismatch negativity. *Frontiers in Human Neuroscience*, *7*. https://doi.org/10.3389/fnhum.2013.00591

Tan, A. Y. Y., Chen, Y., Scholl, B., Seidemann, E., & Priebe, N. J. (2014). Sensory stimulation shifts visual cortex from synchronous to asynchronous states. *Nature*, *509*(7499), 226–229. https://doi.org/10.1038/nature13159

Tanabe, S. (2013). Population codes in the visual cortex. *Neuroscience Research*, *76*(3), 101–105. https://doi.org/10.1016/j.neures.2013.03.010

Tanaka, K. (1983). Cross-correlation analysis of geniculostriate neuronal relationships in cats. *Journal of Neurophysiology*, *49*(6), 1303–1318. https://doi.org/10.1152/jn.1983.49.6.1303

Tanaka, K. (1985). Organization of geniculate inputs to visual cortical cells in the cat. *Vision Research*, *25*(3), 357–364. https://doi.org/10.1016/0042-6989(85)90060-4

Tao, X., Zhang, B., Smith, E. L., Nishimoto, S., Ohzawa, I., & Chino, Y. M. (2012). Local sensitivity to stimulus orientation and spatial frequency within the receptive fields of neurons in visual area 2 of macaque monkeys. *Journal of Neurophysiology*, *107*(4), 1094–1110. https://doi.org/10.1152/jn.00640.2011

Theunissen, F. E., & Miller, J. P. (1991). Representation of sensory information in the cricket cercal sensory system: II. Information theoretic calculation of system accuracy and optimal tuning-curve widths of four primary interneurons. *Journal of Neurophysiology*, *66*(5), 1690–1703.

Thomas, J. P., & Gille, J. (1979). Bandwidths of orientation channels in human vision. *Journal of the Optical Society of America*, *69*(5), 652.

https://doi.org/10.1364/JOSA.69.000652

Thorpe, S., Delorme, A., & Van Rullen, R. (2001). Spike-based strategies for rapid processing. *Neural Networks: The Official Journal of the International Neural Network Society*, *14*(6–7), 715–725. https://doi.org/10.1016/s0893-6080(01)00083-1

Thurman, S. M., Davey, P. G., McCray, K. L., Paronian, V., & Seitz, A. R. (2016). Predicting individual contrast sensitivity functions from acuity and letter contrast sensitivity measurements. *Journal of Vision*, *16*(15), 15. https://doi.org/10.1167/16.15.15

Tolhurst, D. J., Movshon, J. A., & Dean, A. F. (1983). The statistical reliability of signals in single neurons in cat and monkey visual cortex. *Vision Research*, *23*(8), 775–785. https://doi.org/10.1016/0042-6989(83)90200-6

Tootell, R. B. H., Silverman, M. S., Switkes, E., & De Valois, R. L. (1982). Deoxyglucose Analysis of Retinotopic Organization in Primate Striate Cortex. *Science*, *218*(4575), 902–904. https://doi.org/10.1126/science.7134981

Tootle, J. S., & Berkley, M. A. (1983). Contrast sensitivity for vertically and obliquely oriented gratings as a function of grating area. *Vision Research*, *23*(9), 907–910. https://doi.org/10.1016/0042-6989(83)90060-3

Troyer, T. W., Krukowski, A. E., & Miller, K. D. (2002). LGN Input to Simple Cells and Contrast-Invariant Orientation Tuning: An Analysis. *Journal of Neurophysiology*, *87*(6), 2741–2752. https://doi.org/10.1152/jn.2002.87.6.2741

Tschopp-Junker, C., Gentaz, E., & Viviani, P. (2010). Effect of selective and distributed training on visual identification of orientation. *Experimental Brain Research*, *202*(3), 605–611. https://doi.org/10.1007/s00221-010-2167-9

Ts'o, D. Y., Frostig, R. D., Lieke, E. E., & Grinvald, A. (1990). Functional Organization of Primate Visual Cortex Revealed by High Resolution Optical Imaging. *Science*,

249(4967), 417–420. https://doi.org/10.1126/science.2165630

Tsou, B. C., & Bressler, N. M. (2017). Visual Acuity Reporting in Clinical Research Publications. *JAMA Ophthalmology*, *135*(6), 651. https://doi.org/10.1001/jamaophthalmol.2017.0932

Ungerleider, L. G., & Desimone, R. (1986). Cortical connections of visual area MT in the macaque. *Journal of Comparative Neurology*, *248*(2), 190–222. https://doi.org/10.1002/cne.902480204

Ungerleider, L. G., Galkin, T. W., Desimone, R., & Gattass, R. (2008). Cortical Connections of Area V4 in the Macaque. *Cerebral Cortex*, *18*(3), 477–499. https://doi.org/10.1093/cercor/bhm061

Van Den Berg, T. J. T. P., Van Rijn, L. J. R., Michael, R., Heine, C., Coeckelbergh, T., Nischler, C., Wilhelm, H., Grabner, G., Emesz, M., Barraquer, R. I., Coppens, J. E., & Franssen, L. (2007). Straylight effects with aging and lens extraction. *American Journal of Ophthalmology*, *144*(3), 358–363. https://doi.org/10.1016/j.ajo.2007.05.037

Van Der Velden, H. A. (1946). The Number of Quanta Necessary for the Perception of Light of the Human Eye. *Ophthalmologica*, *111*(6), 321–331. https://doi.org/10.1159/000300352

Van Essen, D. C., Newsome, W. T., & Maunsell, J. H. R. (1984). The visual field representation in striate cortex of the macaque monkey: Asymmetries, anisotropies, and individual variability. *Vision Research*, *24*(5), 429–448. https://doi.org/10.1016/0042-6989(84)90041-5

Van Hooser, S. D., Heimel, J. A. F., Chung, S., Nelson, S. B., & Toth, L. J. (2005). Orientation Selectivity without Orientation Maps in Visual Cortex of a Highly Visual

Mammal. *Journal of Neuroscience*, *25*(1), 19–28.
https://doi.org/10.1523/JNEUROSCI.4042-04.2005

van Kerkoerle, T., Self, M. W., Dagnino, B., Gariel-Mathis, M.-A., Poort, J., van der Togt, C., & Roelfsema, P. R. (2014). Alpha and gamma oscillations characterize feedback and feedforward processing in monkey visual cortex. *Proceedings of the National Academy of Sciences*, *111*(40), 14332–14341.
https://doi.org/10.1073/pnas.1402773111

Vancleef, K., Read, J. C. A., Herbert, W., Goodship, N., Woodhouse, M., & Serrano-Pedraza, I. (2017). Overestimation of stereo thresholds by the TNO stereotest is not due to global stereopsis. *Ophthalmic and Physiological Optics*, *37*(4), 507–520.
https://doi.org/10.1111/opo.12371

Vandenbussche, E., & Orban, G. A. (1983). Meridional variations in the line orientation discrimination of the cat. *Behavioural Brain Research*, *9*(2), 237–255.
https://doi.org/10.1016/0166-4328(83)90130-4

Vandenbussche, E., Vogels, R., & Orban, G. A. (1986). Human Orientation Discrimination: Changes With Eccentricity in Normal and Amblyopic Vision. *Investigative Ophthalmology & Visual Science*, *27*(2), 9.

Vanni, S., Hokkanen, H., Werner, F., & Angelucci, A. (2020). Anatomy and Physiology of Macaque Visual Cortical Areas V1, V2, and V5/MT: Bases for Biologically Realistic Models. *Cerebral Cortex*, *30*(6), 3483–3517. https://doi.org/10.1093/cercor/bhz322

Varano, M., Eter, N., Winyard, S., Wittrup-Jensen, K., Navarro, R., & Heraghty, J. (2015). Current barriers to treatment for wet age-related macular degeneration (wAMD): Findings from the wAMD patient and caregiver survey. *Clinical Ophthalmology*, *9*, 2243–2250. https://doi.org/10.2147/OPTH.S92548

Vidyasagar, T. R., & Eysel, U. T. (2015). Origins of feature selectivities and maps in the mammalian primary visual cortex. *Trends in Neurosciences*, *38*(8), 475–485. https://doi.org/10.1016/j.tins.2015.06.003

Vidyasagar, T. R., & Siguenza, J. A. (1985). Relationship between orientation tuning and spatial frequency in neurones of cat area 17. *Experimental Brain Research*, *57*(3). https://doi.org/10.1007/BF00237851

Vidyasagar, T. R., & Urbas, J. V. (1982). Orientation sensitivity of cat LGN neurones with and without inputs from visual cortical areas 17 and 18. *Experimental Brain Research*, *46*(2), 157–169. https://doi.org/10.1007/BF00237172

Vilidaite, G., & Baker, D. H. (2017). Individual differences in internal noise are consistent across two measurement techniques. *Vision Research*, *141*, 30–39. https://doi.org/10.1016/j.visres.2016.10.008

Villeneuve, M. Y., & Casanova, C. (2003). On the use of isoflurane versus halothane in the study of visual response properties of single cells in the primary visual cortex. *Journal of Neuroscience Methods*, *129*(1), 19–31. https://doi.org/10.1016/S0165-0270(03)00198-5

Vogels, R. (1990). Population coding of stimulus orientation by striate cortical cells. *Biological Cybernetics*, *64*(1), 25–31. https://doi.org/10.1007/BF00203627

Vogels, R., & Orban, G. A. (1985). The effect of practice on the oblique effect in line orientation judgments. *Vision Research*, *25*(11), 1679–1687. https://doi.org/10.1016/0042-6989(85)90140-3

Vogels, R., Orban, G. A., & Vandenbussche, E. (1984). Meridional variations in orientation discrimination in normal and amblyopic vision. *Investigative Ophthalmology and Visual Science*, *25*(6), 720–728.

6649 Volgushev, M., Pei, X., Vidyasagar, T. R., & Creutzfeldt, O. D. (1993). Excitation and
6650 inhibition in orientation selectivity of cat visual cortex neurons revealed by whole-cell
6651 recordings in vivo. *Visual Neuroscience*, *10*(6), 1151–1155.
6652 https://doi.org/10.1017/S0952523800010257
6653 Walker, G. A., Ohzawa, I., & Freeman, R. D. (1998). Binocular Cross-Orientation
6654 Suppression in the Cat's Striate Cortex. *Journal of Neurophysiology*, *79*(1), 227–239.
6655 https://doi.org/10.1152/jn.1998.79.1.227
6656 Wang, F., Zhong, X., Huang, J., Ding, Y., & Song, Y. (2013). Comparison of perceptual
6657 learning of real and virtual line orientations: An event-related potential study. *Vision*
6658 *Research*, *93*, 1–9. https://doi.org/10.1016/j.visres.2013.10.004
6659 Wang, G., Ding, S., & Yunokuchi, K. (2003). Representation of Cardinal Contour Overlaps
6660 Less With Representation of Nearby Angles in Cat Visual Cortex. *Journal of*
6661 *Neurophysiology*, *90*(6), 3912–3920. https://doi.org/10.1152/jn.00219.2003
6662 Wang, Y.-Z., He, Y.-G., Mitzel, G., Zhang, S., & Bartlett, M. (2013). *Handheld Shape*
6663 *Discrimination Hyperacuity Test on a Mobile Device for Remote Monitoring of Visual*
6664 *Function in Maculopathy*. *54*(8), 5497–5505. https://doi.org/10.1167/iovs.13-12037
6665 Wassle, H., & Boycott, B. B. (1991). Functional architecture of the mammalian retina.
6666 *Physiological Reviews*, *71*(2), 447–480.
6667 https://doi.org/10.1152/physrev.1991.71.2.447
6668 Watson, A. B., & Ahumada, A. J. (2005). A standard model for foveal detection of spatial
6669 contrast. *Journal of Vision*, *5*(9), 717–740. https://doi.org/10.1167/5.9.6
6670 Watson, A. B., & Robson, J. G. (1981). Discrimination at threshold: Labelled detectors in
6671 human vision. *Vision Research*, *21*(7), 1115–1122. https://doi.org/10.1016/0042-
6672 6989(81)90014-6

Webb, B. S., Ledgeway, T., & McGraw, P. V. (2007a). Cortical pooling algorithms for judging global motion direction. *Proceedings of the National Academy of Sciences*, *104*(9), 3532–3537. https://doi.org/10.1073/pnas.0611288104

Webb, B. S., Ledgeway, T., & McGraw, P. V. (2007b). Cortical pooling algorithms for judging global motion direction. *Proceedings of the National Academy of Sciences of the United States of America*, *104*(9), 3532–3537. https://doi.org/10.1073/pnas.0611288104

Webb, B. S., Ledgeway, T., & McGraw, P. V. (2010). Relating spatial and temporal orientation pooling to population decoding solutions in human vision. *Vision Research*, *50*(22), 2274–2283. https://doi.org/10.1016/j.visres.2010.04.019

Webb, B. S., Ledgeway, T., & Rocchi, F. (2011). Neural computations governing spatiotemporal pooling of visual motion signals in humans. *Journal of Neuroscience*, *31*(13), 4917–4925. https://doi.org/10.1523/JNEUROSCI.6185-10.2011

Webster, M. A. (2015). Visual Adaptation. *Annu Rev Vis Sci.* https://doi.org/10.1016/j.physbeh.2017.03.040

Webster, M. A., & De Valois, R. L. (1985). Relationship between spatial-frequency and orientation tuning of striate-cortex cells. *Journal of the Optical Society of America A*, *2*(7), 1124. https://doi.org/10.1364/JOSAA.2.001124

Webster, M. A., & MacLeod, D. I. A. (1988). Factors underlying individual differences in the color matches of normal observers. *Journal of the Optical Society of America A*, *5*(10), 1722. https://doi.org/10.1364/JOSAA.5.001722

Webster, M. A., Switkes, E., & De Valois, K. K. (1990). Orientation and spatial-frequency discrimination for luminance and chromatic gratings. *Journal of the Optical Society of America A*, *7*(6), 1034. https://doi.org/10.1364/JOSAA.7.001034

Wehrhahn, C., Li, W., & Westheimer, G. (1996). Patterns That Impair Discrimination of Line Orientation in Human Vision. *Perception*, *25*(9), 1053–1064. https://doi.org/10.1068/p251053

Wells-Gray, E. M., Choi, S. S., Bries, A., & Doble, N. (2016). Variation in rod and cone density from the fovea to the mid-periphery in healthy human retinas using adaptive optics scanning laser ophthalmoscopy. *Eye*, *30*(8), Article 8. https://doi.org/10.1038/eye.2016.107

Westheimer, G. (2003a). Meridional anisotropy in visual processing: Implications for the neural site of the oblique effect. *Vision Research*, *43*(22), 2281–2289. https://doi.org/10.1016/S0042-6989(03)00360-2

Westheimer, G. (2003b). The distribution of preferred orientations in the peripheral visual field. *Vision Research*, *43*(1), 53–57. https://doi.org/10.1016/S0042-6989(02)00398-X

Westheimer, G. (2017). Preferential processing of cardinal over oblique orientations in human vision. *Journal of Vision*, *17*(13), 1–14. https://doi.org/10.1167/17.13.8

Westheimer, G., & Beard, B. L. (1998). Orientation dependency for foveal line stimuli: Detection and intensity discrimination, resolution, orientation discrimination and Vernier acuity. *Vision Research*, *38*(8), 1097–1103. https://doi.org/10.1016/S0042-6989(97)00248-4

Westheimer, G., & Lavian, J. (2013). Perceptual learning of orientation judgments in oblique meridians. *Attention, Perception, & Psychophysics*, *75*(6), 1252–1259. https://doi.org/10.3758/s13414-013-0478-1

Westheimer, G., Shimamura, K., & McKee, S. P. (1976). Interference with line-orientation sensitivity. *Journal of the Optical Society of America*, *66*(4), 332. https://doi.org/10.1364/JOSA.66.000332

White, A. L., Runeson, E., Palmer, J., Ernst, Z. R., & Boynton, G. M. (2017). Evidence for unlimited capacity processing of simple features in visual cortex. *Journal of Vision*, *17*(6), 19. https://doi.org/10.1167/17.6.19

Whittingstall, K., Stroink, G., & Schmidt, M. (2007). Evaluating the spatial relationship of event-related potential and functional MRI sources in the primary visual cortex. *Human Brain Mapping*, *28*(2), 134–142. https://doi.org/10.1002/hbm.20265

Wilder, H. D., Grünert, U., Lee, B. B., & Martin, P. R. (1996). Topography of ganglion cells and photoreceptors in the retina of a New World monkey: The marmoset Callithrix jacchus. *Visual Neuroscience*, *13*(2), 335–352. https://doi.org/10.1017/s0952523800007586

Williams, D., Tweten, S., & Sekuler, R. (1991). Using metamers to explore motion perception. *Vision Research*, *31*(2), 275–286. https://doi.org/10.1016/0042-6989(91)90118-O

Wilson, H. R., & Bergen, J. R. (1979). A four mechanism model for threshold spatial vision. *Vision Research*, *19*(1), 19–32. https://doi.org/10.1016/0042-6989(79)90117-2

Wilson, H. R., Mcfarlane, D. K., & Phillips, G. C. (1983). Spatial frequency tuning of orientation selective units estimated by oblique masking. *Vision Research*, *23*(9), 873–882. https://doi.org/10.1016/0042-6989(83)90055-x

Wilson, J. R., & Sherman, S. M. (1976). Receptive-field characteristics of neurons in cat striate cortex: Changes with visual field eccentricity. *Journal of Neurophysiology*, *39*(3), 512–533. https://doi.org/10.1152/jn.1976.39.3.512

Wilson, M. E., Cragg, B. G., Ainsworth, A., & Toyne, M. J. (1969). Projections from the medial geniculate body to the cerebral cortex in the cat. *Brain Research*, *13*(3), 462–475. https://doi.org/10.1016/0006-8993(69)90260-1

6745 Wissig, S. C., & Kohn, A. (2012). The influence of surround suppression on adaptation
6746 effects in primary visual cortex. *Journal of Neurophysiology*, *107*(12), 3370–3384.
6747 https://doi.org/10.1152/jn.00739.2011
6748 Witzel, C., O'Regan, J. K., & Hansmann-Roth, S. (2017). The dress and individual
6749 differences in the perception of surface properties. *Vision Research*, *141*, 76–94.
6750 https://doi.org/10.1016/j.visres.2017.07.015
6751 Wong, W., & Price, N. S. C. (2014). Testing Neuronal Accounts of Anisotropic Motion
6752 Perception with Computational Modelling. *PLoS ONE*, *9*(11), e113061.
6753 https://doi.org/10.1371/journal.pone.0113061
6754 Wurtz, R. H., & Goldberg, M. E. (1971). Superior Colliculus Cell Responses Related to Eye
6755 Movements in Awake Monkeys. *Science*, *171*(3966), 82–84.
6756 https://doi.org/10.1126/science.171.3966.82
6757 Xie, X. (2002). Threshold behaviour of the maximum likelihood method in population
6758 decoding. *Network: Computation in Neural Systems*, *13*(4), 447–456.
6759 https://doi.org/10.1088/0954-898X_13_4_302
6760 Xing, D., Ringach, D. L., Shapley, R., & Hawken, M. J. (2004). Correlation of local and
6761 global orientation and spatial frequency tuning in macaque V1: Spatial frequency and
6762 orientation tuning in macaque V1. *The Journal of Physiology*, *557*(3), 923–933.
6763 https://doi.org/10.1113/jphysiol.2004.062026
6764 Xu, X., Collins, C. E., Khaytin, I., Kaas, J. H., & Casagrande, V. A. (2006). Unequal
6765 representation of cardinal vs. Oblique orientations in the middle temporal visual area.
6766 *Proceedings of the National Academy of Sciences of the United States of America*,
6767 *103*(46), 17490–17495. https://doi.org/10.1073/pnas.0608502103
6768 Xu, X., Ichida, J., Shostak, Y., Bonds, A. B., & Casagrande, V. A. (2002). Are primate lateral

geniculate nucleus (LGN) cells really sensitive to orientation or direction? *Visual Neuroscience*, *19*(1), 97–108. https://doi.org/10.1017/S0952523802191097

Yacoub, E., Harel, N., & Ugurbil, K. (2008). High-field fMRI unveils orientation columns in humans. *Proceedings of the National Academy of Sciences*, *105*(30), 10607–10612. https://doi.org/10.1073/pnas.0804110105

Yang, T., & Maunsell, J. (2004). The Effect of Perceptual Learning on Neuronal Responses in Monkey Visual Area V4. *Journal of Neuroscience*, *24*(7), 1617–1626. https://doi.org/10.1523/JNEUROSCI.4442-03.2004

Ye, R., & Liu, X. (2020). How the known reference weakens the visual oblique effect: A Bayesian account of cognitive improvement by cue influence. *Scientific Reports*, *10*(1), 20269. https://doi.org/10.1038/s41598-020-76911-8

Yen, C. C.-C., Fukuda, M., & Kim, S.-G. (2011). BOLD responses to different temporal frequency stimuli in the lateral geniculate nucleus and visual cortex: Insights into the neural basis of fMRI. *NeuroImage*, *58*(1), 82–90. https://doi.org/10.1016/j.neuroimage.2011.06.022

Yoshida, K., & Benevento, L. A. (1981). The projection from the dorsal lateral geniculate nucleus of the thalamus to extrastriate visual association cortex in the macaque monkey. *Neuroscience Letters*, *22*(2), 103–108. https://doi.org/10.1016/0304-3940(81)90071-9

Yu, C., Klein, S. A., & Levi, D. M. (2002). Facilitation of contrast detection by cross-oriented surround stimuli and its psychophysical mechanisms. *Journal of Vision*, *2*(3), 4–4. https://doi.org/10.1167/2.3.4

Yu, H.-H., & Rosa, M. G. P. (2014). Uniformity and diversity of response properties of neurons in the primary visual cortex: Selectivity for orientation, direction of motion,

and stimulus size from center to far periphery. *Visual Neuroscience*, *31*(1), 85–98. https://doi.org/10.1017/S0952523813000448

Yu, H.-H., Verma, R., Yang, Y., Tibballs, H. A., Lui, L. L., Reser, D. H., & Rosa, M. G. P. (2010). Spatial and temporal frequency tuning in striate cortex: Functional uniformity and specializations related to receptive field eccentricity. *European Journal of Neuroscience*, *31*(6), 1043–1062. https://doi.org/10.1111/j.1460-9568.2010.07118.x

Zemon, V., Gutowski, W., & Horton, T. (1983). Orientational Anisotropy In The Human Visual System: An Evoked Potential And Psychophysical Study. *International Journal of Neuroscience*, *19*(1–4), 259–286. https://doi.org/10.3109/00207458309148661

Zhang, T., Godara, P., Blanco, E. R., Griffin, R. L., Wang, X., Curcio, C. A., & Zhang, Y. (2015). Variability in Human Cone Topography Assessed by Adaptive Optics Scanning Laser Ophthalmoscopy. *American Journal of Ophthalmology*, *160*(2), 290-300.e1. https://doi.org/10.1016/j.ajo.2015.04.034

Zheng, J., Zhang, B., Bi, H., Maruko, I., Watanabe, I., Nakatsuka, C., Smith, E. L., & Chino, Y. M. (2007). Development of Temporal Response Properties and Contrast Sensitivity of V1 and V2 Neurons in Macaque Monkeys. *Journal of Neurophysiology*, *97*(6), 3905–3916. https://doi.org/10.1152/jn.01320.2006

Zipser, K., Lamme, V. A. F., & Schiller, P. H. (1996). Contextual Modulation in Primary Visual Cortex. *The Journal of Neuroscience*, *16*(22), 7376–7389. https://doi.org/10.1523/JNEUROSCI.16-22-07376.1996

Zohary, E., Shadlen, M. N., & Newsome, W. T. (1994). Correlated neuronal discharge rate and its implications for psychophysical performance. *Nature*, *370*(6485), 140–143. https://doi.org/10.1038/370140a0